INTERNATIONAL GEMMOLOGICAL CONFERENCE

Nantes - France
August 2019

36th International Gemmological Conference IGC

August 2019
Nantes, France

Dear colleagues of IGC,

It is our great pleasure and pride to welcome you to the 36th International Gemmological Conference in Nantes, France. Nantes has progressively gained a reputation in the science of gemmology since Prof. Bernard Lasnier created the Diplôme d'Université de Gemmologie (DUG) in the early 1980s. Several DUGs or PhDs have since made a name for themselves in international gemmology. In addition, the town of Nantes has been on several occasions recognized as a very attractive, green town, with a high quality of life. This regional capital is also an important hub for the industry (e.g. agriculture, aeronautics), education and high-tech. It has only recently developed tourism even if has much to offer, with its historical downtown, the beginning of the Loire river estuary, and the ocean close by.

The organizers of 36th International Gemmological Conference wish you a pleasant and rewarding conference

Dr. Emmanuel Fritsch, Dr. Nathalie Barreau, Féodor Blumentritt MsC.

The organizers of the 36th International Gemmological Conference in Nantes, France
From left to right Dr. Emmanuel Fritsch, Dr. Nathalie Barreau, Féodor Blumentritt MsC.

Organization of the 36th International Gemmological Conference

Organizing Committee
Dr. Emmanuel Fritsch (University of Nantes)
Dr. Nathalie Barreau (IMN-CNRS)
Feodor Blumentritt
Dr. Jayshree Panjikar (IGC Executive Secretary)
IGC Executive Committee

Excursions
Sophie Joubert, Richou, Cholet
Hervé Renoux, Richou, Cholet

Guest Programme
Sophie Joubert, Richou, Cholet

Homepage
Dr. Michael Krzemnicki (Swiss Gemmological Institute SSEF)
Dr. Laurent Cartier (Swiss Gemmological Institute SSEF)

Proceedings
Dr. Michael Krzemnicki (Swiss Gemmological Institute SSEF)
Dr. Laurent Cartier (Swiss Gemmological Institute SSEF)

Abstract Review Board
Prof. Dr. Henry A. Hänni
Prof. Dr. Emmanuel Fritsch
Dr. Ulrich Henn
Dr. Karl Schmetzer
Dr. Hanco Zwaan
Dr. Michael Krzemnicki

Special thanks
Mrs. Isabelle Berthaud for helping with registrations, and IMN-CNRS for general support.

The IGC Executive Committee

Members of the IGC Executive Committee at the opening ceremony of the 35th IGC in Windhoek, Namibia. Photo by Roman Serov.

Dr. Jayshree Panjikar, Executive Secretary, India (center right, in red traditional sari). Then from left to right: Prof. Dr. Henry A. Hänni, Switzerland; Mr. Gamini Zoysa, Sri Lanka; Dr. Karl Schmetzer, Germany; Prof. Dr. Emmanuel Fritsch, France; Mrs. Willow Wight, Canada; (Namibian officials and Dr Ulrich Henn, organizer of 35th IGC, second row); Mr. Thye Sun Tay, Singapore; Dr. J. C. Hanco Zwaan, The Netherlands. Not featured: Dr. Michael Krzemnicki, Switzerland; Dr. Dietmar Schwarz, Germany

About the venue in Nantes

Nantes is the regional capital of Pays de Loire, and historically the home of the Duke of Brittany. Nantes with its suburbs has grown to over 630,000 inhabitants in recent years. La Cité Nantes Congress Center offers an ideal setting for the conference, with its high-quality facilities and organizing experience, walking distance from downtown.

Sponsors

Diamond sponsors: 10,000 Euros

Ruby sponsors 5,000 Euros

INTERNATIONAL GEMMOLOGICAL CONFERENCE

History of the IGC

The International Gemmological Conference (IGC) owes much of its origin to BIBOA (Bureau International pour la Bijouterie, Orfèvrene, Argenterie), the International Jewellery and Gemstone Federation, the first Congress of which in 1926 recommended and defined use of the term cultured pearl.

Experts from various European gem testing laboratories were invited to attend a series of expert meetings that aimed to formulate the policies of BIBOA. In 1936, at the fifth conference of experts, collaboration among laboratories was acclaimed by traders and they encouraged Laboratory Directors to meet each other at a technical conference from which all commercial delegates would be excluded.

Technical meetings were held annually, and in 1951 a Technical Conference was held in Idar Oberstein to prepare for the next London Congress in 1952. Those attending the 1951 conference included Mr B.W. Anderson, Mr G. Göbel, Dr E. Gübelin, Mr F. Wolf, Mr A. Bonebakker, Mr H. Tillander, Mr A. Strondahl, and Mr O. Dragstead. It has been suggested that the future framework of the IGC was established at this meeting in Idar Oberstein.

The London Congress saw the restructuring of BIBOA in which Gemmological Associations were replaced by National Federal Committees, and BIBOA evolved into BIBOAH – the forerunner of CIBJO, now known as The World Jewellery Confederation.

A Technical Conference met at Lugano from 23rd to 25th October 1952 at the initiative of Prof. K. Schlossmacher and Dr. E. Gübelin. Also present at this conference were Messrs B.W. Anderson, A. Bonebakker, O. Dragstead, G. Göbel, K. Siess and H. Tillander. At this historic meeting Dr E. Gübelin proposed creation of a "Committee of an International Gemmological Association" that would consist of one member per country; this member being the Director of a Gem Testing Laboratory, or a gemmologist of the calibre who could attend that meeting. This was agreed to, and this meeting was later considered to be the inaugural meeting of the IGC.

The first meeting of the IGC in Lugano was followed by subsequent meetings in Amsterdam, The Netherlands (1953), Copenhagen, Denmark (1954), London, UK (1955), Munich, Germany (1956), Oslo, Norway (1957), Paris, France (1958), Milano, Italy (1960), Helsinki, Finland (1962), Vienna, Austria (1964); Barcelona, Spain (1966); Stockholm, Sweden (1968); Brussels, Belgium (1970); Vitznau, Switzerland (1972); Washington D. C., USA (1975), The Hague, The Netherlands (1977), Idar Oberstein, Germany (1979), Kashiko-Jima, Japan (1981), Beruwela, Sri Lanka (1983); Sydney, Australia (1985); Rio de Janeiro, Brazil (1987), Tremezzo, Italy (1989); Stellenboch (1991), Paris, France (1993); Bangkok, Thailand (1995); Idar Oberstein, Germany (1997); Goa, India (1999); Madrid, Spain (2001), Wuhan, China (2004); Moscow, Russia (2007); Arusha, Tanzania (2009), Interlaken, Switzerland (2011); Hanoi, Vietnam, (2013); Vilnius, Lithuania (2015); Windhoek, Namibia (2017).

Over the history of the IGC, that now in its fourth decade, it can therefore be seen that the International Gemmological Conference is the longest surviving gemmological conference to remain largely in its original format. Over its history, have been invited to participate in IGC meetings gemmologists from over 40 countries or areas – including Australia, Austria, Bahrein, Belgium, Brazil, Canada, China, Czech Republic, Denmark, Dubai (UAE), England, Finland, France, Greece, Germany, Greenland, Hong-Kong, Israel, India, Italy, Japan, Kenya, Korea, Liechtenstein, Lithuania, Namibia, the Netherlands, Norway, Russia, Singapore, South Africa, Spain, Sri Lanka, Switzerland, Sweden, Tanzania, Thailand, U.S.A., Vietnam and Zimbabwe.
During the 20th IGC, which was held in Sydney, Australia, the members present elected nine members to Honorary Members status. The first Honorary Members of the IGC were Oliver Chalmers (Australia), Prof. A. Chikayama (Japan),

and Mr R. Crowningshield (U.S.A), Mr. O. Dragsted (Sweden), Prof. E. Gübelin (Switzerland), Mr. R. T. Liddicoat (U.S.A), Mr.
M. Masso (Spain), Dr. F. H. Pough (U.S. A) and Dr. J. M. Saul (Kenya).

In Italy, the IGC logo was designed by Roberto Sambonet, made in gold by Roberto Cusi, and offered to the conference delegates during the Tremezzo 1989 edition.

In Italy, in 1989, the following rules were agreed for future meetings of the IGC:

1. The prime objective was to be the exchange of gemmological experiences.
2. Gemmology was to be the platform for all topics and was to be regarded as the principal theme.
3. It was decided that attendance at all further Conferences should be by invitation that would be determined where necessary by the Conference Secretary and the Executive Committee.
4. All delegates were to be encouraged to present papers; but this would not be mandatory.
5. All delegates must have a publishing record and all papers at IGC meetings must presented in English, both when written or spoken.
6. The Conference must keep foremost in mind the prime objectives and avoid dilution/confusion of this objective which, if not maintained, could result in a blank organization without true status or credibility.
7. Peripheral commercial activity must be kept to a minimum, and there should be no blatant sponsorship of any kind.

These rules, combined with the original concepts, have been kept as the basis for all conferences since. Any invitation is specific to the person invited and is not transferable.

Rules/Standard Operating Procedures of the IGC as of the 2019 revision

Introduction

Over the years, the Rules/Standard Operating Procedures for the IGC have evolved. These were last published in the Proceedings of the 35th IGC 2017 (Windhoek, Namibia).

The following Rules and Procedures have been revised in 2018 and 2019 by the Executive Committee of the IGC and agreed for future meetings.

I. GENERAL RULES

1. The prime objective is the exchange of gemmological experiences. Gemmology is to be regarded as the principal theme.
2. Attendance at the IGC is by invitation only (see Categories of Membership following).
3. All Members (delegates and observers) are encouraged to present a paper or poster. To receive further invitations, it is mandatory for observers to present a paper or poster, at least at their second attendance at the conference.
4. All Members (delegates and observers) must have a publishing record. All papers at IGC meetings must be presented in English, both written and spoken.
5. The Conference must keep foremost in mind the prime objective and avoid dilution or confusion of this objective, which if not maintained could result in the loss of status or credibility.
6. Peripheral commercial activity must be kept to a minimum, and there should be no blatant sponsorship of any kind.

These rules, combined with the original concepts, have been kept as the basis for all conferences since. Any invitation is specific to the person invited and is not transferable.

Membership
Honorary Members are senior members of the IGC who are elected by Delegates at the Business Meeting following each IGC, following nomination by the Executive Committee.

Delegates are those who are elected from Observers who have established eligibility by presenting worthwhile presentations (either lectures and/or posters) at three IGC meetings. Following recommendation by the Executive Committee, new Delegates shall be elected by majority vote of Delegates at the Business Meeting following each IGC.

Observers are those who are invited to attend an IGC meeting by majority vote of the Executive Committee. Invitations shall be given only to internationally recognized gemmologists who have published in the gemmological field. Applications for Observer status, which shall be supported by a pertinent CV and list of publications, should be submitted to the Executive Committee for consideration. An invitation will then be offered by the Secretary of the IGC.

Executive Committee (Execo)
The day-to-day administration and decision making of the IGC shall be overseen by an Executive Committee that meets formally at IGC meetings, and between meetings conducts the routine business of the IGC electronically by email. New members of the Executive Committee are chosen from among IGC Delegates. Following nomination, new members of the Executive Committee shall be elected by majority vote of Delegates at the Business Meeting that follows each IGC.

From time to time, the Executive Committee shall elect a Secretary, who will be responsible for detailed administration, especially activities related to invitations to the conference, and the distribution of decisions of the Executive Committee to Honorary Members and Delegates.

Written minutes shall be kept for all meetings of the Executive Committee and approved by the Executive Committee.

After a Conference, written minutes of the General Business Meeting shall be distributed by email to all Members to inform everyone, including those not present, about decisions and further activities.

The Executive Committee elects a Chairman of the Abstract Review Committee, who organizes the handling and review process of the Abstracts. Delegates and Observers shall submit the title and a three-page extended abstract of a paper proposed for presentation at an IGC meeting to the Abstract Review Committee for approval.

II. MEETINGS OF THE IGC
IGC meetings should be held every two years in a host country approved by Honorary Members and Delegates.

IGC meetings should be timed so as not to clash with other meetings (e.g. IMA meetings) that Delegates are likely to attend.

A country wishing to host an IGC meeting shall submit a proposal first to the Executive Committee, and then present it formally to Delegates. The decision to accept or reject a proposal to host an IGC meeting will be made by majority vote of Honorary Members and Delegates present at the IGC Business Meeting, or electronically if an IGC meeting is not being held at the time a decision needs to be made.

Countries hosting IGC meetings shall establish their own administrative structures to ensure the efficient planning and operation of the Conference. Costs involved in hosting the Conference shall be met by registration fees paid by Honorary Members, Delegates and Observers attending the meeting, and financial sponsorship from private, institutional and government sources.

Day-to-day administration shall be the responsibility of a Conference Organizer, who is either an Honorary Member or a Delegate. The Conference Organizer is chosen at a Business Meeting following recommendation by the Executive Committee. The Conference Organizer may appoint a Conference Secretary and further members of a Committee as needed.

General responsibilities of the Conference Organizer of each IGC include:

Planning and implementation of
- pre-conference activities
- post-conference activities
- the formal IGC conference
- associated cultural activities and events
- entertainment program for registered Guests of Members
- all finances
- receipt and compilation of abstracts of papers after acceptance by the abstract review committee
- publication of Proceedings of the IGC conference
- implementation of poster presentations
- coordination with the Execo, and updates on progress of arrangements for members

Obtaining the necessary government permissions and other political requirements, including organisation of formalities required for different foreign visitors in the host country, e.g. visas, special permissions etc.

The Conference Organizer is responsible for informing Honorary Members, Delegates and Observers of the prospective dates of the next IGC at least 10 months in advance.
Attendance at IGC meetings of Delegates and Observers from countries other than the host country shall be restricted to a maximum of five registrations per country. This restriction does not include Honorary Members.

Local Guests are gemmologists who may be invited by the Conference Organizer to attend an IGC meeting held in the country in which they are resident.

Each IGC shall consist of a minimum of:

1.Two to three day pre- and post-conference study excursions to areas and facilities of gemmological interest.

2. A one-day session, prior to the IGC at which previously nominated Delegates and/or Observers will be invited to give presentations to gemmologist members of the host country

3. A three to five-day professional conference to consist of:
   - Formal papers of 15 minutes duration, followed by 5 minutes of questions and answers; and,
   - Poster presentations that shall be scheduled independently so that adequate time is allowed for each poster to be presented by its authors and then have its content available for discussion.

4. A Business Meeting for Honorary Members, Delegates and Observers that traditionally follows closure of the IGC professional conference to exchange opinions on further directions of IGC, and to decide the location for further IGC meetings. Only Honorary Members and Delegates are allowed to vote at the Business Meeting.

IGC 2019 programme

23 - 26 August 2019 Pre-conference tour
27 - 31 August 2019 Conference, La Cité Nantes Congress Center, Nantes
01 - 04 September 2019 Post-conference tour

Tuesday 27 August 2019

10h – 18h Open Colloquium
18h 30 Welcome reception and buffet dinner: multi-purpose area R0
20:30 -21:30 Executive Committee Meeting. Room F

Wednesday 28 August 2019

La Cité Nantes Congress Center
9h-10h registration room 300 lower Foyer
10h Opening ceremony
10h40 -11:20 Coffee breaks and posters

Sessions in the lower Foyer, room 300

Session 1: **Diamonds.** Chairman: Henry Hänni

11:20 - 11:40 Lucille Daver, Hélène Bureau, Éloïse Gaillou, Benoit Baptiste, Oulfa Belhadj, Églantine Boulard, Nicolas Guignot, Eddy Foy, Pierre Cartigny and Daniele L. Pinti: The genesis of lithospheric blue diamonds.

11:40 - 12: 00 Marie Schoor, Jean-Claude Boulliard, Emmanuel Fritsch, Eloïse Gaillou, Benjamin Rondeau : characterization of growth sectors in asteriated diamonds

12:00 - 12:20 Roman Serov, Sergey Sivovolenko: Fluorescence influence on diamond performance

12:20 – 12.40 Aurélien Delaunay, Emmanuel Fritsch, Annabelle Herreweghe: Proposed classification of type IIa diamonds on the basis of the DiamondView image

12: 40 – 14:00 Lunch in the multipurpose area R0

Session 2 **Synthetic & treated diamonds.** Chairman: Emmanuel Fritsch

14:00 – 14:20 Hiroshi Kitawaki, Kentaro Emori, Mio Hisanaga, Masahiro Yamamoto: Current Production of Synthetic Diamond Manufacturers in Asia.

14:20 – 14:40 Tian Shao, Jinqiu Zhang, Andy Histien Shen : Phosphorescence of type IIb HT-HP synthetic diamonds from China.

14:40 – 15:00 Jean-Pierre Chalain, Ly Phan, Michael S. Krzemnicki, Hao Wang, Jörg Pausch, Michael Steinacher: Study of a recut HPHT synthetic diamond: colour vs size vs SWUV transmission

15:00 – 15:20 Thomas Hainschwang, Gianna Pamies: The effects of HPHT treatment on previously irradiated and annealed diamonds of all types and colors

15:20 –16:00 Coffee breaks and posters

Session 3 **History and age dating** Chairlady: Jayshree Panjikar

16:00 – 16:20 H. Albert Gilg, Ulrich Schüssler , Joachim Krause , Bernhard Schulz : The use phosphate inclusions in origin determination of ancient and medieval red garnet.

16:20 - 16:40 Karl Schmetzer, H. Albert Gilg: A gothic crown in the treasury of the Munich residence museum : examination of the English royal insignia from the late Middle-age.

16:40 - 17:00 Michael S. Krzemnicki, Hao A.O. Wang, Myint M. Phyo: Age dating applied as testing procedure to gemstones and biogenic materials

17:00 -17:20 Elisabeth Strack , Bernd Augustin : gemmological examination of four Mogul jewellery objects daing from the first half of the 17th century.

19:00 Diner at "La Cigale" restaurant, a historical monument in the center of Nantes

Thursday 29 August 2019

9h – 12 h Visit of the "Machines de l'Ile" an ensemble of articulated machines inspired by Jules Verne.

12: 40– 14:00 Lunch in the multi-purpose area R0

Session 4 **Colored stones 1**- Chairlady: Willow Wight

14:00 – 14:20 Carolina Santiago and Jurgen Schnellrath : Cat's eye opal from Brazil: A second look.

14:20 – 14:40 Alessandra Costanzo , Martin Feely: Review gem-materials from Connemara, Western Ireland.

14:40 – 15:00 Cho Cho, Thet Tin Nyunt , Tay Thye Sun and Tin Kyaw Than: jadeitite deposit from Khamti, Sagaing region, Myanmar

15:00 – 15:20 Gamini Zoyza, Pantaree Lomthong, Dietmar Schwarz, Chen Yanyu, Arūnas Kleišmantas: Spinels from Sri-Lanka.

15:20 – 15:40 Shengsi Wang, Andy Shen, Aaron Palke, Peter Heaney : Color origin of the Oregon sunstone – The reabsorption on exsolution of Cu inclusions.

15:40 – 16:20 Coffee breaks and posters

Session 5 **Colored stones 2** – Chairman Gamini Zoysa

16:20 - 16:40 Feodor Blumentritt, Emmanuel Fritsch, Maria Teresa Caldes, Stephane Jobic: Introduction to mine ralomimetism : the case of photochromic sodalite hackmanite

16:40 - 17:00 Peter Lyckberg, Vsevolod Chournousenko, Oleksandr Chournousenko : Giant heliodor and topaz pocket of the Volodarsk-Volinsky chamber pegmatites, Korosten pluton, Ukraine.

17:00 -17:20 Gagan Choudhary: Recent challenges in identification of filled emeralds

17:20 – 17:40 Shang I (Edward) Liu, Kyaw Thu, Hexiong Yang: A study of pezzotaite from Pyi-Gyi-Taung, Myanmar.

17:40–18:00 Tasnara Sripoonjan , Montira Seneewong Na Ayutthaya , Pimtida Bupparenoo , Nalin Narudeesombat , Thanong Leelawatanasuk , and Malin Sawatekititthum : Gemological and chemical characteristics of Yiqisong peridot, Jilin, People Republic of China.

19:15 Transportation from Cité des Congrés
20:00 Gala dinner along the Erdre river on a boat- restaurant from " les bateaux de l'Erdre"

Friday 30 August 2019

Session 6 **Colored Stones 3** Chairman: Thye Sun Tay

9:00 – 9:20 Pignatelli Isabella, Giuliani Gaston, Morlot Christophe, Pham Van Long: Trapiche texture in emeralds and rubies

9:20 – 9:40 Jarolsav Hyrsl : Genetic classification of mineral inclusion in quartz

9:40 – 10:00 Willow Wight, Aaron J. Lussier and T.S. Ercit : Canadian gem tourmaline and the Leduc mine.

10:00 – 10:20 Hänni, H.A., Milisenda, C., Wang, H.A.O.: Tourmaline with Coltan ore inclusions – an example of auto-irradiation

10:20 – 10:40 Lutz Nasdala, Manfred Wildner, Doris Blaimauer , Manuela Zeug , Chutimun Chanmuang N. , E. Gamini Zoysa : Ekanite from Sri-Lanka : what can we learn from a radioactive gemstone ?

10:40 – 11:20 Coffee breaks and posters

Session 7 **Corundum 1**: Chairman Claudio Milisenda

11:20 - 11:40 Rainer Schultz-Guttler, Bruno Zampaulo: unusual corundum (ruby) bearing rocks from Brazil and India

11:40 – 12:00 Jayshree Panjikar, Aatish Panjikar: Investigation of ruby from a new occurrence from Paramathi in Karur district of Tamil Nadu, India.

12:00 – 12:20 Wilawan Atichat, Supparat Promwongnan, Saengthip Saengbuangamlam, Visut Pisutha-Arnond, Thanong Leelawatanasuk, Marisa Maneekrajangsaeng, Jirapit Jakkawanvibul, Pornsawat Watha nakul, Nalin Narudeesombat, Pimtida Bupparenoo, Apitchaya Buathong. Review of Rubies and sap phires from Chantaburi – Trat and Kanchanburi gems field, Thaïland.

12:20 – 12:40 Stephen Kennedy Review of iron and titanium diffusion treated synthetic sapphire

12: 40 – 14:00 Lunch in the multi-purpose area R0

Session 8 **Corundum 2** : Chairman Michael Krzemnicki

14:00 – 14:20 Kentaro Emori, Hiroshi Kitawaki , Akira Miyake : Be-containing nano-inclusions in untreated blue sapphire from Diego, Madagascar.

14:20 – 14:40 Wiwat Wongkokua , Natthapong Monarumit, Aumaparn Phlayraharn, Somruedee Satitkune, Pornsawat Wathanakul: Update of Fe and Ti oxidation states in ruby and blue sapphire.

14:40 – 15:00 Tom Stephan, Claudio C.Milisanda, Angunguka TH.Jepsun: Low temperature and flux assisted heat treatment of rubies and pink sapphires from Mozambique and Greenland.

15:00 – 15:20 Sutas Singbamroong, Panjawan Thanasutthipitak, Thawatchai Somjaineuk, Nirawat Thammajak, Chatree Saiyasombat, Nazar Ahmed, Phisit Limtrakun: Beryllium heat-treated blue sapphire from Sri-Lanka.

15:20 – 16:00 Coffee break and posters

Session 9 **Corundum 3** Chairman Karl Schmetzer

16:00 - 16:20 Thanong Leelawattanasuk, Thanapong Lhuaamporn, Papawarin Ounorn, Budsabakorn Srisataporn and Nattapat Karava: Blue sapphires heated with pressure and effect of low temperature annealing on the OH-related structure.

16:20 - 16:40 Wasura Soonthorntantikul, Sudarat Saeseaw, Shane McClure, Ungkhana Atikarnsakul, Charuwan Khowpong, Suwasan Wongchacree, Jonathan Muyal: An examination of sapphires treated with heat and pressure before and after treatment.

16:40 - 17:00 Martial Bonnet, Emmanuel Fritsch: Little known absorption bands in infrared spectra of corundum: what do they mean?

Free evening
Suggestion: The Fetes de l'Erdre, a jazz and historic boat festival will take place along the Erdre river

Saturday 31 August 2019

Session 10 **Pearls and amber.** Chairlady Pornsawat Wathanakul

9:20 – 9:40 Bahareh Shirdam, Andy H. Shen, Soheila Aslani, Zhiqing Zhang: Persian amber: A Myth or Reality ?

9:40 – 10:00 Laurent E. Cartier, Michael S. Krzemnicki, Bertalan Lendvay, Nadja Morf, Joana B. Meyer: DNA finger printing of precious corals on pearls.

10:00 – 10:20 Stefanos Karampelas, Fatima Mohamed, Hasan Abdulla, Abeer Al-Alawi: New insights on X-ray luminescence of natural on cultured pearls from fresh waters and salt water bivalves.

10:20 – 10:40 Abeer Al-Alawi, Zainab Ali, Fatema Albedal, Stefanos Karampelas: Pinctata radiata saltwater cultured pearls from Abu Dhabi (U.A.E.)

10:40 – 11:20 Coffee breaks and posters

Session 11 **General gemmology 1** Chairlady Wilawan Atichat

11:20 - 11:40 Anette Juul-Nielsen, Hans Lange: Greenlandic ivory: past and present use

11:40 – 12:00 Ahmadjian Abduriyim: Update of worldwide gemstone discovery activities after 2000

12:00 – 12:20 Brendan M. Laurs: Writing scholarly gems locality articles : perspectives from geologist, gemmologist, and editor.

12:20 – 12:40 Hao A.O. Wang, Michael S. Krzemnicki, Susanne Büche, Ramon Schmid, Judith Braun: Multi-element analysis of gemstones and its application in geographical origin and determination

12: 40 – 14:00 Lunch in the multi-purpose area RO

Session 12 **General gemmology 2** Chairman Stefanos Karampelas

14:00 – 14:20 Menahem Sevdermish: Exploring gem commercial names using big data color analysis technology, expert traders' opinions and geographical and trade interpretation.

14:20 – 14:40 Lore Kiefert, Klaus Schollenbruch: Laser damage in gemstones caused by jewelry repair laser.

14:40 – 15:00 Tom Stephan, Tobias Häger , Ulrich Henn, Wolfgang Hofmeister : Spectral fitting of UV/Vis/NIR, spectra for the quantitative determination of Cr^{3+} and V^{3+} in gemstones, with special emphasis on ruby and emerald.

15:00 – 15:20 Martine Philippe, Emmanuel Fritsch : Dissolved dislocations in gems : an overview.

15:20 – 16:00 Coffee break

16:00 - 17:00 Closing ceremony

Posters

Gagan Choudhary, Sandeep Vijay: A review of commercially available turquoise imitations

Claude Drouin, Emmanuel Fritsch: A history of gem-quality cubic zirconia

Karen Fox, Kenneth Fox: Gemmological applications of Arduino

Seung Kwon Lee, Randy Luo: Optical properties of hackmanite ad sodalite

Zemin Luo, Mingxing Yang, Qin Fang, Ren Lu, Luwu Cai, Yang Hu: provenance of emerald from Prince Liangzhuang's tomb in Ming dynasty, Hubei, China.

Nalin Narudeesombat, Namrawee Susawee, Pimtida Buppareno , Apitchaya Buathong, Supparat Promwongnan and Thanong Leelawatanasuk,: Characteristics of Tairus synthetic hydrothermal ruby and blue sapphire

Thet Tin Nyunt, Thye Sun Tay : Amber from Khamti, Sagaing region, Myanmar

Chen Quanli, Liu Xianyu: Turquoise from Zhushan county in Hubei province of China

Elizabeth Su: The vivid world of jadeite

Manuela Zeug, Lutz Nasdala, Radek Škoda, Chutimun Chanmuang N., Martin Ende, Christoph Hauzenberger, Dan Topa, Manfred Wildner, Richard Wirth: Mineralogical characterization of the unusual gemstone parisite-(Ce)

Zhiqing Zhang, Andy H. Shen: Amber with violet fluorescence from Myanmar.

The genesis of lithospheric blue diamonds

Lucille Daver[1,*], Hélène Bureau[2], Éloïse Gaillou[3], Benoit Baptiste[2], Oulfa Belhadj[4], Églantine Boulard[2], Nicolas Guignot[5], Eddy Foy[6], Pierre Cartigny[7] and Daniele L. Pinti[1]

1– GEOTOP and Département des sciences de la Terre et de l'atmosphère,
Université du Québec à Montréal, Montréal, QC, H2X 3Y7, Canada,
2– Institut de Minéralogie, de Physique des Matériaux et de Cosmochimie (IMPMC),
Sorbonne Université, CNRS UMR 7590, Paris, France
3– MINES ParisTech, PSL Research University, Musée de Minéralogie, 60 boulevard Saint-Michel, 75006 Paris, France,
4– Centre de recherche sur la conservation, Muséum National d'Histoire Naturelle, 75005 Paris, France,
5–Synchrotron Soleil, 91191 Gif-sur-Yvette, France
6– LAPA-IRAMAT, NIMBE, CEA, CNRS, Université Paris-Saclay, CEA Saclay 91191 Gif-sur-Yvette, France
7- Laboratoire de Géochimie des Isotopes Stables, Institut de Physique du Globe de Paris, 75005 Paris, France,
*Correspondence to: eloise.gaillou@mines-paristech.fr

Blue diamonds are among the rarest type of gems (< 0.1% of the extracted diamonds in the most productive area). They were mainly extracted from Indian (Kollur mine) and now mostly from the South African (Cullinan mine) deposits. Their blue color is due to trace amounts of boron (and the absence of nitrogen) in its lattice structure as seen by Fourier-Transform infrared spectroscopy (FTIR), which defined them as type IIb diamonds (see Gaillou et al., 2012 and references therein). They remain poorly studied, because of their rarity and scarce availability. Thus, their genesis and boron source remain misunderstood. The latest research conducted on similar blue diamonds (Smith et al., 2018) concluded to a formation model in the lower mantle (> 660 km), with boron derived from slab dehydration, thanks to the analyses of some inclusions, but no direct analyses of boron.

Here, we studied solid and fluid inclusions in four rough monocrystalline blue diamonds from the Cullinan mine, South Africa. We use a combination of in situ non-destructive methods in order to characterize the inclusions trapped in diamonds. FTIR enabled to measure volatile elements (B, N, H_2O etc.) as well as synchrotron x-ray diffraction and micro-Raman (532nm laser) spectroscopy allowed identification of the different mineral phases (Fig. 1 & 2).

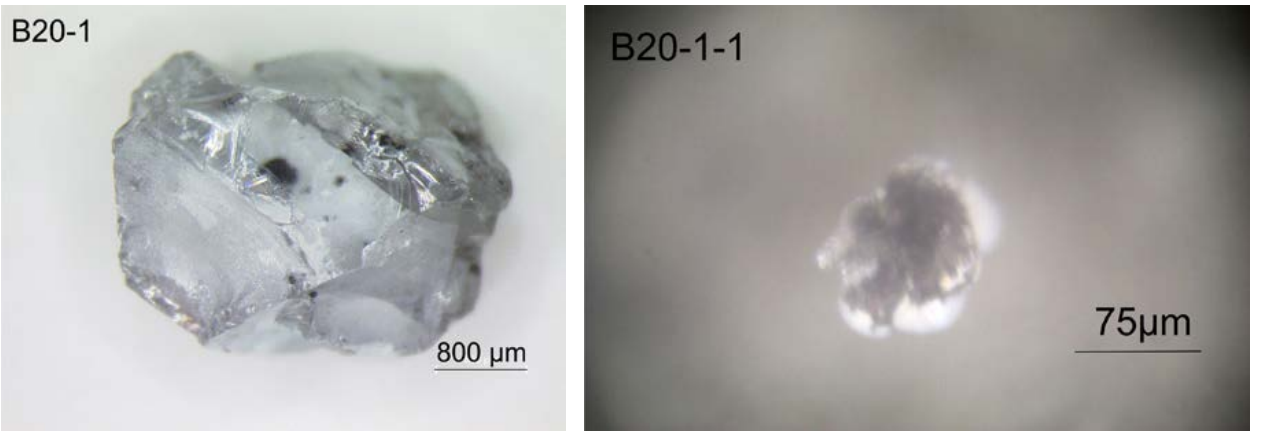

Fig. 1: Left- Full view of type IIb blue diamond B20, containing on average 0.31ppm of boron. Right- Primary inclusion within the same diamond, containing a mixture of graphite and water, as determined by Raman spectroscopy.

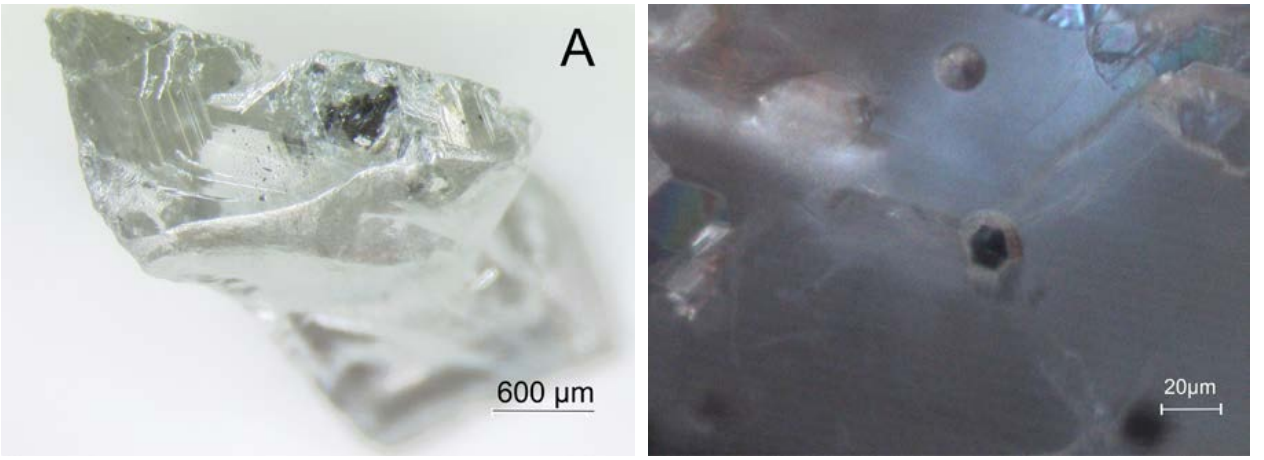

Fig. 2: Left- Full view of type IIb blue diamond B8, containing on average 0.23ppm of boron. Right- Secondary bi-phase hegaxonal inclusion (linked to other inclusions), containing graphite (dark) in its core and a mixture of water and methane in its colorless rim, as recognized by Raman spectroscopy.

These diamonds hold primary (Fig. 1) and secondary (Fig. 2) inclusions of $C_{graphite}$-H_2O composition precipitated from the same parent aqueous fluid and probably reflecting the diamond forming fluid. The secondary $C_{graphite}$-H_2O inclusion set up in a healed fracture and formed as multiple two-phase inclusions (Fig. 2) with H_2O as ice VII and a residual pressure of 2.5 GPa. Alongside, we observed the presence of a lithospheric mineral assemblage. Such a mineral assemblage and the residual pressure (Angel et al., 2014) indicate a genesis for these studied blue diamonds in a B-C-H_2O-rich fluid in the lithospheric mantle, at about 9-10 GPa, for 1000 – 1100°C (~ 200 km) which corresponds to the deep roots of the Kaapvaal craton (Niu et al., 2004). Type IIb blue diamonds therefore may form at any depth below the deep roots of a craton, and are not necessarily "superdeep".

References

Angel, R. J., Mazzucchelli, M. L., Alvaro, M., Nimis, P., & Nestola, F., 2014. Geobarometry from host-inclusion systems: the role of elastic relaxation. American Mineralogist, 99(10), 2146-2149.

Gaillou, E., Post, J. E., Rost, D., & Butler, J. E., 2012. Boron in natural type IIb blue diamonds: Chemical and spectroscopic measurements. American Mineralogist, 97 (1), 1-18.

Niu, F., Levander, A., Cooper, C.M., Lee, C.T.A, Lenardic, A., James, D., 2004. Seismic constraints on the depth and composition of the mantle keel beneath the Kaapvaal craton. EPSM, 224 (3-4), 337-346.

Smith, E. M., Shirey, S. B., Richardson, S. H., Nestola, F., Bullock, E. S., Wang, J., & Wang, W., 2018. Blue boron-bearing diamonds from Earth's lower mantle. Nature, 560 (7716), 84.

CHARACTERIZATION OF GROWTH SECTORS IN ASTERIATED DIAMONDS

Marie Schoor[1,2]*, Jean-Claude Boulliard[3], Emmanuel Fritsch[2], Eloïse Gaillou[4], Benjamin Rondeau[2]

[1]Cellule Gemmologie, Cartier Joaillerie International, France
[2]Institut des Matériaux Jean Rouxel (IMN), University of Nantes, France
[3]Collection de Minéraux de l'Institut de Minéralogie et de Physique des Matériaux et Cosmochimie (IMPMC), Université Pierre et Marie Curie (UPMC), France
[4] MINES ParisTech, PSL Research University, Musée de Minéralogie, France
*marie.schoor@cartier.com

Keywords: diamond, mixed-habit, Rose channels

Asteriated diamonds, known for nearly two centuries, attract again attention, in particular since many cropped out recently from the Marange region of Zimbabwe. These diamonds are characterized by gray or brown sectors in a colorless crystal. A precise cut in slices highlight fairly spectacular figures, often formed of lobes or dark triangles radiating from the center. They are known with certainty before 1822 (Rondeau et al., 2004), and were studied with interest by René-Just Haüy (1743-1822), and also intrigued Alfred Descloizeaux (1817-1897) a few years later, around 1845 (Descloizeaux, 1845). Studies continued only fifteen years ago (Rondeau et al., 2004). No official name really exists for these particular diamonds. Some call them "mixed-habit growth diamonds" (Lang et al., 2004; Howell et al., 2013); a more commercial name used at gem trade shows refers to them as "star diamonds" (Rakovan et al., 2014). They are also called "asteriated diamonds" (Rondeau et al., 2004) because of their star-shape pattern.

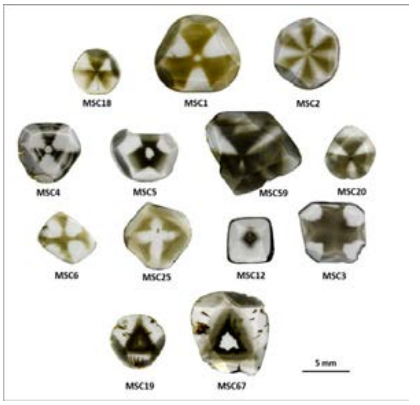

Figure 1: Pictures of the samples used for this study. The first two lines regroup asteriated diamonds showing black and brown 3-lobed patterns. The third line corresponds to the 4-lobed ones and the last line illustrates two non-asteriated diamonds.

Materials and methods

We studied thirteen asteriated diamonds. Their octahedral sectors are always near-colorless and their cuboid sectors can be gray or brown and form patterns with 3, 4 or 6 lobes. Some others samples have no lobe, only darker sectors. The samples have been observed with a microscope (Leica DM 2500P) using both un-polarized and polarized light in order to evaluate any polarization anomalies. We also acquired infrared spectra (FTIR Bruker Vertex 70) in the different

sectors at a resolution of 4 cm^{-1} by averaging 100 scans. To investigate the differences between the two sector types we also performed some Raman maps (MicroRaman Renishaw inVia Raman Microscope) with a 514 nm laser, at 50x magnification and with an exposure time of 0.1 second. Luminescence imaging techniques (DiamondView, JEOL 5800LV for cathodoluminescence), as well as X-ray fluorescence analyses (Rigaku NexCG EDXRF), were finally used.

Results

Magnification shows that the color of the cuboid sectors is not homogeneous but is produced by very small inclusions (fig. 1). The average size of these inclusions ranges from 2 to 7 µm. Octahedral sectors exhibit a double refraction anomaly under crossed polarized filters, while cuboid sectors are globally isotropic and show a granular appearance. Infrared spectra confirm that these asteriated diamonds are nitrogen and hydrogen-rich but not in all sectors. Absorptions at 2812, 3079 and 3255 cm^{-1}, characteristics of the cuboid sectors (Rondeau et al., 2004), are also observed. Raman mapping highlighted differences of the FHWM and the intensity of the diamond peak at 1332 cm^{-1} between octahedral and cuboid sectors. Luminescence finally shows major variations. Luminescence is yellowish-green in cuboid sectors (with UV lamp and DiamondView) while octahedral sectors are inert. However, the two types of sectors show a luminescence in cathodoluminescence. X-ray fluorescence analysis of the samples reveals the presence of nickel in cuboid and octahedral sectors.

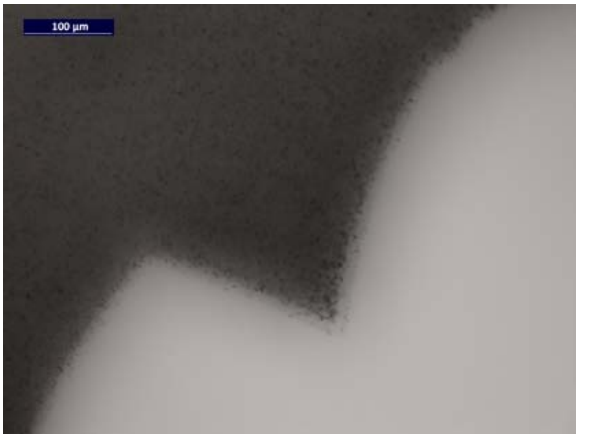

Figure 2: Very sharp border between the octahedral (colorless) and cuboid (gray with microscopic inclusions) sectors

Discussion and conclusion

The analyses carried out allowed us to answer the many questions we had about these particular diamonds. Firstly, the cause of color of cuboid sectors could be related both to the microscopic graphitized-discoid inclusions and to interference hues. Secondly, contrary to the commonly admitted hypothesis that asteriated diamonds are H-rich, our infrared observations go against this affirmation as some of the sectors, mostly octahedral, are not. Then, based on the X-ray fluorescence, yellowish-green luminescence of the cuboid sectors is found to be related to the presence of nickel. But, in the meantime, cathodoluminescence of the octahedral sectors remains unexplained yet. Finally, we present a new interpretation concerning the nature of the channels existing in two of our samples. The channels are usually associated to dissolution of dislocations depending on their appearance. However, a closer look at these inclusions suggests that it could be Rose channels instead, i.e. a mechanical twinning created by intense plastic deformation.

References

Descloizeaux A. (1845) Note sur deux diamants offrant une astérie fixe due à un phénomène particulier de cristallisation. Annales de Chimie et de Physique, Série 3, Tome 14, p. 301-306.

Howell D., Griffin W. L., Piazolo S., Say J. M., Stern R. A., Stachel T., Nasdala L., Rabeau J. R., Pearson N. J., O'Reilly S. Y. (2013) A spectroscopic and carbon-isotope study of mixed- habit diamonds: Impurity characteristics and growth environment. American Mineralogist, Vol. 98, p. 66-77.

Lang A. R., Yelisseyev A. P., Pokhilenko N. P., Steeds J. W., Whotherspoon A. (2004) Is dispersed nickel in natural diamonds associated with cuboid growth sectors in diamonds that exhibit a history of mixed-habit growth. Journal of Crystal Growth, Vol. 263, p. 575-589.

Rakovan J., Gaillou E., Post J. E., Jaszczak J. A., Betts J. H. (2014) Optically sector-zoned (star) diamonds from Zimbabwe. Rocks & Minerals, Vol. 89, No. 2, p. 173–178.

Rondeau B., Fritsch E., Guiraud M., Chalain J. P., Notari F. (2004). Three historical 'asteriated'hydrogen-rich diamonds: growth history and sector-dependent impurity incorporation. Diamond & Related Materials, Vol. 13, p. 1658-1673.

FLUORESCENCE INFLUENCE ON DIAMOND PERFORMANCE

Roman Serov[1], Sergey Sivovolenko[2]

[1] Octonus Software, Moscow, Russia, [2] Octonus Finland Oy, Tampere, Finland
potom_skajy@mail.ru

Keywords: Fluorescence, Diamond, Performance, Colour, Grading

It is well known in the gemmological community and diamond industry that fluorescence can alter the perceived diamond colour. However, there are certain controversies whether fluorescence gives a positive or negative contribution to diamond colour, appearance and performance.
In our current work, we want to show the reasons of this situation related to the fluorescence and the future possibilities to account for fluorescence more objectively. We will consider the influence of the blue fluorescence only. Other fluorescence colours are much rarer and expected to be the subjects of future studies.

Background
From the trade, dealers and consumers point of view, fluorescent diamonds are traded rightfully with discount because of four main reasons:
1) Gemmological laboratories colour grading is not consistent for fluorescent stones.
2) Gemmological laboratories do not indicate in the reports diamonds where fluorescence creates a milky appearance
3) Consumers do not have possibility to separate fluorescent non-milky from fluorescent milky diamonds
4) Positive fluorescence impact on diamond colour and performance is debatable
If these four problems could be addressed and solved – there would be no major reasons to penalize all fluorescent diamonds. Fluorescent stones could get premium or discount on the basis of real fluorescence influence on diamond appearance.

Correlation between diamond Milkiness and Fluorescence
There is a myth in the trade that all diamonds with Very Strong Blue Fluorescence appear milky or hazy. Practically there is no clear correlation between diamond Very Strong Blue Fluorescence and milkiness.
It is very difficult to find diamonds where milkiness is related solely with fluorescence by human observation. Only one such stone was listed in the article by Moses et al., 1997, which also mentioned: "we did not include those diamonds with extremely strong blue fluorescence and a hazy appearance, because we could not obtain sufficient numbers of such stones".
During our research of milkiness/haziness in fluorescent diamonds we found that commonly milkiness was related with graining or clouds/multiple pinpoints and could be observed in completely UV free lighting. In smaller number of stones, milkiness was related solely with fluorescence.
The common example of milky diamond is shown on Fig. 1. The first diamond (Sample 1) does not have transparency loss (and used as a reference). The second diamond shows significant transparency loss caused by internal graining (it was graded SI2 by GIA).
In Darkfield lighting (that is UV free) the transparency loss and milkiness in Sample 2 is quite obvious. In White Dome lighting (also UV Free) this diamond appears darker than the reference (because of the milkiness). However in White Dome lighting with UV content (comparable with CIE D65) Sample 2 appears comparable in brightness with reference. So fluorescence for this stone shows the same positive contribution in color and brightness as for non-milky stones.

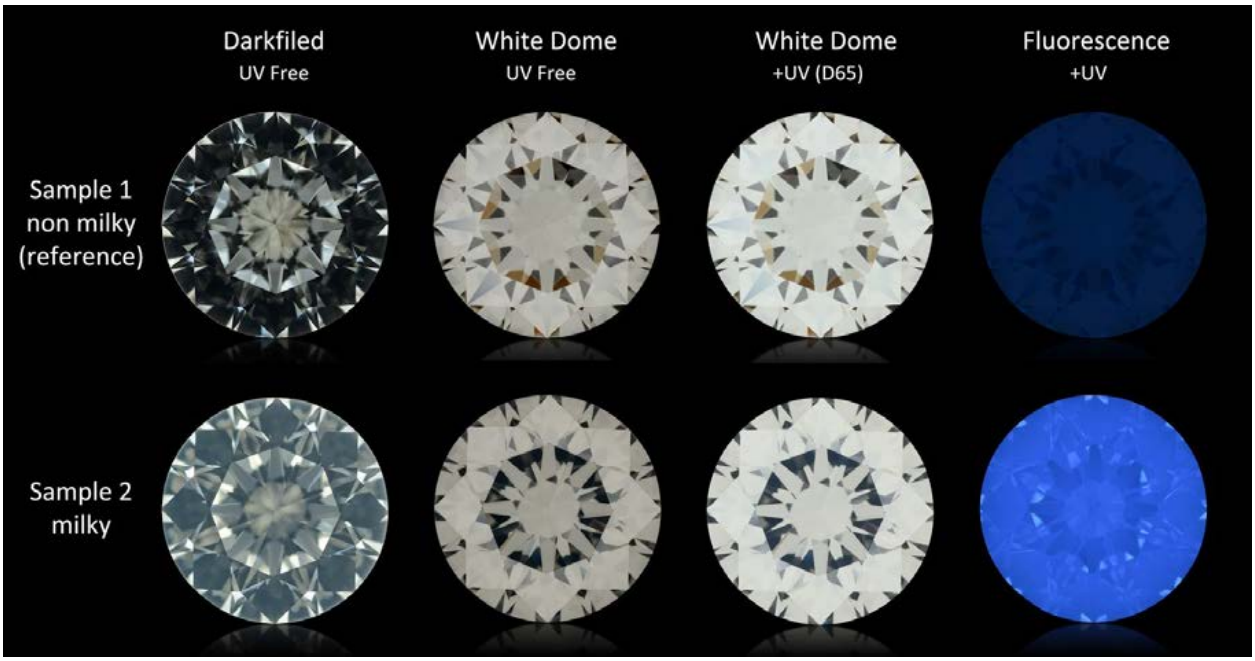

Fig. 1. Comparison between non milky and milky diamonds in different lighting conditions. Images were captured in DiBox 2.0 system.

Fancy Light Yellow cushion with Strong Blue fluorescence (Fig. 2) appears saturated yellow in UV Free lighting, but shifts its color to pale yellow in D65 lighting (lighting with UV content). The areas with long ray path are more affected by fluorescence. In this diamond such areas lose about 20% of transparency in D65 lighting and this significantly reduces the cushion brightness. On the other hand, the areas with short ray path do not show perceptible transparency reduction, even in this diamond with strong fluorescence.

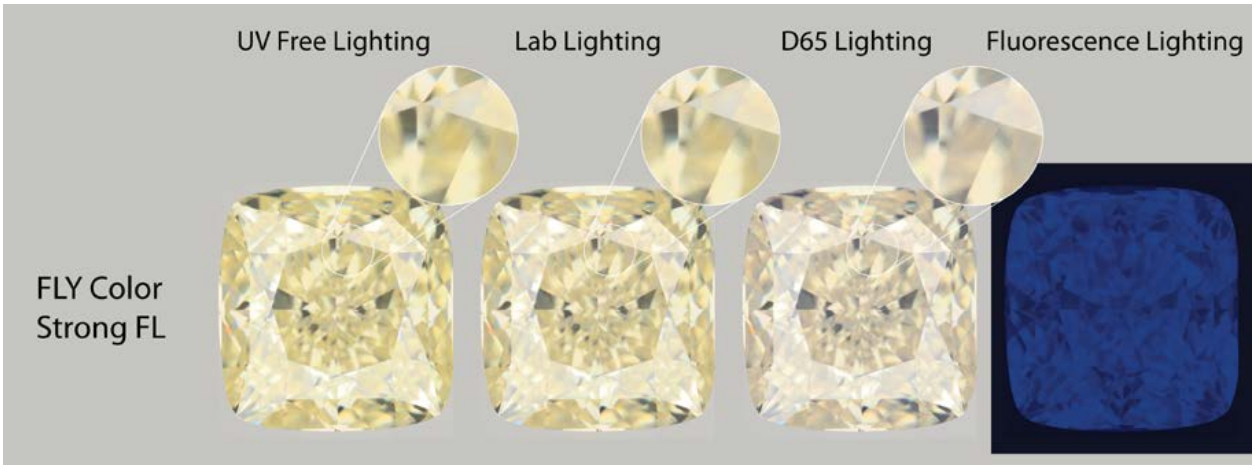

Fig. 2. Fancy Light Yellow Cushion with Strong Blue Fluorescence observed in DiBox 2.0 in lighting conditions with different UV content.

So, fluorescence can affect diamond transparency in certain diamonds. Such stones should be distinguished from the diamonds which brightness benefits from fluorescence.

Conclusion

The current penalty and discounts on fluorescent diamonds are due to high risks of incorrect color and clarity (milkiness) grading for such stones and lack of awareness on all types of possible fluorescence influence on diamond performance.

The end users consume diamonds in a spectrum of very different lighting conditions: from completely UV free (LED lighting) to lightings with moderate UV (daylight) and very high UV (disco). It is not possible to tell on the base of fluorescence strength only if it has positive or negative impact on the overall diamond appearance and value in consumers eyes.

Instead, there is a suggestion to assess color in a set of consumer-oriented lighting conditions (for example LED (UV free) lighting, office lighting and daylight outdoor lighting) to avoid practice of discounting all fluorescent stones regardless of the actual impact of fluorescence on diamond color. It is reasonable to consider fluorescence contribution to diamond appearance in a way, which is close to consumers' manner of diamond appreciation and enjoyment.

References

Moses, T., Reinitz, I.M., Johnson, M.L., King, J.M., and Shigley, J.E, 1997. The effect of blue fluorescence on the appearance of diamonds. Gems & Gemology, 33(4), 244–59

Acknowledgements

We want to thank Janak Mistry and Lexus Softmac staff for their contributions, discussions and data collection.

Proposed classification of type IIa diamonds on the basis of DiamondView™ images

[1]Aurélien Delaunay, [2]Emmanuel Fritsch, [1]Annabelle Herreweghe
[1]Laboratoire Français de Gemmologie (French Gemmological Laboratory), a.delaunay@lfg.paris
[2]Institut des Matériaux Jean Rouxel (I.M.N.) Université de Nantes, emmanuel.fritsch@cnrs-imn.fr

Type IIa diamonds are now analyzed in detail by many gemmological laboratories worldwide. They could be natural or synthetic, untreated or HPHT treated. In the French Gemological Laboratory in Paris, all diamonds (both type Ia and type IIa diamonds) are screened with the luminescence imagery system developed by the DTC, the DiamondView™. Since each type IIa diamond submitted is observed with the DiamondView™, we realized the greater-than-expected diversity and heterogeneity of observed patterns. Our purpose is to classify those and relate them to their growth conditions. In this way, further arguments are given to separate natural from synthetic diamonds, and potential post-growth events (deformation, HPHT treatment) are indicated. Based on experience, we use both colour and texture as basic parameters.

Colour classification

It is sometimes difficult to attribute the colour viewed in DiamondView images to a specific defect. Yet, correlation with classical photoluminescence (PL) brings useful elements to interpret the colour origin of the emission observed.

- violetish blue : linked to dislocations (band-A : electron hole recombination)
- greenish blue : several possibilities
- Associated with HPHT-treated CVD synthetic diamond
- Nitrogen or boron induced phosphorescence in IIa.
- green : presumably linked to H3 centers
- greenish yellow : possibly $N\text{-}V^0$ plus H3 seems to correlate with a band at 561.5 nm
- orange : linked to $N\text{-}V^0$ centers
- red : $N\text{-}V^-$ dominant centers
- pink to purple : combination of orange and blue (either violetish or greenish)

Textural classification

Consideration of crystal growth and further data brings us to classify the observed patterns in two broad categories

1) – Growth-related patterns :

- a) Growth sectors distribution (Sectoring): this is a geometric pattern (often with straight edges) showing a cross section of the volumes created by each growth sector. It is often easy to observe in natural type I diamonds, but it is a rarity in natural type IIa diamonds. It is the rule with HPHT synthetics, and may help interpret one pattern of CVD growth ("step flow growth")

- "classic" sectoring (figure 1), with geometric patterns (cf. classical HPHT synthetic diamond)

- step flow growth: in the model of step flow growth (Martineau et al, 2004), the striations resemble growth sectors (curved), developing behind the steps between terraces. The two dominant growth sec-

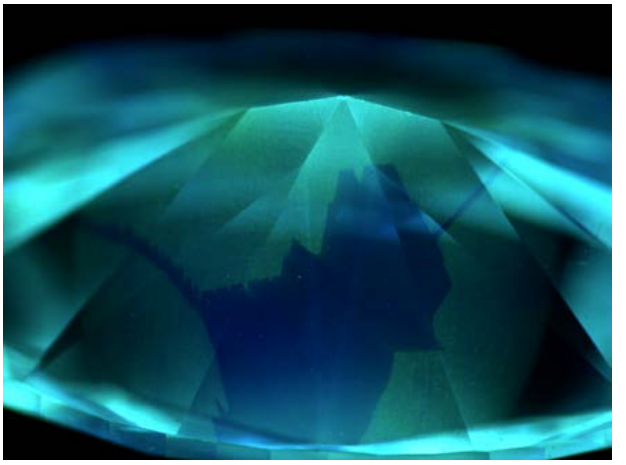

Figure 1: Classic sectoring with straight, planar sector boundaries in a 3.72 ct type IIa diamond

tors in CVD synthetics are the cube and the octahedron (Tallaire et al., 2006) as the terrace represent the cube faces, it is logical to interpret the steps as octahedral faces, the other most common growth sector in not only synthetics but also natural diamonds. This would be a classic case of micro-faceting ("striations"), with dominant cube faces and minor octahedral ones, a classic in the growth of many crystals (quartz, pyrite; Sunagawa, 2005).

- b) Banding: this occurs within one growth sector, and reflects variation in the incorporation of impurities or creation of defects in that sector, as a continuous growth progresses. It translates in the DiamondView as parallel bands of different color or intensities (figure 2).

- c) Layering: this occurs in synthetic CVD diamond only. It comes from interrupted growth, then (typically after cleaning and lowering of the crystal) restarting the growth. Visually, it is quite different from banding (figure 2). The limit is always quite sharp. A layer usually starts with many dislocations, emitting in the blue, and finishes with incorporation of nitrogen, creating an orange glow.

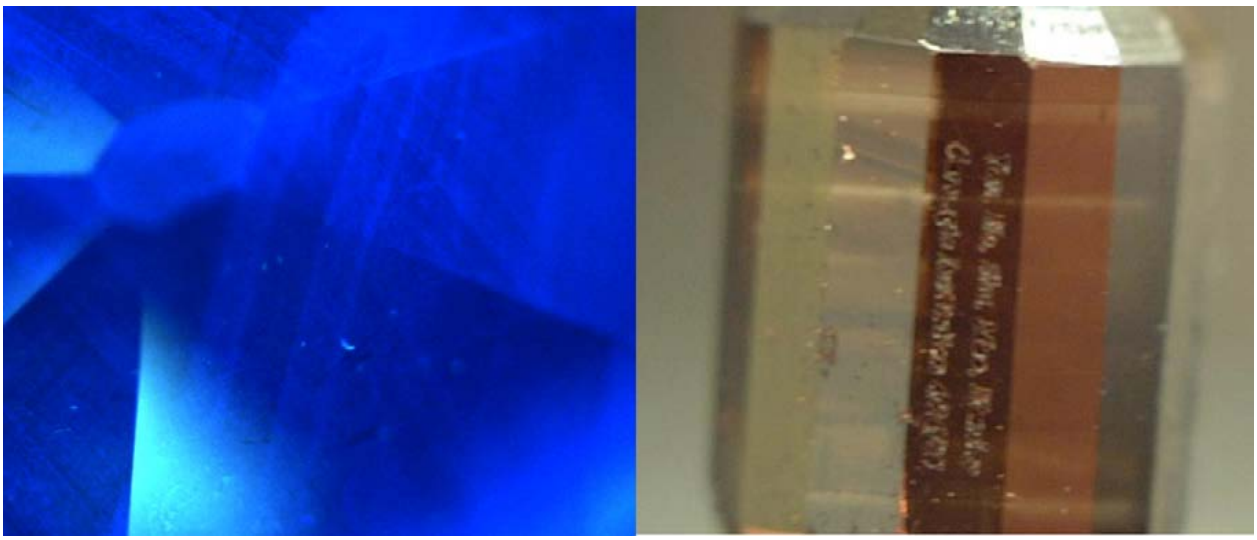

Figure 2: straight parallel banding (left; 2.86 ct pear) as compared to layering (right: the 5 ct "bullet" CVD synthetic diamond from the Carnegie Institution; photo courtesy Carnegie Institution)

2) - Deformation related patterns:

Deformation related patterns strictly occur in natural diamonds, and are thus proof of natural origin.

- Polygonal dislocation network and its variations: the most common image is that of a violetish blue emission in the dislocation network, with a relatively inert matrix. Yet, the opposite is possible, showing an inert network, and a relatively strongly fluorescing matrix. This may be due to a contrast effect, when the emission of the dislocation network is much weaker than that of the diamond matrix. The pattern is rarely very distinct, often weak, sometimes hard to see. This maybe partly due to the small width of the network lines (which are very fine).

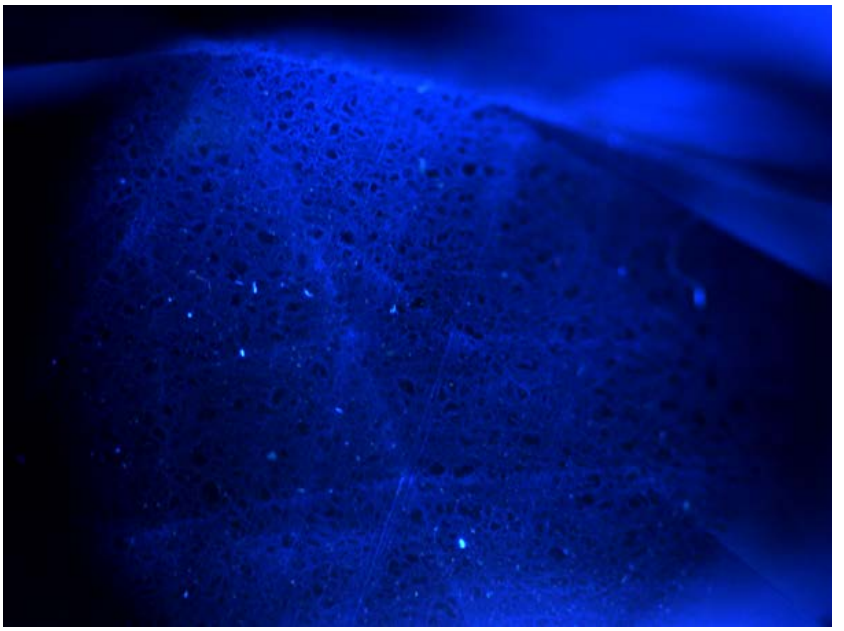

Figure 3: polygonal dislocation network in a typical 10.23 ct type IIa

- Graining: This is a well-known classic deformation pattern with straight parallel lines, in one direction, or being superimposed in three different directions, parallel to octahedral planes. The appearance suggests sometimes that H3 centers concentrate in this graining, as in type Ia stones.

- Curved patterns: (including feather-like patterns) these are the rarest growth structures of type IIa diamonds.

References

Martineau P.M., Lawson S.C., Taylor A.J., Quinn S.J. Evans D.J.F., Crowder M.J. (2004) Identification of synthetic diamond grown using chemical vapour deposition (CVD) Gems & Gemology, 40-1, 2-25.

Sunagawa I. (2005) Crystals: growth, morphology and perfection. Cambridge University Press. Cambridge, England

Tallaire A., Achard J., Secroun A., De Gryse O., De Weerdt F., Barjon J., Silva F., Gicquel A. (2006) Multiple growth and characterization of thick diamond single crystals using chemical vapour deposition working in pulsed mode. Journal of Crystal Growth, 291, 533-539.

Current Production of Synthetic Diamond Manufacturers in Asia

Hiroshi Kitawaki[1], Kentaro Emori[1], Mio Hisanaga[1], Masahiro Yamamoto[1]

[1]Central Gem Laboratory (Miyagi Bldg. 6th Fl. 5-15-14, Ueno Tito-ku, Tokyo, Japan), kitawaki@cgl.co.jp

Keywords: synthetic diamond, HPHT, CVD

1. Introduction

Synthetic diamonds for jewellery use are evolving in size and quality every year. For example, polished HPHT-grown diamonds have reached over 15 ct (Ardon et al., 2018) and CVD-grown diamonds over 9 ct (WD Lab Grown Diamonds 2018). On the other hand, the development and large volume production of colourless melee-sized synthetic diamonds has resulted in contamination of jewellery, which is currently one of the major challenges facing the jewellery industry (e.g., Soonthorntantikul et al., 2015; Lan et al., 2015).

Commercial production of HPHT synthetic diamonds of gem-quality started in the 1990s in Russia. This know-how later spread over to the U.S. and India. In 2003, Apollo Diamond Co. Ltd. was the first to announce the commercial sale of CVD synthetic diamonds of gem-quality (Wang et al., 2003), using a production technology which had been developed mainly in the U.S.

In recent years, the main manufacturers of gem-quality synthetic diamonds are located in Asia, such as in China, Singapore and India. They produce a huge quantity of synthetic diamonds in a large range of colour, size and quality.

In this report, we present about 10 major manufacturers and related facilities in several locations in Asia which we visited between 2016 and 2019 (Figure 1).

Fig.1 Major synthetic gem diamond manufactures and related facilities in several locations in Asia

2. HPHT Synthesis in China

China is one of the world's main producers of industrial synthetic diamonds and it reportedly supplies 95 % of world demand. By State policy, the city Zhengzhou in Henan, China, has become the manufacturing centre for HPHT-synthetic diamonds between the late 1970s and 1980s. Among the many diamond manufacturers in Zhengzhou, the "top three" companies, ZhongNan Diamond Co. Ltd., Huanghe Whirl Wind Co. Ltd., and Zhengzhou Sino Crystal Co. Ltd. largely dominate the other producers (Jia 2016).

In Zhengzhou, colourless synthetic melee diamonds in gem quality have been produced since the end of 2014, and their vast amount of production quickly dominated the world jewellery market. Since 2018, the production is focused on faceted stones of 0.2-0.5 ct size, with some 1-2 ct stones. For the HPHT synthesis (figure 2 & 3), the manufacturers in China use metal solvents such as Fe, Co or Ni, but their compositions vary from producer to producer, suggesting that they have developed their technology each by themselves. They are aiming at producing synthetic diamonds of higher colour grades (D and E), but they still have problems controlling the trace elements related to colour such as Ni, B or N.

Fig.2 HPHT synthesis equipment of Huanghe Whirl Wind Co. Ltd.. Photo by H. Kitawaki

Fig.3 Melée sized rough synthetic diamonds made by Huanghe Whirl Wind Co. Ltd. (five day's production). Photo by H. Kitawaki

3. CVD Synthesis in China

Besides HPHT synthetic diamonds, for which China is reputed, CVD synthetic diamonds are also produced in the country. In early 2013, the technology to grow CVD synthetic single crystals in China was developed by the Ningbo Institute of Materials Technology & Engineering Chinese Academy of Science, and the Ningbo Crysdiam Industrial Technology was established. The company produces colourless and pink gem-quality CVD synthetic diamonds up to 2 ct in size.

According to the technical manager of this company, the colourless material is treated by LPHT under high-vacuum conditions after CVD growth to enhance their colour. Another company, ZS Technology, established in December 2014 in the Zhangjiang High-Tech Park in Shanghai, produces high quality colourless diamonds from 1 to up to 5 ct in size. According to a spokesman for this company, the material is not HPHT-treated after synthesis and we have confirmed it with PL analysis.

4. CVD Synthesis in India

Surat, India is well-known for diamond cutting and polishing. In the 1990s they used the HPHT synthesis techniques that were introduced from Russia. However from around 2011-2012 they started producing CVD synthetic diamonds

for gem use. Today there are many CVD diamond distributors located in Mumbai and Surat who cut and polish the diamonds, but most of them purchase rough stones from the few actual synthetic producers.

The manufacturers that produce synthetic diamonds include larger producers such as New Diamond Era and Diamond Nation, as well as some ten smaller companies such as Diamond Elements and Unique Lab Grown Diamond. As an individual manufacturer, the Singapore-based company IIa Technologies Pte. Ltd. is assumedly the largest producer, whereas India as a country produces the largest quantity of gem- quality CVD synthetic diamonds for jewellery use (figure 4).
The companies New Diamond Era and Diamond Nation situated in the special economic zone in Surat, have integrated production, cutting and polishing facilities. Most of their production is subjected to post-growth HPHT treatment. Their products are directly exported to other countries.

Fig.4 CVD synthetic diamonds made in India (2-4ct). Photo by H. Kitawaki

References

Ardon T., Eaton-Magaña S., 2018. 15 carat HPHT synthetic diamond. Gems & Gemology, 54(2), 217-218. Jia Xiaopeng., 2016. HPHT synthetic diamonds in China. CGL report vol.35 (in Japanese).

Lan Y., Liang R., Lu T., Zhang T., Song Z., Ma H and Ma Y., 2015. Identification characteristic of near- colourless melee-sized HPHT synthetic diamond in Chinese jewelry market. Journal of Gems & Gemmology, 17(5), 12-17 (Chinese)

Soonthorntantikul W and Siritheerakul P., 2015. Near-colorless melee-sized HPHT synthetic diamonds identified in GIA laboratory. Gems & Gemology, 51(2), 183-185

Wang W., Moses T., Linares R., Shigley J. E., Hall M. and Butler J.E., 2003. Gem-quality synthetic diamonds grown by a chemical vapor deposition (CVD) method. Gems & Gemology, 39(4), 268-283 WD Lab Grown Diamonds. Press release May 22, 2018. http://www.wdlabgrowndiamonds.com/

Phosphorescence of Type IIb HTHP Synthetic Diamonds from China

Tian Shao[1], Jinqiu Zhang[1], Andy Histien Shen[1]*

[1] Gemmological Institute, China University of Geosciences, Wuhan, Hubei, China, 430074
ahshen1@live.com

Type IIb diamonds which contain boron (B) are very rare in the gem market, especially the blue ones such as the Hope Diamond or the Blue Moon Diamond [1-3]. They can exhibit characteristic blue and/or red phosphorescence centred at 500 and/or 660 nm by short wave ultraviolet light excitation, and their phosphorescence can last up to 1 min [4]. It was explained reasonably in published theoretical model, the donor-acceptor pair recombination theory (DAPR) [5-7]. The DAPR theory suggested that phosphorescence may come from boron and nitrogen impurity [8] recombination in the diamond's band gap [7]. Both the energy levels and spatial distances between donors and acceptors will determine the phosphorescence band position in the spectra.

Fig.1 Samples' photography, nine colourless IIb diamonds

Nine colourless type IIb HPHT synthetic diamonds produced in China (Fig.1 and Tab.1) with long-time phosphorescence phenomena are reported in this work. Like other IIb diamonds reported, SWUV can induce greenish blue phosphorescence. Visual observation revealed the colours of the phosphoresence are different - greenish blue and/or yellowish orange. Peculiarly, their phosphorescence can be observed with the naked eyes in a darkened environment for 5 min or longer.

Tab.1 Basis gemmological properties of samples studied

No.	Cut	Weight/ ct	Clarity	Type*	Thickness/ cm	Colour¤	Phosphorescence	
							LWUV	SWUV
1	Round Brilliant	0.191	SI	IIb	0.200	colourless	/	Strong greenish blue
2		0.192			0.198			Strong greenish blue
3		0.198			0.200			Strong greenish blue
5		0.206			0.206			Strong greenish blue
6		0.205			0.204			Strong greenish blue
7		0.213			0.210			Strong greenish blue
8		0.222			0.210			Greenish blue to Orange
9		0.205			0.206			Greenish blue to Orange
10		0.227			0.200			Greenish blue to Orange

** Type of diamonds are determined by averaging micro-MIR spectroscopic mapping scan*
¤Colours were not graded and colourless is base on naked eye observation

Small culets were cut parallel to the tables to guarantee that the optical pathlength equals thickness, so we can collect Ultraviolet-Visible (UV-Vis) and Middle Infrared (MIR) absorption spectrum in a quantitative manner. The UV-Vis spectra were measured by a JASCO MSV-5200 micro UV-Vis-NIR spectrometer, which featured a 100 µm light spot. And the MIR mapping scan on samples' tables were performed by Bruker v80 spectrometer + Hyperion 3000 microscope with 10 µm size light spot.
Based on transmission at 230 nm in ultraviolet region and the presence of the 2802 cm^{-1} peak in the MIR region (Fig.2), samples were classified. We calculated uncompensated boron concentration by measuring integral area under the 2802 cm^{-1} peak [9]. The concentration of boron varies, the highest one is 0.072 ppm while the lowest one is 0.006 ppm (Tab.2).

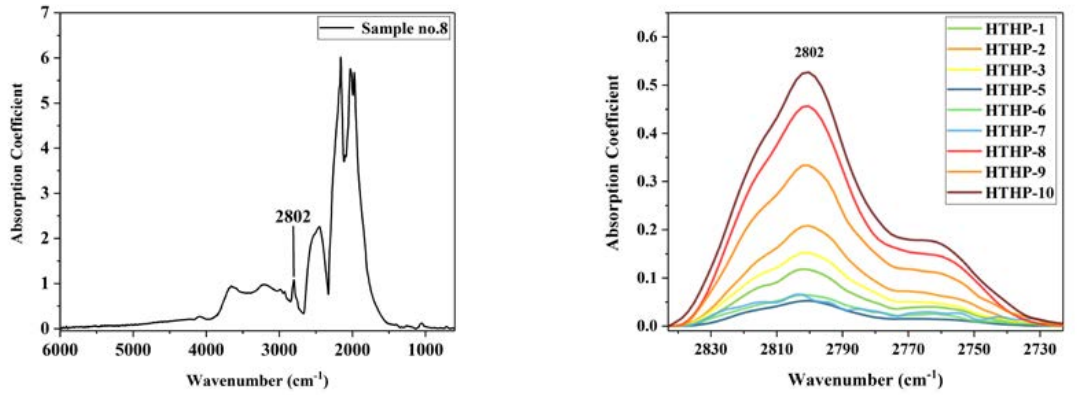

Fig.2 (a) MIR spectrum on sample no.8 which contain a well-developed 2802 cm^{-1} peak; (b) After baseline calibration uniformly, each sample's 2802 cm^{-1} peak has different height and area.

Tab.2 Concentration of uncompensated boron in samples

No.	1	2	3	4	5	6	7	8	9
Area/cm-2	*25.72*	*47.96*	*34.92*	*10.5*	*14.38*	*12.91*	*100.95*	*77.14*	*129.4*
Concentration*/ppm	*0.014*	*0.027*	*0.019*	*0.006*	*0.008*	*0.007*	*0.056*	*0.043*	*0.072*

**Concentration determined by function from Fisher, et al. 2009 [10]: $[B_0] = (5.53 \times 10^{-4}) \times I_{2802}$*

A JASCO FP8500 Fluorescence spectrometer with EPI attachment was employed to gather steady-state excitation-emission spectra. Excitation with monochromatic 230 nm xenon light induces intense phosphorescence centred at 460 nm with a 500 nm shoulder (Fig.3).

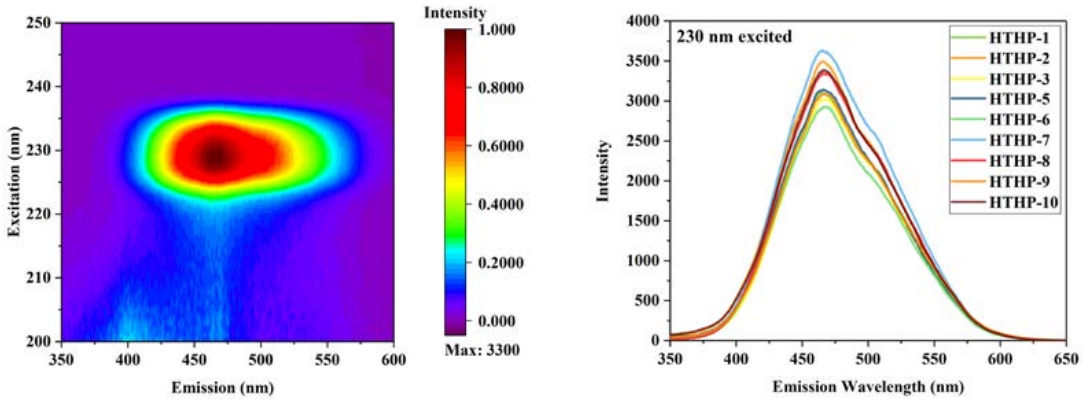

(a) *(b)*

Fig.3 (a) 3-D emission spectrum on sample no.8, which showed intense steady-state fluorescence; (b) Samples' fluorescence spectra excited by 230 nm xenon light.

Once the light source is cut off (pseudo-phosphorescence spectra), the intensity of subsequent phosphorescence spectra would decrease generally, meanwhile in sample no.8, a new band centred at 560 nm appeared. Waiting over five minutes, the diamond still exhibits phosphorescence to the naked eye. To express these phenomena intuitively, by using black paper to cover the excitation light, we gather the emission spectra every thirty seconds (Fig.4).

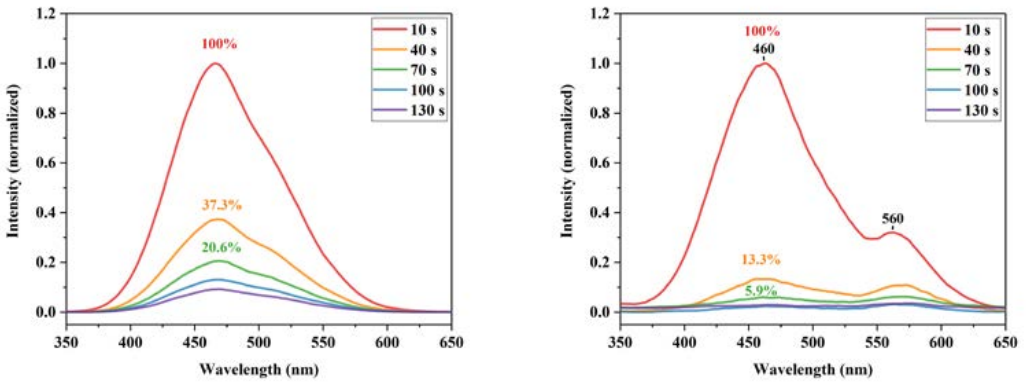

(a) *(b)*

Fig.4 (a) Emission spectra on sample no.8 after light cut off; (b) Emission spectra on sample no.3 after light cut off; the numbers represent duration after the excitation source is turned off.

Samples with relatively higher uncompensated boron, have seemingly shorter phosphorescence life-time compared to those with lower concentration. A correlation is given in Fig.5. There is a negative correlation between the uncompensated boron concentration and phosphorescence decay time. According to our measurements, after forty seconds' darkness, low boron samples' emission intensity is reduced to 32.2% of the original intensity, while high concentration ones have their emission reduced to 15%. After seventy seconds' darkness, samples still appear to phosphoresce, but intensities had further decayed, with the low concentration one's back to about 15% of the original emission.

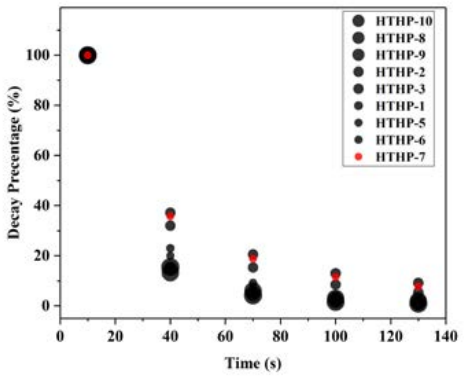

Fig.5 Relationship between the 460 nm phosphorescence lifetime, decay percentage and boron concentration. The spot's area is dependent on uncompensated boron concentration, and the intensity was normalized represent decay percentage.

The results are different from previous studies, and demonstrate some correlation between the uncompensated boron concentration and the phosphorescence lifetime. To further study this kind of phosphorescence in synthetic diamonds, we need to explore the total boron concentration more accurately using techniques such as EPR or SIMS.

References

[1] Gaillou, E., Post, J. E., Rost, D., Butler, J. E. "Boron in natural type IIb blue diamonds: Chemical and spectroscopic measurements." American Mineralogist 97.1(2012):1-18.

[2] Eaton-Magaña, S., Post, J. E., Heaney, P. J., Freitas, J., Klein, P., Walters, R., Butler, J. E. "Using phosphorescence as a fingerprint for the Hope and other blue diamonds." Geology 36.1(2008):83-86

[3] Gaillou, E., Post, J. E., Byrne, K., S., Butler, J. E. "Study of the Blue Moon Diamond." Gems & Gemology 50.4(2014):280-286.

[4] Eaton-Magaña, S and Lu. R "Phosphorescence in type IIb diamonds." Diamond and Related Materials 20.7(2011):983-989.

[5] Thomas, D. G., Hopfield, J. J., and Augustyniak, W. M. "Kinetics of Radiative Recombination at Randomly Distributed Donors and Acceptors." Physical Review 140.1A(1965): A202-A220.

[6] Klein, P. B., Crossfield, M. D., Freitas, J. A., Collins, A. T. "Donor-acceptor pair recombination in synthetic type-IIb semiconducting diamond." Physical Review B 51.15(1995):9634-9642.

[7] Watanabe, K., Lawson, S. C., Isoya, J., Kanda, H., Sato, Y. "Phosphorescence in high-pressure synthetic diamond." Diamond and Related Materials 6.1(1997):99-106.

[8] Collins, A. T., and Williams A. W. S. "The nature of the acceptor centre in semiconducting diamond." Journal of Physics C: Solid State Physics 4.13(1971):1789-1800.

[9] Breeding, C. M., Shigley, J.E. "The "Type" Classification System of Diamonds and Its Importance in Gemology." Gems & Gemology 45.2(2009):96-111.

[10] Fisher, D., Sibley S. J and Kelly C.J. "Brown colour in natural diamond and interaction between the brown related and other colour-inducing defects." Journal of Physics: Condensed Matter 21.36(2009):364213.

STUDY OF A RECUT HPHT SYNTHETIC DIAMOND: COLOUR VS SIZE VS SWUV TRANSMISSION

Jean-Pierre Chalain[1]*, Ly Phan [1], Michael S. Krzemnicki [1], Hao Wang [1], Jörg Pausch[2], Michael Steinacher[3]

[1] Swiss Gemmological Institute SSEF, Basel, Switzerland
[2] Synova SA, Duillier, Switzerland
[3] Department of Physics, University of Basel, Basel, Switzerland
*jean-pierre.chalain@ssef.ch

Keywords: Diamond, type Ib, nitrogen concentration, colour, SWUV absorption, SWUV transmission, water guided MicroJet Laser sawing, SYNOVA

Non-treated nitrogen-rich HPHT synthetic diamonds are of type Ib, they contain solely single substitutional nitrogen atoms responsible for their typical yellow colour, sometimes referred by the trade as a "canary" colour (Collins, 1982). The yellow saturation of type Ib diamonds is directly proportional to their nitrogen concentration and of course to the path length of light (Kiflawi, et al., 1994). Thus, the colours of type Ib diamonds of equal nitrogen concentration are only depending on the path length of light inside the stone (Figure 1).

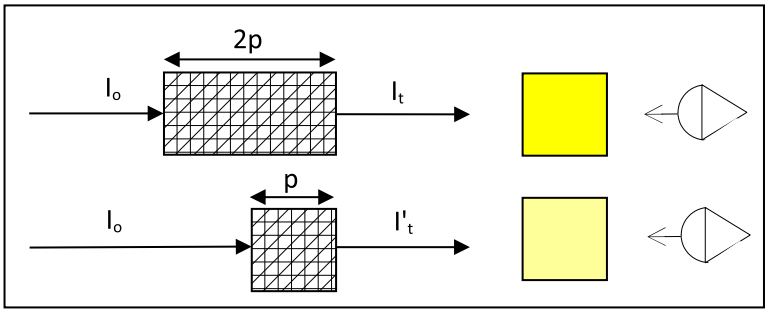

Figure 1: When a light source (I_0) passes through two samples of the same transparent material, the colour of the thicker sample appears more saturated than that of the thinner sample (from the "Lambert law"). The yellow squares represent the different saturations seen when observing the samples in the direction of the light source (I_0).

This study presents the comparison of the colours and of the Short-Wave Ultra-Violet (SWUV) transmissions of four as-grown HPHT synthetic diamonds of type Ib of equal and very low nitrogen concentrations (approximately 1 ppm). This enables a better understanding on the effectiveness of Diamond Verification Instruments (DVI) such as the "ASDI" instrument (Chalain, 2014) which screens melee-size colourless diamonds for separating natural diamonds from possible synthetic diamonds based on their relative SWUV transmission.

Before recut, the large diamond was weighting 0.532 ct and had a diameter of 5.21 mm. Its colorimetric measurements (Table 1) were recorded on an in-house colorimeter (Figure 2).

Table 1

Reference	Ø (mm)	CIE (L*a*b*)	Colour Grade	Transmission (1) @ 270 nm	Absorption coefficient @ 270 nm
97768	5.2	(103.4152, -2.1697, 6.2871)	S-Z	NA	4.9 cm^{-1}
97768A	3.0	(101.4331, -0.1404, 1.5446)	G	7.5 V	2.5 cm^{-1}
97768B	2.0	(98.6827, -3.0896, 7.8891)	S-Z	0.2 V	14.3 cm^{-1}
97768C	1.5	(76.0195, 0.3616, 3.1669)	M-R	0.7 V	NA

(1) Voltage measured by the ASDI device
NA: Not Applicable due to the size out of specifications

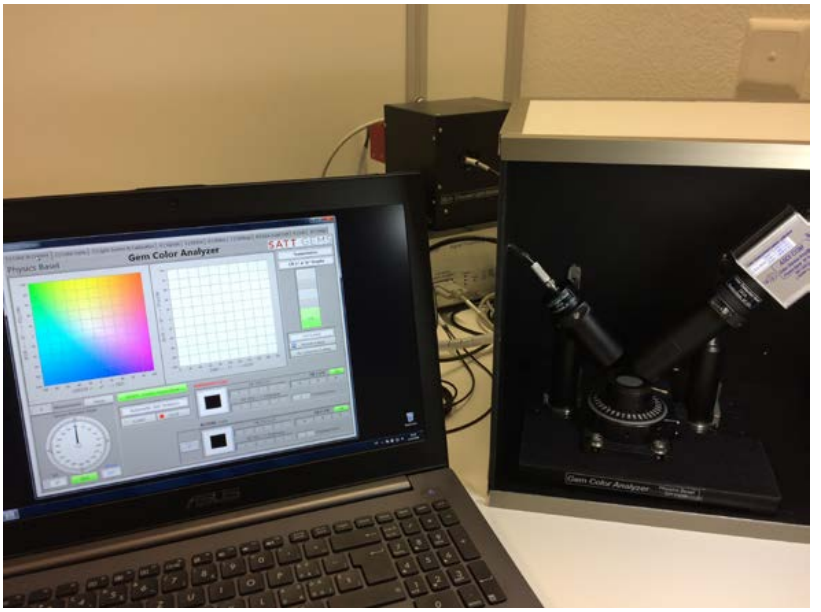

Figure 2: The in-house built "SSEF Gem Colour Analyzer" was used to measure the CIE Lab colour coordinates of the studied stones. They are placed table down in a dark chamber (not shown). A very thin beam of calibrated light is focused on their pavilion. The detector measures the colour coordinates of the stone during a 360° rotation.

After the colour measurement of the large stone, the infrared and UV-Vis absorption spectra were recorded and finally it was recut into three melee-size round brilliant stones as shown in Figure 3.

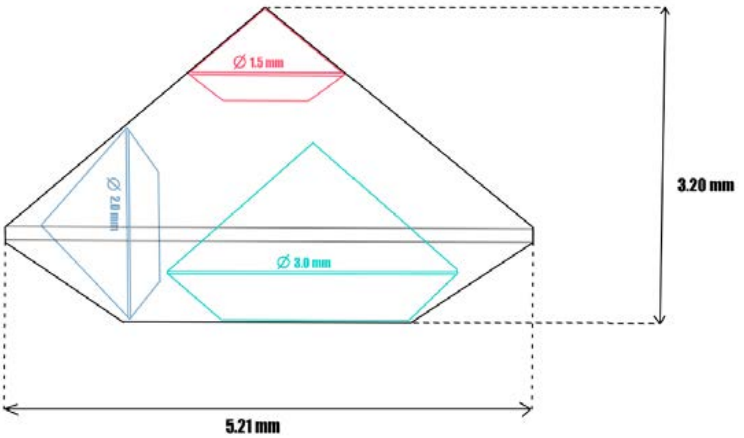

Figure 3: Recut specification of the 0.532 ct synthetic diamond into three melee-size stones

The pre-shaping of the three melee-size stones was performed at Synova SA (www.synova.ch) on a 5 axes high precision water guided Laser MicroJet LCS 305 machine (Figure 4). This unique technology enables parallel kerfs of only 50 to 65 µm.

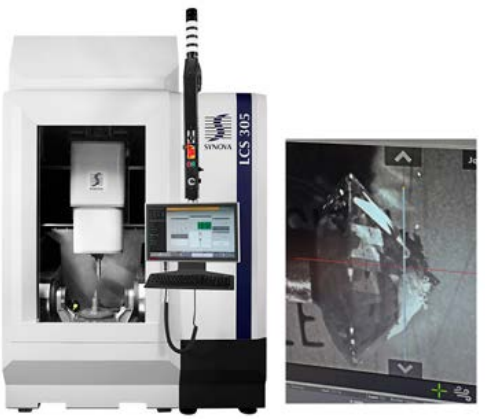

Figure 4: The SYNOVA LCS 305 sawing device (left image) is a 5 axes water-guided laser-MicroJet machine which enables very precise (+/- 0.1°) cutting profile. The precise positioning of the stone (right image) is observed via the help of a digital camera. Please note the white substance lying at the culet side of the stone enables the laser to easily penetrate into the stone.

Later these 3 stones were polished in three full-cuts (32/24) on a traditional scaife. Their final diameters are: 3.0 mm, 2.0 mm and 1.5 mm. Later, the CIE lab colour-coordinates of the three stones were measured (Table 1). And their SWUV absorptions were recorded on an in-house built spectrometer.
The comparison of the SWUV absorptions, SWUV transmissions and colour coordinates of the four stones enables establishing the correlation between colour and SWUV transmission.
It illustrates why and how it is efficient to screen colourless (D to J) synthetic diamonds based on the measurement of their SWUV transmission, even though some of them would have a very low nitrogen concentration.

References

Chalain, J-P., 2014. in Facette SSEF,v.21, p.11-12.

Collins, A. T., 1982. Colour centres in diamond. Journal of Gemmology, v. 18, no. 1, p. 37-75.

I. Kiflawi, A.E. Mayer, P.M. Spear, J.A. Van Wyk and G.S. Woods, 1994. Phil. Mag. B 69, 6 p.1141-1147

Acknowledgement

The authors would like to thank Dr. Bernold Richerzhagen, CEO and President of SYNOVA SA for letting us getting in contact with the Synova team.

THE EFFECTS OF HPHT TREATMENT ON PREVIOUSLY IRRADIATED AND ANNEALED DIAMONDS OF ALL TYPES AND COLORS

Thomas Hainschwang[1], Gianna Pamies[1]

[1]GGTL Laboratories Liechtenstein, Balzers, Liechtenstein
thomas.hainschwang@ggtl-lab.org

Keywords: HPHT treatment, irradiation, defects

For this study a series of over 100 natural and synthetic diamonds selected by type and color were irradiated by 2 or 10 MeV electrons for 2 to 3 hours and consequently heated, the majority up to 1300°C in steps of 100°C. Certain samples were only heated to 140°C and then directly to 900°C. After the annealing experiments in the regular high temperature furnace were finished, some of the diamonds were treated by HPHT under conditions of 2000 to 2500°C and 60 to 75 kBar. Prior to the treatment steps and after each step the diamonds' body color and color of fluorescence under 6 different UV excitations from 220 to 400 nm of the DFI system was documented. Equally, the diamonds were tested by infrared spectroscopy, UV-Vis-NIR spectroscopy at 77K and photoluminescence spectroscopy with 5 laser excitations from 360 to 635 nm, at 77K. While one main aspects of this study was the detailed documentation of the defects created directly by irradiation and at temperatures below 400°C, there was also a great interest in the behavior of the diamonds and their defects after HPHT treatment. Much has been published about the HPHT treatment of brown type I and type II diamonds (e.g., Chalain et al, 1999; Collins et al, 1999; Fisher and Spits, 2000), but there is virtually no data available on the behavior of the defects in other colors and types of diamonds, such as "Cape" diamonds.

The results after HPHT showed that at the lower HPHT temperatures the color of non-deformed diamonds was only slightly modified, but the fluorescence and especially PL spectra changed significantly. The nitrogen aggregation state was only slightly modified and single nitrogen remained undetectable by high resolution IR spectroscopy. At the higher temperature of 2500°C the diamonds appearance changed significantly, mostly through the creation of single nitrogen by the splitting up some of the aggregated nitrogen. All the originally cape yellow diamonds turned non-fluorescent deep brown orange, a color one would expect to originate from a combination of single nitrogen plus strong plastic deformation (Hainschwang et al., 2013). No such plastic deformation could be observed for the treated samples – and any such deformation-related defects would not survive HPHT treatment at 2500°C anyways –, but nevertheless the appearance of the UV-Vis-NIR spectra was virtually identical to the spectra of plastically deformed type Ib diamonds (Fig. 1). It is speculated that the reason for this brown color originates from the destruction of the high concentrations of N3/N2 defects that were present prior to the treatment; whatever defect the N2/N3 centers transform to when they anneal out seems to be responsible for the continuum absorption seen at >550 nm in the UV-Vis-NIR absorption spectrum (Fig. 1, trace e). Even though the very high nitrogen content alone was thought to have an influence on the single nitrogen absorption, this could be refuted since none of the near-colorless samples with equally high nitrogen contents but far lower N2/N3 content did not turn brown orange but plain yellow because of the creation of C centers. The very defective nature of the lattice can be indirectly observed via the FWHM of some of the defects created by HPHT treatment: for sample TH 2.411 a FWHM of 2.8 nm was observed for the NV- center ZPL and a FWHM of 2.1 nm for the H3 center ZPL; as a comparison, in colorless type IIa diamonds the FWHM of these defects are usually around 0.3 nm or lower. The defects as detected in PL spectroscopy change very distinctly with such high temperature HPHT annealing, and the initially typical "Cape" diamond PL resembles much more to a type Ib diamond PL after the treatment.

The extensive amount of data that we have acquired through this still ongoing study that was started all the way back in 2009 allows us to have a much better and detailed insight into the behavior of diamonds and their defects upon irradiation, annealing and HPHT treatment.

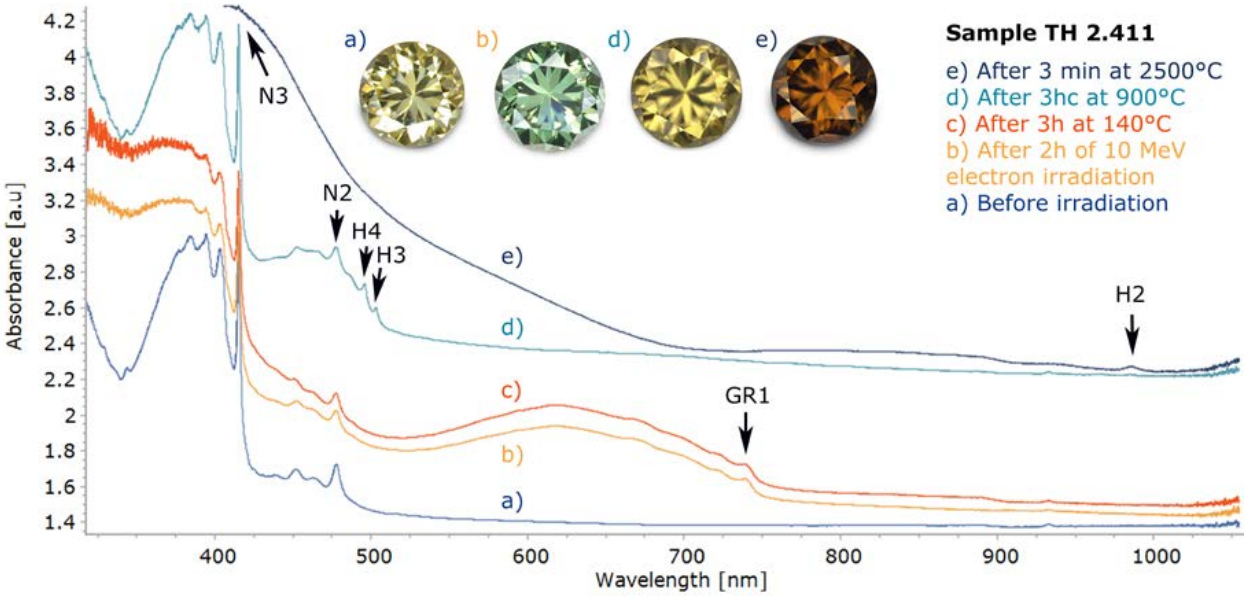

Figure 1. The UV-Vis-NIR spectra of an originally cape yellow diamond of its initial state (a), after 10 MeV electron irradiation (b), after heating at 140°C (c), after heating at 900°C (d) and after HPHT treatment at 2500°C (e). At 2500°C the N3/N2 and H3/H4 centers are all very strongly reduced and only detected in PL; the spectrum is dominated by the continuum absorption induced by the C centres created during the HPHT treatment. The colour of the sample changed from fancy light yellow to green after irradiation to intense yellow after 900°C annealing to deep brown orange after HPHT treatment.

References

Chalain J.P., Fritsch E., Hänni H.A. (1999) Detection of GEPOL diamonds, a first stage. Revue de Gemmologie, No. 138–139, pp. 30–33.

Collins A. T., Kanda H., Kitawaki H. (2000). Colour changes produced in natural brown diamonds by high-pressure, high-temperature treatment. Diamond and Related Materials, Vol. 9, No. 2, pp. 113-122.

Hainschwang T., Fritsch E., Notari F., Rondeau B., Katrusha A. (2013) The origin of color in natural C center bearing diamonds. Diamond and Related Materials, Vol. 39, pp 27-40.

Fisher D., Spits R. A. (2000) Spectroscopic Evidence of GE POL HPHT-treated Natural Type IIa Diamonds. Gems & Gemology, Vol. 36, no. 1, p. 42-49.

THE USE OF PHOSPHATE INCLUSIONS IN ORIGIN DETERMINATION OF ANCIENT AND MEDIEVAL RED GARNETS

H. Albert Gilg[1*], Ulrich Schüssler[2], Joachim Krause[3], Bernhard Schulz[4]
[1] Chair of Engineering Geology, Technical University of Munich, Arcisstr. 21, 80333 Munich, Germany, *agilg@tum.de
[2] Institut für Geographie und Geologie, Universität Würzburg, Germany
[3] Helmholtz-Zentrum Dresden-Rossendorf, Helmholtz Institute Freiberg for Resource Technology, Chemnitzer Straße 40, 09599 Freiberg/Saxony, Germany
[4] Institute of Mineralogy, Division of Economic Geology and Petrology, TU Bergakademie Freiberg, Brennhausgasse 14, 09596 Freiberg/Saxony, Germany

Keywords: Almandine, Inclusions, Monazite, Apatite, Provenance

Red garnets of almandine to pyrope composition were highly appreciated gemstones and frequently employed in jewellery during Hellenistic, Roman and Early Medieval times. To date at least six distinct types or clusters have been distinguished based on characteristic chemical compositions as well as inclusion assemblages (Calligaro et al., 2002; Calligaro et al., 2006-2007; Gilg et al., 2010; Schmetzer et al., 2017). The sources of these red gemstones have been disputed for a long time and are still not firmly established with the exception of chromium pyropes from Bohemia, Czech Republic (Gilg and Hyršl, 2014) and almandines from Garibpet, India (Schmetzer et al., 2017). The knowledge of the garnets' origins, however, is important for understanding trade routes and connectivity in the past. Major problems in provenance research of archaeological gemstones are 1) the required non- or at least micro-destructive analytical approach leading to reduced precision and detection limits, 2) the non-unique chemical compositions and similarity of mineral inclusions of the gems, both related to comparable geological processes, 3) the knowledge of chemical and inclusion variations within a deposit, and finally 4) the possibility that former gem deposits have been mined-out or completely forgotten.

Here we show that the chemical compositions of phosphate mineral inclusions in red garnets can be used as an additional aid in origin determination. The phosphate minerals apatite and monazite are frequent inclusions in metamorphic and metasomatic almandine and pyrope, and show considerable variations in shape and chemistry. Frequently, they even host distinct mineral or fluid inclusions themselves. Furthermore, monazite incorporates significant amounts of thorium and uranium, but little common lead and is, therefore, amenable to age determination, thus dating the growth of the host garnet. We used a combination of optical microscopy, Raman spectroscopy, automated scanning electron microscopy (MLA), electron probe microanalysis (EPMA) and laser-ablation inductively coupled mass spectrometry (LA-ICP-MS) to characterize apatite and monazite in garnets from archaeological contexts as well as from their potential sources. These data can be used as additional criteria for origin determination, but also for in- or excluding possible source areas for garnet types of unknown origin on the basis of age data. Four examples are presented:

We studied the phosphate inclusions in garnet beads from the ancient port of Arikamedu, Tamil Nadu (figure 1), and in garnets of the Garibpet deposit in Telangana state, India, that has been suggested as the primary source based on major and trace element compositions, chemical zonation of garnets, mineral inclusion assemblages and their characteristic zonal arrangement (Schmetzer et al., 2017). The apatite inclusions in garnet from Arikamedu beads and the Garibpet deposit both have characteristic long prismatic shapes (Fig. 1A) and include numerous graphite flakes (cf. Schmetzer et al., 2017). The major and trace element compositions of the apatites are strongly overlapping and characterized by high and in part variable contents of F, Mn, Sr, Y and Pb, while Cl, La and U contents are comparatively low. The monazite inclusions are 10 to 40 µm in diameter, show typical brownish radiation haloes and have quartz, biotite and graphite inclusions. The REE phosphates in three Arikamedu garnet beads yield chemical U-Th-Pb isochron age data of 1171 ± 4 Ma, 1180 ± 26 Ma and 1172 ± 8 Ma that are consistent with 65 analyses of monazites in Garibpet garnets (1163 ± 10 Ma) thus confirming the provenance.

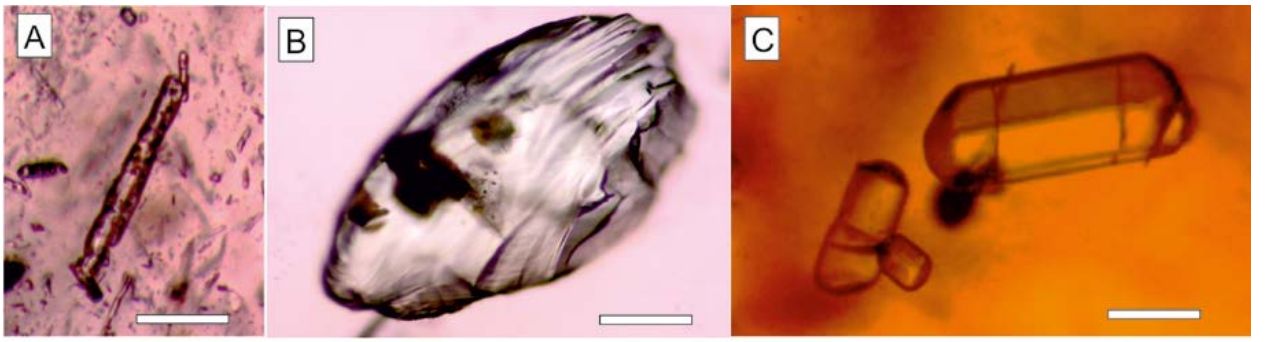

Figure 1 A: long-prismatic graphite-bearing apatite in garnet bead from Arikamedu, India. B: xenomorphic greenish apatite from the Lali deposit, Rajasthan, India, with biotite and sulfide inclusions, the possible source of Cluster B. C: euhedral short-prismatic inclusion-poor apatite from the Sjönevad deposit, Sweden. Scale bars: 200 µm

The apatite inclusions in the most abundant garnet type used in early medieval cloisonné jewellery, cluster B (type I) almandines (Calligaro et al., 2002; Gilg et al., 2010), are compared to those in gem garnets from the Lali deposit, Rajasthan, India, a possible source for cluster B garnets based on similar major element composition. Apatites in cluster B garnets from cloisonné object found in an early medieval cemetery near Munich, Germany, and those from the Lali deposit are both xenomorphic, slightly greenish and can reach diameters of more than 1 mm (Fig 1B). They may contain tiny (<2 µm) spherical sulphide blebs and brownish biotite flakes. The major and trace element compositions of apatites in artefacts and the Lali deposit are identical, but quite distinct from those of the Garibpet deposit showing lower F, Mn, Sr, La, Y, and Pb, but higher Cl and U contents. Monazite inclusions in garnet from the Lali deposit mostly yield U-Th-Pb ages of 807 ± 21 Ma, a few samples having older cores. Monazites are rare in cluster B garnets, only about 20% of the observed stones have those inclusions. No inclusion was observed on the surface of the artefacts that could be used for dating.

Garnets from the Sjönevad deposits, Hallam, Sweden, have been considered as the source for Ca-rich almandines (cluster C) used in Scandinavian early medieval cloisonné jewellery on the basis of garnet composition (Löfgren, 1973; Mannerstrand and Lundqvist, 2003; Gilg et al., 2010). The euhedral apatite inclusions are short prismatic and inclusion-free. Our study reveals distinctly high Cl and low F contents for Sjönevad samples that are quite different to the published values from the artefacts excavated in Paviken, Gotland (Löfgren, 1973). Thus, the Sjönevad deposit cannot be considered the source for the medieval gemstones.

The second most common almandine type in cloisonné jewellery, Cluster A, has almost no apatite inclusions, but frequent monazite inclusions. No specific source deposit, only regions have been vaguely suggested for them (Calligaro et al., 2006-7; Périn and Calligaro, 2016). Our study shows that the monazites in these garnets contain rutile and graphite inclusions and yield an isochron age of 2485 ± 19 Ma. This Late Archean age rules out previously suggested, but poorly supported origins in the Proterozoic Aravalli-Delhi-Belt of Rajasthan or the Eastern Ghats Belt of Odisha.

Thus, we conclude that consistent major element compositions of garnets and even presence of specific inclusion minerals may not be sufficient for a source attribution. Shape, chemical composition and geochronological data on apatite and monazite inclusions in garnets can yield additional supporting constraints for the source.

References

Calligaro, T., Colinart, S., Poirot, J.-P., and Sudres, C., 2002. Combined external-beam PIXE and μ-Raman characterisation of garnets used in Merovingian jewellery. Nuclear Instruments and Methods in Physics Research B, 189(1-4), 320-327.

Calligaro, T., Périn, P., Vallet, F., and Poirot, J.-P., 2006–2007. Contribution á l'étude des grenats mérovingiens (Basilique de Saint-Denis et autres collections du musée d'Archéologie nationale, diverses collections publiques et objects de fouilles récentes). Antiquités Nationales, 38, 111–144.

Gilg, H.A., Gast, N., and Calligaro, T., 2010. Vom Karfunkelstein. In: Wamser, L. (ed.), Karfunkelstein und Seide. Ausstellungskataloge der Archäologischen Staatssammlung, München, Band 37, pp. 87-100.

Gilg, H.A., and Hyršl, J., 2014. Garnet Deposits in Europe. In: Toussaint, J. (ed.), Rouges et Noirs. Rubies, grenat, onyx, obsidienne et autres minéraux rouges et noirs dans l'art et l'archéologie. Monographies du Musée Provincial des Arts du Namurois-Trésor d'Oignies (TreM.a), Société Archéologique de Namur, Namur, pp. 144-173.

Löfgren, J., 1973. Die mineralogische Untersuchung der Granaten von Paviken auf Gotland. Early Medieval Studies, 6(9), 78-96.

Mannerstrand, M., and Lundqvist, L., 2003. Garnet chemistry from the Slöinge excavation, Halland and additional Swedish and Danish excavations - Comparisons with garnet, occurring in a rock context. Journal of Archaeological Science, 30(2), 169–183.

Périn, P. and Calligaro, T., 2016. Note sur l'origine des grenats utilisés par les orfèvres du haut Moyen Âge occidental européen. In: Böllök, A., Csibky G, and Vida, T. (eds.) Between Byzantium and the steppe: archaeological and historical studies in honour of Csánad Bálint on the occasion of his 70th birthday. Institute of Archaeology, Research Center for the Humanities, Hungarian Academy of Sciences, Budapest, pp. 75-86.

Schmetzer, K., Gilg, H.A., Schüssler, U., Panjikar, J., Calligaro, T., and Périn, P. (2017) The linkage between garnets found in India at the Arikamedu historical site and their source at the Garibpet deposit. The Journal of Gemmology 35(7), 589-627.

Acknowledgements

We like to thank Dr. H. Brätz for help in LA-ICP-MS analyses and Dr. K. Schmetzer for fruitful discussions.

A GOTHIC CROWN IN THE TREASURY OF THE MUNICH RESIDENCE MUSEUM: EXAMINATION OF ENGLISH ROYAL INSIGNIA FROM THE LATE MIDDLE AGES

Karl Schmetzer[1], H. Albert Gilg[2]

[1] Taubenweg 16, 85238 Petershausen, Germany; SchmetzerKarl@hotmail.com
[2] Chair of Engineering Geology, Technical University of Munich, Arcisstr. 21, 80333 Munich, Germany

Keywords: 14th century Gothic regalia, diamonds and colored stones, imitations

Introduction

The examination of historical jewellery, and especially the examination of regalia richly decorated with gemstones, can provide insights into historical connections and trade routes of bygone times, as well as the development of faceting technology. Only two English crowns from the Late Middle Ages are known to have survived to the present day: the crown of Blanche of Lancaster, dated to the 1380s; and the crown of Margaret of York, dated to approximately 1461. The former was part of the dowry of Blanche of Lancaster (1392-1409), daughter of the English King Henry IV, when in 1402 she married Louis (1378-1436), the son of Rupert III, Elector Palatine and German King. On the basis of its features, historians generally agree that the crown preserved in the Munich treasury is the same crown as was mentioned in two English royal inventories of Richard II, dated 1398 and 1399 (Stratford, 2012). The crown (Figure 1) is highly embellished with diamonds, colored stones (blue, pink and green), and pearls, but no detailed gemmological examination of the gemstones, beyond visual inspection, has ever been performed, and no description of the gem materials is available. In English and German inventories of the 14th to 19th centuries, the gemstones are described as diamonds, sapphires, balas rubies (i.e., spinels) or rubies, and emeralds. According to the information available from these inventories, only a very small number of stones were lost during the crown's past and subsequently replaced. Thus, the Gothic crown can serve to elucidate the gem materials available and used in late 14th-century Europe.

Experimental Techniques

The crown was examined by microscopy, X-ray fluorescence, and Raman spectroscopy using mobile instrumentation, insofar as removal of the crown from the museum was not possible.

Results and Discussion

The crown was composed of a circlet of twelve gold segments that served as bases for the stems of twelve fleurons (Figures 1, 2). These twelve segments each consisted of a framework displaying a hexagon in the center of a circle, backed by a vertical bar. The vertical bar then is connected with a gold stem topped by a lily. The hexagons were bedecked with enameled white flowers overlaid onto a translucent blue or red background. The twelve segments and the lilies of the fleurons, alternating in size, were heavily jeweled and decorated with diamonds, colored stones, and pearls.

Figure 1. The crown, which became part of the dowry of Princess Blanche of Lancaster in 1402, was first mentioned in English inventories dated 1398 and 1399 and was most likely made for and used by the English Queen Anne of Bohemia. The crown came to Heidelberg, Germany, in 1402, and to Munich at the end of the 18th century. Diameter approx. 18 cm, height 18 cm.

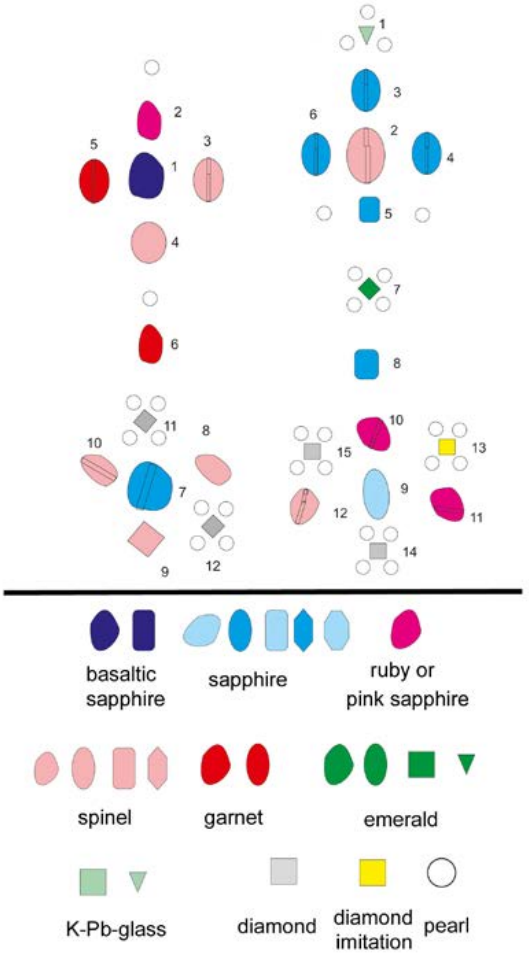

Figure 2. Schematic representation of the rich gemstone adornment of the crown's larger and smaller fleurons, consisting of diamonds, colored stones, and pearls.

The stones or purported stones adorning the crown consisted of 22 diamonds, 13 diamond imitations, 47 blue sapphires, one blue sapphire doublet, 10 pink sapphires or light rubies, 53 pink spinels, five garnets, nine emeralds, six green pieces of lead-glass, and one pink lead-glass (Figures 2, 3).

Figure 3. Gemstones and imitations decorating the crown comprised diamonds (a), diamond imitations (b), blue sapphires (c, d, e), pink sapphires (f), pink spinels (g, h,), garnets (i), pink lead glass (j), emeralds (k) and green lead glass (l); for further details see text. The larger faceted stones (e, h) measure approx. 14 x 10 mm; the pink lead glass (j) measures 7.1 x 6,8 mm; the diamond (a), the diamond imitation (b), and the emerald (k) measure approx. 4.3 mm (with bezel setting).
All photos by the authors.

Diamonds were used in the form of natural crystals with an octahedral habit (Figure 3a). Diamond imitations, however, were present as well and had already been mentioned in some inventories. All these were of the same type, a four-sided pyramid is made of four planar or almost planar gold "faces". The gold faces are now completely or partly covered by a black layer (Figure 3b), which was identified as a lead-bearing glass (black enamel, schwarzlot).

Blue sapphires were found in a dark blue, translucent type (Figure 3c) and in a light to intense blue, transparent type (Figure 3 d,e). Several sapphires were irregularly shaped pebble-like samples with curved domes, frequently with drill holes and/or surface indentations, while others were faceted. The faceted sapphires showed planar tables with four, six, or eight crown facets, depending on whether the sample was rectangular, hexagonal, or octagonal. The majority of the pink sapphires or rubies were irregularly shaped and polished pebbles or cabochons, frequently exhibiting drill holes (Figure 3f).

Most pink spinels displayed irregular pebble-like forms, commonly with surface indentations where impure parts had been removed (Figure 3g). Nonetheless, two groups reflected a certain degree of fashioning. One of these groups lacked sharp edges and had flat or slightly curved tables, suggesting only minor shaping and polishing. The other group was characterized by planar faces resulting from faceting and polishing. Amongst the spinels that had been shaped or faceted, both rectangular and hexagonal forms were extant (Figure 3h).

Garnets likewise existed primarily as irregularly shaped pebbles (Figure 3i). X-ray fluorescence analysis revealed that the garnets used were pyropes or almandines. Conversely, one pink stone proved to be an irregularly shaped "pebble" of pink lead glass (Figure 3j).

The emeralds used to embellish the crown were irregularly shaped polished pebbles or cabochons with triangular or square shapes (Figure 3k). Green lead glass was used as an emerald substitute (Figure 3l).

Notably, the gem materials adorning Blanche of Lancaster's crown chronicled the development of faceting in the late 14th century and the transition from irregularly shaped and polished pebbles to shaped and polished rectangular, hexagonal, or octagonal forms. The first faceted gemstones with planar faces and sharp edges featured only table and crown facets, occasionally combined with girdle facets. Most likely one blue sapphire with crown and pavilion facets, a sapphire doublet, the pink lead glass and at least two garnets were added to the crown after 1600 to replace lost stones. In contrast, most pieces of green lead glass and the gold pyramids covered with black enamel were original, showing the shortage of diamonds and emeralds at the end of the 14th century.

Reference

Stratford, J., 2012. Richard II and the English Royal Treasure. The Boydell Press, Woodbridge, 470 pp.

AGE DATING APPLIED AS A TESTING PROCEDURE TO GEMSTONES AND BIOGENIC GEM MATERIALS

Michael S. Krzemnicki [1*], Hao A.O. Wang [1], Myint M. Phyo [2]

[1] Swiss Gemmological Institute SSEF, Switzerland
[2] Institute of Mineralogy and Petrography, University Basel, Switzerland
* michael.krzemnicki@ssef.ch

Keywords: Radiometric age dating, radiocarbon, U-Pb titanite dating, gem testing

Radiometric age dating is a well-established method in geochronology (earth sciences) and archaeology. There are numerous studies highlighting the use of radioactive decay of U-Pb, K-Ar (among many others) for geological age dating and radiocarbon ^{14}C for biogenic material (bones, shells) of antique to pre-historic age. In gemmology, the application of age dating as an analytical method is still rather limited, although pioneering work was already published many years ago (Coenraads et al., 1990; Sutherland et al., 2002).

With the recent progress of analytical capabilities (e.g. GemTOF: LA-ICP-TOF-MS, see Wang et al., 2016) we have been able in the past few months to carry out radiometric age dating on a large number of gemmological samples, partly from our research collection, but in great number also as part of our testing procedure on gemstones and biogenic materials (pearls and corals) from our clients (Figure 1).

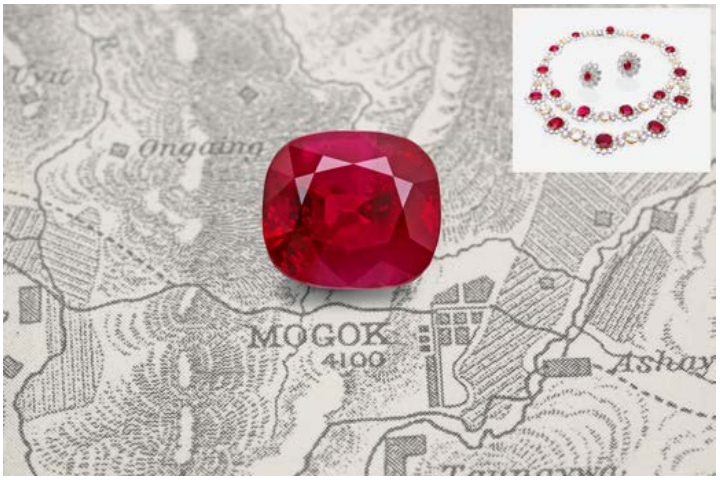

Figure 1: Radiometric age dating of a titanite inclusion at the surface of a Burmese ruby (12.8 ct), originally set in an iconic necklace by Harry Winston. Photo: V. Lanzafame, SSEF

In the context of a gemmological laboratory, radiometric age dating of gem materials or their inclusions is often a very useful addition to data gained by more traditional gem testing procedures. It may bolster conclusions deduced from other tests and may even deliver crucial information without which a conclusion would not be possible. Specifically, when applying (radiocarbon) age dating to biogenic gem materials such as pearls, we may gain information a) to confirm a historic age ("provenance") of a historic pearl (Krzemnicki et al., 2017), and b) it may support the identification of a natural pearl based on its formation age dating prior to pearl cultivation (Krzemnicki & Hajdas, 2013). Geological age dating (e.g. U-Pb) on gemstones and their inclusions is mainly interesting as it may offer further evidence when deducing their origin (see also Link, 2016; Sorokina et al., 2017).

Radiometric age dating is a promising but complex analytical method with limitations and challenges, well-known and described in literature (Reiners et al., 2018 and references therein). For radiocarbon ^{14}C dating, these include contamination effects from the jewellery mounting, during sampling, or over-assessed ages (i.e. too old) when the skeleton of the biogenic material (e.g. shell, pearl, coral) uses/recycles bicarbonate from older sources (so-called hard water effect, Shotton, 1972). In geochronological dating (e.g. U-Pb of zircon), leaching/contamination effects and complex growth zoning (e.g. old detrital zircon grain is overgrown by a much younger rim) may affect the results considerably, for example resulting in "mixed" ages (Schoene, 2014; Reiners et al., 2018). The ability of TOF-MS to analyse not only a small number of isotopes necessary for age dating, but to provide nearly the full mass spectrum simultaneously is in this respect very helpful (Wang et al., 2019), as it is possible to detect complex growth zoning and epitaxial overgrowth patterns (e.g. zirconolite grown on zircon, Phyo et al., 2018), thus supporting the interpretation of radiometric age dating results.

In the past few months we have applied radiometric age dating (Th-Pb and U-Pb) on a large number of corundum and spinel samples, many of them submitted by our clients for testing and origin determination. For this, we used surface-reaching inclusions present as time-capsules in these gemstones. So far, we were able to apply radiometric age dating not only on zircon inclusions, but additionally on inclusions of zirconolite, xenotime, monazite, baddeleyite, rutile, apatite, and titanite. This range of inclusions considerably increases the ability to apply dating as an additional method in gemmological testing in the laboratory. In addition to this, certain sapphires may contain considerable trace amounts of high-field-strength-elements (HFSE) such as Sn, Nb, Ta, W, Pb, Th, U, presumably accumulated as fine dispersed sub-microscopic (syngenetic) inclusions within these sapphires (Shen et al., 2009). As a consequence of this, it is in such cases possible to carry out radiometric age dating in-situ and simultaneously with the chemical analysis of the sapphire independently of the presence of any surface-reaching inclusion (e.g. zircon) (Wang et al., 2019).

In our presentation, we will present case studies which show the potential of radiometric age dating for testing gemstones and biogenic gem materials. These include radiocarbon dating on the so-called "Ana Maria Pearl", which will be offered at auction in May 2019. Our radiocarbon analyses confirmed that this pearl (presumably from Pinctada mazatlanica) formed in the early 16th to late 17th century. Our age dating thus provides supporting evidence for its documented historic provenance. We also will present the case of a pearl with internal structures reminiscent of beadless cultured pearls, which could be identified as saltwater natural pearl based on radiocarbon analyses, dating this pearl to the late 17th to mid 19th century, thus well before commercial pearl cultivation was developed. Furthermore, we will present age dating results of cultured pearls from Pinctada maxima from Australia harvested in the past three decades.

Radiometric age dating of coloured gemstones is presented on a number of real cases for which origin determination was only possible by combining a classical approach (microscopy, chemical composition and spectroscopy) with radiometric age dating. Among others, we discuss a sapphire of 8.27 ct which shows features and analytical data fitting for both, a Kashmir or Madagascar origin, and a 76 ct ruby cabochon originating from a marble deposit. Based on the geologically "young" U-Pb age of a (protogenetic) zircon inclusion (23.36 ± 0.40 Ma) in the sapphire and the "old" U-Pb age of a tiny surface-reaching xenotime (562.65 ± 5.76 Ma), we were able to finalise the origin of the sapphire (Kashmir) and the ruby (East-Africa), as the calculated ages were well in agreement with the age of sapphire formation in the Himalayan mountain range in India and with ruby formation in marbles along the Mozambique Mobile Belt in East Africa.

Based on our research, age dating is a very promising tool and will become increasingly important in gem testing in future. As could be demonstrated, it provides additional and unique information which may substantially help to establish the origin of a gemstone or the historic provenance and identity (cultured or natural) for biogenic materials.

References

Coenraads R.R., Sutherland F.L., and Kinny P.D. 1990. Origin of sapphires: U-Pb dating of zircon inclusions sheds new light. Mineralogical Magazine, 54, 113-122.

Krzemnicki M.S. and Hajdas I., 2013. Age determination of pearls: A new approach for pearl testing and identification. Radiocarbon, 55(3), 1801–1809.

Krzemnicki M.S., Cartier L.E., and Hajdas I., 2017. Radiocarbon age dating of 1000-year-old pearls from the Cirebon Shipwreck (Java, Indonesia). Journal of Gemmology, 35(8), 728-736.

Link K., 2015. Age determination of zircon inclusions in faceted sapphires. Journal of Gemmology, 34 (8), 692-700.

Phyo M.M., Guillong M., Franz L., Berger A., Krzemnicki M.S., and Wang H.A.O., 2018. U-Pb age dating and trace element analysis of zircon inclusions in ruby, spinel and host rock from Mogok, Myanmar using LA-ICP-TOF-MS and LA-ICP-SF-MS. Proceedings of the 14th European Workshop on Laser Ablation, Pau, France, 26-29 June 2018.

Reiners P.W., Carlson, R.W., Renne P.R., Cooper K.M., Granger D.E., McLean N.M,. Schoene B., (editors), 2018. Geochronology and Thermochronology. John Riley & Sons Ltd., West Sussex, UK. 464 pp.

Schoene B., 2014. Causes of Discordance in the U–Th–Pb System, in: Treatise on Geochemistry, 2nd edition, editors Holland H.D. & Turekian K.K., Elsevier, (4), 10, 347-351.

Shen A., McClure S., Scarratt K., 2009. Beryllium in pink and yellow sapphires. GIA News from Research (April 3, 2009). https://www.gia.edu/doc/Beryllium-in-pink-and-yellow-sapphire-20090401_so-ahs.pdf

Shotton F.W. 1972. An example of hard-water error in radiocarbon dating of vegetable matter. Nature, 240, 460-461.

Sorokina E.S., Rösel D., Häger T., Mertz-Kraus R., and Saul J.M., 2017. LA-ICP-MS U–Pb dating of rutile inclusions within corundum (ruby and sapphire): new constraints on the formation of corundum deposits along the Mozambique belt. Miner. Deposita, 52 (5), 641-649.

Sutherland F.L., Bosshart G., Fanning C.M., Hoskin P.W.O., Coenraads R.R., 2002. Sapphire crystallization, age and origin, Ban Huai Sai, Laos: age based on zircon inclusions. Journal of Asian Earth Sciences, 20, 841-849.

Wang H.A.O., Krzemnicki M.S., Chalain J.P., Lefèvre P., Zhou W. and Cartier L.E., (2016) Simultaneous high sensitivity trace-element and isotopic analysis of gemstones using laser ablation inductively coupled plasma time-of-flight mass spectrometry. Journal of Gemmology, 35(3), 212-223.

Wang H.A.O., Krzemnicki M.S., Braun J., and Schmid R., 2019. Multi-element analysis of gemstones and its applications in geographical origin determination. Proceedings of the 36th IGC Conference 2019, Nantes, France.

Gemmological examination of four Mogul jewellery objects dating from the first half of the 17th century

Elisabeth Strack[1], Bernd Augustin[2]

[1]Gemmologisches Institut Hamburg, Poststrasse 33, 20354 Hamburg, Germany
info@strack-gih.de
[2] Herbert-Weichmann-Strasse 21, 21085 Hamburg, Germany
karinaugustin@gmx.de

Introduction

The Mogul dynasty, founded in 1526, ruled for more than 200 years over a large part of India, establishing itself as an Islamic world power dominated by Persian culture and language The height of Mogul culture was reached under rulers Jahangir (reigned from 1605 – 1627) and Shah Jahan (reigned from 1628 -1658).

Jewellery, at first characterized by the use of rubies (predominantly of Burmese origin), red spinels and pearls, received a new emphasis when, after the Spanish conquest, Colombian emeralds found their way to India (Lane, 2010).

Consequently, in the first half of the 17th century objects were produced that stand unique in the history of jewellery making (Augustin, 1993, 2006, 2014). Four pieces of the higher courtly type were made availalble from a private collection; a forehead ornament, two sash belt ornaments and a figure pendant, set with diamonds, rubies, emeralds, red spinels and pearls respectively. Gemmological examination, due to testing at the premises, was limited to a microscope and a UV lamp. In addition, two objects (No. 1 and No. 4) were made available for x-ray testing of the pearls and respectively Raman testing of the red spinels.

Four Mogul jewellery objects from the first half of the 17th century

The four objects examined are witnesses of the high courtly culture under Jahangir and Shah Jahan. Made of 22 carat gold, they are characterised by balanced colour schemes, rhythmic linearism, intricate forms and an influence of European Renaissance jewellery, the gemstones are set in the Indian kundan technique (Nigam, 2001; Augustin, 2006).

A characteristic feature in Jahangir's time is the dominant use of rubies and red spinels. Emeralds, after imports from Colombia had started in the second half of the 16th century (Lane, 2010), were at first used sparsely.It was only with the development of style under Shah Jahan that they took up an equal position to rubies, replacing turquoise (Augustin, 2006). Colombian emeralds reached India by way from Europe or they were sent directly via the Pacific Ocean to Manila, a thriving Spanish trading post since 1570 (Lane, 2010), and from there to India.

General description of jewellery objects examined

1. Forehead ornament (tikka), ca. 4.5 x 3.5cm, 11.7 grams (Fig. 1a,b)

Fig. 1 a. Forehead ornament or tikka, around 1620- 1640

Fig. 1b: Under longwave ultraviolet light (366nm)

Date: ca. 1620 – 1640 (late Jahangir/early Shah Jahan rule)
Gemstones: 1 rectangular, mirror-cut diamond, ca.5x4x2.4mm,ca.0.40carats
1 domed cabochon ruby, ca. 10.5x8.5mm, ca. 5 carats
11 small trapezoid-shaped rubies
1 emerald slab in the loop (2 attached pearls are later additions)
5 pearls, irregular shapes, max.length ca.12mm, white to creamish, good to diminished lustre, one pearl has an inner crack

2. Eight-sided rosette-shaped sash belt ornament, ca. 4.3cm, 37.1 grams (Fig. 2a,b)

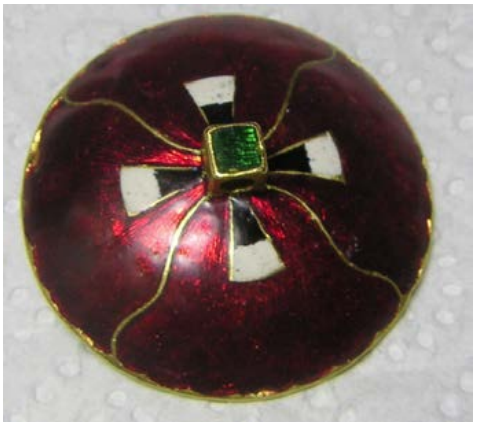

Fig. 2.a,b. Round button-shaped sash belt ornament, ca. 1640 – 1660

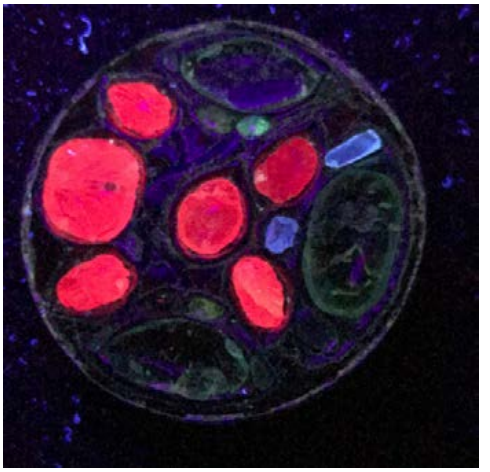

Fig. 2c. Under longwave ultraviolet light (366nm)

Date: around 1634 (early Shah Jahan rule) - the engraving „1043 AH" corresponds to the year 1634
Gemstones: 1 highly-domed ruby, ca. 11x10mm, ca. 6 – 8 carats
Lining of spaces with small rubies, below 5mm
8 drop-shaped emerald cabochons,ca.8x7mm, ca. 3-4 carats each
9 small triangular emeralds on the rim, below 4mm

3. Round button-shaped sash belt ornament, ca. 3.8cm, 23.8 grams (Fig. 3a,b)

Fig. 3 a.b.. Intricate figural pendant, ca. 1620 – 1625

Fig.3c. Under longwave ultraviolet light (366nm)

Date: around 1640 – 1660 (late Shah Jahan rule)
Gemstones: 11 diamonds: macles, early rose cuts and table cuts
6 rubies: 1 cabochon, 5 carved in floral patterns, max.size 10mm
3 emerald cabochons, max. size 13x6mm

4. Intricate figure pendant, ca. 5.1 x 3.25cm, 29.5 grams
Date: around 1620 – 1625 (late Jahangir rule)
Gemstones: 2 red spinels, composing an engraved angle, total length 25mm
2 emeralds, cut as angles in a serving posture, ca. 10x3mm
Small emeralds and rubies in a linear/mosaic arrangement

Methods and results of gemmological examination

Gemmological examination of the four objects was limited, as the pieces could not be taken out of the premises (with the exception of No. 1 having been made available for x-ray testing of the pearls and No. 4 for Raman testing of the red spinels), to a microscope (10x to 60x) and a UV lamp with both longwave and shortwave ultraviolet light (366nm and 254nm).

Diamonds
The rectangular diamond in object No. 1 is an example of a rare mirror cut (Falk, 1980; Tillander, 1995). The 11 diamonds in object No. 3 are a mixture of early rose cuts, table cuts and macles. Only 2 out of 11 diamonds in No. 3 fluoresced a strong blue and 1 fluoresced a strong green under 366nm; fluoresences were weaker under 254nm.

Rubies
Under the microscope, the larger rubies in No. 1 to 3 showed patches of rutile silk, characteristic of Burmese origin, a result that is in concordance with findings by M. Tschistijakowa for rubies in Mogul objects at the Hermitage Museum (Tschistijakowa,1984); foiling or artificial colouring could not be detected. All rubies showed a strong fluorescence under longwave uv light and fluoresced slightly less intensively under shortwave. While the central rubies in No. 1 and in No. 3 had no eye-visible inclusions, the one in No.2 showed, under a pointed light source, a silk line extending in the direction of its length.

Spinels
The two red stones that make up the central figure in No. 4 were identified by Raman spectroscopy as red spinels, using the BW Tek Gem Raman instrument, thus confirming the description given by Augustin (Augustin, 2014). Under longwave uv light the red spinels showed a strong red fluorescence that was slightly weaker under shortwave.

Emeralds
All emeralds had eye-visible fissures; foiling or artificial colouration could not be detected. Under the microscope, a pattern of liquid inclusions with jagged outlines, characteristic for Colombian emeralds, was observed. Comparable inclusion patterns were described for eme- ralds in Mogul objects at the Hermitage Museum (Tschistijakowa, 1984; Strack, 2004). 1 emerald in object No. 2 and 3 in object No. 3 contained a filling substance and corresponding- ly showed a yellowish fluorescence on internal flaws under longwave ultraviolet light.

Pearls
The size of the pearls in object No.1 indicates their origin from Pinctada margaritifera, possibly from the Persian Gulf or the Red Sea. It cannot be excluded that pearls from the Pacific central American coast (from Pinctada mazatlanica) may have reached India together with emeralds from Colombia. All pearls fluoresced whitish-blue under both long and shortwave uv light. X-radiography revealed characteristic features of natural pearls, showing inner cores and curves of organic substance.

Conclusion

Testing of gemstones in four 17th century Mogul jewellery objects, limited to a microscope and a UV lamp, confirmed the Burmese origin of rubies and the Colombian origin of eme-ralds, as described by B. Augustin (Augustin, 1993, 2006, 2014). The result is in concordance with findings by M. Tschistijakowa and this author in Mogul objects at the State Hermitage Museum (Tschistijakowa, 1984; Strack, 2004). Identification of two red spinels by Raman spectroscopy confirmed the description given by B.Augustin (Augustin, 2014). Diamonds showed a mixture of 17th century rose cuts, table cuts and macles, one was a rare mirror cut. The natural origin of the pearls was tested by x-radiography.

References

Augustin, B., 1993. Jewellery, 231. In: Oriental Splendour – Islamic Art from German Private Collections. Exhibition at the Museum für Kunst und Gewerbe Hamburg 18th June – 22nd August, 1993 (ed. C.-P. Haase, J. Kröger, U Lienert), Edition Temmer, 296 pp.

Augustin, B., 2006. Schmuck des westlichen Indien zu Beginn des 17. Jahrhunderts. Eine Meisterschaft der Kundantechnik in der hinduistischen Tradition unter islamischem und europäischem Einfluss. Indo-Asiatische Zeitschrift. 10, 72 – 81.

Augustin, B., 2014. Drei imperiale Juwelen. Ein Beitrag zur Schmuckkunst unter Jahangir und Schah Jahan. Indo-Asiatische Zeitschrift. 8, 56-70.

Falk, F., 1980. The Cutting and Setting of gems in the 15th and 16th centuries. V&A Exhibition Catalogue: Princely Magnificence – Court Jewels of the Renaissance 1500 – 1630, 20 – 26.

Lane, K., 2010. Colour of Paradise. The Emerald in the Age of Gunpowder Empires. Yale University Press, New Haven and London, 280 pp.

Nigam, M.L., 2001. Indian Jewellery. Lustre Press Poli Bookd, New Delhi, 96 pp.

Strack, E., 2004. The origin of the emeralds in some of the Moghul objects in the olletion of the State Hermitage Museum., St. Petersburg. Juweliernoe Iskusstwo i Materialnaja Kultura. Tesis Dokladow, 12- 18. April 2004, 101-107.

Tillander, H., 1995. Diamond Cuts in Historic Jewellery 1381 – 1910. Art Book International, London, 248 pp.
Tschistijakowa, M.B., 1984. Juweliernie Isdeljy Wostowka (in Russian, edited by A.A.Iwanow, B.G.Lukonin, L.C. Smesova.). The Hermitage Museum, St. Petersburg.

CAT'S EYE OPALS FROM BRAZIL: A SECOND LOOK

Carolina Santiago[1] and Jurgen Schnellrath[2]

[1] Andreas Lüttge Mineralogy Group, Center for Marine Environmental Sciences (MARUM) & Department of Earth Sciences (FB5), Klagenfurter Strasse 4, 28359 Bremen, Germany *souzasan@uni-bremen.de
[2] Gemmological Research Laboratory (LAPEGE), Mineral Tecnology Center (CETEM), Boullevard Pedro Calmon, 900, University City, 21941-908, Rio de Janeiro, RJ, Brazil * jurgen@cetem.gov.br

Keywords: Green opal, Cat's eye, Bahia

Opal is a gemological material appreciated worldwide for its unique characteristics, such as wide range of colors and optical effects. Opals showing cat's-eye effect are rare and only two occurrences are known until today, one in Brazil (BR) and another in Tanzania. The African material occur in a variety of colours between white, yellow (Srithai, Puangcharoen & Srichan, 2014), orange and brown (Fritsch, 2007) while the Brazilian one is characterized by greenish to brownish hues (Cassedanne & Ledoux, 1990).

Discovered in 1983 nearby the emerald deposit of Socotó, Campo Formoso (Bahia, BR), the opal veins occur erratically spread in the rock layers of the Campo Formoso mafic-ultramafic complex (Barbosa, Cruz & Souza, 2012) and in the 30 m of weathered profile on top of that. The veins, with widths ranging from 0.4 mm to 5 cm (figure 1), can present several hues and tones of green and brown, and the cat's eye effect can be seen locally in areas where a fibrous mineral (chrysotile) and enough opal meet.

Figure 1 – Opal veins within a matrix, with and without cat's eye effect, several sizes and erratic color distribution. Photo by C. S. Santiago

Figure 2- Cut opals (2.29, 10.06, and 9.27 ct) from Socotó, Bahia. Photo by C. S. Santiago

The heterogeneous characteristic of the deposit is directly linked with its genesis. At least four events of hydrothermal alterations affected the host rocks (Rudowski, 1989), resulting in changes of the original mineralogical assembly and remobilization of chemical elements. The serpentinization process was the first one to take place, transforming the primary iron-magnesium silicates into lizardite and chrysotile, while the opal formation is related to the third hydrothermal episode, carbonation, which converted the serpentine assembly into one made up of magnesite, talc, dolomite, opal and quartz, and intensified the alteration of spinel (Zaccatini, Garuti & Martin, 2006).

Basic gemmological properties were checked using a refractometer, scale and ultraviolet (UV) lamp with short (365 nm) and long (253 nm) waves. Measured refractive indices ranged from 1.469 to 1.498, higher than the values expected for pure opal (1.42 – 1.47 at Lazzarelli, 2002), and the material showed birefringence. Densities ranged between 2.173 and 2.219 and these values lay inside the expected interval (1.99 – 2.23 at Lazzarelli, 2002). No reaction under UV light was observed.

X-ray diffraction (XRD) and Raman spectroscopy were the tools chosen to identify the mineral phases that outcrop associated with the opal vein and the nature of the fibers responsible for the chatoyancy. Clinochlore, chromite and chrysotile were identified as the major phases in the host rock's diffractogram, while chrysotile and opal are the major phases inside the opal veins, regardless of showing or not a cat's eye effect. Chalcedony and quartz are present only as minor phases in some samples. With Raman spectroscopy it was possible to conclude that the fibrous mineral responsible for the optical effect is chrysotile, a member of the serpentine group, and to confirm the volcanogenic origin of these opals as proposed by Fritsch et al (1999), with the main peak centred around 340cm^{-1}. Due to the nature of this mineralization, the minerals included in the opal are the same present in the host rocks.

The results from the XRD were additionally used to identify the degree of crystallinity of these opals. It is important to mention that classification of crystallinity degree by the relationship between refractive index and density was not suitable for this work since opal was found to be always associated with chrysotile. Graetsch et al. (1994) proposed a separation through the ratio between intensities of the 4.3 and 4.1 Å reflections vs d-spacing values (graphic 1). Accordingly, the opals belong to the CT-type.

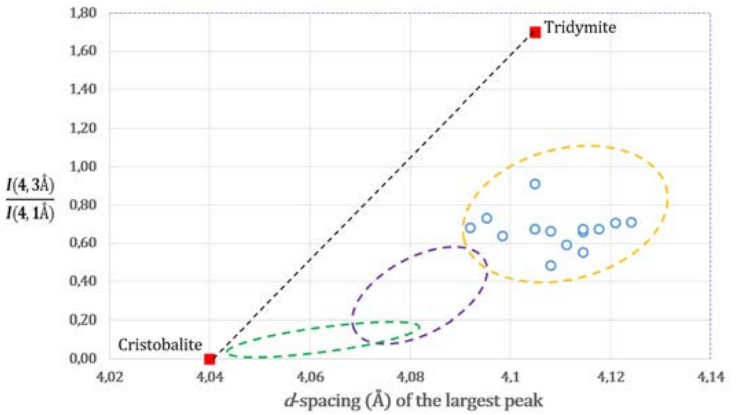

Graphic 1 – Plot intensities ratio 4,3 – 4,1Å versus d-spacing of the largest peak. Blue circles represent this work data while dotted circles indicate approximately the boundaries proposed by Graetsch et al. (1994): Opal-CT (yellow), opal-C (purple) and disordered cristobalite (green). Red squares: low-cristobalite and low-tridymite.

Scanning electron microscopy (SEM) coupled with energy dispersive spectroscopy (EDS) was used to investigate less abundant mineral inclusions and to shed light on the micro-scale texture and spatial relationship between opal and chrysotile. "Manganese dendrites" and nickel and cobalt spinels, possibly nichromite and/or cochromite, were observed, beyond chrysotile, clinochlore and chromite. SEM pictures revealed an arrangement of thin parallel fibers of chrysotile, with opal filling existing gaps in between those fibers.

Opals, if one considers only their main composition (hydrated silica) and structure, should be either colourless, white (when porous) or, only in very special cases, show a play of colour caused by diffraction of white light at the spaces between very small, uniformly sized silica spheres arranged in an orderly, three-dimensional array. Consequently, the green and brown hues found in the Socotó samples are likely linked with the presence of mineral inclusions, such as many other coloured opals (Fritsch et al, 1999). Using UV-VIS-NIR spectrophotometry and semiquantitative X-ray micro-fluorescence three main ions contributing to the colour were identified: Fe^{3+}, between 0.23 and 1.23 wt% of Fe_2O_3; Ni^{2+}, from 0.04 to 0.22 wt% of Ni_2O_3; and Cr^{3+} between 0.04 to 0.58 wt% of Cr_2O_3. Considering the data collected with SEM, clinochlore, chrysotile and chromite are the iron and chromium bearing phases while nichromite represent the nickel bearing one.

In addition to the chromophores mentioned above, a physical effect was observed contributing to the final colour, Rayleigh scattering. The same spot was observed using transmitted and reflected light conditions under the UV-VIS-NIR spectrometer. The absorption intensities under 450 nm, due to iron and oxygen ligand to metal charge transfer (LMCT) (Fritsch & Rossman, 1988a), are less strong with reflected light conditions when compared to the transmitted ones. This difference can be explained by the Rayleigh scattering effect, produced by the interaction of visible light with non-ordered structures smaller than the incident wavelength, which is more effective in that region of the electromagnetic spectrum (Fritsch & Rossman, 1988b). The result is that, when observed by transmitted light, these opals have more brown hues than when observed by reflected light (greener), comparing the same spot.
Despite being marketed nationally and internationally since the early 1980s, the lack of a steady production and the erratic nature of the deposits make the gem quality material a rarity in the trade. In order to maximize production yield, many opals cut from rough of this area, have chatoyant bands randomly crossing the stone, as can be clearly seen in Figure 2. Some of them may even completely lack the bands with fibers responsible for the cat´s eye effect. These opals are known among lapidaries as instable and are normally treated with fillers before the cutting process.

References

Barbosa, J. S., Cruz, S. S., & Souza, J. S. (2012). Terrenos Metamórficos do Embasamento. In J. S. Barbosa, Geologia da Bahia: pesquisa e atualização (1), 101-201.

Cassedanne, J. P., & Ledoux, L. A. (1990). Une curieuse opale chatoyante. Association Française de Gemmologie, 102, 3-5.

Fritsch, E. (Summer, 2007). Cat's-eye K-feldspar and other chatoyant gems from Tanzania. Gems & Gemology - Gem News International, 170-171.

Fritsch E., Rondeau B., Ostrooumov M., Lasnier B., Marie A.M., Barreau A., Wery J., Connoué J., Lefrant S. (1999) Découvertes récentes sur l'opale. Revue de gemmologie a.f.g. vol. 138/139, pp. 34-40.

Fritsch, E., & Rossman, G. R. (Spring, 1988a). An update on color in Gems. Part 2: Colors involving multiple atoms and color centers. Gems & Gemology, 3-15.

Fritsch, E., & Rossman, G. R. (Summer, 1988b). An update on color in Gems. Part 3: Colors caused by band gaps and physical phenomena. Gems & Gemology, 2, 81-102.

Graetsch, H., Gies, H., & Topalovic, I. (1994). NMR, XRD and IR study on microcrystalline opals. Physics and Chemistry of Minerals, 21, 166-175.

Lazzarelli, H. N. (2002). Blue Chart - Gem Identification: Natural / Treated / Synthetic / Imitation, first edition, 20.

Rudowski, L. (1989). Pétrologie et géochimie des granites transamazoniens de Campo Formoso et Carnaiba (Bahia, Brésil), et des phlogopites à émeraudes associées. PHD thesis, Paris, France: Université Pierre et Marie Curie - Paris VI.

Srithai, B., Puangcharoen, P., & Srichan, W. (2014). Causes of colour and optical phenomenon of Cat's eye opal from Tanzania. The 4th International Gem & Jewelry Conference. Chiangmai.

Zaccatini, F., Garuti, G., & Martin, R. F. (2006). Exotic accessory minerals in layered chromitites of the Campo Formoso complex (Brazil). Geologica Acta, 4(4), 461-469.

A REVIEW OF IMPORTANT GEM MATERIALS FROM CONNEMARA, WESTERN IRELAND

Alessandra Costanzo [1*], Martin Feely [2]

[1,2] Gemmology Lab, Earth and Ocean Sciences, National University of Ireland Galway, Ireland,
* alessandra.costanzo@nuigalway.ie
martin.feely@nuigalway.ie

Keywords: Ireland, Connemara, gem materials

Introduction

The geology, mineralogy and gemmological features of three separate gem material occurrences from the world-renowned region of Connemara, western Ireland, are described. Two (Connemara marble and sapphire) occur in the Connemara Metamorphic Complex while the third (fluorite) occurs in the younger Galway Granite Complex (Figure 1).

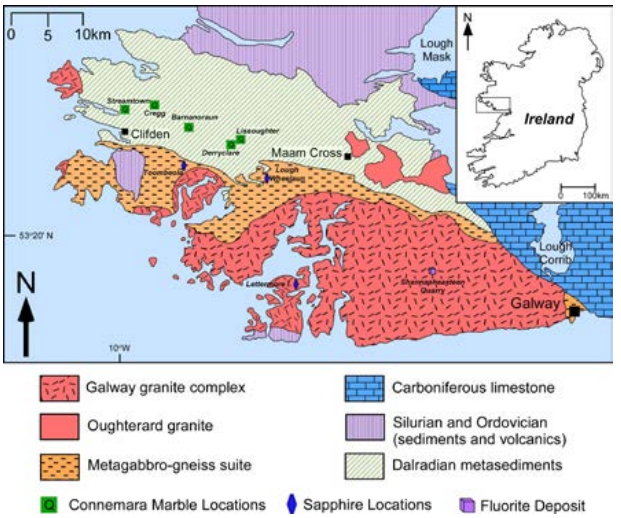

Figure 1. Map of Connemara and environs showing the distribution of the main geological units and the locations of the gem material described in the text. Geology and gem locations adapted from Leake and Tanner (1994), Pracht et al. (2004), Feely et al., (2017) and Feely et al., (2019).

Connemara is composed of a number of major rock units (Leake and Tanner, 1994 and Pracht et al., 2004) i.e. the Connemara Metamorphic Complex (CMC) composed of Dalradian (c.650Ma) metasediments, the Metagabbro Gneiss Suite (475-463Ma) and the Oughterard Granite (~462Ma) (Friedrich and Hodges, 2016). Silurian and Ordovician sediments and volcanics (Leake and Tanner, 1994) occur to the North and South while to the east the Carboniferous limestones are in faulted contact (Lees and Feely, 2016). To the south lie the younger Caledonian Galway granites (~425-380Ma; Feely et al., 2018).

The Connemara Marble

The Connemara marble occurs within the Connemara Marble Formation that belongs to the Lower Dalradian and is a metamorphosed impure siliceous dolomitic limestone (Leake et al., 1975). Its mineralogy includes olivine, diopside, tremolite, talc, chlorite, calcite and dolomite. Later hydrothermal metamorphism triggered pervasive serpentinisation of olivine, diopside and tremolite (Leake et al., 1975; Feely et al., 2019). The stone exhibits intricate millimetre- to metre-scale corrugated layers that range from white through sepias to various shades of green. Five Connemara Marble quarries (Figure 1) occur along an E-W corridor between Clifden and Recess. There is a rich heritage of quarrying the

marble and its use as a decorative building stone in civic and ecclesiastical buildings in Ireland, the UK and the USA. The Connemara marble is an important gem material widely used in jewellery and souvenir gift items during the 19th and early 20th century. The deep green variety known as Irish Jade was in high demand and the manufacture of green Connemara Marble jewellery at this time put this marble from the west of Ireland on the world stage of much sought after gemstones. Birmingham (UK) was one of the major centres for the manufacture of Connemara marble jewellery. Harry Grant & Co., Torquay, UK (1847- early 1980s), produced a large range of silver and gold jewellery inlaid with Connemara marble (Figure 2). The Design and Craft Council of Ireland are advocating special EU protection for the Connemara marble because they believe it qualifies for Protected Geographical Indication (PGI) status as it is unique to Connemara.

Figure 2. A range of Connemara marble jewellery items showing iconic Irish symbols e.g. shamrock, harp, St Bridget's Cross (Connemara Marble Visitor Centre, Moycullen).

Connemara Sapphire

Sapphire bearing hornfelsed desilicated pelitic xenoliths within the 470 Ma metagabbros of Connemara's Grampian Metagabbro-Gneiss Suite occur at two localities i.e. Lough Whelaun and Toombeola. A sapphire bearing erratic of similar lithology containing visible (~5mm) and micro-sapphires (<1mm), was discovered on the granite island of Lettermore, south Connemara (Figure 3). Well established constraints on the timing of magmatism and on metamorphic conditions show that colourless corundum and a hercynite-magnetite spinel formed 470 Ma ago at > 900°C. The spinel later (~468 Ma) unmixed to form sapphire, and magnetite at temperatures of ~750°C and 3.5–6 kb. Consideration of global sapphire occurrences indicates that sapphire can form over a wide range of P and T i.e. greenschist to granulite facies; the Connemara sapphire formed during contact granulite facies metamorphism (Feely et al., 2017).

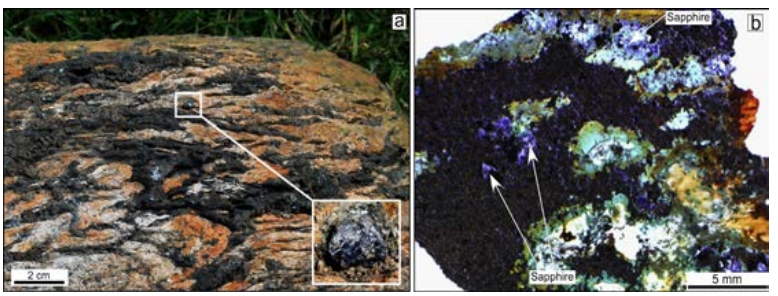

Figure 3. a) The sapphire-bearing granulite hornfels erratic from the island of Lettermore, south Connemara with visible sapphire (~5mm). b) Photomicrograph of micro-sapphire crystals with magnetite patches.

Connemara Fluorite

A vein of gem quality fluorite has been recently (2015) exposed in Larkin's Shannapheasteen Granite Quarry (Figure 4). The vein, probably Upper Triassic in age (Jenkin et al., 1997), also contains galena, chalcopyrite, sphalerite and pyrite, together with quartz, calcite and barite and is similar to other base metal veins in and around the Galway Granite Complex. This mineralization in Connemara is broadly synchronous with, and is similar to other Triassic-Jurassic mineralization in the N. Atlantic margins and Europe. The fluorite varies from deep to light purple and green in colour. Rare bicolour (clear and deep purple) crystals are also observed and these are the most sought after specimens from this quarry and have made an impact on the international mineral collector's market. Euhedral crystals are commonly found with a combination of cube and octahedron forms and rare pyritohedron-cube crystal combos. Numerous inclusions are visible within the crystals mainly two-phases (liquid+vapour) but three-phase (liquid+vapour+solid) and monophase inclusions are also present. Under LW UV light the crystals display a brilliant purple fluorescence.

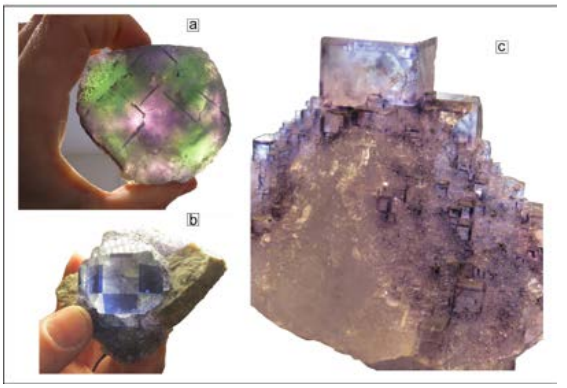

Figure 4. Three examples of gem quality fluorite from Larkin's Shannapheasteen Granite Quarry. a) A backlit crystal of green to purple fluorite (5cm across); b) a bicolour single fluorite crystal (4 cm across) showing a combination of cube and octahedron forms. The octahedral faces possess the darker purple hue; c) an aggregate of cubic fluorite crystals of ~10cm in height. The darker purple hue is evident at the crystal edges.

References

Feely, M., Gaynor, S., Venugopal, N., Hunt, J., Coleman, D.S., 2018. New U-Pb zircon ages for the Inish Granite Pluton, Galway Granite Complex, Connemara, Western Ireland. Irish Journal of Earth Sciences 36 (2018), 1-7

Feely, M., Leake, B.E., Costanzo, A., Cassidy, P., Walsh, B., 2017. Sapphire occurrences in Connemara: field and mineralogical descriptions from an erratic, and from bedrock in the Grampian Metagabbro Gneiss Suite. Irish Journal of Earth Sciences, 35, 45-54.

Feely, M., Wilton, D., Costanzo, A., Koller, J., Joyce, A., 2019. Mineral Liberation Analysis and Scanning Electron Microscopy of Connemara Marble: new mineral distribution maps of an iconic Irish gem material. The Journal of Gemmology, 36 (5).

Friedrich, A.M. and Hodges, K.V., 2016. Geological significance of $^{40}Ar/^{39}Ar$ mica dates across a mid-crustal continental plate margin, Connemara (Grampian orogeny, Irish Caledonides), and implications for the evolution of lithospheric collisions Canadian Journal of Earth Science 53, 1258-1278.

Jenkin, G.R.T., O'Reilly, C., Feely, M. & Fallick, A.E., 1997. The geometry of mixing of surface and basinal fluids in the Galway Granite, Connemara, Western Ireland. In: Hendry, J., Carey, P., Parnell, P., Ruffell, A. & Worden, R. (eds), Proceedings of Geofluids II '97. ISBN 1-897799-83-7. 374-377.

Leake, B.E. and Tanner, P.W.G., 1994. The geology of the Dalradian and associated rocks of Connemara, Western Ireland. Dublin. Royal Irish Academy.

Leake, B.E., Tanner, P.W.G. & Senior, A., 1975. The composition and origin of the Connemara dolomitic marbles and ophicalcites, Ireland. Journal of Petrology, 16(1), 237-257.

Lees, A. and Feely, M., 2016. The Connemara eastern boundary fault: a review and assessment using new evidence. Irish Journal of Earth Sciences 34, 1-25.

Pracht, M., Lees, A., Leake, B.E., Feely, M., Long, B., Morris, J. and McConnell, B., 2004. Geology of Galway Bay: A geological description to accompany the Bedrock Geology 1:100,000 Scale Map Series, Sheet 14, Galway Bay. Dublin. Geological Survey of Ireland.

JADEITITE DEPOSIT FROM KHAMTI, SAGAING REGION, MYANMAR

Cho Cho[1], Thet Tin Nyunt [2]*, Tay Thye Sun [3] and Tin Kyaw Than[4]

[1] Myanma Gems Enterprise, Nay Pyi Taw, Myanmar
[2] Deputy Director General, Department of Higher Education, Ministry of Education, Nay Pyi Taw, Myanmar
[3] Far East Gem Lab, 12 Arumugam Road, #04-02 LTC Building B, Singapore 409958
[4] Principal, Gemmological Science Centre, No. 59, 3rd Floor, 27th Street, Pabedan Township, Yangon, Myanmar
* corresponding author: thettinnyunt@gmail.com

Keywords: Natmaw, Khamti, Jadeitite, jadeite, eclogite, omphacite, garnet, glaucophane, albitite

Abstract

The world's largest commercial production source of jadeitite is the Pharkant-Tawmaw Jade Mine Tract, Kachin State, northern Myanmar and Natmaw (also spelled Nammaw) and Nansibon Jade Mine Tract, Khamti (Hkamti) Township, Sagaing Region. Natmaw is located about 80 km southeast of Khamti in Sagaing Region. It is bounded by Latitudes 25° 53' 13.79"N and 25° 57' 05.73"N and Longitude 95° 55' 20.78"E and 95° 58' 14.23"E (Figure 1)(Cho Cho, 2016). The exposed rock units are granodiorite, serpentinized peridotite, eclogite, complex schists, sandstone and shale interbedded unit, sandstone and conglomerate interbedded unit and alluvium. Serpentinized peridotite is the most abundant unit and schist unit is the second most abundant, including graphite schist, mica schist, chlorite schist, epidote schist and glaucophane schist (blue schist). Jadeitite is found in serpentinite mélange associated with high-pressure low-temperature (HP/LT) metamorphic rocks, such as eclogite and blueschist. The serpentinized peridotite is host rock for primary jadeitite dikes or veins in Natmaw area which are associated with albitite, albite-jadeite unit, amphibolite and blackwall zone (Figure 2). Natmaw jadeitite dikes or veins are surrounded by blackwall zone (such as chlorite zone, amphibolite zone) which is similar to that of Tawmaw jadeitite dikes. Jadeite is the principal constituent mineral in jadeitite and accessory minerals include amphiboles (glaucophane, actinolite and tremolite), kosmochlor, omphacite, albite, phlogophite and chromite. Jadeitites from Natmaw can be subdivided in three groups of textures: (i) primary (ii) deformed and (iii) recrystallized. In the first group, the rocks are coarse-grained with granoblastic or granular texture, radiated texture, porphyritic texture and some crystals are chemically zoned; such rocks can be porous and thus are rarely seen as gem quality even green in colour. In the second group jadeitites are finer grain size, generally formed by metamorphism and deformation of the coarse-grained jadeitites, with textures showing variable fibroblastic or fibrous texture, foliated texture, cataclastic texture, and the third group shows recrystallized texture and corona texture (Figure 3)(Cho Cho, 2016). The best quality jadeitite is related to the transparency which are the consequence of texture and are evidence of their formation (Figure 4)(Shi et al, 2009b). A small block of eclogite and garnet amphibolites are found in the Makyan stream near the jadeitite body. The main constituent minerals are omphacite and garnet porphyroblasts with minor amphiboles (glaucophane) and greenish micas and epidote in eclogite and glaucophane, garnet, hornblende and actinolite in amphibolite. P-T condition of Natmaw jadeitite and associated metamorphic rocks (glaucophane schist and amphibolite) which is about 1.6-2.2 GPa and 470-590°C (Cho Cho & Thet Tin Nyunt, 2018), can be compared with similar lithological and mineralogical characteristics of the previous research works from Pharkant-Tawmaw jade mines area (Thet Tin Nyunt, 2009).

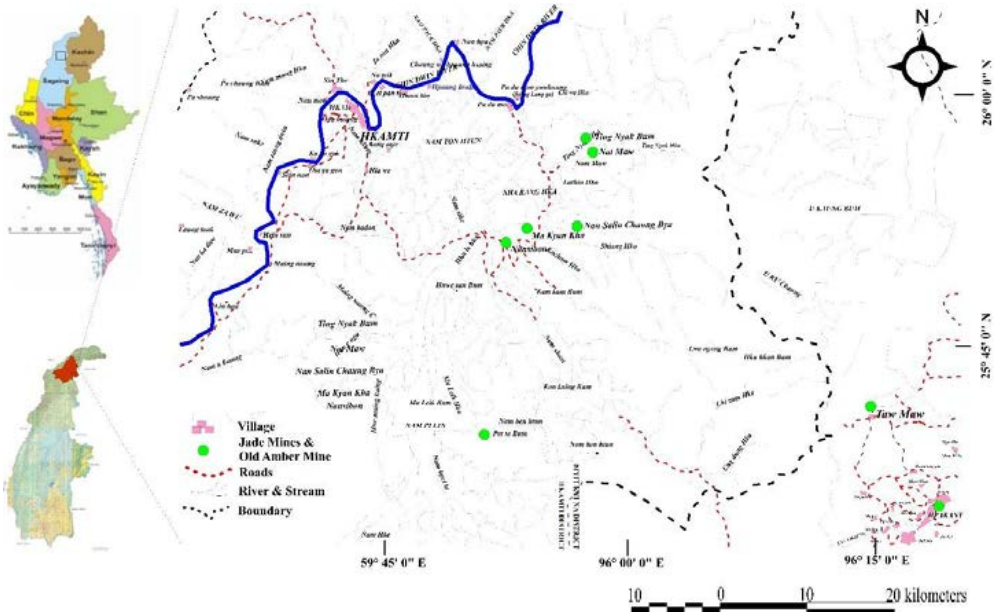

Fig. 1 Location map of the Khamti Jade mine area.

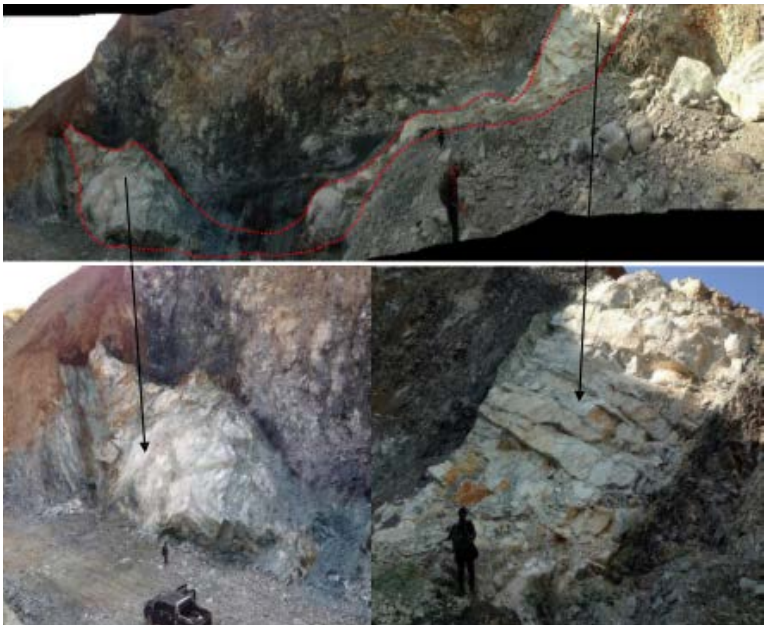

Fig. 2 Outcrop nature of jadeitite in serpentinized peridotite with blackwall association; Outcrop nature of jadeite dyke at Natmaw, Khaing Nan Shwe worksite, trending is 43°- 223°(NE-SW).

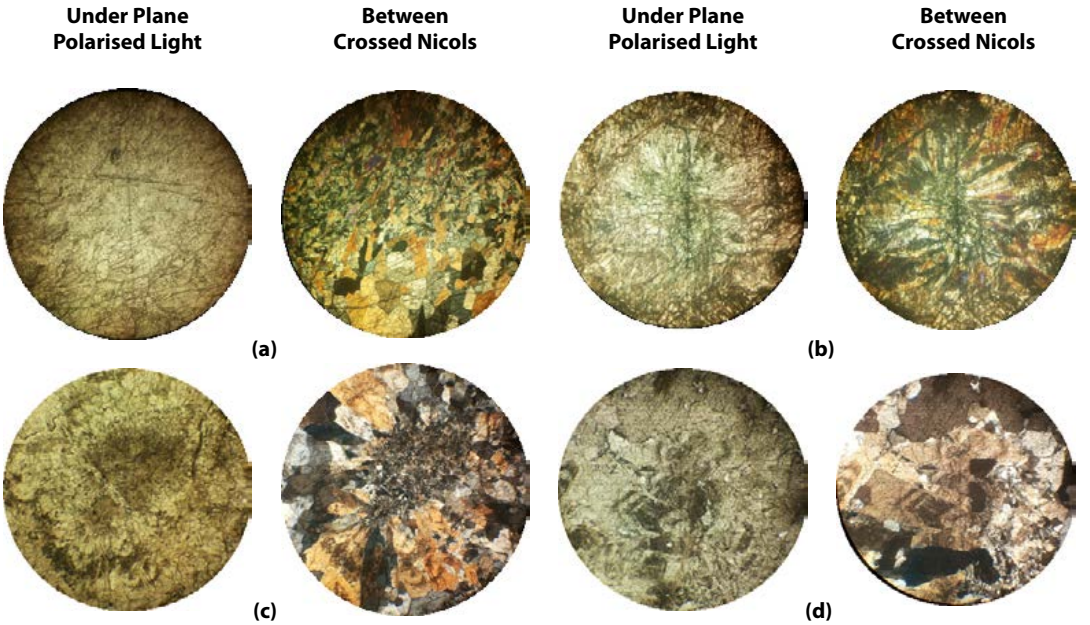

Fig. 3 Some textures of Khamti Jadeitites: (a) Granular or granoblastic texture, A4, (b) Radiated texture, NLP; (c) Radiated texture and zoning, E-31 and (d) Oscillatory zoning in jadeite, E-31, 4xs.

Fig. 4. Jadeite from Khamti, Sagaing Region, Myanmar.

Acknowledgement
We are very grateful to H.E Prof. Dr Myo Thein Gyii, Union Minister, Department of Education, Union of Myanmar and Dr Thein Win, Director General, Department of Higher Education, Ministry of Education, Prof. Dr Day Wa Aung, Head of Geology Department and also Prof. Dr Htay Lwin, Department of Geology, University of Yangon for their permission to study this area. We also express our sincere thanks to Khaing Nan Shwe Co., for their generous support and also to Daw Ma Gjam, Ko Aung Naing, Dr Ko Hein for providing financial support to attend the International Gemmological Conference (IGC), Nantes, France.

References

Cho Cho, 2016. Mineralogy and occurrences of jadeite jade and associated rocks from Natmaw area, Hkamti Township, Sagaing Region, Unpublished, M.Sc. (Thesis), Department of Geology, Yangon University, 101 p.

Cho Cho and Thet Tin Nyunt, 2018. Petrology and occurrence of eclogite and glaucophane-bearing rocks around Khamti-Natmaw jade mine area, Sagaing Region, The Second Myanmar National Conference on Earth and Sciences, Hinthada.

Shi, G.H., Wang, X., Chu, B.B. & Cui, W.Y., 2009b. Jadeite jade from Myanmar: its texture and gemmological implications. J. Gem., 31, 185–195.

Thet Tin Nyunt. 2009. Petrological and Geochemical Contribution to the Origin of Jadeitite and Associated Rocks of the Tawmaw Area, Kachin State, Myanmar. Doctoral Dissertation. Institut für Mineralogie und Kristallchemie der Universität Stuttgart, 176 p.

SPINELS FROM SRI LANKA

Gamini Zoyza[1], Pantaree Lomthong[2], Dietmar Schwarz[3], Chen Yanyu[4], Arūnas Kleišmantas[5]

[1] Ceylon Gemmological Services, Colombo 3, Sri Lanka : gaminigz@hotmail.com
[2] ICA GemLab, Bangkok, Thailand : pantaree@icagemlab.com
[3] ICA GemLab, Bangkok, Thailand :drdietmarschwarz@hotmail.com
[4] TGI Tongji University,Shanghai, China :
[5] Department of Geology and Mineralogy, Vilnius University, Lithuania: arunas@kleismantas.eu

Keywords: chemical fingerprinting, spectral fingerprinting, internal features

More than three hundred fifty unheated, faceted spinels (mostly of gem quality) ranging in weight from 0.06 to 4.05 carats were fully documented for this study. They originate from the following mining areas: Horana (181 samples), Eheliyagoda (77 samples), Ratnapura (32 samples) and Okkampitiya (58 samples); these are all located in the so-called Highland Complex (Figure 1).

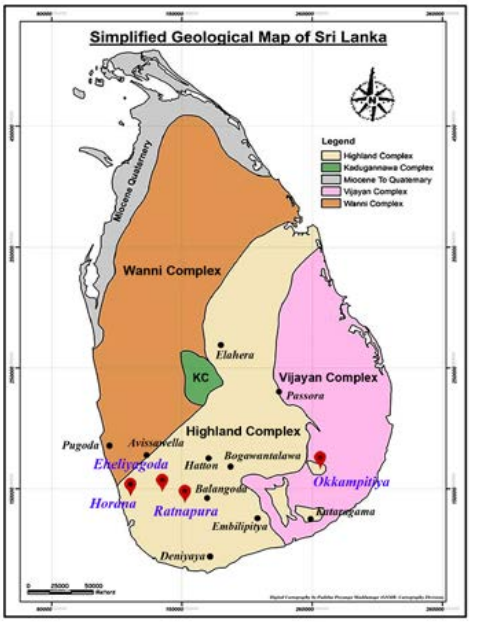

Figure 1: The geological map of Sri Lanka with lithotectonic subdivisions. The locations of the spinel sampling areas used in this study are indicated (after Zoysa, 2019).

The mineralogical-gemological documentation of the samples included UV-vis-NIR spectroscopy, FTIR spectroscopy, RAMAN spectroscopy (detection of heat treatment), chemical fingerprinting (using EDXRF and LA-ICP-MS) and the study of the internal features (using gem microscope and LASER RAMAN spectroscope for the identification of solid inclusions). The color of the analyzed spinels typically varied from pink-to-red, orange, purple-to-violet with some green-to-blue stones.

The gemological properties (especially the internal features) of spinels have been discussed in many papers (e.g. Gübelin and Koivula, 2008; Malsy and Klemm, 2010; Huong et al., 2012). The most interesting inclusion type in the internal world of spinels are the solid inclusions. A huge variety of mineral inclusions (representing the internal mineral association) has been identified. These reflect the nature of the external mineral associations in which spinels have formed in different genetic environments.
The internal features of the spinels from all four Sri Lankan locations are characterized by the presence of different inclusion minerals. Unhealed and healed fissures (mostly displaying typical "spinel textures") are common, growth structures are generally only poorly developed. Figure 2 gives some examples of internal features observed in spinels from Eheliyagoda (left), Horana (center) and Okkampitiya (right). Kleismantas et al. (2017) identified the following inclusion minerals in "Sri Lanka" spinels (using scanning electron microscope): paragonite, clinochlorite, biotite/phlogopite, florensite, baddeleyite, zircon, pyrite, diopside, chlorite and magnesite.

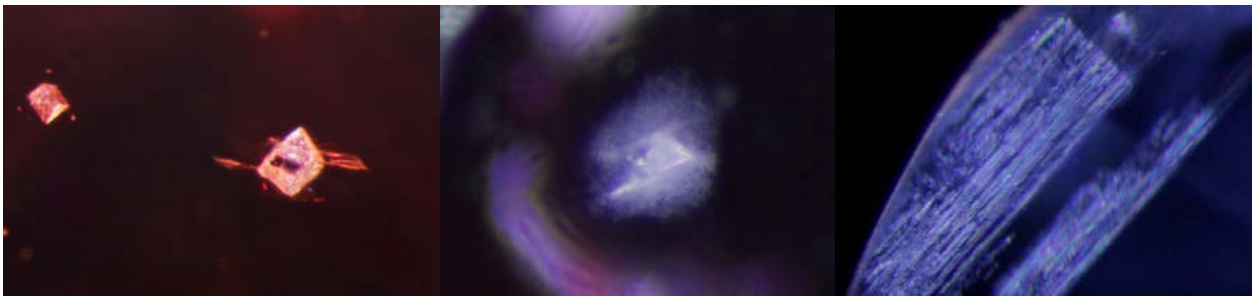

Figure 2: (from left to right) octagonal crystals; crystal surrounded by tiny particles in a cloud-like formation; bands with iridescent, needle-like inclusions.

The chemical properties of spinels originating from various locations (especially those situated in the SE-Asian ruby belt) have been published by different authors. Peretti et al. (2015) found the trace elements Li and Be in natural spinels from different origins. The elements Si, Ti, V, Cr, Zn and Ga are highly variable, they were detected in many natural spinels and in synthetic spinel from Russia (except Zn). In the spinels from Burma, Vietnam, and Tajikistan, analyzed by Malsy and Klemm (2010), the elements V, Cr, Fe, and Zn were commonly present in highest concentrations, whereas Ti, Ga, and Mn contents were generally low. Traces of Li, Be, Co, Ni, Cu, Zr, and Sn were detected, other investigated elements were below the detection limit.

Table 1 illustrates the chemical fingerprinting of the spinels examined for this study using EDXRF-data. It is structured considering the four locations and four "color groups" (pink-to- red, orange, purple-to-violet, blue-green). The following elements are discussed in detail: vanadium, chromium, iron and zinc. The lower limit for the element gallium in Sri Lanka spinels is about 0.01 wt.% Ga_2O_3; the upper limits measured were 0.05 for Eheliyagoda, 0.06 for Horana and Okkampitiya and 0.08 for Ratnapura spinels. The manganese content is often below the detection limit in Sri Lanka spinels; the upper MnO-limits found were 0.05 wt.% for Eheliyagoda, 0.10 wt.% for Horana, 0.11 wt.% for Okkampitiya, and 0.07 wt.% for Ratnapura. Figure 3 shows the correlation diagram [Cr_2O_3] vs [V_2O_3] for pink-to-red and orange Sri Lanka spinels.

In Figure 4, the representative UV-vis-NIR absorption spectra for pink-to-red, orange, purple- to-violet and blue-green Sri Lanka spinels are shown. They are combination spectra with variable ratios of the spectral components [Cr^{3+}], [V^{3+}] and [Fe^{2+}]. Detailed studies on the color and absorption behavior of spinels from Burma, Vietnam and Tajikistan were published by Malsy et al. (2012) and Huong et al. (2012). Peretti et al. (2015) distinguish three color groups (purple to green - brown or orange-red - pink to vivid red) to describe and compare Burmese spinels from Mogok and Namya. Malsy and Klemm (2010) give the following assignments of absorption bands (based on literature data and general principles of ligand field theory). Absorption maxima at about 410 and 540 nm are attributed to Cr^{3+} and maxima at

391 and 558 nm to V^{3+} at octahedral sites. As natural spinels usually contain both elements, a superposition of the individual absorption is present. Purple spinels with dominant amounts of iron showed absorption maxima at 372, 387, 457 and 544 nm. Investigations of that authors by Mössbauer spectroscopy indicate Fe^{2+} at tetrahedral sites responsible for these maxima, except a broad band at 544 nm, which results from superimposition of Cr and Fe.

Table 1: Chemical fingerprinting of spinels from Sri Lanka.

Locality	Color	V_2O_3	Cr_2O_3	Fe_2O_3	ZnO
Eheliyagoda	Pink-Red	0.04-0.89	0.03-0.66	0.11-0.55	0.04-1.55
	Orange	0.10-1.06	0.01-0.17	0.05-0.48	0.02-1.35
	Purple-Violet	0.01-0.15	0.01-0.22	0.21-1.33	0.08-0.78
	Blue-Green	0.01-0.02	bdl-0.01	0.69-1.18	0.06-0.47
Horana	Pink-Red	0.02-1.67	0.01-1.32	0.05-1.57	0.03-3.42
	Orange	0.25-0.96	0.01-0.32	0.05-0.60	0.05-1.11
	Purple-Violet	0.02-0.08	bdl-0.09	0.21-1.23	0.05-0.97
	Blue-Green	0.01-0.07	0.06-0.99	0.21-2.08	0.13-3.92
Okkampitiya	Pink-Red	0.01-1.36	0.06-0.99	0.21-2.08	0.02-1.36
	Orange	0.23-0.76	0.03-0.17	0.06-0.48	0.05-1.71
	Purple-Violet	bdl-0.10	0-0.15	0.41-1.92	0.04-0.37
	Blue-Green	bdl	bdl	1.04-3.38	0.47-1.53
Ratnapura	Pink-Red	0.01-0.23	0.01-0.20	0.38-0.88	0.05-0.61
	Orange	0.21-0.65	0.01-0.08	0.05-0.31	0.05-0.61
	Purple-Violet	0.01-0.03	bdl-0.09	0.47-2.35	0.06-0.62
	Blue-Green	0.01-0.02	0-0.02	0.60-5.04	0.07-3.54

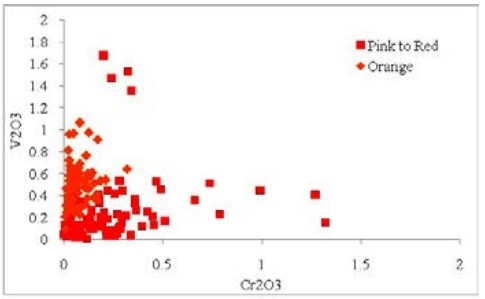

Figure 3: Correlation diagram [Cr_2O_3] vs [V_2O_3] of pink-to-red and orange Sri Lanka spinels.

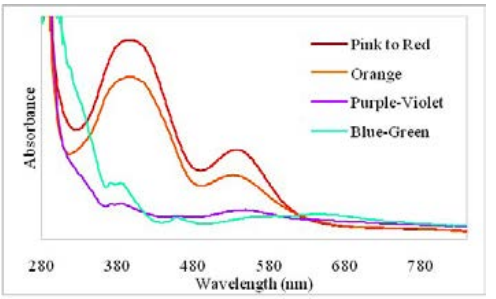

Figure 4: Representative UV-vis-NIR absorption spectra of Sri Lanka spinels.

A random selection of ca. seventy samples were tested for heat treatment using RAMAN- and FTIR spectroscopy. All samples did show no indications for heat treatment.

References

Chauvire, B., Rondeau, B., Fritsch, E., Ressigeac, P., Devidal, J. -L., 2015. Blue Spinel from the Luc Yen District of Vietnam, Gems & Gemology, 51 (1)

Fernando, G.W.A.R., Attanayake, A.N.B., Hofmeister, W., 2005. Corundum-Spinel-Taafeite- Scheelite bearing Metasomatites in Bakamuna, Sri Lanka: Modeling of its Formation. Proceedings of the International Symposium, Hanoi, September 26-October 2, 2005, 117-122.

Gubelin, E.J., Koivula, J.I., 2004, Photoatlas of Inclusions in gemstones. Spinel and its inclusions, 372-382.

Huong, L.T.T., Hager, T., Hofmeister, W., Hauzenberger, C., Schwarz, D., Long, P.V., Wehrmeister, U., Khoi, N.N., Nhung, N.T., 2012. Gemstones from Vietnam: An update. Gems & Gemology, Vol. 48, No. 3, pp. 158-176.

Kleismantas, A., Zoysa, G.E., Shang I, E.L., 2017. Chemistry and gemological features of spinels from Sri Lanka and Vietnam. 35th IGC, Windhoek, Namibia.

Malsy, A., Klemm, L., 2010. Distinction of Gem Spinels from the Himalayan Mountain Belt. Chimia 64, No. 10, 741-746.

Malsy, A.-K., Karampelas, S., Schwarz, D., Klemm, L., Armbruster, T., Tuan, D.A., 2012. Orangey-red to orangey-pink gem spinels from a new deposit at Lang Chap (Tan Huong- Truc Lau), Vietnam The Journal of Gemmology, 33, 1-4, 19-27.

Peretti, A., Kanpraphai-Peretti, A., & Gunther, D., 2015 World of magnificent spinel: Provenance and identification. Contributions to Gemmology, 11,293pp

Phyo, M.M., Bieler, E., Franz, L., Balmer, W., Krzemnicki, M. S., 2019. Spinel from Mogok, Myanmar - A detailed inclusion study by Raman Microspectroscopy and scanning electron microscopy. The Journal of Gemmology, 36 (5),2019, 418-435

Schmetzer, K., Haxel, C., Amthauer, G., 1989. Colour of natural spinels, gahnospinels and gahnites, Neues Jahrbuck fur Mineralogie Abhandlungen, 160, 2 , 159-180

COLOR ORIGIN OF THE OREGON SUNSTONE -THE REABSORPTION AND EXSOLUTION OF CU INCLUSIONS

Chengsi Wang[1], Andy Shen [1*], Aaron Palke [2], Peter Heaney [3]

[1] Gemmological Institute, China University of Geosciences, 388 Lumo Road, Wuhan, Hubei, China, 430074, *578871876@qq.com
[2] Gemological Institute of America, 5431 Armada Dr, Carlsbad, CA, USA, 92008
[3] Department of Geosciences, Pennsylvania State University, University Park, PA, USA, 16802,
* 1469209352@qq.com

Keywords: Oregon Sunstone, Nanoparticle inclusions, Colour origin

Oregon sunstone, a variety of gem quality plagioclase ($Ab_{30-50}An_{70-50}$), is known for its unique optical property which produces very appealing, transparent, red and green colours and even shows the apparent aventurescence effect of pure native copper flakes in the crystal. Because of the popularity and high value of Oregon sunstones, the artificially diffused imitations appeared in the gem market since 2002 and raised concern for gemmological institutes around the world (Rossman, 2011). Our previous research showed that the red colour of both natural and artificially diffused Oregon sunstone was caused by Cu nanoparticles with a diameter of approximately 10 nm (Figure 1) in the crystal, as a consequence of localized surface plasmon resonance (LSPR) (Wang et al., 2018). In further experiments, we found that samples diffused for ten days (D01-1) and three days (AD707) in the same conditions can develop a similar colour appearance (Figure 2). The result made us recognise that the colour may form during the low-temperature cooling-down process instead of the high-temperature diffusion process. Based on the existence of nanoparticles and previous research (Hofmeister and Rossman, 1985), we assumed that the formation of nanoparticles in the crystal is a process of exsolution. To confirm this hypothesis, we did a series of heat treatments and recorded the reabsorption and exsolution of the inclusions and red colour. Gemmological properties of samples mentioned in this abstract are listed in Table 1.

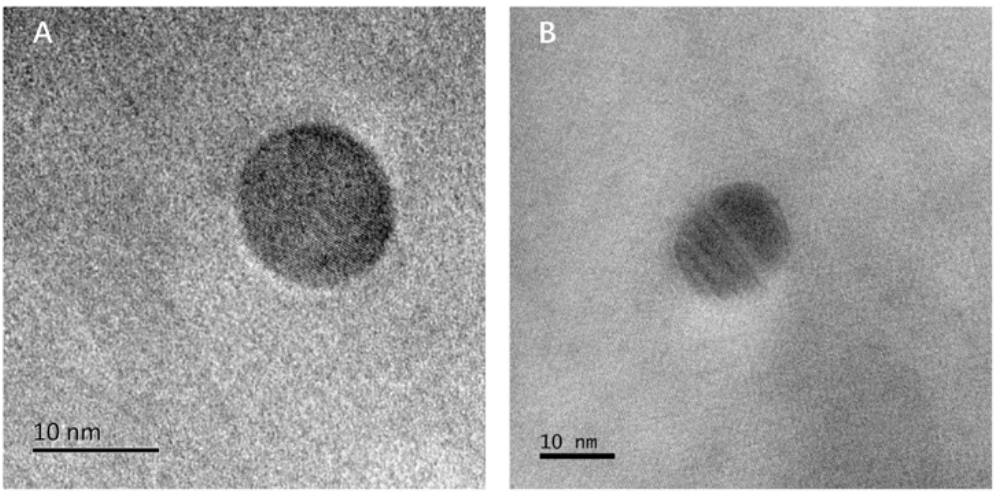

Figure 1. Copper nanoparticles in the natural Oregon sunstone (A) and artificially diffused red sunstone (B).

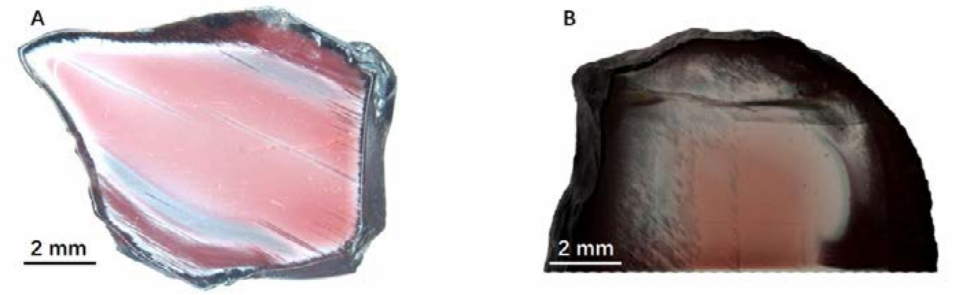

Figure 2. Artificially diffused samples treated for ten days (D01-1) (A) and three days (AD707) (B) at 1170°C in the air with powder of 1% Cu + Zr_2O_3, which have a similar colour appearance.

Table 1. Gemmological properties of samples

Sample Label	D01-1	AD707	AD747	N001-3
Composition	labradorite	labradorite	labradorite	labradorite
Colour Origin	artificially diffused (10 days)	artificially diffused (3 days)	natural	natural
Optical Character	green and red	green and red	aventurescence	red
Weight	0.19 g	0.51 g	0.62 g	0.23 g
Index of Refraction	1.56	1.56	1.56	1.56
Fluorescence	none	none	none	none

A quenching heat treatment was performed to compare with the slow-cooling-down treatment. The red colour in the slow-cooling-down treated sample was significantly more intense than the quenched one (Figure 3), which confirmed that the colour mainly formed under the low temperature. In order to observe the reabsorption process, samples were heated at 1170 °C for 5 minutes and quenched in the air. In the natural glitter sample (AD747), the large platelet inclusions were partially reabsorbed and the small ones entirely disappeared (arrowed in Figure 4). Similarly, the red colour of a natural coloured sample (N001-3) faded after being quenched from 1170 °C. The exsolution experiment was performed at 850 °C for 24 hours, and the colour of the N001-3 sample reappeared (Figure 5). Since the colour is caused by the Cu nanoparticles, we believed that the variation of colour intense is the evidence of the reabsorption and exsolution of the Cu nanoparticles in the crystal. A further transmission electron microscopy (TEM) test is still underway. In addition, spheroid-shaped nanoparticles were found by TEM in the green area of natural samples, which confirmed the role of Cu nanoparticles in the colouration of Oregon sunstone.

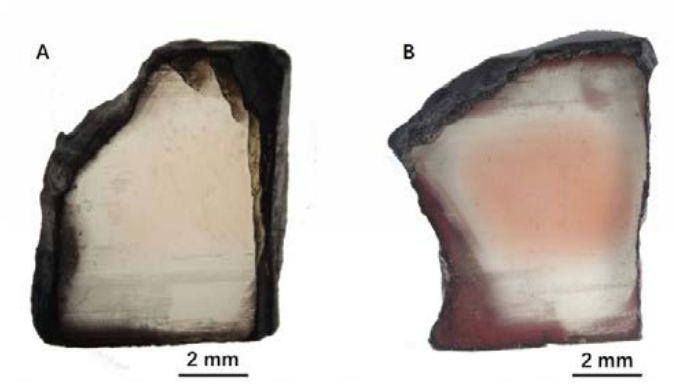

Figure 3. Comparison of the quenched sample (A) and the slow-cooling-down treated sample (B), both of which were cut from the same colourless Oregon labradorite crystal.

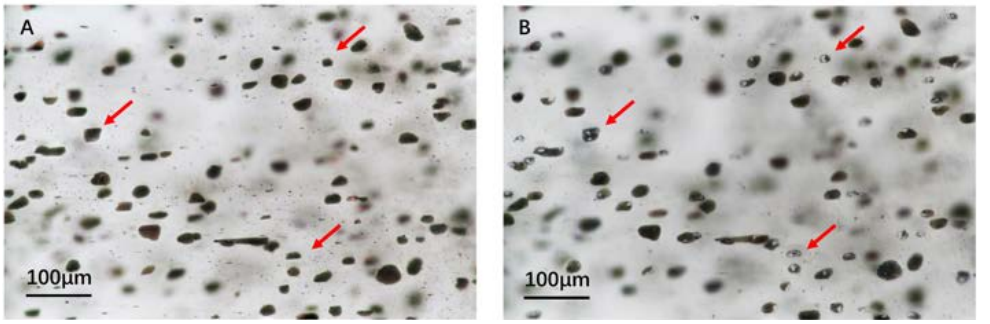

Figure 4. Platelet inclusions in the natural glitter Oregon sunstone (AD747) before (A) and after (B) being quenched from 1170 °C. The small inclusions entirely disappeared, and the large platelets were partially reabsorbed.

Figure 5. Variation of the red colour zone in the natural red sample (N001-3) before treatment (A), after being quenched from 1170 °C (B), and after being held under 850 °C for 24 hours (C). The red colour faded in (B) and reappeared in (C).

References
Hofmeister, A.M., and Rossman, G.R., 1985. Exsolution of metallic copper from Lake County labradorite. Geology, 13(9), 644-647.

Rossman, G.R., 2011. The Chinese Red Feldspar Controversy: Chronology of Research Through July 2009. Gems & Gemology, 47(1), 16-30.

Wang, C., Shen, A.H., Saiyasombat, C., and Krongthong, K., 2018. A Preliminary synchrotron-radiation XAS study of diffusion treatment Oregon sunstone. XXII Meeting of the International Mineralogical Association, Melbourne, Australia, 348 pp.

Acknowledgment
We would like to show our immense gratitude to the Gemological Institute of America (GIA) and Gübelin Gem Lab (GGL) (time-ordered) for their sample and financial support. We also appreciated the suggestions and sample support from Prof. George Rossman.

Introduction to mineralomimetism: the case of photochromic sodalite hackmanite

Féodor Blumentritt[1]*, Emmanuel Fritsch[1], Maria-Teresa Caldes[1], Stéphane Jobic[1]

[1] Institut des Matériaux Jean Rouxel (IMN) & University of Nantes, Faculté des Sciences et des Techniques, 2, rue de la Houssinière, BP 32229 Nantes, cedex 3 France
*feodor.blumentritt@cnrs-imn.fr

Keywords: Hackmanite, mineralo-mimetism, photochromism, synthesis, XRD, XPS

Photochromism can be defined as the reversible color change of a compound typically under ultraviolet illumination (Bouas-Laurent & Dürr, 2001). Other terms are also used to name this phenomenon, such as tenebrescence or darkening. Several gems are reported photochromic in the literature such as sodalite-hackmanite (Medved, 1953; Kirk, 1955; Milisenda et al., 2015; Norrbo et al., 2015, 2016, 2018), scapolite-marialite (Kirk, 1955; McClure et al., 2005), tugtupite (Warner & Andersen, 2012) and others. The ultimate goal of this study is to duplicate interesting behaviors or properties observed in natural minerals and optimize them for a potential industrial application. We call this mineralo-mimetism, to emphasis the parallel with biomimetism. If they are well defined and controlled, photochromic gem-inspired materials could replace organic ones with better (even infinite) cyclability. The fast change from the colored to the colorless state could lead to a new system for data storage for example.
Here we focus on hackmanite, the photochromic variety of sodalite ($Na_8Al_6Si_6O_{24}Cl_2$). This mineral presents a remarkable change of color from near-colorless to deep purple (Figure 1). The crystalline structure of this aluminosilicate contains "cages" holding [Na_4] tetrahedra with an anion at the center (Cl^-, HO^-, CO_3^{2-}, SO_4^{2-},...) (Günther et al., 2015). The substitution of this central anion is believed to induce the photochromism (Figure 2). However, the mechanism behind this phenomenon is not yet fully understood even if some theoretical models involve sulfur polyanions (Norrbo et al., 2015, 2016, 2018; Zahoransky et al., 2016; Curutchet & Le Bahers, 2017).

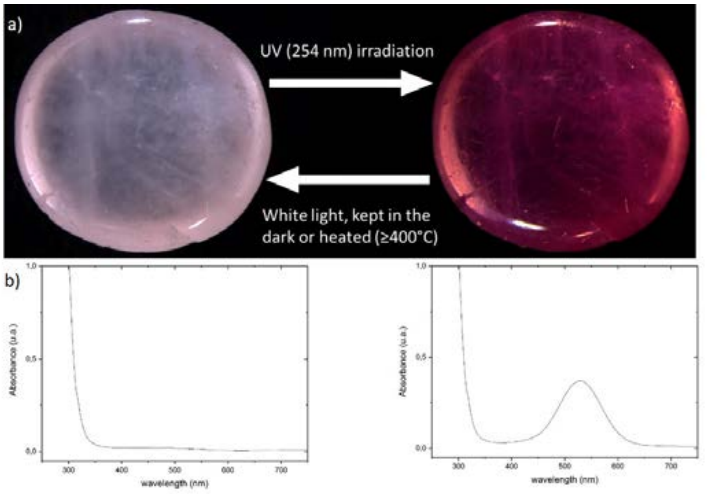

Figure 1: (a)Photochromic sodalite-hackmanite before and after UV (254nm) irradiation during 2 minutes. (b) Corresponding absorption spectra before and after UV irradiation.

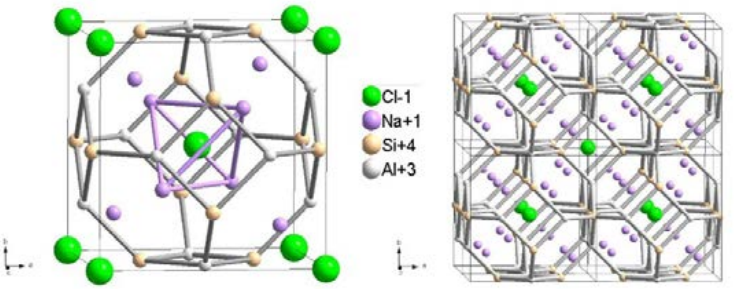

Figure 2: *Structure of the sodalite with the central tetrahedron of [Na4] and Cl inside it.*

Figure 2: Structure of the sodalite with the central tetrahedron of [Na4] and Cl inside it.

Namely, chemical and fluorescence analyses of natural stones (ICPMS-LA, XRF, XPS) do reveal the presence of noticeable amount of sulfur (Medved, 1953; Kirk, 1955). This observation was the starting point of the aforementioned model : chloride (Cl^-) would be substituted by a S_2^{2-}(or more generally S_n^{2-}) ion. The excess of negative charge brought by S_2^{2-} replacing Cl^- would be hence compensated by a chlorine vacancy in an adjoining cage (Curutchet & Le Bahers, 2017).

Here, when irradiated by UV light, electrons of sulfur species are trapped in vacancies creating color centers responsible for the purple color. The charge transfer is followed by a structural relaxation which induces a change in the electronic structure. Once in the colored state, the reverse reaction could occur by irradiating the sample with wavelength corresponding to the new maximum absorption (typically 540nm in chlorosodalite) or by heating the sample. The photochromic reaction could then be written as: $S_2^{2-} + V_{cl}^{0} \rightarrow S_2^{-} + V_{cl}^{-}$.

Whereas the model presented above is consistent with observations, formal justifications are rare, mainly because of the difficulty to analyze sulfur in such natural gems. That is why much work has been devoted to the synthesis of hackmanites (Medved, 1953; Kirk, 1955). It began in the mid XXth century and noticeable improvements have been made since (Williams et al., 2010; Warner & Andersen, 2012). Today, synthesis of hackmanite is relatively easy. Zeolite A ($Na_{12}Al_{12}Si_{12}O_{48}$), halite (NaCl) and sodium sulphate (Na_2SO_4) are used as starting materials, mixed together and heated under reducing atmosphere (e.g. Ar/H_2), to produce photochromic sodalite:

$$5\ Na_{12}Al_{12}Si_{12}O_{48} + 18\ NaCl + Na_2SO_4 = 10\ Na_8Al_6Si_6O_{24}(Cl_{1.8}S_{0.01})$$

Synthetic hackmanites have many advantages compared to naturals such as controlled composition and adaptable stoichiometry. Hence, chlorides in the cage can also be replaced by other halogens (Br, I). Pure bromosodalite and iodosodalite can be synthetized and adding sulfur seems to induce the photochromism in these compounds. Substituting the halogen changes the color of the photo-generated state (Williams et al., 2010).

So far we have analyzed 28 natural hackmanites (24 from Myanmar, two from Quebec, and two from Afghanistan) and synthesized 47 sodalites, mostly sulfur-doped. For the sake of simplicity, we produced powders and not single crystals (which could be achieved with an hydrothermal process). The quality and kinetics of the change was measured with UV-visible absorption spectra. We achieved similar kinetics of change between natural and synthetic samples by modifying the initial sulfate amount. For possible applications, a fast switch is the most desirable. XRD analysis confirms the sodalite structure of synthetic samples. Moreover, we recently initiated XPS analyses to try to prove which sulfur species are involved in the photochromism phenomenon.

Our current researches aim to have an overview of all mechanisms involved in the photochromism of hackmanite. This, or these mechanisms could be extended to other related materials such as scapolite and tugtupite.

References

Bouas-Laurent, H. & Dürr, H. (2001). Organic photochromism (IUPAC Technical Report). Pure and Applied Chemistry 73(4): 639–665.

Curutchet, A. & Le Bahers, T. (2017). Modeling the Photochromism of S-Doped Sodalites Using DFT, TD-DFT, and SAC-CI Methods. Inorganic Chemistry 56(1): 414–423.

Günther, C., Richter, H., Voigt, I., Michaelis, A., Tzscheutschler, H., Krause-Rehberg, R. & Serra, J.M. (2015). Synthesis and characterization of a sulfur containing hydroxy sodalite without sulfur radicals. Microporous and Mesoporous Materials 214: 1–7.

Kirk, R.D. (1955). the Luminescence and Tenebrescence of. American Mineralogist 40(1–2): 22–31.

McClure, S.F., Rossman, G.R. & Shigley, J.E. (2005). Tenebrescent scapolite from Afghanistan. Gems & Gemology 41(Fall): 269–271.

Medved, D.B. (1953). The Optical Properties of Natural and Synthetic Hackmanite. The Journal of Chemical Physics 21(7): 1309–1310.

Milisenda, C.C., Koch, S., Müller, S., Stephan, T. & Wild, M. (2015). Gemstones with photochromism. 34th International Gemmological Conference, Vilnius, Proceedings 107–109.

Norrbo, I., Curutchet, A., Kuusisto, A., Mäkelä, J., Laukkanen, P., Paturi, P., … Lastusaari, M. (2018). Solar UV index and UV dose determination with photochromic hackmanites: From the assessment of the fundamental properties to the device. Materials Horizons 5(3): 569–576.

Norrbo, I., Gluchowski, P., Hyppänen, I., Laihinen, T., Laukkanen, P., Mäkelä, J., … Lastusaari, M. (2016). Mechanisms of Tenebrescence and Persistent Luminescence in Synthetic Hackmanite $Na_8Al_6Si_6O_{24}(Cl,S)_2$. ACS Applied Materials and Interfaces 8(18): 11592–11602.

Norrbo, I., Gluchowski, P., Paturi, P., Sinkkonen, J. & Lastusaari, M. (2015). Persistent Luminescence of Tenebrescent $Na_8Al_6Si_6O_{24}(Cl,S)_2$: Multifunctional Optical Markers. Inorganic Chemistry 54(16): 7717–7724.

Warner, T.E. & Andersen, J.H. (2012). The effects of sulfur intercalation on the optical properties of artificial 'hackmanite', $Na_8[Al_6Si_6O_{24}]Cl_{1.8}S_{0.1}$; 'sulfosodalite', $Na_8[Al_6Si_6O_{24}]S$; and natural tugtupite, $Na_8[Be_2Al_2Si_8O_{24}](Cl,S)_{2-\delta}$. Physics and Chemistry of Minerals 39(2): 163–168.

Williams, E.R., Simmonds, A., Armstrong, J.A. & Weller, M.T. (2010). Compositional and structural control of tenebrescence. Journal of Materials Chemistry 20(48): 10883–10887.

Zahoransky, T., Friis, H. & Marks, M.A.W. (2016). Luminescence and tenebrescence of natural sodalites: a chemical and structural study. Physics and Chemistry of Minerals 43(7): 459–480.

GIANT HELIODOR AND TOPAZ POCKETS OF THE VOLODARSK CHAMBER PEGMATITES, KOROSTEN PLUTON, UKRAINE

Peter Lyckberg[1], Vsevolod Chournousenko[2], Oleksandr Chournousenko[3]

[1]MNHN Museum of Natural History Luxembourg
[2]Volyn Quartz Samotsvety
[3]Geology Department, Zhitomir Polytechnical Institute
Lyckberg@pt.lu

Keywords: Gem Pegmatites, Chamber Pegmatites, Giant Pockets, Heliodor, Topaz, Hydrocarbon Pegmatite

Introduction
The Volyn Piezo Quartz deposit at Volodarsk, Zhitomirskaja Oblast, Ukraine where 1900 chamber pegmatites were mined, produced 75% of former Soviet Unions Piezo Quartz. The first author has studied these deposits in situ since 1995, the Chief geologist has worked here daily for some 30 years and the third author weekly visits since January 2013.

Introduction to the geology and mine development
The Volyn deposit is situated on the western endo contact of the Korosten Pluton. The chamber pegmatites are confined to a 22 km N-S stretching 0.5-1.5 km wide zone. Less known is that such zones also exist on the south and eastern endo contacts of the same pluton. Only those in the south were mined to a very limited extent and those to the east just drilled and found. The Volyn piezoquartz deposit, its official name, was developed by sinking 6 shafts to 100 and 150 m respectively and driving 110 km of main access tunnels on three main horizons at the 50, 100 and 150 m levels from which small access tunnels and shafts were made to reach individual pegmatites in the granite. There were also many open pits mined often including several pegmatites with additional "shurfs" (small shafts)

Historical production of gem material and new finds on the dumps
From the 5 main mines (shafts) tunnels reached from 100 to several hundreds of individual pegmatites within the granite. Mined rock and piezo quartz was taken out through the shafts. When we look at the old logbooks of work from each pegmatite body, we can draw the conclusion that about 10% of miarolitic pegmatite bodies contained also topaz and 2% beryl (fig. 1). Both topaz and beryl occur in large high quality gem quality collectors crystals (Fig 2 & 3 & 4) and were partly overlooked during mining. It was often thrown on the dumps from open pits and from the underground mines. In fact the finest perfectly terminated large gem heliodor crystals, one 8.5 kg flawless gem with sharp termination was found as late as 2008 just 10 cm under the surface of a gravel road leading to an open pit. During Soviet times, Illegal removal of a single fragment of piezo quartz carried punishment while such world class gem beryl and topaz was thrown on the dumps. They were not secret or seen as valuable and were often given as gifts to museums and visiting Soviet Geologists.

For years, the chief geologist leading the mines operations, pumping out shafts, one by one, and re-working each access area pegmatites for years at a time, together with the other authors could study known mineralizations but also study pegmatite structure and mineralizations as well as discover many new mineralizations more in detail than previously done. The pegmatite 464 in Shaft 2 had historically produced 4.2 tons topaz in Soviet times known from old logbook.

Figure 1

Figure 2

Figure 3

New studies and new observations on mineralogy, pocket morphology, gem crystal production

During recent explorations of pegmatite 464, an additionally 1.8 tons topaz was recovered in primarily two large niches high on the wall in the tall, vertically extended chamber thus in total an astonishing 6 ton was produced making it the largest documented producer until that time. It also shows that gem material was not the main concern in the past and or less competence to search for and find the often hidden corners were these are concentrated. In 2017-2018 a former believed "empty pocket" in pegmatite 394 locally referred to as "Skorkina" after a miner who worked there in the 1990's, and named "Vsevolods pocket" after the chief geologist produced a record amount of topaz well surpassing P464 thus setting a new record. Here the second author discovered topaz from 6 to 15 m below the original floor level of the 3 m diameter and 23 m deep chimney like pocket, never studied or recorded from the deposit before. Large amounts of topaz crystals from 100g to 230 kg each were collected as collector's items and as gem rough. This topaz is cognac-colored with strong orange tone in its outer zone, sometimes all through the crystals and a sometimes lighter colored core.

Figure 4

In an open pit exploring pegmatite 206 unique bi colored topaz (figure 5) with triangular crystals of white fluorite was found for the first time right near well terminated unetched helidor crystals. One can not help to wonder about the phase diagram during the topaz-fluorite formation.

Figure 5

Giant Chambers of Pegmatite 521 at 96 m depth
Pegmatite 521 contains two giant chambers, one originally smaller which had produced 100 tons quartz in 1982 in its upper section, the second part of the pocket produced less quartz and measuring 30 by 20 by 15 m tall became world famous for producing very distinct etched heliodor crystals discovered here in 1982 when mining commenced (see figure 1 again). That year alone 1 ton was mined and again in 1992 when the Soviet Union had collapsed an additional ton, of which 900 kg was mined in 5 days by five miners from a dark greenish clay matrix zone.

Recent work in 2018-2019 has exploited the quartz pocket and so far work has opened a 45 m long and up to 25 m wide pocket with a vertical extension of some 20 m. This pocket continues towards the beryl chamber and about 10 m of pocket material wall separate the two. This pocket is the largest known discovered in any granitic pegmatite and final length is estimated to 85 m plus possible extensions in all directions. Some beryl was discovered here, the latest gemmy large doubly terminated one on March 30, 2019 weighing 1437 gram and 17 cm tall, 10 cm diameter and a vertical rehealed crack along its length.

Heliodor beryl crystals may have a concentric color zoning where the outer shell may be of a strong yellow or in rare case orange brown color. In pegmatite 521 pocket the top part of heliodor crystals often have a slightly weaker color and larger crystals often have a re healed irregular fracture at an angle across the c-axis below the termination. There were likely some violent events either due to pocket implosion and/or caving in.

Uncolored Topaz from Pegmatite 404
Pegmatite 404 is a large chamber with a maze of pocket tunnels and shafts below the main chamber lined with white tan Oligoclase crystals. Here all topaz was found to be colorless and much was recovered from the upper wall of the main chamber as well as from a couple of spots along its lower sides and below in small shafts and tunnels. The lack of coloration is certainly interesting and may be due to lack or very low concentration of U and Th bearing minerals in this pegmatite.

Structural observation around and inside the pegmatite and pockets

Interesting to note from a geological and genetic point of view is the cooling contraction fractures around those chamber pegmatites in the granite. The red color of the granite within a zone of half a meter around the pegmatite and is strectched out to depth below and above the pegmatite. Below this zone you will also find oscillatory gravitational fractionation/settling bands of alternating darker and lighter colored granite with bands a few cm wide each.

The quartz core (figure 6) is often fractured concentric with the outline of the pegmatite and pocket as is the feldspars and pegmatite around the pockets. Under the original pockets a typical leached zone, where quartz was leached and deposited in the ceiling as giant quartz crystals. This leached zone is heavily albitized and may contain secondary beryl and topaz. Another peculiarity is the sometimes occurring late stage brecciation and deposition of opal between quartz shards and other pegmatite fragments. At Volodarsk, one pegmatite was famous for fibers of the complex hydrocarbon Kerite.

Figure 6

Kerite and Methane

During 2013 the authors searched for additional kerite containing pegmatites in shaft 3 which had just been pumped out. We discovered numerous cavities with kerite in association with oligoclase feldspar, fluorite, topaz. In pegmatite 394 a 2 m tall open cavity was intersected above the pegmatite at shallow depth. The authors have interpreted this as methane gas was intermixed during the magmatic stage and highly contributed to formation of at least some cavities, likely most if not all. It seems as much gas was trapped in individual pegmatites during formation and contributed to the formation of cavities. Methane has been encountered in pegmatite pockets below 100 m depth, while at shallower levels it seems as through 1,7 Ga of geological events gas has escaped at some point in time.

Typical for the Volodarsk Chamber pegmatites is the before mentioned brecciated quartz and feldspar, often healed by opal. The origin of breccia is not fully understood at this stage but may involve lithostatic implosion of cavity, lithostatic overpressure trapped in the cavity during formation and later released due to tectonic movements and or shallower positioning and/or methane gas release/ignition. In 1955 during drilling a gas filled cavity was encountered at 600 m depth which shot up the entire drill steel out of the hole and toppled the drill tower. It took over half an hour before the highly pressurized gas slowed down its escape out of the hole.

1.7 Ga of Radiation from radioactive isotopes of U, Th, K and their daughter products

The long in situ radiation exposure starting 1.7 Ga ago with radiation primarily from Th232, U235 and U 238, K40 and their daughter products, have caused the color of Al containing quartz to become pitch black (morion) in outer sections while some or parts of some may be citrine and often with a white interior. From the gem perspective, topaz has primarily attained a deep orange color from this radiation, which color will fade with time and light exposure thus to be used as an evening-night stone

RECENT CHALLENGES IN IDENTIFICATION OF FILLED EMERALDS

Gagan Choudhary
Gem Testing Laboratory, Jaipur, India
*gagan@gjepcindia.com

Keywords: emerald, resin-filled, films

Introduction

Identification of fracture filling in emeralds typically involve three well established criteria – observations under a microscope, followed by spectroscopic (infrared and/or Raman) analyses, and fluorescence under ultra-violet light (e.g. Kiefert et al, 1999). Observational features mainly depend on the type of filler i.e. whether oil or resin, and their types, the process of filling (whether traditional or modern), and type of illumination used. 'Traditional' process refers to immersion of emeralds in a bowl of oil from few hours to overnight; occasionally warm oil may be used or the bowl containing oil and emeralds is placed under a lamp for gentle heating. 'Modern' process refers to use of pressure for filling, where heated fillers are forced into the fissure with pressures of up to ~3000 psi or even higher (depending on type of filler and temperature). Due to absence of pressure during fissure-filling, 'traditional' process results in uneven filling and thereby reflecting films (Figure 1) within the fissures, while 'modern' process, commonly used for fillers like resins and few oils, such as cedarwood results in smooth and even filling. Infrared spectroscopy (FTIR), using standard diffused reflectance or direct transmission modes, is the most widely used tool to conclusively identify the type of filler, where oils and resins display distinct sets of peaks.

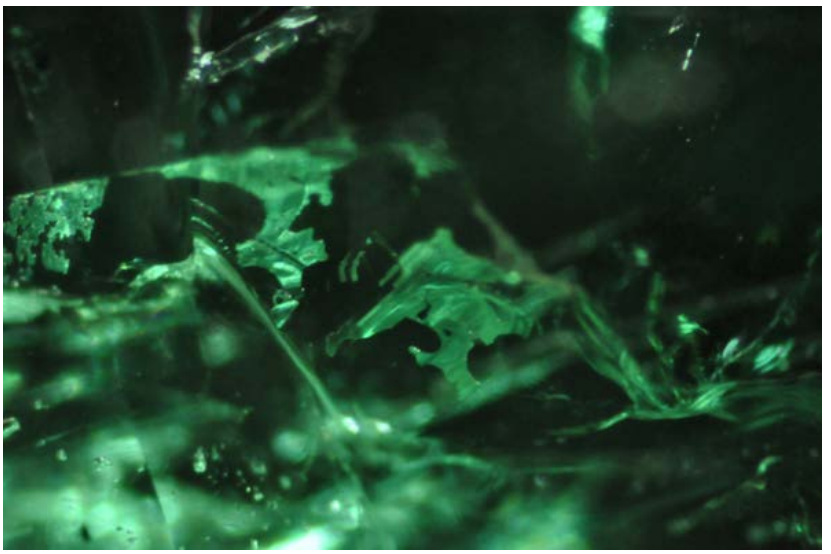

Figure 1: These uneven reflecting films are typically seen in oil-filled stones, using traditional methods, and are being referred to as 'oil-like' films in this presentation. Photomicrograph by Gagan Choudhary; image width: 8.40 mm

The Challenge

Visual Observations

Since the past few months, we at the Gem Testing Laboratory, Jaipur are observing filled emeralds that display uneven films (Figure 2), similar to as described above in figure 1, indicating presence of oil but often with golden reflections (Figure 3). When such fissures are carefully rotated and viewed in vertical direction, they display subtle blue and golden colour flashes (Figure 4), weaker than that typically associated with artificial resins (and some oils, e.g. cedarwood); the observer needs to be extremely careful while observing such stones and one can easily miss these subtle flash-effects. Interestingly, such filling effects are being observed in all qualities of emeralds from low commercial to high commercial, and in various origins.

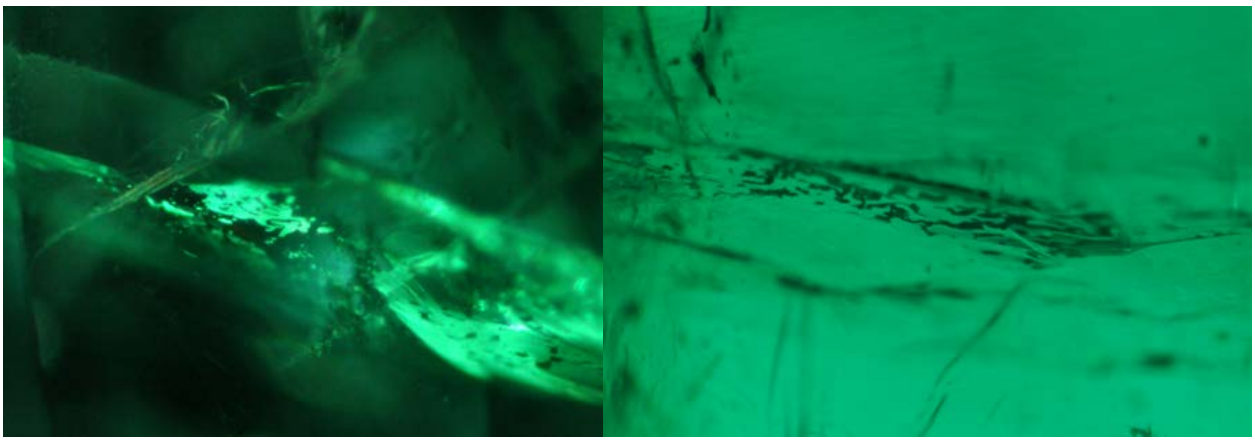

Figure 2: These typical examples of uneven reflecting films in emeralds, associated with 'oil-filling', are areas of concern and recent challenges in filler identification. These emeralds were identified as 'resin-filled', after micro-analyses on FTIR. Photomicrograph by Gagan Choudhary; image width: 6.30 mm (left) and 5.60 mm (right)

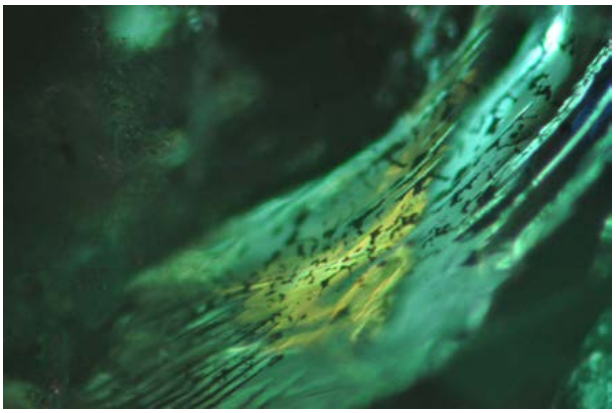

Figure 3: The uneven reflecting 'oil-like' films in resin-filled emeralds, as illustrated in figure 2, are often associated with golden reflections. Photomicrograph by Gagan Choudhary; image width: 6.30 mm

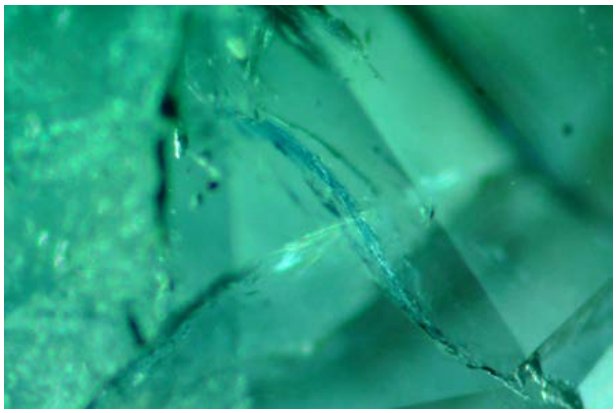

Figure 4: Such subtle blue and golden flash effects easily can be missed during microscopic observations, which is an area of concern, because if the observer is unable to note these weak effects, the emerald will not probably go through detailed micro-analyses under FTIR (microscope) and/or Raman spectrometers. Photomicrograph by Gagan Choudhary; image width: 5.60 mm

Infrared spectral analyses

When such filled stones are analysed in standard diffused reflectance or direct transmission modes of infrared spectrometer, even in several directions, they display features at ~2854, 2927, 2956 and 3010 cm^{-1}, associated with universal oils, only. However, considering the presence of 'subtle' blue and golden flashes, features associated with resins (or cedarwood oil) is expected, but lack of such spectral features intrigue further detailed spectroscopic analyses.

Therefore, a detailed micro-analysis was performed using FTIR, equipped with a microscope, where a single fissure is analysed from several points, although this analyses is a laborious and time-consuming process. Such multi-point analyses under FTIR microscope reveal two sets of features (figure 5) – one set consists of peaks at ~2854, 2927, 2956 and 3010 cm^{-1}, while the other set consists of peaks at ~2872, 2927, 2966, 3035 and 3055/64 cm^{-1}; the first set of peaks is associated with oils, while the second set is related to resins (e.g. Johnson et al., 1999; Kiefert et al., 1999). In many cases, a confocal micro-Raman spectrometer is also used for performing multi-point analyses of a single fissure.

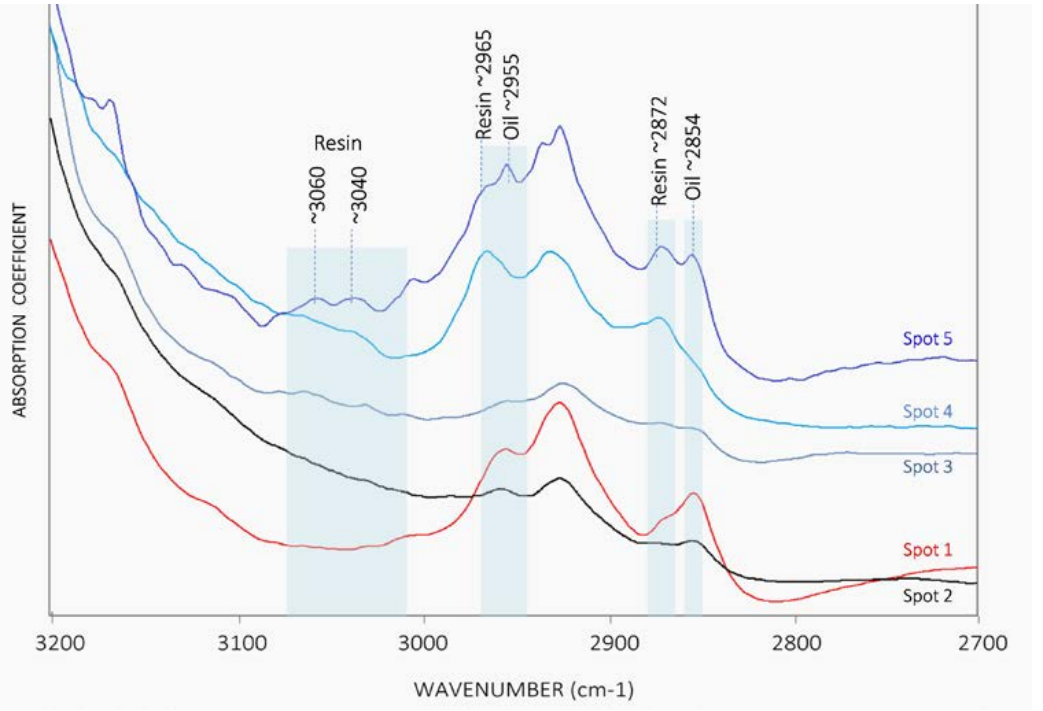

Figure 5: An example of micro-FTIR analyses of a single fissure with uneven 'oil-like' films. Note the shift in peak positions, where spots 1 and 2 (red and black traces) display features associated with universal oil, while spots 3, 4 and 5 (blue traces) display peaks associated with resins, such as opticon, araldite, etc. Analyses using standard diffused reflectance or direct transmission modes, reveal features associated only with universal oil (red and black traces), and may result in (mis)identification of the filler.

Cause of subtle visual and spectral features

So, what causes such visual i.e. reflective films along with a subtle flash effect, and spectral patterns? We don't have a definitive answer to this, but such effects may be a result of instability or inhomogeneity of the filler; or a problem with the filling process i.e. the fissure not cleaned thoroughly before filling, or the required time, pressure and temperatures were not achieved; or the stone has undergone through several generations of filling. To find out the reason for these visual and spectral patterns, we spoke to owners of such stones, and tried to track down the processing line.

As per the available information, such emeralds were never subjected to resin-filling process, but, they were 'only' immersed in oil. However, non-disclosure of an earlier filling on rough itself cannot be ruled out.

On further discussions on processing techniques, some manufacturers revealed that the cutters often apply 'glue' or 'epoxy' at the opening of fissures to prevent polishing compound (such as chromium oxide) to enter into the fissures and/or to prevent the fissures from further expansion, resulting in splitting of the emerald. On the basis of this information, several adhesives including 'epoxy-based' and 'super-glue' types, being used in the Jaipur trade were analysed using infrared and Raman spectrometers for their characterization. Out of the many, only epoxy-based adhesives (e.g. araldite) displayed spectral features similar to those observed in these emeralds, as seen previously for resin-filled stones using opticon, ExCel, Permasafe, etc. Therefore, it may be deduced that the epoxy-based glue applied at the opening penetrates into the fissure due to the pressure created during polishing; and because of lack of proper filling process, it could not fill the fissure completely, resulting in reflective films. However, considering the depth of filling and the flash-effects, this theory is applicable only for few specimens. Further, use of proper filling techniques, such as achieving required pressure (in vacuum) or temperature would have resulted in complete and smooth filling, and hence no such film-effects. Therefore, on the basis of observational and spectroscopic features, we believe that majority of these emeralds have gone through several generations of filling with improper cleaning of pre-existing resin-filled fissures, and refilling with oil.

Conclusions

Reflecting films are not usually associated with resin, therefore, such filled-emeralds can easily be misidentified as 'oiled', also because the majority of filled-emeralds are analysed using diffused reflectance or direct transmission modes of the infrared spectrometer. The challenge remaining here is the observation of 'faint' flash effects! Once the flash effect is detected, it is equally important to focus the infrared laser precisely at several points of a fissure producing 'spot-on' results; alternatively, confocal Raman micro-spectrometer is also very useful in such analyses. Both types of analyses however become a laborious and time consuming process. In our experience, if the flash-effect is missed in microscopic observations, the emerald will not go through micro-analyses in infrared or Raman spectrometers, and hence no resin-related features will be resolved. In such cases, a 'resin-filled' stone may be (mis)identified as 'oil-filled', therefore, it is imperative to observe individual fissures carefully under a microscope from all possible angles.

References

Kiefert L., Hänni H.A, Chalain J-P., Weber W., 1999. Identification of filler substances in emeralds by infrared and Raman spectroscopy. The Journal of Gemmology, 26(8), 501-520

Johnson M.L., Elen S., Muhlmeister S., 1999. On the identification of various emerald filling substances. Gems & Gemology, 35(2), 82–107

A study of Pezzottaite from Pyi-Gyi-Taung, Myanmar

Shang I (Edward) Liu[1], Kyaw Thu[2], Hexiong Yang[3]
[1] The Gemmological Association of Hong Kong, Hong Kong; gemedward@hotmail.com
[2] MACLE Gem Trade Laboratory, Yangon, Myanmar; macle45@googlemail.com
[3] The University of Arizona, Tucson, US

Keywords: Pezzottaite, Pyi-Gyi-Taung, reciprocal lattice

Introduction

Pyi-Gyi-Taung Mountain is located 6km east of Letpanhla village, Singu Township, Mandalay region (Fig 1). There are many LCT type pegmatites distributed over this mountain range producing mainly rubellite (elbaite variety) and pink beryl. Recently, the discovery of "mushroom" (and "wheatsheaf") tourmaline in this area has aroused one of the author's (EL) interest to investigate the unusual pink "beryl". Finally, they are identified to be Cs-, Li-rich beryls and few of them are pezzottaites.

Geology and Production

Pyi-Gyi-Taung area lies in the southern continuation of Mogok Metamorphic Belt (MMB) (Latitude 22°33'52"N and longitude 96°07'58"E, 466m elevation – location of the mine shown in Fig 2). It comprises mainly marble and calc-silicate rocks which intruded by rubellite bearing pegmatite dykes. Structurally, the area is rather complex, consisting of Pyin Gyi Taung anticline with intricate numerous minor folds mostly in calc-silicate rocks. In addition, four minor fault systems of NNW-SSE, NNE-SSW, NE-SW and E-W trending are recognized. Generally, the prominent pegmatites occur as concordant to discordant dykes trending in nearly E-W to NE-SW directions and dipping at 40° - 80°. Most dykes occur in tabular and mostly irregular with long narrow branches. The width of pegmatite dykes are approximately 1 m to 10 m and the length measures about 7 m to 50 m.

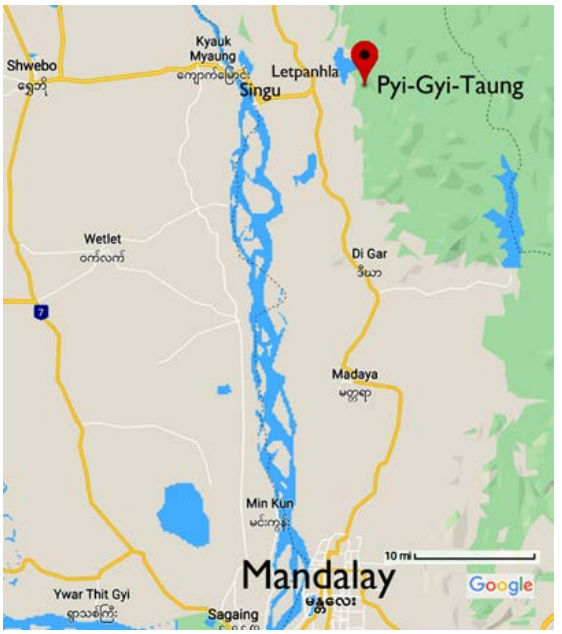

Figure 1. Location of pezzottaite deposits in Pyi-Gyi-Taung. (Image: modified from Google Map)

Figure 2. Shaft mining in Pyi-Gyi-Taung Mountain

Radiometric dating by zircon U-Pb method using LA-ICP-MS indicates that the age of pegmatite is 24.56 Ma (Late Oligocene) (Phyu Phyu Lwin, 2012). These pegmatites are classified as zoned pegmatite, rare-element type and complex lepidolite subtype. The outer zone of the dyke composes mainly albite, perthite, orthoclase and quartz. The core zone is characterized by containing mainly lepidolite, zinnwaldite, cleavelandite, fine-grained rubellite (green, yellow and pink tourmaline) and purple apatite that are generated by pneumatolitic action, and eventually hydrothermal fluid metasomatic alteration.

More than 10 shafts have been found in Pyi-Gyi-Taung area. The gem pits are rather deep (around 25-30 m). This area was originally explored by local miners for rubellite. Recently, they discovered goshenite and pink "beryl" with rock crystal and green tourmaline in some small pockets near the surface. The production of pink "beryl" is small and amounted to about 1kg of crystals in last 5 years. Most of the materials occur in shade of pale pink to milky white colour and subtransparent to translucent with plenty of visible inclusions. They are notable for their prismatic form (size usually 10-20mm, exceptional large crystal can up to 30mm width) and a distinct clear pink banding (cap) at termination (Fig 3a & 3b). Euhedral crystals are common and usually appear in the form of hexagonal prism terminated by basal pinacoid with a length/ width ratio of 1:1-1:2.

(a) *(b)*

Figure 3. Pyi-Gyi-Taung (a) Pezzottaite crystal (46.62 ct- MP1);(b) Cs-, Li-rich beryl crystal (44.44 ct- MP2)

Experimental

Apart from using conventional gemmological instruments, X-ray single-crystal diffraction studies were performed for four crystals of "beryl" with a Bruker X8 APEX2 CCD X-ray diffractometer equipped with graphite-monochromatized MoKα radiation. UV-Vis-NIR spectra were collected using a Gem3000 UV-Vis spectrophotometer. Raman spectroscopy was performed on oriented samples using a TSI SR EZR-A7. Chemistry was determined using CAMECA SX100 Ultra electron probe microanalyzers (EPMA) and also Shimadzu EDX-LE EDXRF Analyzer.

Results

All samples show a higher values for R.I. (ne=1.598 and no=1.607, DR=0.008-0.009) compare to common beryl. Their specific gravity were found to be slightly higher than morganite (average SG=2.85). X-ray single crystal diffraction revealed that sample MP1 consists of both pezzottaite and Cs-, Li-rich beryl, whereas the other three samples are Cs-, Li-rich beryl. The pezzottaite (in the outer rim of MP1) showed a distinct superstructure with additional weak reflections in the beryl diffraction pattern in reciprocal lattice (Fig 4) (Lafuente et al., 2015; Aurisicchio et al., 1988; Liu et al., 2008). Its unit cell parameter: a=b=1.59563(8)nm, c=2.78281(14)nm, c/a ratio=1.7440, alpha=beta=90°, gamma=120°, V=6.1359nm^3; space group = $R\bar{3}c$ (Trigonal system); R=0.0499 for the structure refinement.

Chemical analysis revealed that Pyi-Gyi-Taung Pezzottaite has high Cs contents (Cs_2O up to 14.85 wt.%). Backscattered-electron (BSE) imaging shows that the distribution of Cs contents in sample MP1 is uneven and increase discontinuously from colourless prism and core of Cs-, Li-rich beryl (average Cs_2O=5.67 wt.%) to pink pezzottaite termination (average Cs2O=14.41 wt.%). A thin milky layer which contains less Cs contents (average Cs2O=3.64 wt.%) has been found below the pink layer. Distinct compositional discontinuities reflect fluctuations in fluid chemistry and changing in driving force during the multiple stages of crystallization.

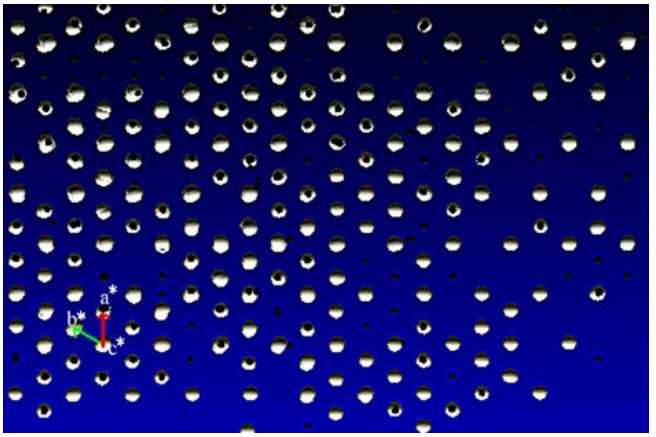

Figure 4 The superstructure diffractions in reciprocal lattice of pezzottaite (View along C)*

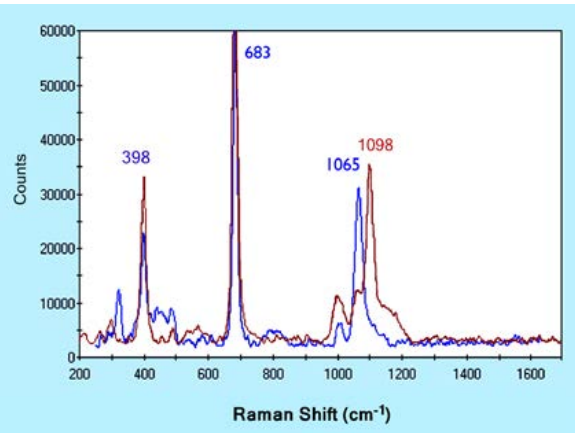

Figure 5 Oriented Raman spectra of Pyi-Gyi-Taung Pezzottaite (Red: along C-axis; Blue: perpendicular to C-axis)

Both pezzottaite and Cs-, Li-rich beryl exhibit similar Raman spectrum with distinct bands at 112 cm^{-1} and 1100 cm^{-1}, which has not been observed in common beryl. The intensity of 1100 cm^{-1} band (corresponding to Si-O-(T) bonds) is highly oriented (Fig 5) (Liu & Peng, 2005). Strong to intense peak may appear where laser beam is oriented along c-axis. However, it becomes very weak (or disappear) when spectra were collected perpendicular to c-axis. Misleading results may be obtained using unoriented samples.

Growth conditions and discussion

Homogenization temperature measurements of fluid inclusions in Madagascar pezzottaite suggested that they were formed in the range of 180-340˚C (Liu et al., 2006). This temperature is in line with the formation temperature of some pegmatites (210-410˚C) in Myanmar (Zaw, 1998). The order-disorder (Be and Li ions arrangement in tetrahedral sites) transformation in the beryl structure was suggested to be happened mainly at relatively low temperature around 180-260˚C where pezzottaite and Cs-, Li-rich beryl crystallized syngenetically.

Since "mushroom" tourmaline has only been found in those pezzottaite mines in Madagascar, Momeik and Pyi-Gyi-Taung, Myanmar, its textural and compositional changes at different parts of the stone reflects the changes of crystallization conditions during late stages of evolution of this complex type rare element miarolitic pegmatite (Lussier et al., 2008). Further investigation will be focused on its potential use as one of the pezzottaite-indicator minerals in pegmatite exploration.

Acknowledgements
The authors are grateful to Dr Kenneth J. Domanik of the University of Arizona Lunar and Planetary Laboratory for providing Electron Microprobe experiments. Tsui Kin Wah Tommy, Lau Chun Kit, Ho Nang Chi James and Li Sheung Yin Timothy of China Gems Laboratory Limited are thanked for providing Raman spectroscopy and EDXRF experiments.

References
Aurisicchio C. et al. 1988. Reappraisal of the crystal chemistry of beryl. American Mineralogist, 73, 826-837

Liu S.I., Li Guo-Wu, Peng M.S., 2008. Crystal Structure Analysis of Pezzottaite and Its Application. Acta Mineralogica Sinica, 28(4), 350-356 (in Chinese with English abstract)

Liu S.I., Peng M.S., Li X.G., 2006. Formation and Occurrence of Pezzottaite from Madagascar. Bulletin of Mineralogy, Petrology and Geochemistry, 25(2), 133-136 (in Chinese with English abstract)

Liu S.I, Peng M.S., 2005. A new gem mineral – The Vibrational Spectroscopic Characterization of Pezzottaite, Acta Mineralogica Sinica, 25, 60-64 (in Chinese with English abstract). American Mineralogist, 2006, 91, 222 (New Minerals: abstract)

Lussier A.J., Hawthorne F.C., Herwig S. et al. 2008. Mushroom elbaite from the Kat Chay mine, Momeik, near Mogok, Myanmar: II. Zoning and crystal growth. Mineralogical Magazine, 72(5), 999-1010

Lafuente B., Downs R.T., Yang H., Stone N., 2015. The power of databases: the RRUFF project. In: Highlights in Mineralogical crystallography, T Armbruster and R M Danisi, eds. Berlin, Germany, W. De Gruyter, 1-30

Phyu P.L., 2012. Geology and mineralogical study of Kaduta – Pyin Gyi Taung area, Singu Township, Mandalay Region, Myanmar. Unpublished PhD thesis, Yangon University

Zaw K, 1998. Geological Evolution of Selected Granitic Pegmatites in Myanmar (Burma): Constraints from Regional Setting, Lithology, and Fluid-Inclusion Studies, International Geology Review, 40(7), 647-662

Gemmological and Chemical Characteristics of Yiqisong Peridot, Jilin, People Republic of China

Tasnara Sripoonjan [1*], Montira Seneewong Na Ayutthaya [1], Pimtida Bupparenoo [1], Nalin Narudeesombat [1], Thanong Leelawatanasuk [1], and Malin Sawatekitithum [1]

[1] The Gem and Jewelry Institute of Thailand (Public Organization), ITF-Tower Building, Silom Road, Suriyawong, Bangrak, Bangkok, 10500 Thailand
* stasnara@git.or.th

Keywords: peridot, China, Yiqisong, Jilin, Fuli, gemstone

Introduction

China has traditionally been a territory of a great conundrum with a diversity of natural resources including minerals and gems, and especially green colored stones (e.g. jade, prehnite and peridot). Peridot has been found in a number of different areas of China. Since 1979, China has mined the peridot from the Zhangjiakou-Xuanhua area of Hebei Province (Koivula and Fryer, 1986; Keller and Fuquan, 1986). Recently, the significant deposit of gem-quality peridot has been found in the area called Yiqisong, Yanbian of Jilin province. At first glance, these peridots strikingly show a medium toned yellowish green attribute with high clarity. The average size of relatively clean stones was up to 2 ct. This article describes their detailed gemological characteristics, namely, basic properties, internal features, absorption spectra and chemical compositions.

Figure 1 Representative samples of Yiqisong peridot from China ranging in weight from 1.60 to 2.80 ct (Photograph by T. Sripoonjan)

Materials and methods

In this investigation, we used a total of 26 peridot samples provided by the Yanbian Fuli Olivine mining Co., Ltd. Of those, there are 9 faceted stones (Figure 1) and 17 rough specimens (5.38 to 26.94 ct). The samples' gemological properties were collected by basic gem equipment and various advanced instruments, such as UV-Vis-NIR, FTIR, EPMA, and Raman spectroscopies.

Results and Discussion

Gemological properties. Peridots from Yiqisong typically have light yellowish green to yellowish green and generally showed gemological properties similar to those from the other sources (e.g. Vietnam, Arizona, Italy, Pakistan, Nevada).

In detail, the peridot samples displayed identically biaxial positive with RI values of α = 1.649-1655, β = 1.667-1673, γ = 1.682-1690, and corresponding birefringence of 0.03-0.04. Their SG values ranged from 3.29-3.36. All of them were inert to both short-wave and long-wave UV radiation.

Internal Features. The most prominent inclusions found in almost all Yiqisong peridot samples were various shapes of lily pads (Figure 2A-2C) and delicate wispy veils and tiny crystals (figure 2D and 2E). Protogenetic chromite inclusions (as identified by Raman spectroscopy) exhibit tabular-shaped, brown- to-brownish-red crystals (Figure 2F). Partially healed secondary fractures showing iridescent effect were seen in most of the Yiqisong peridot samples (Figure 2G). Other inclusions rarely observed are peculiarly unidentified crystals which have attractive attributes (Figure 2H).

Spectra. Yiqisong peridots have a typical UV/Vis/NIR spectrum characterized by a broad band at 1086 nm, with a shoulder at about 850 nm in the near IR range, and an increasing absorption toward the UV region (Figure 3). Additional weak bands were also observed at 394, 402, 432, 450, 472, 489, 495, 530, 635 nm. The coloration of these peridots can be referred by spectral features found in peridot from the previous works (Adamo et al., 2009), that confirmed the presence iron (Fe2+) as a main chromophore of green color (Stockton and Manson, 1983; Thuyet et al., 2016).

The characteristic mid-IR spectra of peridot samples revealed several absorption bands, located at 1046, 980, 951, 899, 835, 626 and 530 cm^{-1} (Figure 4). The peak maxima positions of all samples are almost identical and consistent with their very small chemical ranges. Nevertheless, the peak positions of our spectra were shifted to either slightly lower or higher values depending on their contents of Fe (Fe-O stretching). Namely, the frequency of each band would have a decrease with the increase of iron content and vice versa as previously suggested by Duke and Stephens (1964) and Burns and Huggins (1972).

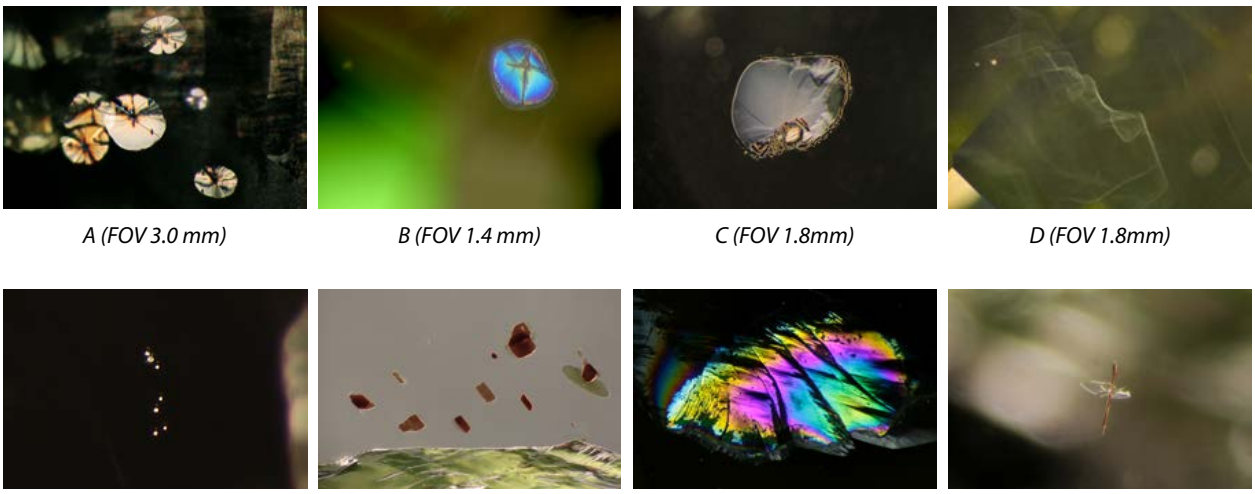

A (FOV 3.0 mm) *B (FOV 1.4 mm)* *C (FOV 1.8mm)* *D (FOV 1.8mm)*

E (FOV 0.8 mm) *F (FOV 2.0 mm)* *G (FOV 3.2 mm)* *H (FOV 1.1 mm)*

Figure 2 Internal features of Yiqisong peridots from China (see text for further details)
(Photomicrographs by T. Sripoonjan)

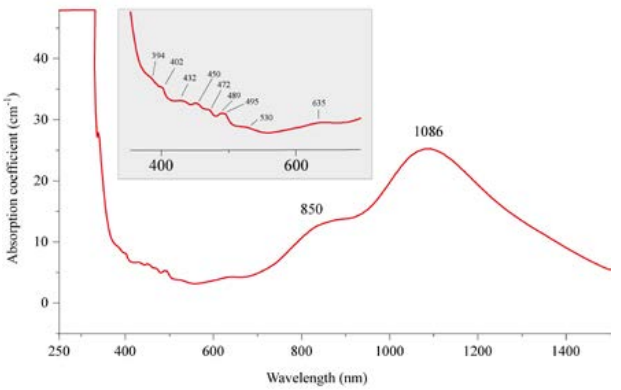

Figure 3 UV-Vis-NIR spectrum of a representative Yiqisong peridot sample.

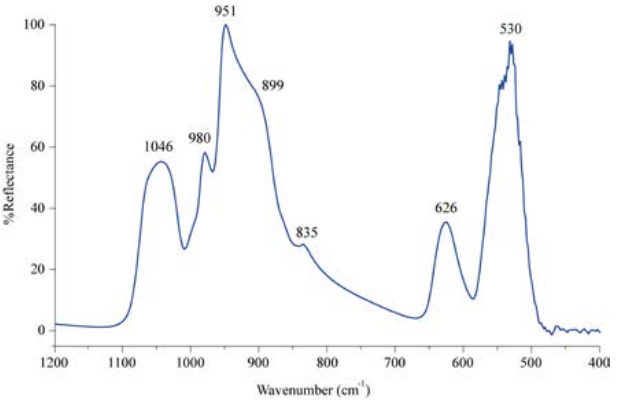

Figure 4 FTIR spectrum of a representative Yiqisong peridot sample

Chemical Composition

The chemical components of Yiqisong samples mostly range from 90.06 to 91.46 % fosterite and 8.38 to 9.83 % fayalite. Their MgO contents vary from 49.43 to 50.87 wt.% that are similar to peridots from Vietnam, Italy and Pakistan, but slightly higher than those from Arizona and Nevada. Their FeO contents range from 8.25 to 9.62 wt.%, that are nearly the same as those from Arizona, Sardinia, and Vietnam, but a bit lower than the specimens from Black Rock, Nevada in the USA (see Table 1). The average MnO content is 0.10 wt.%, while the average NiO content is 0.40 wt.%, that also indicate the mantle's olivine (Jan and Khan, 1996; Ishimaru and Arai, 2007).

Table 1 Chemical composition of Yiqisong peridots and other countries by EPMA (in wt.%).

Source	Yiqisong, China (26 samples)	Central Highlands, Vietnam[a] (9 samples)	Arizona[b] (2 samples)	Sardinia, Italy[c] (2 samples)	Kohistan, Pakistan[d] (7 samples)	Black Rock Summit, Nevada[e] (3 samples)
SiO_2	39.69-41.16 (40.60)	40.27–42.64 (41.02)	40.55–40.77	40.69–40.83	38.75–41.57 (40.47)	37.90-40.55
FeO	8.25-9.62 (8.69)	8.24–9.90 (8.68)	9.68–9.73	8.77–8.98	2.74–9.69 (6.54)	10.27-13.81
MnO	0.06-0.16 (0.10)	0.03–0.24 (0.12)	0.12–0.17	0.11–0.15	0.06–0.15 (0.11)	0.16-0.20
MgO	49.43-50.87 (50.21)	47.22–52.25 (50.36)	48.22–48.98	50.15–50.17	48.52–53.49 (50.80)	47.34-47.62
NiO	0.34-0.48 (0.40)	0.24–0.54 (0.36)	0.37–0.39	0.38–0.39	0.17–0.38 (0.26)	0.27-0.28
CaO	0.00-0.04 (0.01)	0.03–0.1 (0.06)	0.06–0.11	n/a	0.00–0.03 (0.01)	0.15-0.22
Total	99.48-100.89 (100.02)	99.17–100.99 (100.61)	99.29–99.77	100.12–100.50	97.43–99.38 (98.21)	99.92-100.03

[a]Thuyet et al (2016); [b]Stockton and Manson (1983); [c]Adamo et al. (2009); [d]Jan and Khan (1996); [e]Führbach (1998)
n/a: not applicable

Conclusion

Peridots from Yiqisong, Yanbian of Jilin province, China appeared in light yellowish green to yellowish green colors. Their RIs, birefringence, SGs and fluorescence are similar to those from the other sources. Internal features showed various shapes of lily pads, wispy veils, tiny crystals and protogenetic chromite crystals (brown to brownish red). Secondary healed fractures showing iridescent effect were also found. The presence of unusual tabular shape protogenetic chromites (brown to brownish red) have never been reported in peridots from other sources; however, only black and octahedral shape chromite crystals were found in peridot from San Carlos (Koivula, 1981).

The result of UV/Vis/NIR spectrum significantly related to iron (Fe^{2+}). Mid-IR spectra showed several absorption bands from 1046 to 530 cm^{-1}. Contents of MgO (49.43 to 50.87 wt.%) and FeO (8.25 to 9.62 wt.%) were similar to peridots from Vietnam, Sardinia (Italy) and Pakistan.

References

Adamo I., Bocchio R., Pavese A., Prosperi L. (2009) Characterization of peridot from Sardinia, Italy. G&G, Vol. 45, No. 2, pp. 130–133

Burns R.G., Huggins F.E. (1972) Cation determinative curves for Mg-Fe-Mn olivines from vibrational spectra. The American Mineralogist, Vol. 57, No. 5-6, pp. 967–985

Duke D.A. and Stephens J.D. (1964) Infrared investigation of the olivine group minerals. The American Mineralogist. Vol. 49, No. 9-10, pp. 1388–1406

Führbach J.R. (1998) Peridot from the Black Rock Summit lava flow, Nye County, Nevada, USA. G&G, Vol. 26, No. 2, pp. 86–102

Ishimaru S. and Arai S. (2008) Nickel enrichment in mantle olivine beneath a volcanic front. Vol. 1559, pp. 119-131

Jan M.Q., Khan M.A. (1996) Petrology of gem peridot from Sapat mafic-ultramafic complex, Kohistan, NW Himalaya. Geological Bulletin, University of Peshawar, Vol. 29, pp. 17–26

Keller P.C. and Fuquan W. (1986) A Survey of the Gemstone Resources of China. G&G, Vol. 22, No. 1, pp. 3-13

Koivula J.I. (1981) San Carlos peridot. G&G, Vol. 17, No. 4, pp. 205–214

Koivula J.I. and Fryer C.W. (1986) The Gemological Characteristics of Chinese Peridot. G&G, Vol. 22, No. 1, pp. 38-40.

Stockton C.M. and Manson D.V. (1983) Peridot from Tanzania. G&G, Vol. 19, No. 2, pp. 103–107

Thuyet N.T.M., Hauzenberger C., Khoi, N.N., Diep C.T., Lam C.V., Minh N.T., Hoang N., and Häger. T. (2016) Peridot from the Central Highlands of Vietnam: Properties, Origin, and Formation. G&G, Vol. 52, No. 3, pp. 276-287

TRAPICHE TEXTURE IN EMERALDS AND RUBIES

Pignatelli Isabella[1*], Giuliani Gaston [2*], Morlot Christophe [3], Pham Van Long[4]

[1,3] GeoRessources, Université de Lorraine, Faculté des Sciences et Technologies, "Entrée 3B" Rue Jacques Callot BP 70239, 54506 Vandoeuvre-lès-Nancy Cedex, France.
[2] Université Paul Sabatier, GET/IRD, UMR CNRS-IRD-CNES 5563, 14 avenue Edouard Belin, F- 31400 Toulouse, France and Université de Lorraine, CRPG UMR 7358 CNRS-UL, 15 rue Notre- Dame-des-Pauvres, BP20, 54501 Vandœuvre-lès-Nancy cedex, France
[4] Centre for Gems and Gold Research and Identification of Vietnam, 91 Dinh Tien Hoang Hanoi, Vietnam
* isabella.pignatelli@univ-lorraine.fr giuliani@crpg.cnrs-nancy.fr

Keywords: trapiche texture, Colombian emeralds, Vietnamese rubies

The term "trapiche" was used for the first time to describe atypical Colombian emeralds, because their texture remember the shape of a crushing gear used in sugar cane production (McKague, 1964). Trapiche texture in emeralds is characterised by a central core surrounded by growth sectors, dendrites and sometimes an overgrowth (Figure 1A). The dendrites are around the core and separate six crystallographic-equivalent growth sectors; they are made by inclusions or matrix of host-rock.

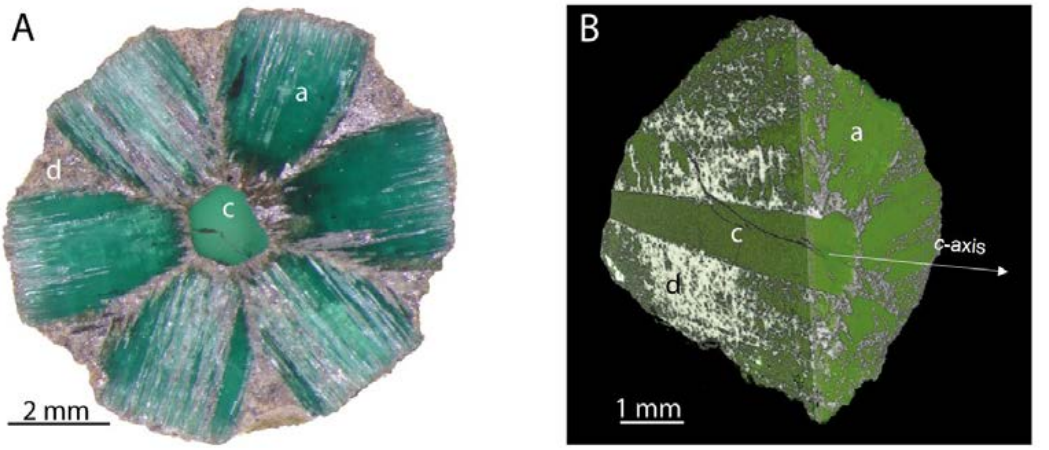

Figure 1: Typical trapiche texture (A) with a central core (c), six arms (a) and dendrites (d). X- ray computed tomography image (B) showing the reduction of the core from the top to the bottom of the sample and how the dendrites develop laterally in the arms. Both samples come from Muzo mine.

Later, the term trapiche was also used to name sapphire and rubies from Southeast Asia with a similar texture that appeared on the gem market in '90s (Koivula et al., 1994; Schmetzer et al., 1996, 1998). These rubies show six triangular or trapezoidal growth sectors separated by yellow and/or white dendrites that generally cross at a central point. In few samples the dendrites start from a hexagonal central core. These similarities with the emeralds trapiche texture can be explained by the symmetry: both beryl and corundum belong to the hexagonal crystal family, which includes two crystal systems: hexagonal (beryl) and trigonal (corundum).

The request of gems with a trapiche texture increased during the 2000s, giving rise to an incorrect use of the term trapiche (e.g. quartz trapiche - Chabrol and Michelou, 2017). This needed a clarification and trapiche minerals were distinguished from trapiche-like minerals (Win, 2005; Schmetzer et al., 2011; Giuliani and Pignatelli, 2016).

The formation of trapiche minerals is controlled both by the geological environment and formation of the deposits, and by the crystal symmetry. Until now the trapiche textures are found only in high symmetry minerals: cubic for garnet, hexagonal for emerald, trigonal for ruby and tourmaline. Nevertheless, the low symmetry of orthorhombic system for andalusite is an exception, but the system is pseudotetragonal ($a \approx b$). No other orthorhombic mineral show the trapiche texture. The symmetry affects the number of arms and dendrites in the trapiche texture, as well as the directions where dendrites develop (Pignatelli et al., 2015). For example, as beryl crystallizes in the hexagonal system, trapiche emeralds have six arms and six dendrites along the a-axis.

Trapiche emeralds formed in the albitized and calicitized black shale host-rock in Colombia (Giuliani et al., 2015), trapiche rubies are found in marble deposits from Central and Southeast Asia (Schmetzer et al., 1996; Garnier et al. 2002a,b; 2008). Although these geological contexts are quite different, there are few common features that play a fundamental role in the trapiche texture formation: (i) the presence of organic matter or graphite, (ii) the thermal reduction of sulfates, (iii) the presence of evaporites, and (iv) the fluid pressure variations.

In the last few years, we provided new mineralogical and geochemical data on Colombian emeralds and Vietnamese rubies obtained thanks to the X-ray Computed Tomography (CT). The originality of this work is based on data acquired with this non- destructive technique that reveals 3D interior details of the trapiche texture without modifying the color of the gems. CT data are useful to facilitate the comparison between trapiche emerald and rubies.

The CT showed that the core of trapiche emeralds has the shape of two opposite hexagonal pyramids. Thus, the core decreases form the top to the bottom of the pyramids as shown by different sections perpendicular to the c axis. The core is surrounded by the dendrites that develop laterally and penetrate into the growth sectors (Figure 1B). The dendrites contain mainly the albite, pyrite and emerald assemblage, but also other solid inclusions, such as carbonates, rutile, muscovite, F-apatite, tourmaline, monazite and parisite. The dendrites occupy 18% of the total volume of the sample, the core and growth sector 81%, the remaining 1% forms the porosity that favour the secondary alteration and consequently formation of clay minerals and iron oxides/hydroxides along the dendrites. The CT data combined with the results of X-ray topography proved that trapiche emeralds are not twinned but they are single crystals whose growth history is quite complex.

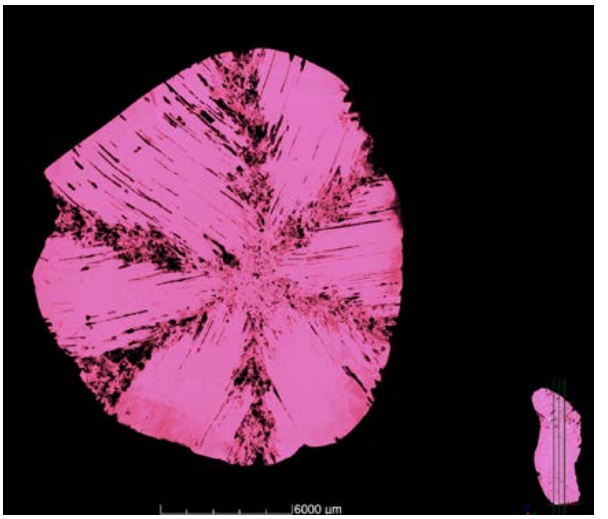

Figure 2. X-ray computed tomography image showing the tube-like inclusions filled by liquid and vapour phases in a Vietnamese ruby.

The trapiche texture of Vietnamese rubies is similar to that of Myanmar ones. The dendrites generally run from the corners of crystals and intersect in a central point, but sometimes a very small core is visible. The dendrite contains: anorthite, calcite, pyrite, rutile, aluminosilicates, titanite, zircon, corundum and margarite, which forms at the expense of corundum during the retrograde metamorphism (Garnier et al., 2008). The CT data underline the presence of tube-like inclusions developing from the dendrites and prolonging them into the growth sectors (Figure 2). The tomographic contrast indicates that the tube-like inclusions can be filled by solid inclusions or by fluid, i.e. a liquid and a vapour.

Based on the acquired data and on the geological context of formation, we reconstructed the steps of growth history of trapiche emeralds and rubies, and we compared them in order to underline the common features of the trapiche texture in different minerals.

References

Chabrol M., Michelou J.C., 2017. Sainte-Marie-aux-Mines – Sun, Fun, Friends and Magnificent Minerals. InColor, 92, 92–95.

Garnier V., Giuliani G., Ohnenstetter D., Fallick A.E., Dubessy J., Banks D., Hoàng Quang V., Lhomme Th., Maluski H., Pêcher A., Bakhsh K.A., Pham Van L., Phan Trong T., Schwarz D., 2008. Marble- hosted ruby deposits from central and Southeast Asia: towards a new genetic model. Ore Geology Reviews, 34, 169–191.

Garnier V., Ohnenstetter D., Giuliani G., Blanc P., Schwarz D., 2002a. Trace-element contents and cathodoluminescence of "trapiche" rubies from Mong Hsu, Myanmar (Burma): geological significance. Mineralogy and Petrology, 76(3–4), 179–193.

Garnier V., Ohnenstetter D., Giuliani G., Schwarz D., 2002b. Rubis trapiches de Mong Hsu, Myanmar. Revue de Gemmologie AFG, 144, 5–12.

Giuliani G., Branquet Y., Fallick A.E., Groat L., Marshall D., 2015. Emerald deposits around the world, their similarities and differences. InColor, special issue, 56–69.

Giuliani G., Pignatelli I., 2016. 'Trapiche' Vs 'Tapiche-like' textures in minerals. InColor, 31, 45–46. Koivula J.I., Kammerling R.C., Fritsch E., 1994. Gem News: "Trapiche" purple-pink sapphire. Gems & Gemology, 30(3), 197.

McKague H.L., 1964. Trapiche emeralds from Colombia. Gems & Gemology, 11(7), 210–223. Pignatelli I., Giuliani G., Ohnenstetter D., Agrosì G., Mathieu S., Morlot C., Branquet Y., 2015. Colombian trapiche emeralds: recent advances in understanding their formation. Gems & Gemology, 51(3), 222–259.

Schmetzer K., Beili Z., Yan G., Bernhardt H.J., Hänni H.A., 1998. Element mapping of trapiche rubies. Journal of Gemmology, 26(5), 289–301.

Schmetzer K., Bernhardt H.J., Hainschwang T., 2011. Chemical and growth zoning in trapiche tourmaline from Zambia – a re-evaluation. Journal of Gemmology, 32(5-8), 151–173.

Schmetzer K., Hänni H.A., Bernhardt H.J., Schwarz D., 1996. Trapiche rubies. Gems & Gemology, 32(4), 242–250.

Win K.K., 2005. Trapiche of Myanmar. Australian Gemmologist, 22(6), 269–270.

Genetic classification of mineral inclusions in quartz

Jaroslav Hyrsl,
Prague
hyrsl@hotmail.com

Keywords: quartz, inclusions

The following genetical types of geological environment are producing the majority of inclusions (with examples of main localities and typical inclusions). They are numbered according to an approximate volume of the specimens, the Alpine fissures being by far the most common ones.

1) Alpine fissures A
Typical localities : the Alps in Austria and Switzerland, Polar Ural Mts. in Russia, Diamantina-Corinto-Curvelo region in northern Minas Gerais and southern Bahia in Brazil, Nepal, Arkansas in the USA
Typical inclusions : mica (white muscovite, brown biotite), chlorite (green clinochlore, black chamosite), epidote, actinolite, quartz, hematite, ilmenite, rutile, anatase, brookite, titanite, carbonates (calcite, siderite), pyrite, black tourmaline (schorl), hollows after anhydrite, galena, chalcopyrite, fibrous sulphosalts (boulangerite, cosalite, meneghinite, etc.), monazite

2) Granitic pegmatites P
Typical localities : Minas Gerais in Brazil, Sahatany in Madagascar, Tongbei in China, northern Pakistan
Typical inclusions : colored tourmaline (elbaite, schorl), mica (muscovite, lepidolite), garnet (spessartite, almandine), albite, apatite, columbite, beryl, microlite, helvite

3) Tungsten deposits W
Typical localities : Panasqueira in Portugal, Kara-Oba in Kazakhstan, Yaogangxian and Xuebaoding in China, Pasto Bueno and Mundo Nuevo in Peru, Kami in Bolivia Typical inclusions : arsenopyrite, chalcopyrite, pyrrhotite, sphalerite, stannite, helvite, cosalite, carbonates (siderite, rhodochrosite), fluorite, apatite, wolframite

4) Dolomitic carbonates C
Typical localities : Herkimer in New York, Bahia in Brazil, Sichuan in China, Baluchistan in Pakistan
Typical inclusions : calcite, pyrite, graphite, hydrocarbons ("anthraxolite"), natural petrol

5) Ore veins O
Typical localities : Berezovsk in Russia, Messina in South Africa, Casapalca in Peru Typical inclusions : pyrite, galena, sphalerite, chalcopyrite, tetrahedrite, stibnite, molybdenite, cinnabar, gold, Cu-silicates (ajoite, papagoite, shattuckite)

6) Alkaline pegmatites AP
Typical localities : Mt. Malosa in Malawi, Row Mt. in Russia, Zegi Mt. in Pakistan
Typical inclusions : aegirine, astrophyllite, epididymite, zircon, riebeckite

7) Quartz monomineral veins with amethyst Q
Typical localities : Mangyshlak in Kazakhstan, Madagascar, Brazil
Typical inclusions : goethite ("cacoxenite"), hematite ("lepidocrocite" or "beetle legs")

8) Amethyst geodes in volcanic basalts V
Typical localities : Rio Grande do Sul in Brazil and Uruguay
Typical inclusions : goethite, fluorite, cristobalite

9) Skarn deposits S
Typical localities : Pampa Blanca in Peru
Typical inclusions : pyrite, chalcopyrite, pyrrhotite, andradite

CANADIAN GEM TOURMALINE AND THE LEDUC MINE

Willow Wight[1], Aaron J. Lussier[1] and T.S. Ercit[1]

[1] Canadian Museum of Nature, Mineralogy, Research & Collections,
P.O. Box 3443, Station D, Ottawa, ON K1P 6P4, Canada
*wwight@nature.ca

Keywords: tourmaline, Canada, fluor-elbaite

Tourmaline from Canada is not a significant gemstone. Among the many localities for tourmaline in Canada, very few contain any material of gem quality. The first mention of coloured gem tourmaline in published literature was in the Geological Survey of Canada (GSC) Annual Report of 1888-89, which states that: "tourmaline occurs generally in long crystals imbedded in the vein matter of Wakefield, and is generally not of a quality fitted for gems, but occasionally pieces are found sufficiently clear for this purpose".
In 1890 and 1894, Ottawa mineral dealers C.P. Willimott & Co., offered for sale tourmaline gems from Wakefield, Quebec (Willimott, C.P., 1890). A family relation, C.W. Willimott, mineralogist at the GSC, published "Canadian Gems and Precious Stones" in The Ottawa Naturalist: "Small stones of one to two carats, of transparent green of various shades, sometimes a bright emerald, also a yellow and a yellowish-green variety, have been cut from the Tourmaline of Wakefield." (Willimott, C.W., 1891, p. 120)

Locality
The Leduc mine, St-Pierre-de-Wakefield, Wakefield Tp., Gatineau Co., Québec, Canada is considered a classic Canadian mineral locality. Now described as the Leduc mine, Val-des-Monts, Les Collines-de-l'Outaouais RCM, Outaouais, Québec, it is situated in a hilly, forested area 3.5 km WNW of St-Pierre-de-Wakefield (~60 km NE of Ottawa, Ontario).
The Leduc mine is a quarry in a well-zoned granitic pegmatite body. The pegmatite is small, as are the quarry workings (25 x 4 x 6 m deep). It has a quartz core; an intermediate zone of often-large crystals of elbaite, amazonite, cleavelandite, lepidolite-zinnwaldite and quartz; a heterogeneous wall zone of schorl, pink perthite and quartz in some areas and finer-textured pegmatite characterized by smoky quartz, peristerite, and biotite in others; and a border zone of graphitic granite (Hogarth et al., 1972; Hilderley, et al., 2006). Among the minor minerals is fluor-elbaite (highly fractured, polychrome crystals to 5 cm d. in matrix; intermediate zone) and schorl (in outer zones and as rims on elbaite). (Hilderley, et al., 2006). The Leduc mine is the only known occurrence of a lithium-enriched granitic pegmatite in all of the Grenville Province (Ercit and Gault, 2007).

History of the Leduc mine
The many pegmatites that occur in the Grenville Geological Province of Ontario and Quebec were considered for their economic potential beginning in the late 1800s. The Leduc mine was originally opened by H.L. Shirley in 1884, producing large sheets of "muscovite" (to 35 x 70 cm) for use as windows in wood-burning stoves. The mine failed because the mica contained lithium, making it too brittle and too readily fusible. In 1908, M.J. O'Brien acquired the property to mine for gem tourmaline, making this the first mine in Canada exploited for gemstones. The venture failed because the tourmaline was too fractured for faceting (Hogarth et al., 1972; Sabina, 1964, 1970). Interest in the Leduc mine has continued over the years as mineralogists and mineral collectors have visited and studied the minerals found there.

Tourmaline specimens from the Leduc mine

Tourmaline crystals at Leduc are up to 5 cm d., but may be up to 45 cm l. Colours range from yellow-green to dark bluish green, and from pink to green and almost black; green is predominant. The Canadian Museum of Nature (CMN) holds several dozen Leduc tourmalines, collected periodically throughout the past ~120 years. Of particular interest are two specimens collected by A.T. McKinnon of the GSC. The first dates from 1908 when the mine was being worked for gem tourmaline. It is a large but unterminated crystal on matrix (CMNMC 43659; 48 x 19 x 7 cm). Most interesting are its colour variations. Mostly a dark green, there are translucent areas toward the top with a mix of mid-green to pink tourmaline. (Figures 1 & 2). The second McKinnon specimen, collected in 1916, has two tourmaline crystals, one of which is terminated, on quartz matrix (CMNMC 54148; 15 x 9 x 8 cm).

In addition, many early mineral specimens from Canada are in the collections of the Natural History Museum (NHM) in London, UK. Two samples labelled elbaite in matrix, Wakefield, Quebec, acquired in 1917, are almost certainly from the Leduc mine.

Figure 1. Fluor-elbaite on quartz, collected in 1908 (CMNMC 43659; 48 x19 x 7 cm)

Figure 2. Leduc tourmaline gem (CMNGE 20003; 3.85 ct)

Faceted tourmaline from the Leduc mine

A few tourmaline gems (colourless to emerald to olive green) were reported as early as 1890 and 1891 (Willimott, C.P., 1890; Willimott, C.W., 1891). The next published report came from amateur faceter G. Grant Waite of Toronto, who specialized in Canadian gemstones. His gem from Wakefield is a "good green matching good Brazilian colour" (Waite, 1944). It is a 1.27-ct, triangular mixed cut (CMNGE 21026). A second Leduc tourmaline gem was faceted by E.J. Letourneau from rough donated by mineral collector Hamilton Stitt. It is a 3.85-ct, blue-green, rectangular step cut (CMNGE 20003). The CMN has recently obtained a 5.52-ct, dark blue-green, square cushion cut (CMNGE 21802; faceted by B.S. Wilson). See Figure 3.

The most extensive collection of Leduc tourmaline gems is the reference suite of Brad Wilson (Alpine Gems, Kingston, ON). The wide variety of colours are shown in one box (Figure 4). Brad kindly loaned these faceted stones for study, and contributed four pieces of transparent rough for detailed chemical analyses.

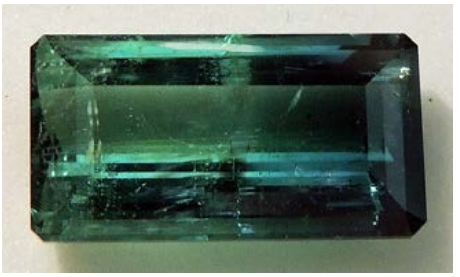

Figure 3. Leduc tourmaline gem (5.41 ct; B.S. Wilson)

Figure 4. Part of reference suite of Leduc tourmaline gems, courtesy of B.S. Wilson, Alpine Gems (Kingston, ON)

The usual gemmological measurements were made on selected stones of different colours. There was very little difference in the RIs of the different shades of green and blue-green (1.621-1.641). Slightly lower values were obtained for one very small colourless stone (1.613-1.635) and two small pink (1.618-1.638). Dichroism was seen as dark and light shades of the specimen's colour. Most of the gems have many inclusions such as curved feathers, twisted veils, parallel tubular inclusions, and two-phase inclusions.

Compositional variation in Leduc tourmalines

Minerals of the tourmaline supergroup are well known for their chemical complexity, with over 30 valid species recognized by the International Mineralogical Association. The general formula for members of the tourmaline supergroup is given as $XY_3Z_6(BO_3)_3(T_6O_{18})VW_3$, where X = Na^+, Ca^{2+}, K^+, and Vacancy; Y = Fe^{2+}, Mg^{2+}, Mn^{2+}, Al^{3+}, Li^+, Fe^{3+}, and Cr^{3+}; Z = Al^{3+}, Fe^{3+}, Mg^{2+}, and Cr^{3+}; T = Si^{4+}, Al^{3+}, and B^{3+}; B = B^{3+}; V = $(OH)^-$ and O^{2-}; and W = $(OH)^-$, F^-, and O^{2-}. The many substitutions result in a wide array of colours.

The core region of Leduc tourmalines commonly shows distinct colour zoning, ranging from greenish-blue to pinkish-red. Crystals also show an outer rind of dark brown-to-black material. Electron microprobe analyses (Figure 5) show that, within a single crystal, compositions vary between fluor-elbaite and schorl, along the exchange vector: $^{Y}Al^{3+} + {}^{Y}Li^+ + {}^{W}F^- \leftrightarrow {}^{Y}2Fe^{2+} + {}^{W}(OH)^-$ (Fig. 5a). The composition of the coloured cores regions, from which gem material would be extracted, ranges from $[^{X}(Na_{0.5}Ca_{0.2}Vac_{.0.3})\ ^{Y}(Li_{1.0}Al_{1.7}Mn_{0.2}Fe_{0.1})\ ^{Z}Al_6(BO_3)_3\ (Si_6O_{18})\ ^{V}(OH)\ ^{W}((OH)_{0.2}F_{0.8})]$ (for blueish green) to $[^{X}(Na_{0.6}Ca_{0.2}Vac_{0.2})\ ^{Y}(Li_{1.0}Al_{1.5}Mn_{0.1}Fe_{0.4})\ ^{Z}Al_6(BO_3)_3\ (Si_6O_{18})\ ^{V}(OH)^{W}\ ((OH)_{0.3}F_{0.7})]$ (for pinkish red). The apparent colour is related to the Fe/Mn ratio, with areas where Fe > Mn apfu and Fe < Mn apfu corresponding to green and pink material, respectively (Fig. 5c).

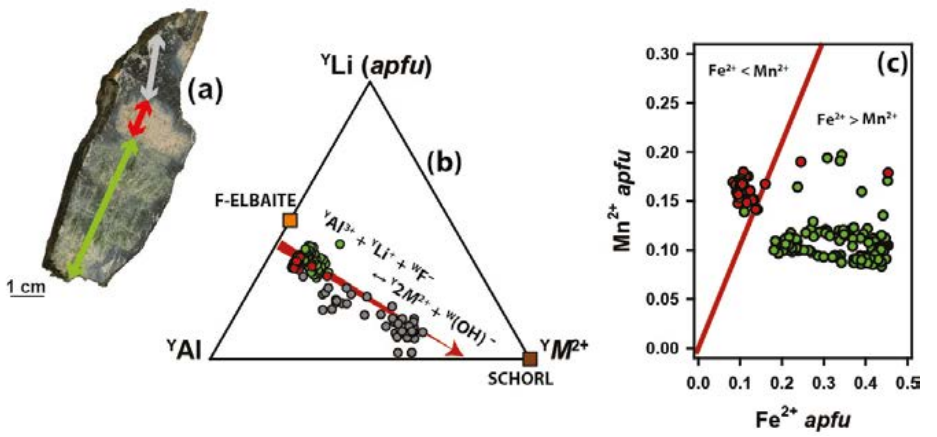

Figure 5. Electron microprobe analysis on Leduc tourmaline; (a) cross-section of single-crystal showing colour variations and location of traverses; (b) ternary plot showing variation in Y-site cations ($M^{2+} = Fe^{2+} + Mn^{2+} + Mg$), with end-member compositions indicated; (c) Mn/Fe ratios as a function of colour (apfu = atoms per formula unit).

Despite much interest in the site for more than one hundred, the Leduc mine has never been a commercial success. It has been the source of small numbers of a few gemstones (amazonite and peristerite as well as tourmaline), but it is mainly of interest to local collectors and to mineralogists or geologists studying lithium-enriched granitic pegmatites.

References

(1888-89) Geological Survey of Canada Annual Report, Volume IV, Class X. Minerals applicable to jewelry and the fine arts decorative purposes, p. 155-56.

Ercit, T.S. and Gault, R.A. (2007) Canadian tourmaline occurrences in the Grenville province, Rocks & Minerals, 82, May/June, p. 235.

Hilderley, M., Ercit, T.S. and Rowe, R.A. (2006) The Leduc mine, St.-Pierre-de-Wakefield, Quebec, Canada, Program 33rd Rochester Mineralogical Symposium, p. 13-14.

Hoffmann, G.C. (1893) Catalogue of Section One of the Museum of the Geological Survey, VIII. Minerals applicable to the fine arts and jewellery, (series of ornamental stones cut and polished and presented by C.P. Willimott & Co.), p. 149-50.

Hogarth, D.D., Moyd, L., Glass, D.J., Rose, E.R. and Steacy, H.R. (1972) Classic mineral collecting localities in Ontario and Quebec, IGC A47-C47 XXIV International Geological Congress Excursions 1972, 79 pp. (Leduc mine p. 29-30.)

Sabina, A.P. (1964) Rock and mineral collecting in Canada, Vol. 2 Ontario and Quebec, GSC Misc. Report 8, 252 pp.

Sabina, A.P. (1970) Rocks and minerals for the collector: Hull-Maniwaki, Quebec; Ottawa-Peterborough, Ontario, GSC Paper 69–50, 177 pp. p. 26 (republished in 1987)

Waite, G.G. (1944) Contributions to Canadian Mineralogy, University of Toronto Studies, Geological Series No. 49. In Notes on Canadian gems and ornamental stones, p. 75-78.

Willimott, C.P. & Co. (1890) Catalogue of Mineralogical Gems. Mineralogists and Lapidaries, 33 Wellington St., Ottawa, 18 pp.

Willimott, C.W. (1891) Canadian Gems and Precious Stones, The Ottawa Naturalist, Transactions Vol. VII, p. 117-142.

Acknowledgements

We are very grateful to Brad Wilson (Alpine Gems), who loaned his reference collection of Leduc tourmaline gems for study, and offered many helpful suggestions. Robin Hansen kindly provided access to tourmaline specimens from Canada in the Natural History Museum, London, UK.

Tourmaline with Coltan ore inclusions – an example of auto-irradiation

Hänni, H.A.[1], Milisenda, C.[2], Wang, H.A.O.[3]
[1] GemExpert, Basel, Switzerland, h.a.haenni@gmail.com
[2] DSEF, Idar-Oberstein, Germany
[3] SSEF Swiss Gemmological Institute, Basel, Switzerland

In an olive green slice of tourmaline with a red rim, tiny inclusions were observed that were surrounded by red haloes (Koivula & al., 2009) (Fig. 1). A TOF LA ICPMS analysis revealed the composition and the tourmaline could be identified as liddicoatite. With a SEM, the composition of the inclusion was analysed and niobium, tantalum, iron, tin and further elements including uranium and lead were found (Fig. 2). In figure 3, a SEM EDS spectrum of the inclusion is shown. Subsequently the inclusions were identified as columbite-tantalite solid solution members that are called coltan. The decay of uranium emits radiation that causes colour centres and created red haloes surrounding the coltan inclusions in the tourmaline host (Nassau, 1975, Calas et al., 2006). The U/Pb concentrations vary significantly and the compositional inhomogeneities are shown in Tab. 1. The higher (brighter areas in Fig. 2) and lower (darker areas in Fig. 3) concentrations of U have been delivered in the main stage of the crystallisation. The darkest areas in the SEM picture have been caused most probably by different processes. They resemble fractures, caused by later brittle deformation, and mineralised in a final process. That the bulk pink colour of the tourmaline is less dark than the haloes around the U-containing coltan inclusion shows that the full potential of red was not reached by the weak primary source of radioactivity of the parent rock in which the tourmaline has formed.

Figure 1 An oval slice (15 x 22 mm) of a tourmaline from Ambosita, Fianarantsoa, SE-Madagascar. In the pale red rim more intensive red clouds are visible that contain a tiny mineral grain. Photo © H.A. Hänni

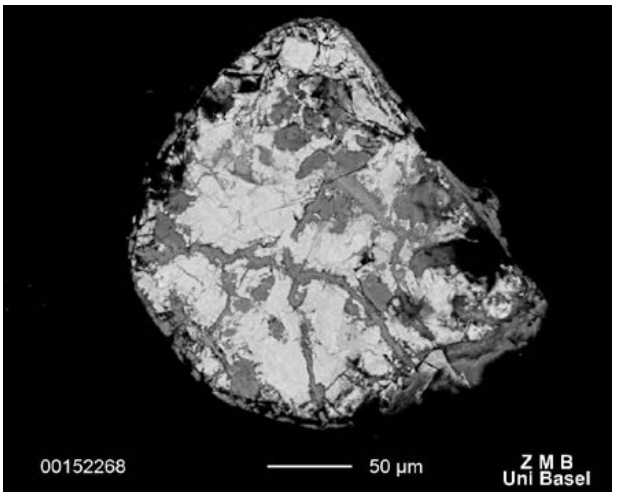

Figure 2 SEM picture of the inclusion in tourmaline produced by backscattered electrons. The different grey tones reflect differences in chemical composition. Image: Nano Imaging Lab, Basel University

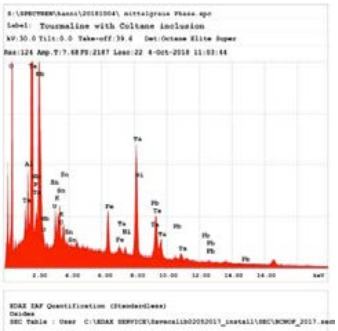

Figure 3 A SEM-EDS spectrum of the investigated inclusion, indicating the qualitative chemical composition by their elemental fluorescence lines: tantalum, niobium, and further elements. Analysis: Nano Imaging Lab, University of Basel

Element	bright (Wt.%)	medium (Wt.%)	dark (Wt.%)
Al_2O_3	1.56	4.67	4.72
Fe_2O_3	0.53	4.61	4.69
Nb_2O_5	35.06	34.78	35.66
P_2O_5	0.00	1.78	1.82
K_2O	1.15	0.88	0.00
SnO_2	11.45	7.28	8.00
UO_2	14.18	7.49	5.76
PbO_2	1.84	3.35	2.40
NiO	1.13	0.91	0.93
TaO	33.11	35.27	36.01
Total	100	100	100

Table 1 Comparison of compositions of three differently grey areas within the columbite-tantalite inclusion, compositions indicated in weight per cent of oxides normalised to 100%. Analysis Nano Imaging Lab, University of Basel.

References

Calas, G.; Allard, T.; Balan, E.; Morin, G. (2006) Radiation Damage in Minerals: From Point Defects to Amorphization. Mineralogical and Environmental Consequences. American Geophysical Union, Fall Meeting 2007, abstract id. M32A-01

Koivula J. I., N. K., Shen A. H-T., Owens P. (2009) Solution-generated pink color surrounding growth tubes and cracks in blue to blue-green copper-bearing tourmalines from Mozambique. Gems & Gemology. 45. 1. 44-47

Nassau, K. (1975) Gamma ray irradiation induced color changes in the color of tourmaline. American Mineralogist, 60, 710-713.

EKANITE FROM SRI LANKA: WHAT CAN WE LEARN FROM A RADIOACTIVE GEMSTONE?

Lutz Nasdala [1*], Manfred Wildner [1], Doris Blaimauer [1], Manuela Zeug [1], Chutimun Chanmuang N. [1], E. Gamini Zoysa [2]

1 Institut für Mineralogie und Kristallographie, Universität Wien, Althanstr. 14, A–1090 Wien, Austria
2 Mincraft Company, No. 4, Gothami Mawatha, Mount Lavinia, Sri Lanka
*lutz.nasdala@univie.ac.at

Keywords: Ekanite, Radioactivity, Metamictisation

In spite of being a highly radioactive mineral (Tennakone, 2011; Nasdala et al., 2017; and references therein), the Ca-Th silicate ekanite has been, and still is, traded as a rare collector's gemstone in the Sri Lankan market. This may perhaps be ascribed to this mineral's transparency and beautiful greenish colour (Fig. 1), often reminiscent of the colour of tender leaves of banana plants. Also, some of the specimens show asterism, then resembling star kornerupine (Gübelin, 1961). Ekanite was first discovered in 1953, in a gem pit near Ellawala, Ratnapura area (Fig. 2; compare Anderson et al., 1961; Gübelin, 1961). More recently, ekanite was found further in the east of Sri Lanka, near Okkampitiya, Monaragala district. The small Okkampitiya gem field is situated atop and around the Buttala klippe, an isolated remnant of the Highland Complex resulting from its overthrust onto the Vijayan Complex (Fig. 2; see Mathavan and Fernando, 2001). Gem-bearing sediments occur, among others, in karstic potholes (Mathavan et al., 2000). Ekanite is found as loose grains in such gravels. The uneven surfaces of rough stones, not showing abrasive rounding (Fig. 1a), indicate short transportation pathways from the primary source rock, which, however, remains unknown.

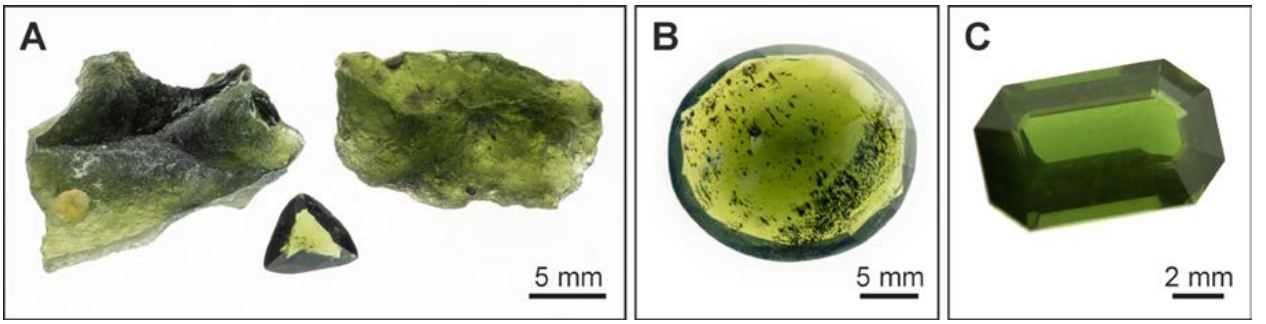

Figure 1: (A) Two rough (14.50 and 11.25 ct) and one small cut ekanite (0.65 ct) from Okkampitiya. (B) A large round-cut stone (28.66 ct) from Okkampitiya shows numerous dark inclusions in transmitted light. (C) Emerald-cut ekanite (2.34 ct) of exceptional colour and clarity, from Sri Lanka (precise origin unknown; purchased in 1992). Specimen M4911 of the collection of the Natural History Museum, Vienna (photo courtesy Vera M.F. Hammer).

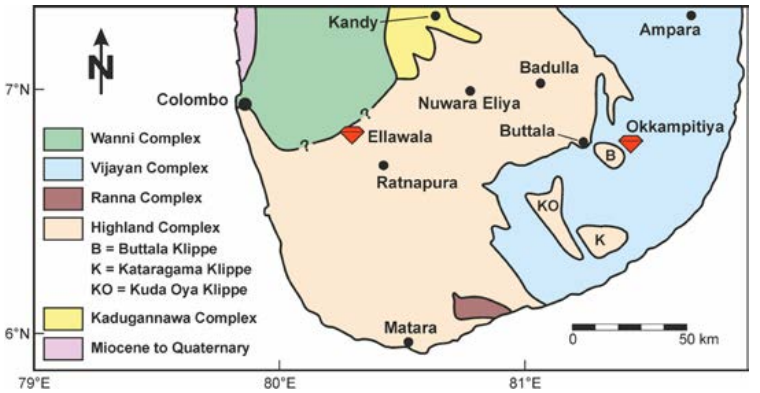

Figure 2: Geological map of southern Sri Lanka (redrawn and modified from Mathavan and Fernando, 2001, and Kröner et al., 2013), showing two locations of ekanite production.

Here we summarise the spectroscopic work done on the Okkampitiya ekanite, which included natural samples and their heat-treated analogues. Results of chemical, isotopic and diffraction analyses have been reported elsewhere (Blaimauer, 2015; Nasdala et al., 2017). The green colour of ekanite was assigned by Tennakone (2011) to ferrous iron and uranyl luminescence. We, however, found no indication of uranyl luminescence (Fig. 3A), and it should also be considered that the Okkampitiya ekanite has a fairly low total Fe concentration of ~0.1 wt% (Nasdala et al., 2017). We found that the optical absorption of natural, green ekanite (Fig. 3B) is mainly characterised by an absorption edge that increases toward the blue and ultraviolet range, and a broad absorption band in the yellow to red range. The combined effect of these to features results in a "transmission window" in the green region of the electromagnetic spectrum. We assign the ~15700 cm^{-1} (~637 nm wavelength) absorption band to an irradiation-induced defect, presumably the O-site vacancy (cf. Nasdala et al., 2017). The ~15700 cm^{-1} band could therefore be considered as an analogue of the irradiation-induced defect (GR1) absorption of green-spotted diamond (Nasdala et al., 2013; and references therein). Our interpretation is supported by the disappearance of the ~15700 cm^{-1} band after recrystallization. After dry heating at ≥ 1000 °C, ekanite appears decoloured to greenish-brownish and appears dull. This is assigned to transformation of the initially amorphous material into a sub-micrometre, polycrystalline form in which many internal grain boundaries cause loss of the initial transparency and increase appreciably the total absorption (Fig. 3B). Attempted colour enhancement by heat treatment, therefore, is ill-advised.

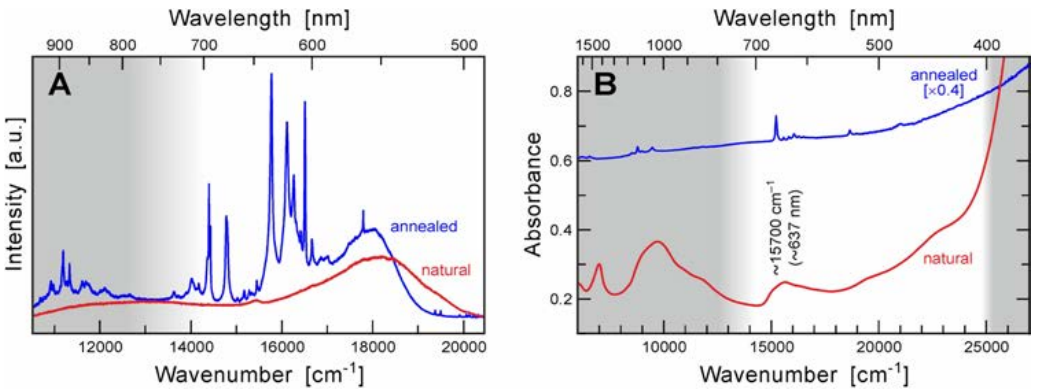

Figure 3: (A) Optical absorption spectra. (B) Emission spectra (488 nm excitation). Spectral ranges that are invisible to the human eye have grey background colour. After annealing at 1400 °C, sharp emissions of trivalent rare earth elements and U^{4+} absorption bands are observed.

There is, however, a most interesting aspect of ekanite that lies beyond its use as collector's gem. In spite of having been exposed to weathering, and in spite of being metamict (i.e. irradiation-amorphised), ekanite has not experienced any Pb loss or other post-growth chemical changes (Nasdala et al., 2017). This should give reason to reconsider to which degree radiation tolerance and amorphisation susceptibility are key factors for the performance of a mineral, or other solid, as possible host material for the immobilisation of nuclear waste. Ekanite from Sri Lanka may indicate that not necessarily irradiation resistance, but rather chemical durability and low aqueous leachability after having become radiation damaged, are crucial properties.

References

Anderson, B.W., Claringbull, G.F., Davis, R.J., and Hill, D.K., 1961. Ekanite, a new metamict mineral from Ceylon. Nature, 190, 997.

Blaimauer, D., 2015. Mineralogische Charakterisierung und Ausheizverhalten des radioaktiven Edelsteins Ekanit. Unpublished B.Sc. thesis, Universität Wien.

Gübelin, E.J., 1961. Ekanite – another new metamict gem from Ceylon. Gems & Gemology, 10, 163–179, 191.

Kröner, A., and Williams, I.S., 1993. Age of metamorphism in the high-grade rocks of Sri Lanka. Journal of Geology, 101, 513–521.

Mathavan, V., and Fernando, G.W.A.R., 2001. Reactions and textures in grossular-wollastonite-scapolite calc-silicate granulites from Maligawila, Sri Lanka: evidence for high-temperature isobaric cooling in the meta-sediments of the Highland Complex. Lithos, 59, 217–232.

Mathavan, V., Kalubandara, S.T., and Fernando, G.W.A.R., 2000. Occurrences of two new types of gem deposits in the Okkampitya gem field, Sri Lanka. Journal of Gemmology, 27, 65–72.

Nasdala, L., Grambole, D., Wildner, M., Gigler, A.M., Hainschwang, T., Zaitsev, A.M., Harris, J.W., Milledge, J., Schulze, D.J., Hofmeister, W., and Balmer, W.A., 2013. Radio-colouration of diamond: a spectroscopic study. Contributions to Mineralogy and Petrology, 165, 843–861.

Nasdala, L., Corfu, F., Blaimauer, D., Chanmuang, C., Ruschel, K., Škoda, R., Wildner, M., Wirth, R., Zeug, M., and Zoysa, E.G., 2017. Neoproterozoic amorphous "ekanite" ($Ca_2Th_{0.9}U_{0.1}Si_8O_{20}$) from Okkampitiya, Sri Lanka: A metamict gemstone with excellent lead-retention performance. Geology, 45, 919–922.

Tennakone, K., 2011. Thorium minerals in Sri Lanka, history of radioactivity and thorium as a future energy source: a compendium to commemorate the International Year of Chemistry 2011. Journal of the National Science Foundation of Sri Lanka, 39, 97–111.

Acknowledgements

Thanks are due to Andreas Wagner for sample preparation, Vera M.F. Hammer for the photograph of a gem ekanite from the collection of the Natural History Museum (NHM), Vienna, and the NHM board for the permission to publish this image herein. L.N. acknowledges funding by the Austrian Science Fund (FWF) through project P24448-N19.

UNUSUAL CORUNDUM (RUBY) BEARING ROCKS FROM BRAZIL AND INDIA

Rainer Schultz-Guttler, Bruno Zampaulo

Gemlab-USP, Geological Institute of Sao Paulo State University, Butanta, Sao Paulo Brazil
rainersgut@gmail.com

keywords : Ruby, Brazil, India, deposit formation

Ruby, due to its high esteem as a gemstone, is extensively described in the gemological and petrological literature (Giuliani et al. 2014 and references therein). The formation of ruby deposits may be classified into secondary, or alluvial, and primary ones, those subdivided into magmatic and metamorphic origin (Simonet et al 2008, Giuliani et al 2014) The interest in the formation of ruby motivated us to the elaboration of this contribution although our study is only preliminary at this point. We present three types of corundum bearing primary deposits, two from Brazil and one from India, which are rarely mentioned or discussed in the literature.
Although of lesser importance in the gem market due their very limited output of cuttable material, their description is nevertheless of interest to better understand the variability of ruby formation.

The three occurrences described below belong to the metamorphic and metasomatic formation of ruby and are hosted in Proterozoic or Archean terrains of Brazil and India. They are fuchsite and/or chlorite bearing ruby deposits which can be found in eastern Brazil (Minas Gerais and Bahia states) and western India (Karnataka state). It may be mentioned that in all three described cases, the whole rock, containing the rubies, can be used for adornment and may be called a "gem rock" due to their spectacular color pattern much alike the so-called anyolite (ruby-zoisite rock) or unakite (metasomatic epidote-feldspar-quartz rock).

In Brazil, the investigated fuchsite-ruby bearing rocks contain varying amounts of k-feldspar and sillimanite. They are found in lenses outcropping in Archean or Proterozoic terrains within the widespread fuchsite-quartzite horizons which stretch over 2500 km along the eastern side of Brazil extending into the states of Minas Gerais, Espirito Santo, Bahia and Rio Grande do Norte. Figure 1 shows the occurrences of fuchsite bearing rocks in eastern Brazil compiled from literature data but without mention of detailed geological, structural and/or metamorphic conditions.

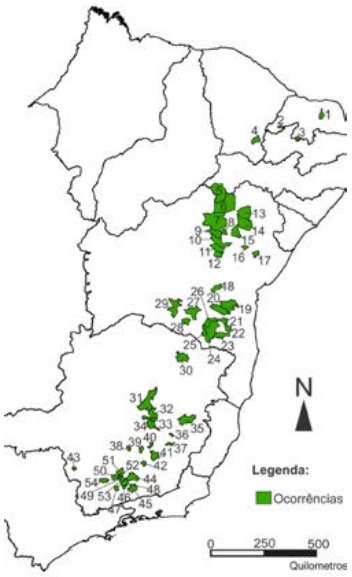

Figure 1: occurrence of fuchsite bearing rocks in eastern Brazil

Depending on the local metamorphic conditions and the presence of nearly monomineralic fuchsitic lithologies one notes the appearance of ruby besides k-feldspar and sometimes small amounts of sillimanite and rutile as shown in Figure 2.

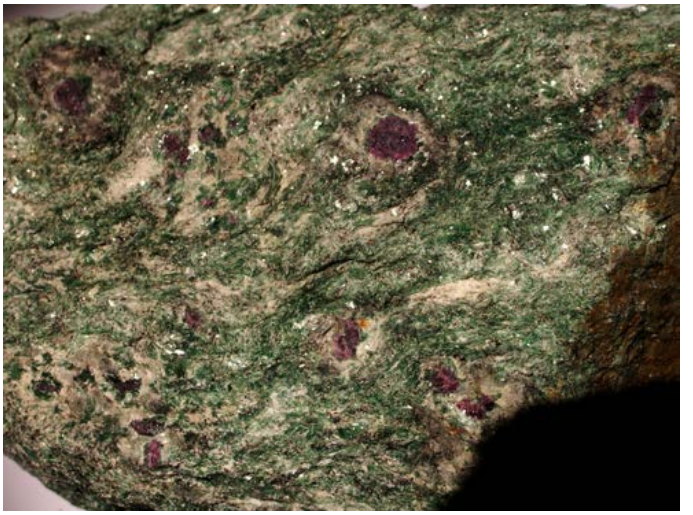

Figure 2: Rubies in this fuchsite-containing rock are encased in K-feldspar

Petrographic studies have shown that the mineral assemblage is derived by the well- known reaction of muscovite = corundum+K-feldspar+water or muscovite+small amount of quartz= sillimanite + corundum + k-feldspar+ water (Velde 1966). As such, these rocks are different from the verdite rocks of Southern Africa (Schreyer et al 1981, Schreyer 1982) For comparison, the well-known, but poorly studied Indian fuchsite-kyanite-ruby mineral assemblage from Karnataka (Ottens 2011, Raith and Schuhmacher 2015, Schultze 2018) has been included in this contribution since textural and mineralogical evidences have shown that its primary mineral assemblage was very similar to the studied Brazilian material. The metasomatic imprint produced the appearance of kyanite eventually leading to a complete absence of ruby as shown in Figures 3 and 4.

Figure 3: Kyanite marks the start of metasomatism and eventually disappearance of ruby

Figure 4: Ruby is progressively transformed in blue kyanite

The second type of ruby bearing rock, much more restricted locally, shows mainly ruby-chlorite and ruby-chlorite-kyanite mineral association with small amounts of tourmaline, plagioclase and vermiculite.(Sa 2012) It can be found in close association to the famous emerald deposits of Campo Formoso in the Mundo Novo Greenstone Belt, Bahia state,(Giuliani et al 1990) along a strike of about 8 km with scattered outcrops of this mineral assemblage. Contrary to the first type described above, the presence of tourmaline, plagioclase and vermiculite (an altered phlogopite) indicates a probable metasomatic origin. The texture varies from very fine grained mineral assemblages (Figure 5) to centimeter sized crystals of darkish red ruby (Figure 6). The preliminary investigation has shown very abrupt changes in the macroscopic texture of samples from each outcrop, revealing the variability of local mineral transformation, which is typical for metasomatic processes. Chemical, geological and phase petrological studies of these interesting rocks are planned.

Figure 5: Fine grained mineral assemblage from Brazil containing ruby and kyanite

Figure 6: Large pluricentimeter ruby from Brazil

References

Giuliani G.,Ohnenstetter,D.,Fallick,A.E.,Fagan,A. 2014 The Geology and Genesis of Gem Corundum Deposits, ed.Groat, L.,A.Vol.2 Chapter 2 Short Course 44, 29-112, Mineralogical Association of Canada

Giuliani, G., Silva, L.J.H.D.,Couto,P., 1990 Origin of emerald deposits of Brazil. Mineralium Deposita 25, 57-64

Ottens B.,2011 Indien : Mineralien-Fundorte-Lagerstaetten, Christian Weise Verlag, Muenchen, 378 pages

Sa, J.H.S, 2012 Corindon na Bahia, CBPM Serie Arquivos Abertos 114p

Schreyer,W., Werding,G., Abraham,K.1981 Corundum Fuchsite Rocks in Greenstone Belts of Southern Africa : petrology, geochemistry and possible origin. J.Petrology 22, 191-231

Schreyer, W. 1982 Fuchsite-aluminium silicate rocks in Archean Greenstone belts : are they metamorphosed alunite deposits? Geol. Rundschau 71, 347-360

Schultze, D. 2018 Dissolution-precipitation reactions in the system Al2O3-SiO2-H2O and the formation of Al2SiO5. PhD Thesis, Technische Universitaet Berlin, Fakultaet VI, 113p

Simonet, C., Fritsch E., Lasnier,B, 2008. A classification of gem corundum deposits aimed towards gem exploaration. Ore Geology Reviews 34,127-133

Velde, B. 1966 Upper stability of muscovite. American Mineralogist 51, 924-929

Acknowledgment

The comments of the reviewer are highly appreciated.

Investigation of ruby from a new occurrence from Paramathi in Karur district of Tamil Nadu, India

Jayshree Panjikar[1] and Aatish Panjikar[2]

[1]Pangem Testing Laboratory, Pune, India
[2]PANGEMTECH – Panjikar Gem Research & Tech Institute, Pune, India
jayshreepanjikar@gmail.com

Keywords: ruby, Paramathi, Karur India, analyses, inclusions

Figure 1 Paramathi rubies ranging from0.91carat to1.94carats

Materials and methods

Selection of 15 rubies (Fig1) ranging from 0.91carats to 1.94 carats was done on basis of their colour and inclusions to cover the range of red colour shades and variety of inclusions observed. Where ever it was possible Laser Raman Spectroscopy was used to determine the identity of the microscopic inclusions crystallizing near the surface. Non-polarized UV-Vis-NIR spectra for all samples were collected using JASCO F660 spectrophotometer over the 350nm - 800nm range. Mid Infrared spectra of 10 samples of ruby were collected in the absorption mode in the infrared region between 4000 and 2000cm^{-1} by JASCO FT/IR-6600 with a resolution of 4cm^{-1}. Chemical analyses were carried out using Thermo Scientific ARL QUANT'X EDXRF having a detector of 30mm^2 to determine the oxide wt% of the elements present in the Paramathi rubies.

Results

Visual Appearance & Gemmological Properties: Rubies from Paramathi village exhibit shades of red colour ranging from bright dark red to light purplish red. Most of the material was transparent and all the samples examined showed prominent inclusions. Specific gravity was found to be in the range of 3.99 to 4.01, refractive indices fell in the range no1.766 to 1.772 and ne1.758-1.764 with a negative birefringence of 0.008. Strong fluorescence under LWUV and moderate to weak fluorescence under SWUV was observed under ultra violet light.

Microscopic Observations: The inclusion scenario of Paramathi rubies involves a variety of crystals of different minerals in varied sizes and shapes. Extremely small to prominently large crystals were observed (Fig 2) in some specimen. These transparent large colourless crystals were identified by Raman spectroscopy as apatite. Prismatic crystals of corundum were seen to be present in some of the specimen. Other mineral inclusions observed and identified were zircon crystals (Fig 3), spinel (Fig 4) and rutile (Fig 5).

Fig 2 Transparent apatite crystals

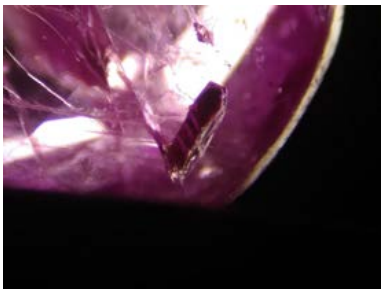

Fig 3 Zircon crystal stands out in relief

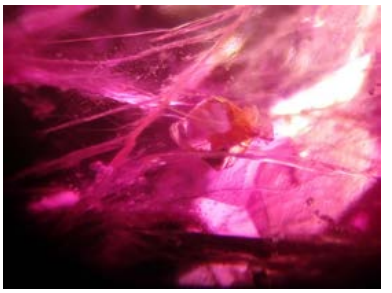

Fig 4 Octahedral crystal of spinel

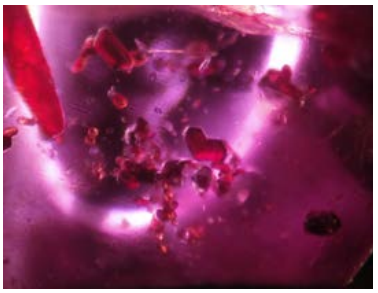

Fig 5 Rutile crystals & Rutile twin

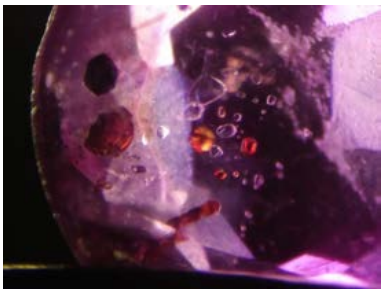

Fig 6 Orange garnet & ilmenite crystals

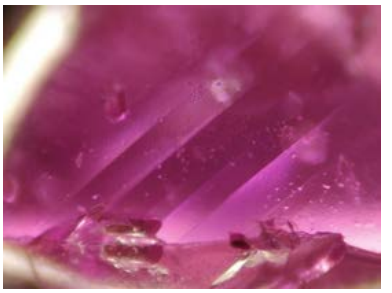

Fig7 Lamellar twinning& zircon crystals

Rutile crystals appear in all shapes even a twin crystal (Fig 5) could be clearly observed. Three of the specimens had very clear orange coloured garnets (Fig 6) which displayed their characteristic crystalline habit whereas some specimen displayed lamellar twinning as well as clusters of zircon crystals (Fig 7).

Laser Raman Spectroscopy

Apatite crystal was identified by its characteristic major peaks of Raman shift at 968cm^{-1} 1036 cm^{-1}, 1063 cm^{-1} and 584 cm^{-1}, zircon was determined by its peaks at 1008 cm^{-1} , 357cm^{-1} , 441cm^{-1} and 975 cm^{-1}. Rutile crystal had peaks at 614 cm^{-1}, 450 cm^{-1} and 802 cm^{-1} whereas the octahedral crystal gave some peaks similar to those for pink spinel at 409 cm^{-1}, 767 cm^{-1} and 668 cm^{-1} . The garnet crystal gave major peaks at 906 cm^{-1}, 850 cm^{-1}, 353 cm^{-1} and 1030cm^{-1} and the ilmenite crystal was determined by peaks of Raman shift at 159 cm^{-1}, 643 cm^{-1}, 516 cm^{-1}, 401cm^{-1} and 1311cm^{-1}.

UV-VIS-NIR Spectra

The UV-VIS-NIR spectra of Paramathi rubies showed similar patterns with a little difference in the band position that may be due the variation of the crystal field strength in individual ruby specimen. General pattern of spectra included the typical Cr^{3+} absorption peaks at 754nm, 700nm and 654nm (Figure 8). In ruby the Cr^{3+} ions occupy smaller Al^{3+} sites (Weast et al., 1981) so that they experience a stronger crystal field than in Cr_2O_3 and this results in ruby getting its red colour. The crystal field strength in ruby is rather strong and variations are dependent on the amounts of trace elements in the ruby. The purplish tinge in these rubies is due to trace elements iron and vanadium. Other peaks

406nm and 559nm have been assigned to iron and vanadium along with chromium.

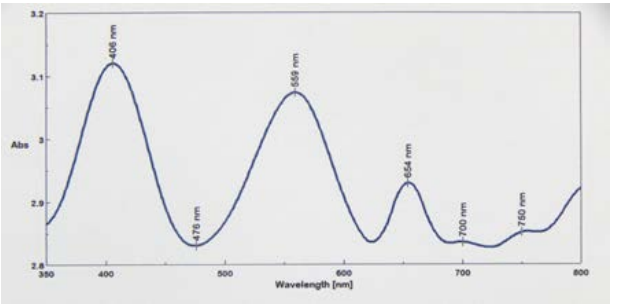

Figure 8 UV-Vis-NIR spectrum of Paramathi Ruby

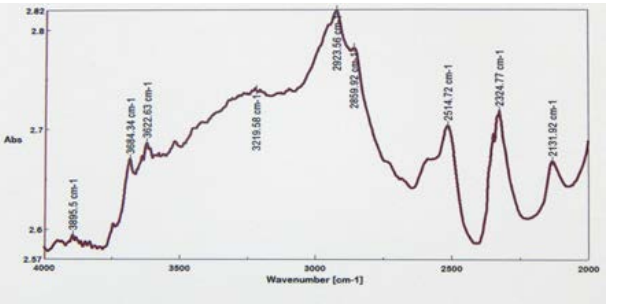

Figure 9 FTIR spectrum of Paramathi Ruby

FTIR Spectra

The FTIR spectra in the mid infrared region between 4000 and 2000cm^{-1} for the Paramathi ruby showed certain distinct features (Figure9). Each spectrum contained bands and peaks in four regions. The absorption peaks in the region between 3900 cm-1 and 3500 cm^{-1} wherein 3895 cm^{-1}, 3684 cm^{-1} and 3622 cm^{-1} peaks may be assigned to ruby. The peaks in the 3600-3700 range may be kaolinite-related, which is commonly present in natural rubies. In the next region between 3500 cm^{-1} and 3000 cm^{-1} where the general hump and peaks around 3219 cm^{-1} may be assigned to diaspore. The third region is that between 3000 cm^{-1} and 2700 cm^{-1} with prominent peaks at 2923 cm^{-1} and 2859 cm^{-1} are probably due to the stretching frequency in diaspore (Frederickson, 1954). The fourth region extending from 2700 cm^{-1} to 2000 cm^{-1} with peaks at 2514 cm^{-1} and 2131 cm^{-1} may be related to OH bending mode. This may indicate the presence of boehmite or diaspore in ruby (Smith, 1995). The peaks around 2324 cm^{-1} can be assigned to C-O bond in CO_2 (Peretti et al 1995) which is seen to be present in the fluid inclusions inside the negative crystals present in these Paramathi rubies.

Chemical Analyses

Chemical analyses by EDXRF for rubies from Paramathi gave the oxide wt % for Al_2O_3 = 94.96 to 98.86 (the concentration of Al_2O_3 in some samples was reduced by the presence mineral inclusions located at or just below the surface of the area measured). And the oxide wt % for Cr_2O_3= 0.850-1.968, for TiO_2= 0.085-0.965, for Fe_2O_3= 0.086-0.895, for V_2O_5= 0.044-0.095 and for Ga_2O_3=0.035-0.091.

Discussion

Characteristic inclusions observed in the Paramathi ruby appear to be zircon, apatite, mica, spinel and garnet. One can to some extent relate the inclusions to the paragenetic mineral assemblage in the primary rocks which are garnet-biotite schists with corundum, rutile with accessory minerals like zircon and spinel. From the infrared spectra collected for Paramathi presence of diaspore is seen from the peaks. The coexistence of Ilmenite +Corundum possibly indicates the existence of a former homogeneous process of iron oxide, diaspore and titanium oxide formed corundum (Carim et al 1997) in these rocks as shown in the following equation:

$AlO(OH)$ (diaspore) $+Fe_2O_3 +TiO_2= FeTiO_3+Al_2O_3$ (Corundum)$+H_2O$

The rutile mineral has crystallized in several forms in the Paramathi ruby. Rutile in the form of needle like crystals, sometimes as thick, short and tabular crystals of rutile or thick almost flat plate like form even twin crystal of rutile were observed. Changes and fluctuations in temperature are said to be responsible for the different morphologies of TiO_2 crystals (Camaratta et al 2011).

Conclusion

Paramathi ruby display a wide range of inclusions especially with titanium oxide. Crystalline inclusions observed and identified were zircon, spinel, garnet, ilmenite and rutile. These rubies from Paramathi, crystallized at a high temperature and with fluctuations in temperature which may have given rise to the voids and negative crystals, liquid feathers and corundum crystals inside the host. The melt had large quantity of diaspore, iron oxide and titanium oxide some of which may have got converted to corundum and ilmenite.

References

Bosshart, G. (1982): Distinction of natural and synthetic rubies by ultraviolet spectrophotometry. Journal of Gemmology 8(2), 145-160.

Camaratta, R., Acchar, W. and Bergmann, C.P. (2011): Phase transformations in the Al_2O_3/TiO_2 system and metastable phase formation at low temperatures. Rev. Adv. Mater. Sci. Vol. 27.pp64-68

Carim, A.H., Rohrer, G.S., Dando, N.R., Shih-Ying Tzeng, Rohrer, C.L. and Perrotta, A.J. (1997): Conversion of diaspore to corundum: a new α-alumina transformation sequence. Journal of the American Ceramic Society 80(10), 2677-2680.

Frederickson, L.D. Jr. (1954): Characterization of hydrated aluminas by infrared spectroscopy. Analytical Chemistry 26 (12), 1883-1885

Peretti, A., Schmetzer, K., Bernhardt, H-J., and Mouwad, F. (1995): Rubies from Möng Hsu. Gems & Gemology 31 (1) 2-26

Smith, C.P. (1995): A contribution to understanding the infrared spectra of rubies from Möng Hsu, Myanmar. Journal of Gemmology, 24(50, 321-325.

Weast R. C. and Astle, M.J. (1981): CRC Handbook of Chemistry and Physics (62nd Edition) CRC press, Inc: Boca Raton, Florida

Acknowledgements

Authors thank Mr. T. Raju for his invaluable help to visit the location and collect samples. Both authors express their sincere gratitude to National Chemical Laboratory, Dept. of Geology, University of Pune and their scientists for their assistance for carrying out some of the analyses.

REVIEW OF RUBIES AND SAPPHIRES FROM CHANTHABURI-TRAT AND KANCHANABURI GEM FIELDS, THAILAND

Wilawan Atichat[1*], Supparat Promwongnan[1], Saengthip Saengbuangamlam[1], Visut Pisutha-Arnond[1], Thanong Leelawatanasuk[1], Marisa Maneekrajangsaeng[1], Jirapit Jakkawanvibul[1], Pornsawat Wathanakul[1], Nalin Narudeesombat[1], Pimtida Bupparenoo[1], Apitchaya Buathong[1]

[1] The Gem and Jewelry Institute of Thailand (Public Organization), ITF-Tower Building, Silom Road, Suriyawong, Bangrak, Bangkok, 10500 Thailand
*awilawan@git.or.th

Keywords: ruby, sapphire, Chanthaburi-Trat, Kanchanaburi

For over 40 years, Thailand has been globally known as an important source of ruby and sapphire. The Geological Survey of Thailand studied numerous gem occurrences in Thailand and found that the potential gem fields were located in Tha Mai and Khlung Districts of Chanthaburi Province and some areas in Khao Saming District of Trat Province (Chanthaburi-Trat gem field); Bo Phloi District of Kanchanaburi Province (Kanchanaburi gem field); Wang Chin, Den Chai and Si Satchanalai (Phrae-Sukhothai gem field); Wichian Buri (Petchabun gem filed); and Nam Yuen (Ubon Ratchathani gem field). Almost all those gem fields were sapphire deposits, except some areas in Trat Province where significant ruby deposits have also been found. In the past, it was estimated that approximately 70% of all good quality rubies in the world came from Thailand. All ruby and sapphire deposits in Thailand were essentially associated with Cenozoic alkaline basaltic volcanism (Barr and MacDonald, 1978, 1981; Vichit, 1992; Sutthirat et al., 1994). They are usually found as secondary deposits, both eluvial and alluvium ones. Among those occurrences, the two most important sources are from the Chanthaburi-Trat gem field (ruby and sapphire); and the Kanchanaburi gem field (sapphire).

Chanthaburi-Trat Gem Field

Gem corundums from the Chanthaburi-Trat gem field have been widely known for a long time by Thais and foreigners as the "Ploy Chanthaboon" (Vichit, 1992). The stones are rubies and blue, green, yellow, purple sapphires as well as parti-coloured stones. The source areas in this gem field can be separated into 3 major zones (see Figure 1).

The Western Zone of Chanthaburi is where only sapphires of different colours have been recovered from the areas of Khao Wua, Khao Ploi Waen, and Ban Bang Kacha areas. The Khao Ploi Waen area has been mined for over 100 years. Nowadays, the stones in this Zone are almost depleted, except some sporadic mining activities are still active at the Ban Bang Kacha area. The deposits of this Zone are related to basaltic volcanism dated from 0.44$\pm$0.11 Ma (Barr and Macdonald, 1981) to 3.3$\pm$0.11 Ma (Sutthirat et al., 1994).

The Central Zone is between Chanthaburi and Trat (East of Chanthaburi). Various quantities of both ruby and sapphire have been recovered in Ban Bo Welu, Ban Tok Phrom, Ban Bo Na Wong, Nong Bon Noi, and many other smaller occurrences.

The Eastern Zone is in Trat. Most of the stones are ruby and rarely sapphire. The areas include Ban Suea Dao, Ban Nong Bon, Ban Bo Rai, and many other smaller deposits (see Figure 1). The geological setting here is mostly tuffaceous sandstones and volcanic agglomerates.

Based on the geochemical studies of mineral inclusions in ruby and sapphire hosts as well as sapphire-bearing and ruby-bearing xenoliths from Chanthaburi-Trat gem field, the researchers suggested that sapphires originated from incompatible-element enriched, volatile-rich, alkaline felsic magma in lower crust/upper mantle conditions (Coen-

raads et al., 1995; Sutherland et al., 1998; Intasopa et al., 1999), whereas the rubies derived from mafic granulite deeper in the mantle (e.g. at 30–50 km depth and 700 - >1000°C, Sutthirat et al. (2001); Sutthirat et al. (2018). The mantle-derived alkaline basalts were later erupted and carried the sapphires in the Western Zone, ruby and sapphire in the Central Zone, and ruby in the Eastern Zone to the surface during <~3 Ma.

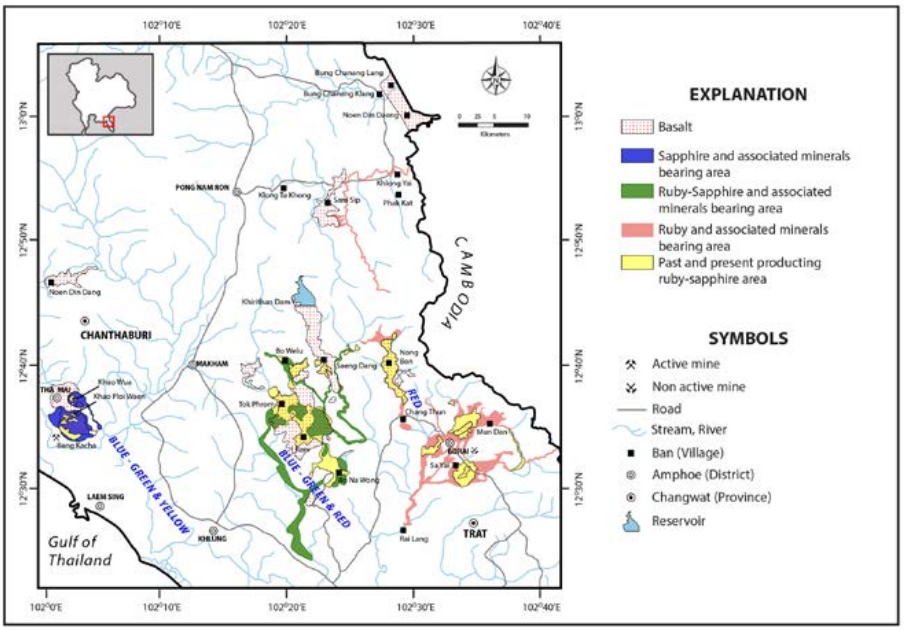

Figure 1 A map illustrating locations of rubies, and blue-green-yellow sapphires in 3 major zones of the Chanthaburi-Trat gem field. (Modified after Vichit (1992)).

Characteristics of rubies and sapphires from the Chanthaburi-Trat gem field

Ruby from this gem field has been famously known as the "Siamese Ruby", and is becoming increasingly rare in the global market. Thai ruby usually contains purple hue, except the stones found in Bo Rai and Bo Welu possess bright red colours with very minor purplish tint. Ruby from Nong Bon is being known for its relatively dark red colour, while blue sapphires from this area are relatively dark with some greenish tint.

Internal characteristics

The most diagnostic inclusions of ruby from the Chanthaburi-Trat gem field are negative crystals with healed fissures, similar to a thin film, locally called "Lai Thai" by gem traders (Figure 2a) and common diopside crystals (Figure 2b).

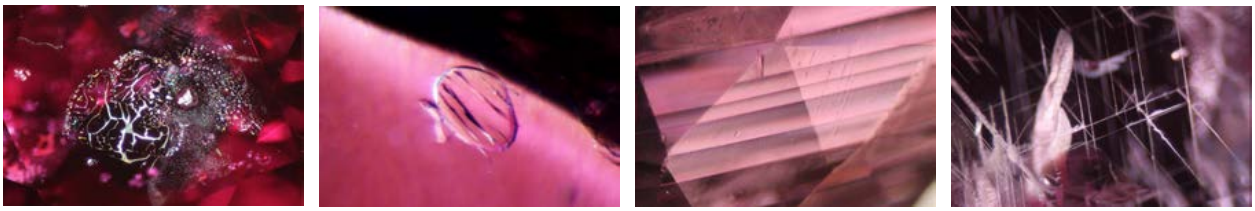

a b c d

Figure 2 Inclusions in ruby samples from Bo Rai: Negative crystals with equatorial thin-film (a; Field of View (FoV) 0.60 mm), diopside crystal (b; FoV 0.76 mm), repeated twinning (c; FoV 3.00 mm), and boehmite tubes in box work pattern (d; FoV 0.80 mm).

Other internal features are repeated twinning (Figure 2c), boehmite tubes in box work pattern (Figure2d). Examples of inclusions in blue sapphires from Chanthaburi gem field are solid crystal (Figure 3a), oriented minute particles along angular growth zones (Figure 3b), healed fissures (Figure 3c), and silks (Figure 3d).

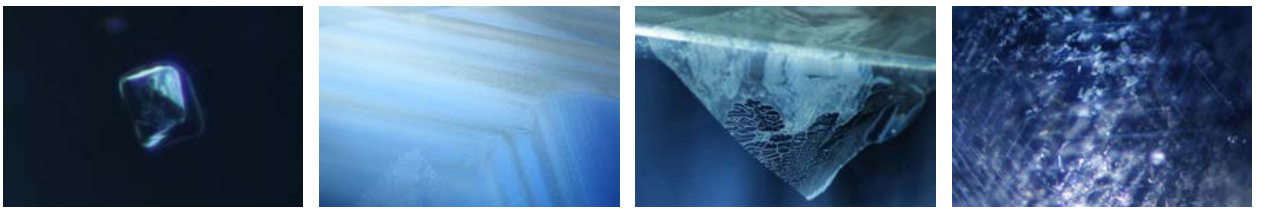

a *b* *c* *d*

Figure 3 Inclusions in blue sapphires from Chanthaburi: solid crystal (a; FoV 0.60 mm), minute particles along angular growth zones (b; FoV 1.50 mm), healed fissure (c; FoV 1.20 mm), and silks (d; FoV 1.75 mm).

Kanchanaburi Gem Field

Bo Phloi District in Kanchanaburi Province is located towards the north of Kanchanaburi town. This gem field was well known in 1990 when there were the largely mechanised mining activities enabling the exploitation of large amounts of sapphire from this source in a short period of time. Nowadays, there is only one small mining operation here. Source areas of sapphire in Kanchanaburi (Figure 4) were found in recent alluvial gravel deposits of the Lam Taphoen river system. The gems were believed to derive from the weathered 3.14-4.17 Ma alkaline basalt nearby that flowed on top of quartzite basement rocks.

Based on the geochemical studies of mineral inclusions and dating of zircon inclusions in the sapphire hosts as well as zircon+sapphire-bearing xenoliths from this gem field, it was proposed that the sapphires were derived from bimodal origins, syenitic melts and contact metamorphic sources, that occurred episodically during ~24-4 Ma as a result of the hybrid interplay of lower crustal and upper mantle materials (Pisutha-Arnond et al., 1999; Khamloet et al., 2014). Later, the eruption of mantle-derived alkaline basalt carried the sapphires from both origins along with other xenoliths and xenocrysts to the surface during ~3-4 Ma.

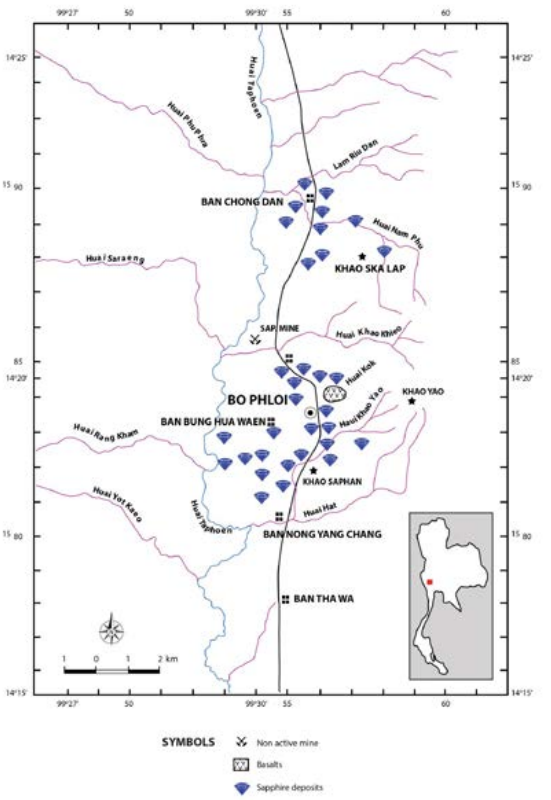

Figure 4 A map illustrating sapphire deposits in Bo Phloi District in Kanchanaburi Province.

Characteristics of sapphires from the Kanchanaburi gem field

Sapphires from this gem field are mostly light to dark blue in colour but brighter and clearer cf those of Chanthaburi. Other rare varieties of sapphire found here are yellow, pink, green, purple, and fancy-coloured (Leelawatanasuk et al., 2017).

Internal characteristics

Examples of internal characteristics of sapphires from Kanchanaburi are twin lamellae with needles (Figure 5a), minute particles (Figure 5b), strong colour bands (Figure 5c), and feldspar crystals (Figure 5d).

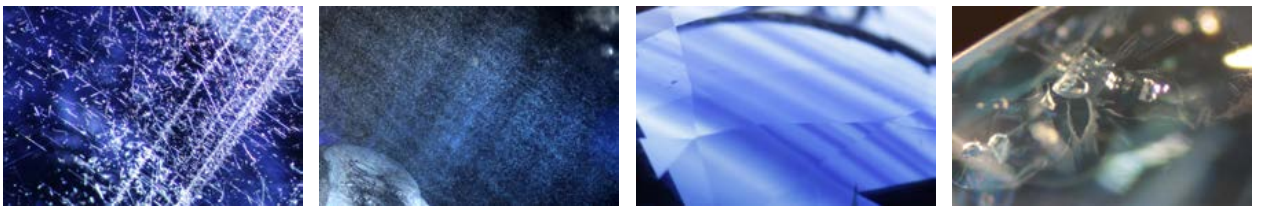

a *b* *c* *d*

Figure 5 Inclusions in blue sapphire from Kanchanaburi:Twin lamellae with needles (a; FoV 1.75 mm), minute particles (b; FoV 1.00 mm), strong colour bands (c; FoV 7.00 mm), and feldspar crystals (d; FoV 1.00 mm).

Conclusions

The important sources of ruby and sapphire in Thailand are still from the Chanthaburi-Trat gem field and the Kanchanaburi gem field. Though the main resources of these two gem fields have been exploited extensively in the past, some stones are still being supplied from the current mining operations in both fields. The ruby and sapphires from these two Thai gem fields possess distinct and unique characteristics for their colours and inclusions, and they are becoming increasingly rare in the market.

References

Barr, S.M. and MacDonald, A.S., 1978. Geochemistry and petrogenesis of Late Cenozoic alkaline basalts of Thailand. The Bulletin of the Geological Society of Malaysia, 10: 25-52.

Barr, S.M. and Macdonald, A.S., 1981. Geochemistry and geochronology of late Cenozoic basalts of Southeast Asia. Geological Society of America Bulletin, 92(Part 2): 1069-1142.

Coenraads, R.R., Vichit, P. and Sutherland, F.L., 1995. An unusual sapphire-zircon-magnetite xenolith from the Chanthaburi Gem Province, Thailand, Mineralogical Magazine, pp. 465-479.

Intasopa, S., Atichat, W., Pisutha-Arnond, V., Sriprasert, B., Narudeesombat, N. and Phuttarat, T., 1999. Inclusions in Chanthaburi – Trat corundums: A clue to their genesis, in Thai. Proceedings of the Symposium on Mineral, Energy, and Water Resources of Thailand: Towards the Year 2000, October 28-29, 1999, Bangkok, Thailand: 471-484.

Khamloet, P., Pisutha-Arnond, V. and Sutthirat, C., 2014. Mineral inclusions in sapphire from the basalt-related deposit in Bo Phloi, Kanchanaburi, western Thailand: indication of their genesis. Russian Geology and Geophysics, 55(9): 1087-1102.

Leelawatanasuk, T., Sripoonjan, T., Susawee, N., Wathanakul, P. and Pisutha-Arnond, V., 2017. Rare fancy sapphires from Bo Phloi Gem Field, Kanchanaburi, Western Thailand. Proceedings of the 35th International Gemmological Conference (IGC 2017), Windhoek, Namibia: 156-158.

Pisutha-Arnond, V., Wathanakul, P. and Intasopa, S., 1999. New evidences on the origin of Kanchanaburi sapphire. Proceedings of the Symposium on Mineral, Energy, and Water Resources of Thailand: Towards the year 2000, Bangkok, Thailand (Abstract).

Sutherland, F.L., Hoskin, P.W., Fanning, C.M. and Coenraads, R.R., 1998. Models of corundum origin from alkali basaltic terrains: a reappraisal. Mineralogy and Petrology, 133(4): 356-372.

Sutthirat, C., Charusiri, P., Farrar, E. and Clark, A.H., 1994. New 40Ar/39Ar geochronology and characteristics of some Cenozoic basalts in Thailand. Proceeding of International Symposium on: Stratigraphic Correlation of Southeast Asia, Bangkok, Thailand, November 15-20: 306-321.

Sutthirat, C., Hauzenberger, C., Chualaowanich, T. and Assawincharoenkij, T., 2018. Mantle and deep crustal xenoliths in basalts from the Bo Rai ruby deposit, eastern Thailand: Original source of basaltic ruby. Journal of Asian Earth Sciences, 164: 366-379.

Sutthirat, C., Saminpanya, S., Droop, G.T.R., Henderson, C.M.B. and Manning, D.A.C., 2001. Clinopyroxene-corundum assemblages from alkali basalt and alluvium, eastern Thailand: constraints on the origin of Thai rubies. Mineralogical Magazine, 65(2): 277-295.

Vichit, P., 1992. Gemstones in Thailand. Proceedings of the National Conference on Geologic Resources of Thailand Potential for Future Development, Supplementary Volume, 17-24 Nov.,1992. Purblished by the Department of Mineral Resources, Bangkok, Thailand, C.Piencharoen (ed.in chief): 124-150.

REVIEW OF IRON & TITANIUM DIFFUSION TREATED SYNTHETIC SAPPHIRE

Stephen Kennedy

The Gem & Pearl Laboratory Ltd, Unit 23, Arundel House, 43 Kirby Street,
London EC1N 8TE
info@thegemlab.co.uk

The 1990's saw the peak of iron and titanium diffused superficial-layered treated blue corundum (Kane, R.E. et al, 1990). This is similar but distinct from the later diffusion of lighter, smaller elements such as beryllium into corundum, which initially penetrated only to an outer layer, but later was allowed to permeate throughout the whole structure, or lattice (Emmett, J.L., et al, 2003).

The last decade has seen a proliferation of iron and titanium superficial-layered surface diffused synthetic sapphires. The differentiation of these surface-diffused natural and synthetic sapphires has been a recurring and seemingly more regular issue in the Laboratory. The concentration of colour on the pavilion facet edges prove the diffusion treatment. The observation of natural inclusions or bubbles then establish the nature of the starting material very easily. Most customers are not concerned about the distinction between natural and synthetic sapphire once they know a gem is diffused. In ten years the Laboratory has only issued 10 reports for diffused natural sapphires and six for diffused synthetic sapphires but there would be many more submissions where a verbal communication was all that was required, for which numbers are not known. The issue of the lack of noteworthy inclusions in a diffused sapphire lead to a review of identification methods, especially for any simple tests, and also the reasons for the increasing prevalence of diffused synthetic sapphires.

An early reaction to their occurrence being accidental was better explained by the commercial imperatives for their prevalence. Many synthesizers who tried growing blue synthetic sapphire have exited the industry or switched to pink, red, or colorless (Stone-Sundberg, J, 2013). The shortfall of blue synthetic sapphire can be met by diffusing synthetic white sapphire.
Additionally natural near-colourless sapphire was being sought for its use in deep lattice diffusion of sapphires with light elements such as beryllium, etc (Scarani, A, et al, 2017). Therefore the iron and titanium superficial-layered surface-diffused treaters filled the gap in supply of natural colourless sapphire with colourless synthetic sapphire.
A review of existing identification criteria is exemplified by an article from The Gem and Jewellery Institute of Thailand (GIT) (Pisuth-Arnon, V, et al, 2018). They compared Ti, Fe, and Ga contents by EDXRF (Table 1). The overlap in EDXRF concentration levels for Fe & Ti mean they are of limited assistance. It would seem that if gallium can be detected by EDXRF this would indicate a natural origin. GIT also used LA-ICP-MS to reveal Be, Mn, and V in the diffused layer of synthetic stones and Mg, B, V, and Cr in the diffused layer of natural sapphires.

	Natural Diffused Sapphire	Synthetic Diffused Sapphire
Fe content (wt %)	0.05 – 0.41	0.07 – 0.20
Ti content (wt %)	0.05 – 0.21	0.19 – 0.29
Ga content (wt %)	0.01- 0.02	< 0.01

Table 1: Comparison weight percentages of iron, titanium and gallium in natural versus synthetic diffused sapphires by EDXRF as determined by GIT

A diffused synthetic blue sapphire, similar to a crackled and healed sapphire for instance, are simply a synthetic in terms of price and disclosure. The fact a diffused synthetic can be passed off as a diffused natural corundum is an obvious advantage for the unscrupulous. So they need to be differentiated. So what if there are no recognisable inclusions.

The UV-VIS spectrum can assist – an appreciable strength in the 450 nm and 375/388 peaks would indicate natural origin. However a lack of peaks is no proof of synthetic origin, since heated sapphires, diffused or otherwise, may also have no peaks. In addition some synthetic sapphires will reveal very weak peaks. With regard to short-wave ultra-violet light fluorescence observation: the facet-related patchy fluorescence indicates diffusion having taken place but cannot be trusted in determing the original nature of the sapphire. There will be exceptions – for instance one suspect sapphire had a blue body colour under SW-UV, no colour concentration on pavilion facets, but slightly brighter facet-related fluorescence on upper girdle facets. This pointed to a synthetic origin and maybe the removal by polishing of most of the diffused outer layer. The last step in differentiating natural from synthetic sapphires is trace element analyses.

The Gemmological Association of Great Britain (Gem-A) analysed four natural colourless sapphires with a Thermo Nicolet Quant'X EDXRF spectrometer. The gallium wt% varied from 0.003 – 0.011 by the parameters employed. The Laboratory submitted one diffused sapphire of uncertain origin to Gem-A for EDXRF analysis – the 0.08 wt% gallium content was taken to indicate a natural origin. Whereas another suspect stone revealed a content of gallium below detection limits and was assumed to be synthetic.

It is possible that natural colourless sapphires may have concentration levels lower than 0.01 wt% (as specified by EDXRF @ GIT) and would therefore require LA-ICP-MS or LIBS to provide a lower cut-off point between natural and synthetic sapphires. However for the time being EDXRF provides a cost-effective back-stop for separating these relatively cheap treated stones.

References

Kane, R.E, et al, 1990. The identification of blue diffusion-treated sapphires. *Gems & Gemology*, Vol. 26, No.2, pp. 115-133

Emmett, J.L., et al 2003. Beryllium Diffusion of Ruby and Sapphire, *Gems & Gemology*, Vol. 39, No.2, pp. 84-135
Pisutha-Arnon, V, et al, 2018. New Blue-diffused Sapphires from Synthetic vs Natural Starting Materials (http://www.git.or.th/eng/testing_center_en/lab_notes_en/glab_en/2018/08/Article-2008201802.pdf)

Scarani, A., et al, 2017. The strange revival of diffused sapphires. But this time they are synthetic (http://www.rivistaitalianadigemmologia.com/en_GB/2017/07/21/lo-strano-revival-degli-zaffiri-termodiffusi-questa-volta-pero-sono-sintetici)

Stone-Sundberg, J., 2013. Sapphire Series Part 4: Gem Synthetic Sapphire and Diffusion-Treated Synthetics, (https://www.gia.edu/gia-news-research-sapphire-series-treated-synthetics)

Acknowledgements

Thanks to Charles Evans and Pat Daly at the Gemmological Association of Great Britain for running the EDXRF spectra

Be-containing nano-inclusions in untreated blue sapphire from Diego, Madagascar

Kentaro Emori [1*], Hiroshi Kitawaki [1], Akira Miyake [2],

[1] Central Gem Laboratory (Miyagi Bldg. 6th Fl. 5-15-14, Ueno Tito-ku, Tokyo, Japan),
[2] Kyoto University (Japan)
*emori@cgl.co.jp

Keywords: corundum, nano-inclusion, TEM, beryllium

Abstract
We studied the origin of Beryllium in natural corundum using the Be-containing untreated blue sapphire from Diego, Madagascar. LA-ICP-MS analysis shows good relationship among Be, Nb and Ta and their molar ratio is about 3: 1: 4. Under TEM, Nano-inclusions which have 20-40 nm in length and 5-10 nm in width are observed and those inclusions have Ti, Nb, Ta and their molar ratio is about 16 :1 :4. Although we couldn't perform structural analysis, those inclusions might be an unknown mineral.

Introduction
Since September 2001, Beryllium diffusion treated corundum has been widely seen in gem market across the world. Initially, it was thought that Beryllium did not exist within untreated corundum, but traces of naturally occurring Be have subsequently been confirmed in untreated corundum (e. g. Shen et al., 2007). At present, methods for determining whether the origin of Be is natural have been established to some extent (Emori et al., 2014), but the origin of natural Be remains unknown.

Shen et al. 2012 found that clouds in samples from Ilakaka, Madagascar, are associated with traces of Be, Nb and Ta, and that there are nano-inclusions 20-40 nm long and 5-10 nm wide which are unnamed high-pressure mineral that has the same composition as rutile, but has the crystal structure of scrutinyite (a-PbO_2). But there was no discussion about Be and nano-inclusions.

The purpose of this study is to reveal the relationship between beryllium and nano-inclusions in naturally Be-containing sapphires.

Material and Method
In this study, we analyzed 30 untreated blue sapphire (rough) from Diego, Madagascar. Each sample polished by one side for analysis. To detect trace elements, we employed LA-ICP-MS system; ESI UP-213 for laser ablation and Agilent 7500a for ICP-MS. Analysis conditions were as follows; Laser ablation setting: laser wavelength 213nm, crater size 80µm, laser power 10 J/cm2, laser frequency 20Hz, ICP-MS setting: ICP 27.15MHz, RF power 1200W, Plasma gas(Ar) 14.93 l/min, Auxiliary gas(Ar) 0.89l/min, Carrier gas(Ar) 1.44l/min, Target Mass 9Be, 24Mg, 27Al, 47Ti, 51V, 53Cr, 57Fe, 69Ga, 90Zr, 93Nb, 118Sn, 178Hf, 181Ta, 182W, 232Th. In addition, in order to perform TEM observation, we used Quanta 200 3DS for FEI (acceleration voltage: 30 kV and 5 kV) and JEOL JED-2100F for TEM (acceleration voltage: 200 kV).

Result and Discussion
Be was detected in 27 out of 30 samples used in this study. The most abundant sample contained 26.0 ppmw of Be. Other than Be, Mg, Ti, V, Fe, Sn, Ta, W and Th were detected. We analyzed sample 10 in detail in which the concentrations of Be from points measured were 14.16 ppm and less. Using laser ablation spots of 80 micron meter, we performed two line-analysis (spots 1 to 30 and spots 31 to 57) with regular intervals. Each result of Be, Ti, Nb and Ta are shown in Figure 1.

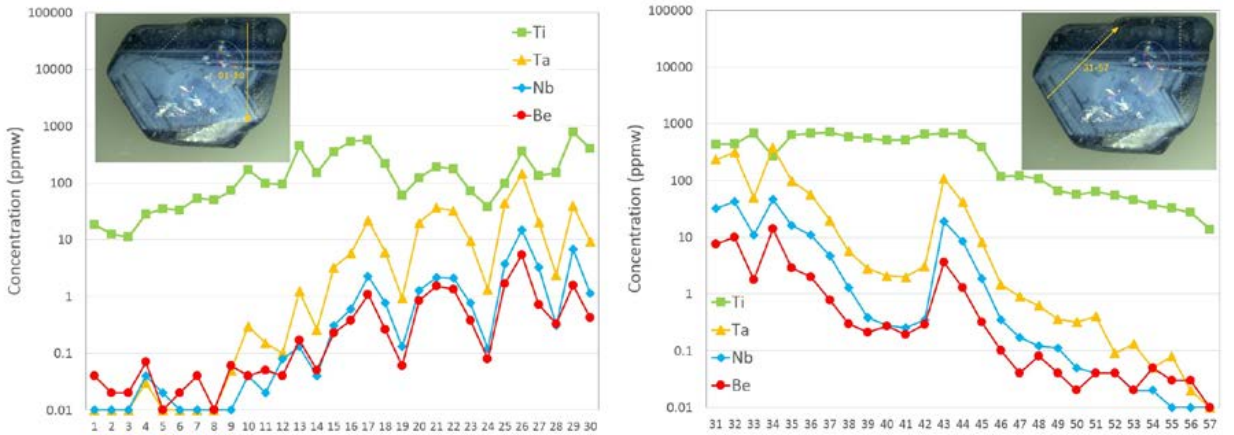

Figure 1. Be, Ti, Nb and Ta concentrations of line analysis in sample 10

There are good correlations among Be, Nb and Ta, and less correlations with Ti Figure 2 shows Be-Nb and Be-Ta plots measured from spots 01-57 in the line analysis. This correlation matches the results of the basaltic blue sapphire from Cambodia, Nigeria and Laos in our previous study (Emori et al. 2014). The molar ratio was estimated from the concentration relationship among Be, Nb and Ta, and the result of Be: Nb: Ta = 3: 1: 4 could be obtained.

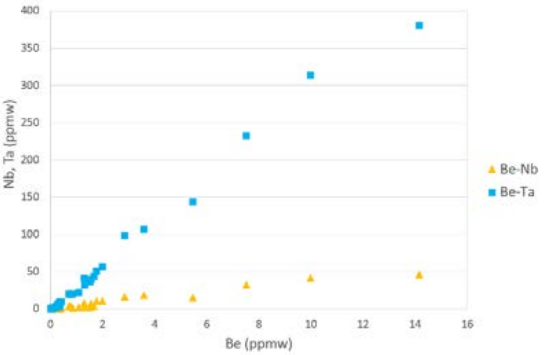

Figure 2. The relations between Be-Ta and Be-Nb in sample 10

We prepared two TEM specimens from areas with maximum concentration of Be and with no-Be from sample 10 using FIB. TEM observation showed nano-inclusions with lengths of 20-40 nm and widths of 5-10 nm in the Be containing specimen (Figure 3), but we could not find any nano-inclusions in the Be free specimen. As a result of EDS analysis of this inclusion, Al, Ti, Fe, Nb and Ta were detected and it was found the molecular ratio of Ti, Nb and Ta was Ti: Nb: Ta = 16: 1: 4. Only Al and Fe were detected from area apart from the nano-inclusion. Moreover, this inclusion turned out to be another phase from corundum, although the phase could not be identified (Figure 4).

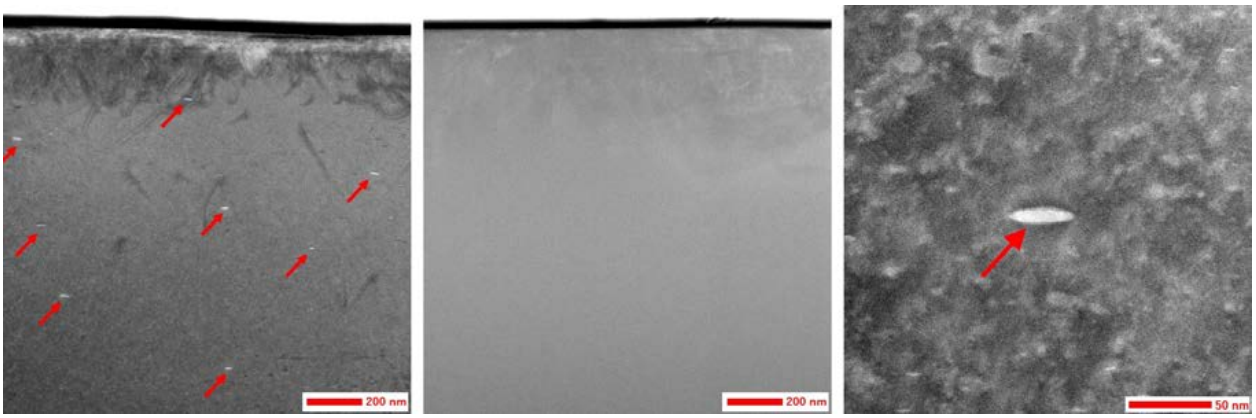

Figure 3. (Left) nano-inclusions in area with maximum concentration of Be. (Center) no inclusions in Be free area. (Right) Nano inclusions with length 40 nm and width 5 nm.

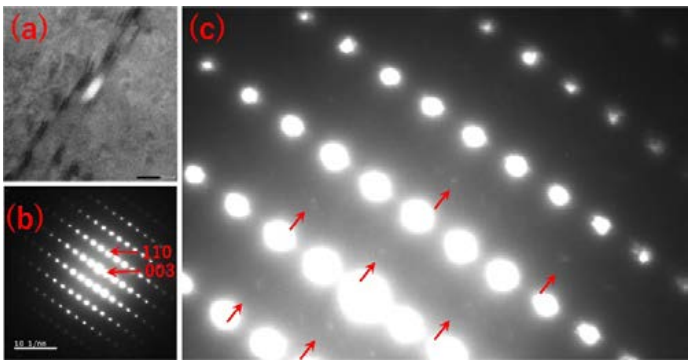

Figure 4. TEM images of a corundum sample containing nano-inclusion. (a) a bright field image showing a nano-inclusion. (b) Diffractions pattern of the area containing nano-inclusions. Strong spots are from corundum structure. (c) an enlarged view of (b). There are other spots (red arrows) between diffraction spots of corundum. The weak spots are of nano-inclusion and have structure different from corundum.

Conclusion

Based on the results above, nano-inclusions in untreated blue sapphire containing Be from Diego, Madagascar, contains Ti, Nb and Ta as well, and showed relationship between with Beryllium and nano-inclusions. Although their crystal structure phase has not been determined, it may be an unknown mineral which have scrutinyite (a-PbO_2) structure (Shen et al. (2012)) and has the chemical composition of Be: Ti: Nb: Ta = 3: 16: 1: 4.

References

Emori K., Kitawaki H., Okano M., 2014. Beryllium-Diffused Corundum in the Japanese Market, and Assessing the Natural vs. Diffused Origin of Beryllium in Sapphire. Journal of Gemmology, 34(2), 130-137

Shen A., McClure S., Breeding C. M., Scarratt K., Wang W., Smith C., Shigley J., 2007. Beryllium in Corundum: The Consequences for Blue Sapphire. GIA Insider, Vol.9, Issue 2 (January 26, 2007)

Shen A., Wirth R., 2012. Beryllium-Bearing nano-inclusions identified in untreated Madagascar sapphire. Gems & Gemology, 48(2), 150-151

UPDATE ON Fe AND Ti OXIDATION STATES IN RUBY AND BLUE SAPPHIRE

Wiwat Wongkokua[1], Natthapong Monarumit[2], Aumaparn Phlayraharn[2], Somruedee Satitkune[2], Pornsawat Wathanakul[2*]

[1] Department of Physics, [2] Department of Earth Science, Kasetsart University, Thailand
* pwathanakul2@gmail.com

Keywords: Fe Ti oxidation state, Ruby and Blue sapphire, XANES

Abstract
The series of experiments on corundum crystal chemistry using X-ray Absorption Near Edge Spectroscopy (XANES) have been conducted on blue sapphires of different natures (natural, synthetic and diffusion), ruby and sapphire samples of different localities, and those experienced heating in oxidising and reducing conditions. The results revealed the Fe and Ti oxidation states in those samples are always present as 3+ and 4+, respectively.
Hence, instead of the Fe^{2+}/Ti^{4+} IVCT, the mixed acceptors in the energy band gap above the valence band of corundum, related to Fe^{3+}/Ti^{4+} pairs have been proposed, and thus assigned for 580 and 710 nm absorptions, leading to the new explanation/understanding of the cause of blue colour in sapphire. The UV-Vis-NIR and FTIR spectroscopic studies have helped support this finding.

Introduction
The gemstone and mineral science research group, Kasetsart University, Bangkok, Thailand, has conducted the series of experiments to unveil questions related to gem corundum crystal chemistry in order to gain more understanding and update the finding to gemmological forum. Gemmologists and mineral scientists have learnt and followed publications made by many authorities in physics and chemistry of colour in gemstones; the crystal field has been used to explain red colour of ruby, blue is according to the intervalence
charge transfer (IVCT) by traces of Fe^{2+} and Ti^{4+} in sapphire structure and the yellow is produced by Fe^{3+} replacing Al^{3+} (e.g., Nassau, 1978, 1987 and 2001; Fritsch and Rossman, 1987 and 1988a). In order to reveal the trace element chemistry in gem corundum in particular ruby and blue sapphire, the oxidation states of Fe and Ti have been measured using the synchrotron facility, mainly the X-ray Absorption Near Edge Spectroscopy (XANES) and sometimes the Extended X-ray Absorption Fine Structure (EXAFS) techniques at the Synchrotron Light Research Institute (SLRI), Nakhon Ratchasima, Thailand. Besides, the UV-Vis-NIR and FTIR have been used to help support the results of XANES study.

Experimental & Results
One of the research experiments is the XANES study of Fe and Ti oxidation states in blue sapphire samples of different natures (natural, synthetic, Be-treated and surface diffusion ones). The standards of different oxidation states were used (see Notes under Table 1). The results of all samples showed the K-absorption edges for iron at 7124 eV corresponding Fe^{3+}, and those of titanium edges at 4984 eV indicating Ti^{4+} (Wongrawang et al., 2016). This certainly surprised the research team since the Fe^{2+}/Ti^{4+} IVCT has always been referred for the cause of blue colour in sapphire, and always labelled as such in UV-Vis- NIR absorption spectra. A measurement on polished rough sapphire samples also showed most of the results in Fe^{3+} and Ti^{4+}; however, one sample showed a mixed K-absorption edge of Fe^{2+} and Fe^{3+}, which later revealed the contamination of exposed ilmenite ($Fe^{2+}TiO_3$) inclusions (Monarumit et al., 2016; 2017b). The consequent series of experimental work was carried out on blue sapphire, and also on ruby samples, from different localities and nature of occurrences (metamorphic vs basaltic) as well as on those undergone heating in oxidising and reducing conditions; again the results indicated Fe^{3+} and Ti^{4+} species in all samples (Monarumit et al., 2017a; Phlayraharn et al., 2018). The XANES results are given in Table 1, with the K-edge energy 7124 eV corresponding to Fe^{3+}, no matter on the natural or heated samples at oxidising or reducing conditions. Hence, the new explanation of the finding has been made based on the energy band theory (see Fritsch and Rossman, 1988b)

instead of the IVCT as usual. The energy states at 2.14 and 1.75 eV have been proposed as being the mixed acceptors in the band gap above the corundum valence band, corresponding to UV-Vis absorptions at 580 and 710 nm, respectively; hence, the Fe^{3+}/Ti^{4+} pairs could have been responsible for those absorptions.

Besides, the polarised FTIR spectroscopy has been used to help understand this finding of the XANES results. The 3309 cm^{-1} series and its side absorption peaks (3232, 3184 cm^{-1}) have been proposed and assigned for Ti-OH stretching (Phlayraharn et al., 2014; 2016). Only the samples with high Ti content in particular, blue sapphire and ruby with blue sectors, normally show those 3309 absorption series peaks. This supports the charge balance of M^{3+}- Ti^{4+} can be made by OH^-. The reason on the gradual change of infrared absorption intensity of 3309 cm^{-1} series has been explained based on the extent of Ti content and structural rearrangements of trace elements in particular on Ti-OH. (Phlayraharn et al., 2018; 2019).

Table 1. Representatives of K-absorption edges obtained by XANES technique, indicating the oxidation states of Fe and Ti (Wongrawang et al., 2016; Monarumit et al., 2017a, b; Phlayraharn et al., 2018; 2019).

Type of sample	Fe K-edge absorption energy (eV)	Ti K-edge absorption energy (eV)	Corresponding to: Fe, Ti
Natural blue sapphire	7124	4984	Fe^{3+}, Ti^{4+}
Synthetic blue sapphires	7124	4984	Fe^{3+}, Ti^{4+}
Diffusion blue sapphire	7124	4984	Fe^{3+}, Ti^{4+}
Be-heated blue sapphire	7124	4984	Fe^{3+}, Ti^{4+}
Heated blue sapphires (oxidising)	7124	4984	Fe^{3+}, Ti^{4+}
Heated blue sapphires (reducing)	7124	4984	Fe^{3+}, Ti^{4+}
Ruby (unheated)	7124	4984	Fe^{3+}, Ti^{4+}
Heated ruby (oxidising)	7124	4984	Fe^{3+}, Ti^{4+}
Heated ruby (reducing)	7124	4984	Fe^{3+}, Ti^{4+}

Notes: K-absorption edges of standards (eV): Fe^0; iron foil (7112), FeO; Fe^{2+}; ferrous oxide (7119), Fe_2O_3; Fe^{3+}; ferric oxide (7124), Ti^0; titanium foil (4966), Ti^{4+}; titanium dioxide (4984).

Concluding Remarks

The research experiments have led to the new understanding of gem corundum crystal chemistry as follows: Fe always presents as Fe^{3+}. Ti oxidation state is 4+ and is a reactive trace element in gem corundum. Hence, for blue colour in sapphire, the 580 and 710 nm absorptions in UV-Vis-NIR spectra have been proposed for Fe^{3+}/Ti^{4+} pairs, instead of Fe^{2+}/Ti^{4+} IVCT, and those absorptions correspond to the energy levels in the band gap of corundum at 2.14 and 1.75 eV above the corundum valence band, respectively. The blue colour appears when undergone reduction and fading under oxidising environment (Pisutha-Arnond et al., 2015) can be explained based on the energy states that the reduction can cause more electron holes on the energy levels 2.14 and 1.75 eV, thus promoting electron transitions from the corundum valence band to those mixed acceptors in the gap, and the 580 and 710 nm absorptions being raised up, i.e. more blue developed; vice versa, on heating under oxidation, electrons are added to holes on those mixed acceptors, i.e. the holes are filled up, therefore no electron transitions required, resulting in hindering/fading of the blue colour. Besides, the energy states of 1.99 and 1.36 eV were also calculated by the simulation of Fe^{2+}/Ti^{4+}pairs in the corundum structure (Na-Phattalung et al., 2018); however, by this postulation, the absorptions could be at 623 and 912 nm, in which the former does not exist in the UV-Vis-NIR spectra of blue sapphire, whilst the latter is beyond the visible perception. Our proposal on the existing of

Fe^{3+}/Ti^{4+} pairs is based on experimental results, enabling to make fit by the explanation using the energy band model. In addition, to make the charge balance by IVCT would require more species of both Fe^{2+} and Ti^{4+} cf the electron-hole model which requires a lesser amount of Fe^{3+} and Ti^{4+} to induce the valence electron transitions. The extent of Ti content in ruby and sapphire samples provides different absorptions of the 3309 cm^{-1} and its side peaks (3232, 3184 cm^{-1}) which have been assigned for Ti-OH stretching (Phlayraharn et al., 2014 and 2016). Only the samples with high Ti content, in particular blue sapphire and ruby with blue sectors, normally show these 3309 cm^{-1} series peaks. To the real space, this helps indicate the charge balance of M^{3+}-Ti^{4+} pairs by OH^-, where M^{3+} could either be Al^{3+}, Fe^{3+}, or Cr^{3+}, depending on the varieties of the samples. Further research on the crystal chemistry of corundum should be conducted.

References

Fritsch E. and Rossman G.R., 1987. An update on color in gems. Part 1: Introduction and colors caused by dispersed metal ions. Gems & Gemol. 23 126-139.

Fritsch E. and Rossman G.R., 1988a. An update on color in gems. Part 2: Colors involving multiple atoms and color centers. Gems & Gemol. 24 3-15.

Fritsch E. and Rossman G.R., 1988b. An update on color in gems. Part 3: Colors caused by band gaps and physical phenomena. Gems & Gemol. 24, 81-102.

Monarumit N., Wongkokua W. and Satitkune S., 2016. Fe^{2+} and Fe^{3+} oxidation states on natural sapphires probed by X-ray absorption spectroscopy. Procedia Computer Science 86 180-183.

Monarumit N., Wongkokua W. and Satitkune S., 2017a. Oxidation state of Ti and Ti-O bond length on natural sapphire probed by X-ray absorption spectroscopy. Key Eng Mater. 737, 585-589.

Monarumit N, Satitkune S. and Wongkokua W., 2017b. Role of ilmenite micro-inclusion on Fe oxidation stats of natural sapphires. J. Phys.: Conf. Ser. 901 012074, 4pp.

Na-Phattalung S., Limpijumnong S., T-Thienprasert J. and Jaejun Y., 2018. Magnetic states and intervalence of Ti and Fe defects in alpha-Al_2O_3: The origin of the blue in sapphire. Acta Mat. 143, 248-256.

Nassau K., 1978. The origins of colour in minerals. The American Mineralogist. 63, 219-229.

Nassau K., 1994. Gemstone Enhancement Science and State of Art. Redwood Book, Wiltshire, 264 p.

Nassau K., 2001. The Physics and Chemistry of Colour: The Fifteen Causes of Color. John Wiley & Son, New Jersey, 481 pages.

Phlayrahan A., Monarumit N., Satitkune S. and Wathanakul P., 2014. If diaspore is responsible for the 3309 cm^{-1} peak in the FTIR spectra of heated ruby samples. 4th GIT2014, Thailand, 211-216.

Phlayrahan A., Monarumit N., Satitkune S. and Wathanakul P., 2016. Phase transformation of diaspore and its application for indicating the low-temperature heat treatment of corundum samples. 5th GIT2016, Thailand. Proceedings paper, 167-170.

Phlayrahan A., Monarumit N., Satitkune S. and Wathanakul P., 2018. Role of Ti content on the occurrence of the 3309 cm^{-1} peak in FTIR absorption spectra of ruby samples. J Appl. Spectros. 85 385-390.

Phlayraharn A., Monarumit N., Lhuaamporn T., Satitkune S. and Wathanakul P., 2019 accepted. Spectroscopic investigation revealing the heating experiment of blue sapphire samples. J Appl.
Spectros.

Pisutha-Arnond V., Rochd C., Atichat W., Wathanakul P., Narudeesombat N., 2015. Role of Be in reduction and oxidation heating of sapphire. 34th IGC 2015, Lithuania. Proceedings paper, 65-68.

Wongrawang P., Monarumit N., Thammajak N., Wathanakul P. and Wongkokua W., 2016. Oxidation states of Fe and Ti in blue sapphire. Mater Res Express 3 02620, 7 p.

Acknowledgements
The institutions namely: Department of Physics, Department of Earth Sciences, and the Graduate School, Kasetsart University, Bangkok, Thailand; The Gem and Jewelry Institute of Thailand; Synchrotron Light Research Institute, Nakhon Ratchasima, Thailand are thanked for their supports on staff, facilities and funding.

Low-temperature and flux assisted heat treatment of rubies and pink sapphires from Mozambique and Greenland

Tom Stephan [1], Claudio C. Milisenda[2], Angunguak Th. Jepsen [3]

[1]German Gemmological Association, Idar-Oberstein, Germany
[2]DSEF German Gem Lab, Idar-Oberstein, Germany
[3]Greenland minerals & gems, Nuuk, Greenland
ccm@dgemg.com

Keywords: Ruby, low-temperature treatment, heat treatment, flux assisted healing

With the new finds of rubies and pink sapphires in Mozambique and Greenland, the supply of material with potential for various treatments significantly increased. Besides origin determination, the identification of these treatments is one of the main goals for gemmological laboratories nowadays. For this study, rubies and pink sapphires from these new occurrences have been treated at different temperatures, partially assisted by chemicals, to reproduce the results observed in stones from the trade and to improve the identification capabilities.

In 2009, first reports and analyses about rubies from a new find in Montepuez, Mozambique were published from various authors (Hänni & Krzemnicki, 2009, McClure & Koivula, 2009). The production increased drastically in 2011 when Gemfields entered a partnership with Mwriti, the earlier owner of the mine. A detailed description of the occurrence is given by Pardieu et al. (2013). The samples from Mozambique used for this study where collected by the second author in 2015 during a field trip to Mozambique.

The Montepuez ruby mine produces a wide range of different qualities starting from high-quality material which enters the market untreated going down to low-quality opaque material, suitable only for lead glass filling.

Possible heat treatments for rubies and pink sapphires from Mozambique start at rather low temperature under 1000°C (Pardieu et al., 2010, 2015, Saeseaw et al., 2018, Stephan et al., 2018, Sripoonjan, 2016). Own experiments show, that it is possible to remove disturbing bluish colour zones by a low-temperature heat treatment at approx. 800°C (figures 1 & 2). It can be identified by a combination of microscopic (especially oxidation of iron hydroxides) and spectroscopic methods (disintegration of aluminium hydroxides and transformation of iron hydroxides to iron oxides).

Stones with more fissures are customarily treated at higher temperatures involving fluxes to improve their colour and clarity as well. Flux assisted heat treatments for this study were undertaken using "borax".

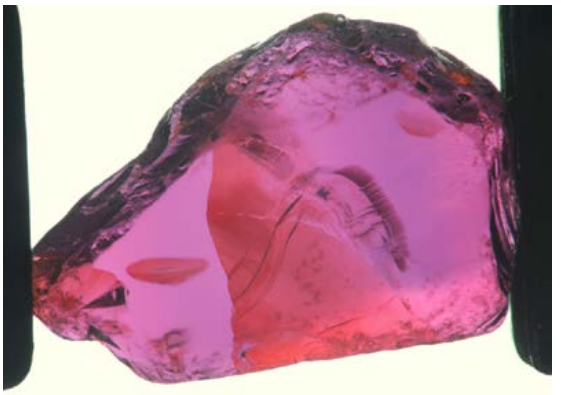

Figure 1: A polished slice of a Mozambican ruby (Mugloto pit), showing its blue colour zone before the heat treatment process (transmitted light, image width 11.09 mm). Note the orangey colour of the "natural staining".

Figure 2: The slice from figure 1 after the low-temperature treatment (900°C, 8h) (transmitted light, image width 11.41 mm). Note the reddish colour of the "natural staining".

Rubies from Greenland are already known since 1966 (Gübelin, 1979, Petersen and Secher, 1993, Rivalenti, 1974, Secher and Appel, 2007). Various occurrences have been discovered in the Archean block of West Greenland and mapped, which, however, did not produce rubies in commercially important amounts since 2014 (granted exploitation license), when True North Gems Inc. (now: Greenland Ruby) obtained a license of a 3600 sq. km area (Thirangoon, 2009). In addition to that operation a number of small scale mining activities is going on and the miners offer a diverse range of minerals from Greenland including ruby and pink sapphires.

The last years rubies from Greenland became more and more popular and begun being available in the trade. The crystals are found in sizes up to a few kilograms but are usually opaque and full with fissures and twinning lamellae, along which aluminium hydroxides are incorporated. Untreated stones over 0.5 ct are rare, most of the stones have to be heat treated involving fluxes before the cutting process (figure 3).

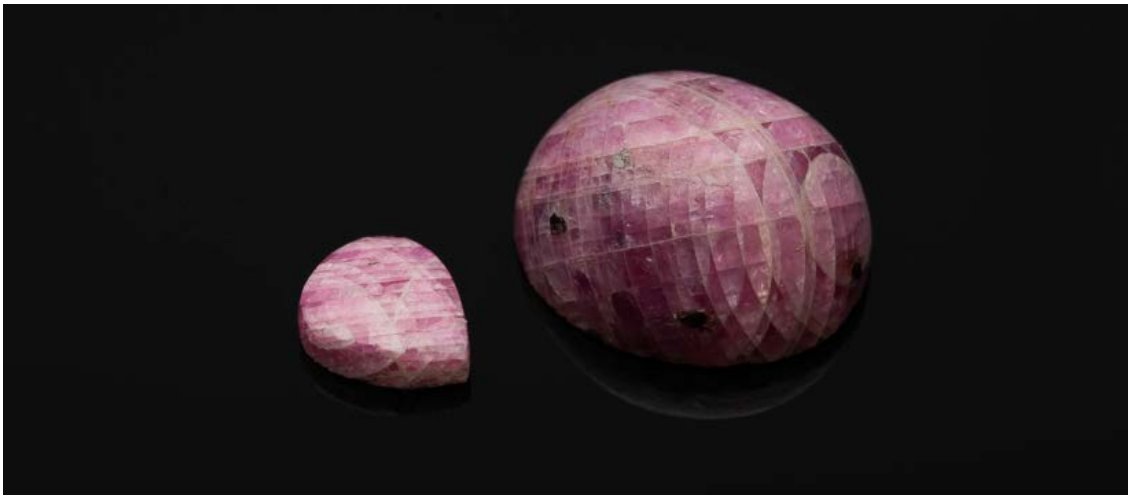

Figure 3: Pink sapphires from Greenland, heated without flux. Note the whitish striation along the twinning lamellae caused by the dehydration of aluminum hydroxides, which form polycrystalline corundum (Photo: Benjamin Huaysan, DSEF).

The samples we are experimenting with now were kindly donated by the company Greenland minerals & gems, Nuuk, Greenland. Our own experiments show, that heat treatments without fluxes are unrewarding: the aluminium hydroxides along twinning lamellae dehydrate, leaving white layers of polycrystalline corundum (Wehrmeister & Häger, 2005). Furthermore, the samples often break caused by the expansion of water. To avoid these circumstances experiments with fluxes are running now (figure 4).

Figure 4: Pair of rubies from Greenland, heated in a borax flux (Photo: Benjamin Huaysan, DSEF).

The heat treatment experiments are part of an ongoing research project of the German Gemmological Association and the DSEF German Gem Lab. All the stones are treated in the Nabertherm high-temperature oven (LHT 02/18/P470) of the German Gemmological Association, which enables temperatures up to 1850°C.

References

Gübelin, E. J. 1979. Fiskenaesset: Rubinvorkommen auf Grönland. Lapis, 4(3), 19-26 (in German).

Hänni, H. A. & Krzemnicki, M. S. 2009. Das neue Rubinvorkommen von Montepuez, Mosambik. Zt. Dt. Gemmol. Ges, 58(3/4), 127-130 (in German).

McClure, S. F. & Koivula, J. I. 2009. Preliminary observations on new rubies from Mozambique. Gems & Gemology 45(3), 224-225.

Pardieu, V., Saeseaw, S., Detroyat, S., Raynaud, V., Sangsawong, S., Bhusrisom, T., Engniwat, S. & Muyal, J. 2015. GIA lab reports on low-temperature heat treatment of Mozambique ruby. https://www.gia.edu/gia-news-research-low-temperature-heat-treatment-mozambique-ruby.

Pardieu, V., Sangsawong, S., Muyal, J., Chauviré, B., Massi, L. & Sturman, N. 2013. Rubies from the Montepuez area (Mozambique). http://www.giathai.net/wp-content/uploads/2015/02/GIA_Ruby_Montepuez_Mozambique.pdf.

Pardieu, V., Sturman, N., Saeseaw, S., du Toit, G. & Thirangoon, K. 2010. Treated Ruby from Mozambique - a preliminary report. http://www.giathai.net/pdf/Flux_heated_and_glass_filled_rubies_from_Mozambique.pdf.

Petersen, O. V. & Secher, K. 1993. Minerals of Greenland. Mineralogical Record, 24(2), 1-65.

Rivalenti, G. 1974. A ruby corundum pegmatoid in an area near Fiskenaesset, South-west Greenland. Bolletino del Servizio Gelogico d'Italia, 93, 23-32.

Saeseaw, S., Konsomart, B., Atikarnsakul, U., Khowpong, C., Vertriest, W. & Soonthorntantikul, W. 2018. Update on "low-temperature" heat treatment of Mozambican ruby: A focus on inclusions and FTIR spectroscopy. https://www.gia.edu/doc/low_HT_Moz_report.pdf.

Secher, K. & Appel, P. 2007. Gemstones of Greenland, Geology and Ore: Exploration and mining in Greenland, 1-12.

Stephan, T., Milisenda, C. C. & Müller, S. 2018. Untersuchungen an Rubinen und pinkfarbigen Saphiren aus Montepuez, Mosambik. Zt. Dt. Gemmol. Ges., 67(3/4), 11-28 (in German).

Sripoonjan, T., Wanthanachaisaeng, B. & Leelawatanasuk, T. 2016. Phase transformation of epigenetic iron staining: indication of low-temperature heat treatment in Mozambique ruby. Journal of Gemmology, 35(2), 156-161.

Thirangoon, K. 2009. Ruby and Pink Sapphire from Aappaluttoq, Greenland. Status of on-going research. GIA Laboratory, Bangkok.

Wehrmeister, U. & Häger, T. 2005. Edelsteine erkennen - Eigenschaften und Behandlungen. Rühle-Diebener-Verlag, Stuttgart (in German).

BERYLLIUM HEAT-TREATED BLUE SAPPHIRE FROM SRI LANKA

Sutas Singbamroong[1,2*], Panjawan Thanasutthipitak[1], Thawatchai Somjaineuk[3], Nirawat Thammajak[4], Chatree Saiyasombat[5], Nazar Ahmed[2], Phisit Limtrakun[2]

[1] Department of Geological Science, Chiang Mai University, Thailand
[2] Dubai Central Laboratory Department, Dubai, United Arab Emirates
[3] Chanthaburi Gem and Jewelry Manufacturer Association, Chantaburi, Thailand
[4] School of Chemistry, Institute of Science, Suranaree University of Technology, Nakorn Ratchasima, Thailand
[5] Synchrotron Light Research Institute (Public Organization), Nakorn Ratchasima, Thailand
*sutas.singbamroong@gmail.com

Keywords: Beryllium, Blue Sapphire, Sri Lanka

Since at least 2000, corundum treated by new technique involving beryllium (Be) heat-treatment has been discovered and developed in Chantaburi, Thailand. The process involved introduction of beryllium into corundum creating yellow, orange or brown color components which turn pink sapphire to a "padparadscha", nearly colorless or pale-colored corundum to yellows and oranges as well as bluish rubies to fine red color. It can also lighten the over-dark blue basaltic sapphires where concentration $[Ti^{4+}] >> [Mg^{2+}]$ to $[Ti^{4+}] > [Mg^{2+}+Be^{2+}]$ condition which reducing blue color saturation resulted in more attractive color.

For this study, samples of transparent to translucent milky-white to yellow, purple to violet, and light to medium blue sapphires from Sri Lanka (metamorphic origin) were heat treated with Be in three types of furnace (gas, electric and fuel) at various temperatures and in both oxidizing and reducing atmospheres. The technique of Thawatchai Somjaineuk (a Thai gem heating specialist) was used to intensify blue color, improve clarity, and distribute uneven color. Somjaineuk's technique has been used to enhance Sri Lankan corundum with a milky/silky appearance since 2004 and supplies approximately 50 kg of beryllium-treated blue sapphire per year to the gem market.

The samples were studied after each step of heating for basic gemological properties, spectroscopic properties using ultraviolet/visible/near-infrared (UV-Vis-NIR) and Fourier-transform infrared (FTIR) absorption spectroscopy, and chemical composition using laser ablation–inductively coupled plasma–mass spectrometry (LA-ICP-MS). X-ray absorption spectroscopy (XAS) in fluorescence mode is a non-destructive technique that can be used to study the oxidation state of transition metal defects down to 50 ppm levels in solid-state samples. X-ray absorption near edge structure (XANES) is therefore employed to study *K*-edge absorptions of Fe and Ti cations in the samples before and after each heating steps. The corundum samples were first heated in a traditional O_2/LPG mixed-gas furnace to about 1500°C for two hours in an oxidizing atmosphere. The white to yellow and light to medium blue sapphires turned colorless, whereas the purple to violet sapphires became pink. The second step of heating was done with Be in an electric furnace at about 1700°C for 48 hours in an oxidizing atmosphere. After this process, the milky/silky colorless sapphires become a more transparent yellow, while the pink sapphires became orange-pink. These stones were enhanced in the final step by reheating in a fuel furnace at about 1700°C for 72 hours in a reducing atmosphere. All samples became blue with light to strong saturation and tone.

The combination of the color appearance, the absorption spectra analyzed after oxidation with Be and reduction heating (figure 1), and the chemical data suggest that Be and/or Mg trapped-hole yellow color centers—created during oxidation heating with Be—were made inactive after reduction heating. The blue coloration is mainly caused by strong broad absorption bands of Fe^{2+}/Ti^{4+} intervalence charge transfer (IVCT) mechanism without Fe^{2+}/Fe^{3+} IVCT. However, chemical data were analyzed for those samples and showed relatively high Mg and Be concentrations in comparison with the Ti composition, which does not fit well with the model that indicates $[Ti^{4+}] > [Mg^{2+}+Be^{2+}]$ causes blue coloration. XANES results showed an Fe absorption edge at 7124 eV, corresponding to the Fe^{3+} state; and Ti at 4984 eV, corresponding to Ti^{4+}. Fe^{2+} state was not found in any samples before and after each heating step which

contrasted with the IVCT theory that the blue color caused by charge transfer between Fe^{2+} and Ti^{4+}. There is no influence of Be observed from the Fe and Ti *K*-edge due to its low electron density therefore detailed local structure analyses by extended X-ray absorption fine structure (EXAFS) must be further investigated. This heating technique is still not well understood. Further experiments and analyses are being carried out to confirm the role of beryllium in blue sapphires.

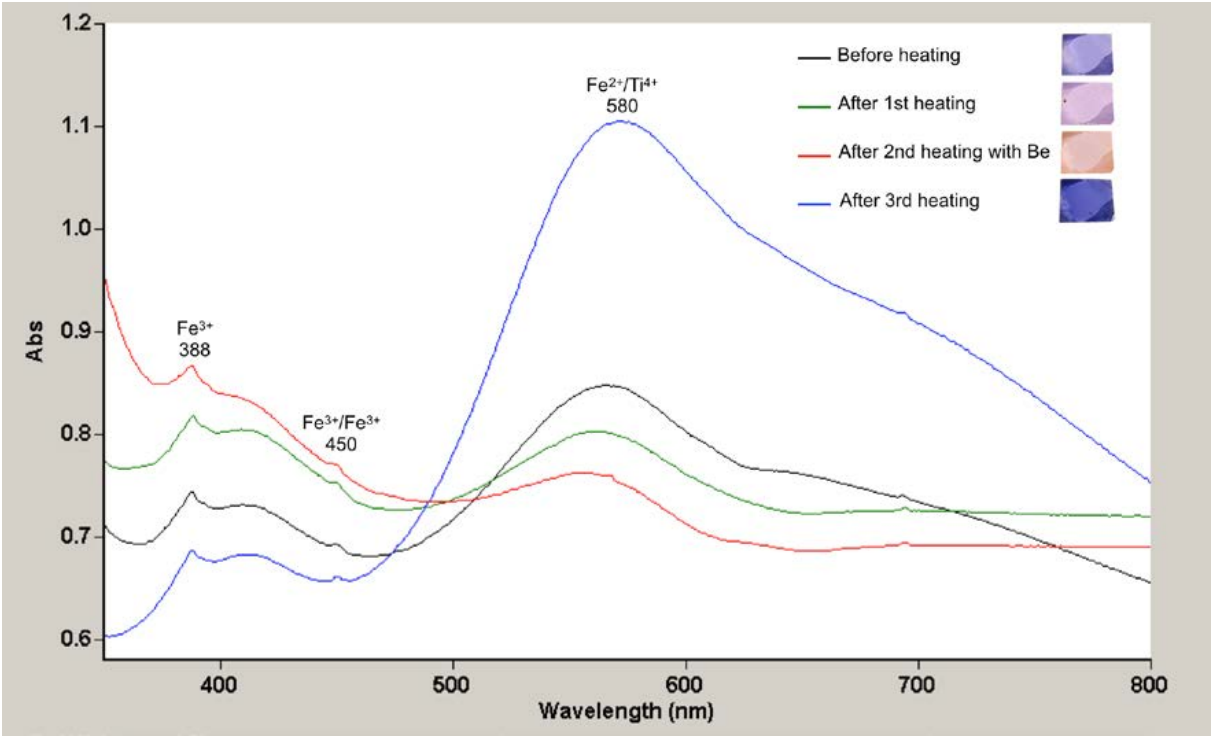

Figure 1. UV-Vis spectra of a violet sapphire before treatment (A), after a first heating in an oxidizing atmosphere (B), after a second heating with beryllium in an oxidizing atmosphere (C), and after a third heating in a reducing atmosphere (D).

References

Crowningshield R. 1966, Developments and highlights at GIA's Lab in New York: Unusual items encountered. Gems & Gemology, 12(3), 73.

Crowningshield R. 1979, Developments and highlights at GIA's Lab in New York: Treated blue sapphires. Gems & Gemology, 16(5), 147.

DuToit, G., Thanachakaphad, J. and Scarratt, K. 2009, Beryllium treated blue sapphires: Continuing market observations and updated including the emergence of larger sized stones. www.gia.edu/gia-news-research-nr62609, June 25.

Emmett, J., Scarratt, K., McClure, S.F., Moses, T., Douthit, T.R., Hughes, R., Novak, S., Shigley, J.E. and Wang, W., Bordelon, O., Kane, R.E. 2003, Beryllium diffusion of ruby and sapphire. Gems & Gemology. 39(2), 84- 135

Fritsch, E. and Rossman, G.R. 1988, An update on color in gems, Part 2: colors involving multiple atoms and color centers, Gems & Gemology, 24(1), 3-15.

Fritsch, E., 1993, Blue color in sapphire caused by Fe^{2+}/Fe^{3+} Intervalence charge transfer. Gem & Gemology, 29(3), 151-226.

Nassau, K. 1983, The Physics and Chemistry of Color: The fifteen causes of color. John Wiley & Sons, Inc., New York. 454 pp.

Peretti, A. 2006, Report on the occurrence of a Be-treated blue sapphire of commercial importance. www.gemresearch.ch/beryllium-treated-sapphires-report, March 1.

Wongrawant, P., Monarumit, N., Thammajak, N., Wathanakul, P. And Wongkokua, W. 2016, Oxidation states of Fe and Ti in blue sapphire, Materials Research Express, 3(2016)026201.

Blue sapphires heated with pressure and the effects of low temperature annealing on the OH-related structure

Thanong Leelawattanasuk[1], Thanapong Lhuaamporn[1], Papawarin Ounorn[1], Budsabakorn Srisataporn[1] and Nattapat Karava[1]

[1] The Gem and Jewelry Institute of Thailand (Public Organization), ITF-Tower Building, Silom Road, Suriyawong, Bangrak, Bangkok, 10500 Thailand
* lthanong@git.or.th

Keywords: heated blue sapphire with pressure, gemstone, PHT

Introduction

Blue sapphire treated with pressure and high temperature heating (PHT sapphire) has been circulated in the gem market since 2009 and many gemological studies have been continuously released to public since 2014 (Hyun-Min Choi et al., 2014). In 2019, the LMHC (Laboratory Manual Harmonization Committee) launched their press release that, based on the current scientific knowledges, this treatment was essentially a form of heating similar to the normal heating technique and need no specific disclosure at the moment. However, one of the most prominent characteristics of the PHT sapphire is its strong OH-related absorption in Mid- IR range that could be eliminated by normal heating the stones at high temperatures (e.g., ~1500^{o}C for 5 hrs; Leelawatanasuk et al., 2018). In this article, we report our further study on the effect of low temperature annealing (800 -1200^{o}C) on its color and their IR spectrum.

Brief process of blue sapphire heated with pressure treatment

The graphite powder was used to fill a crucible with the sapphire samples placed at the center, and a few drops of water. The crucible was then sealed with a metal plate and took to a press machine that was able to pressurize below 1 kilobar and heat the samples around 1200- 1800°C that set by a controller. (Hyun-Min Choi et al., 2018)

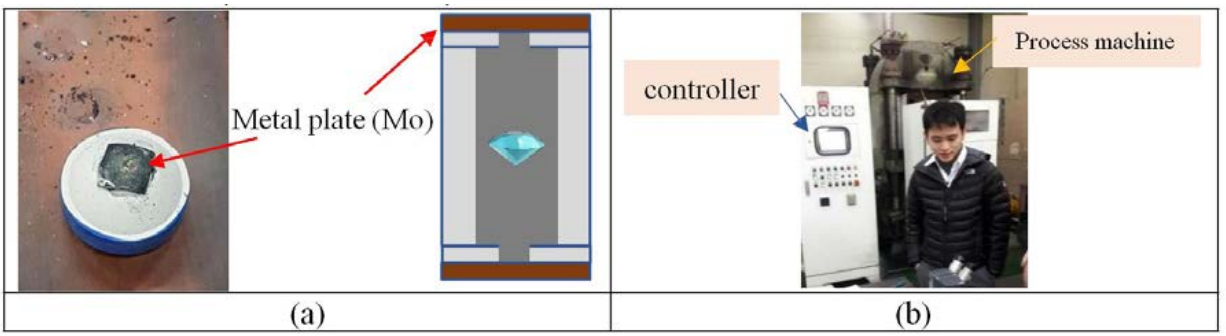

Figure 1 (a) The crucible was sealed by the metal plate
(b) The process machine and controller of the heat with pressure process.

Characteristic of heated blue sapphire with pressure

In our previous studies, the diagnostic internal features of the PHT blue sapphire which treated from Korea were the slightly healed border of the clear and flattened tension discs or narrow gab tension thin films (fig.2b,c), the exploded crystals (fig.2a) and the black graphite residue in the cavities (fig.2d).

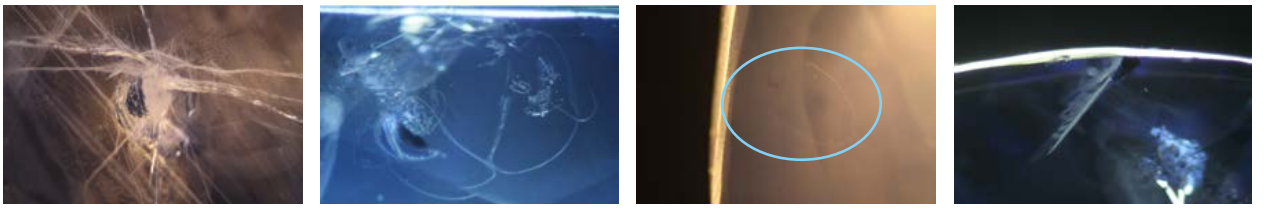

(a) (b) (c) (d)

Figure 2 (a) A crystal exploded after enhancement, (b, c) Tension cracks become a narrow-gap tension thin-film, (d) Black graphite residue in the cavities

The UV-Vis-NIR spectra revealed that the cause of blue coloration is mainly due to the Fe-Ti intervalence charge transfer (IVCT) mechanism like those of the blue sapphires originated from metamorphic origin (fig.3).

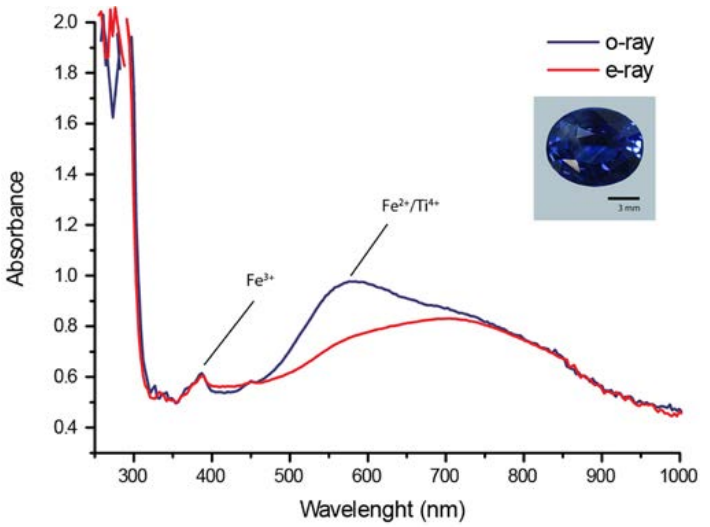

Figure 3 UV-Vis-NIR spectra show the absorption due to Fe-Ti IVCT mechanism

Their FTIR spectra showed four main different patterns. The first pattern was a unique strong OH-related absorption band and small shoulders or peaks (fig.4a); the second was an OH-related absorption band around 2700-3500 cm^{-1} and centered at 3048 cm^{-1} with the strong sharp peaks at 3424, 3262, 3232, 3187 and the main strong peak at 3309 cm^{-1} (fig.4b); the third was a small broad OH-related absorption band around 2700 and 3500 cm^{-1} with the strong sharp peaks at 3417, 3367, 3309, 3232 and 3185 cm^{-1} (fig.4c); and the forth was a wide broad absorption band with some small peaks around 2700 and 3500 cm^{-1} (fig.4d).

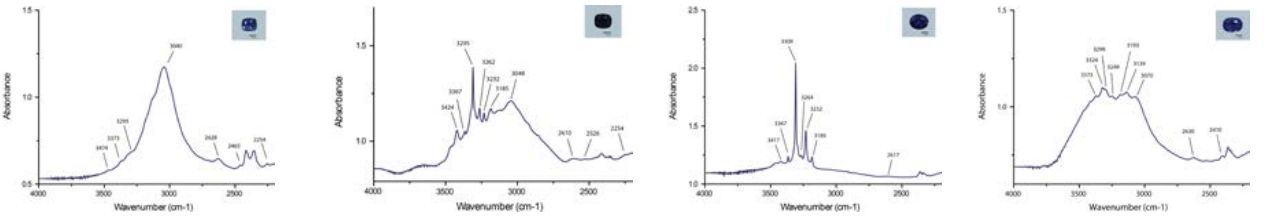

Figure 4 (a) A strong OH-related absorption band centered at 3040 with small shoulders or peaks (b) A board OH-related absorption around 2700-3500 cm^{-1} with strong sharp peaks at 3424, 3262, 3232, 3187 and the main strong peak at 3309 cm^{-1} (c) A small broad OH-related absorption band around 2700-3500 cm^{-1} with strong sharp peaks at 3417, 3367, 3309, 3232 and 3185 cm^{-1} (d) A wide broad absorption band with some small peaks about 2700-3500 cm^{-1}

Low temperature annealing experiments

In this study, three PHT treated blue sapphires from our reference collection that claimed to be treated from Korea were selected for low temperature annealed under an oxidation condition for two hrs at 800, 1000 and 1200°C, respectively. The blue hue of those sapphires are still remaining essentially the same after annealing at 800 and 1000°C but are obviously faded at 1200°C (fig.5). In term of internal features, the tension discs, fingerprints and cloud pattern, that usually occur in the heated stones, are rather changed (fig.6).

No.	Before	800°C	1000°C	1200°C
a				
b				
c				

Figure 5 The color comparison of blue sapphire before and after annealing at 800, 1000 and 1200°C

Before	800°C	1000°C	1200°C
	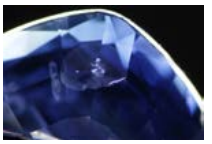	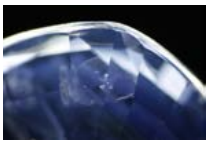	
			
	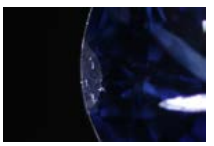		
	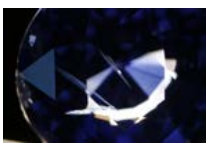	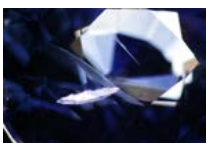	

Figure 6 The internal features before and after annealing at 800, 1000, 1200°C

The UV-Vis-NIR spectra displayed theabsorptionduetothe Fe-Ti (IVCT mechanism that clearly decreased after annealing at 1200°C in consistent with their faded colors (fig.7). The FTIR spectra of the blue sapphires still showed the OH related absorption peaks around 3000 to 3500 cm-1 after annealing at those three temperatures, but were decreasing progressively at higher temperatures (fig 8).

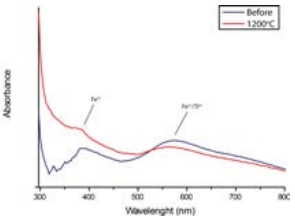

Figure 7 UV-Vis-NIR spectra of a blue sapphire before and after annealing at 1200°C

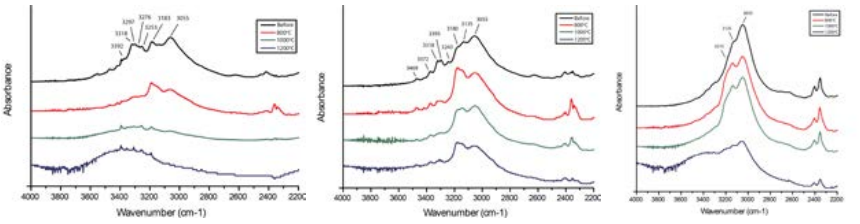

Figure 8 FTIR absorption spectra of blue sapphire (a-left, b-center, c-right) before and after annealing at 800, 1000, 1200°C

Conclusion

This study has revealed that the characteristically strong OH-related absorption band in Mid-IR spectrum of the PHT blue sapphire is still present but somewhat altered or eliminated when the stones were simply annealed at temperature around 1000^{O}C for a 2 hours without any effect on the stone's coloration and internal inclusions. Hence, since blue sapphire heated with pressure is multistep process mostly subsequence treatment on previously high temperature heated blue sapphires aim to deepen their color. However, it is also possible that the burner can also attempt low temperature annealing to lighten color of these PHT sapphires if the result color is too dark. According to the experiment, the temperature that can affect the color is around 1,000 c and at this stage the IR spectrum can be partially or completely eliminate but however, as long as the OH-related absorption band is still noticeable, the positive identification of PHT sapphire is possible.

References

Choi, H.M., Kim, S.K. and Kim, Y.C., 2014. New Treated Blue Sapphire by HPHT Apparatus. The 4th International Gem and Jewelry Conference Proceeding, 104-105

Choi, H.M., Kim, S.K., Kim, Y.C., Leelawatanasuk, T., Lhuaamporn, T., Atsawatanapirom, N., Ounorn, P., 2018. Sri Lankan Sapphire Enhanced by Heat with Pressure. The Journal of The Gemmological Association of Hong Kong, vol.34, 16-25

Leelawatanasuk, T., Lhuaamporn, T., Atsawatanapirom, N., Ounorn, P., 2018. Characteristics of commercial grade blue Sapphire enhanced by heat & pressure, XXII IMA Meeting Melbourne, Australia, IMA2018, Abstract Book, 336.

Acknowledgements

The authors would like to express ours thanks to Dr. Visut Pisutha-Anond and Mrs. Wilawan Atichat for their extensive reviews of this article.

AN EXAMINATION OF SAPPHIRES TREATED WITH HEAT AND PRESSURE BEFORE AND AFTER TREATMENT

Wasura Soonthorntantikul[1], Sudarat Saeseaw[1], Shane McClure[2], Ungkhana Atikarnsakul[1], Charuwan Khowpong[1], Suwasan Wongchacree[1], Jonathan Muyal[2]

[1] GIA Gemological Institute of America, Bangkok, Thailand
[2] GIA Gemological Institute of America, Carlsbad, California, USA
smcclure@gia.edu

Keywords: Sapphire, Pressure, Heat

Late last year and early this year a treatment that has been around since 2009 suddenly drew a lot of attention. This treatment involves heating sapphire at high temperatures with pressure. In that brief time and for several years prior much has been written and discussed on the subject. Primarily these discussions have focused on describing the procedure and the reasons why it should or should not require a separate disclosure (Choi et al., 2014, Choi et al., 2018, Leelawatanasuk et al., 2016, Song et al., 2015, Peretti et al., 2018, LMHC, 2019.

This presentation will not focus on these issues. Instead it will describe the results of the treatment on a group of sapphires both before and after treatment.

In January of 2019, GIA sent a team to Korea to visit the treatment facility and have a number of sapphires from our research collection treated by this process. This was at the kind invitation of Mr. Imam Faris, part owner of the facility and distributor of the treated sapphires. The company doing the treatment is HB Laboratory Co. Ltd., which is run by Mr. Dong Sung Ham who is also part owner and operator of the lab.

Mr. Ham kindly offered to not only treat stones for us but to let us witness every step of the operation. The only thing they asked us not to do was take pictures of the press itself. He also allowed us to experiment with changing the treatment parameters.

This process is mostly applied to metamorphic blue sapphires that have already been heat treated. They feel they can improve heated stones that didn't turn out well enough to make a profit. With this in mind the majority of the stones we took were metamorphic blue stones from Sri Lanka and Madagascar (with 3 from Myanmar), albeit mostly unheated. However, we also took magmatic stones from several localities (Australia, Cambodia, Thailand, Nigeria and Montana) and five yellow stones (Madagascar, Sri Lanka, Thailand, Australia), just to see what would happen. There were 48 samples in total, all of which were cut into wafers (some oriented, some not) to facilitate observation of inclusions and to increase the quality of spectra.

All of the stones turned blue or got darker blue after treatment, including the yellow stones (Figure 1). The degree of change for the metamorphic stones was related to the amount of rutile inclusions present, whether it be clouds or silk, just like would be expected with normal high temperature heat treatment.

Figure 1. All the samples in the test set changed color to some degree. In this stone figure A is before heating and the clouds of rutile are clearly visible. After heating (B) this is where the blue developed. Photos by Jonathan Muyal.

The most interesting thing about this process is how fast it takes place. The total treatment time, from start to finish, is about 25 minutes. However, the soak time, when the stones are at the desired pressure (about 800 bars) and temperature (they estimate to be 1800 degrees C) is only about 750 seconds, or 12.5 minutes. This, compared to standard high temperature heat treatment which can take days and sometimes even weeks.

The physical changes that happen to these stones is very interesting given the duration of the treatment. In many respects they are quite similar to changes seen in beryllium diffused stones that are heated for days at temperatures of 1800 to 1850 degrees C.

The first thing one notices about these stones after treatment (aside from the change in color) is their surfaces are now frosted. There is clear surface damage, although not severe, and every low area on the rough surfaces, cavities or surface reaching fractures was now full of graphite. The graphite had penetrated into even the smallest of openings, sometimes crystallizing in a dendritic pattern (Figure 2). Another consequence in some (but not the majority) of the stones was the growth of randomly oriented corundum crystals along the edges of cavities (Figure 3). This effect is very similar to that seen in some beryllium treated sapphires.

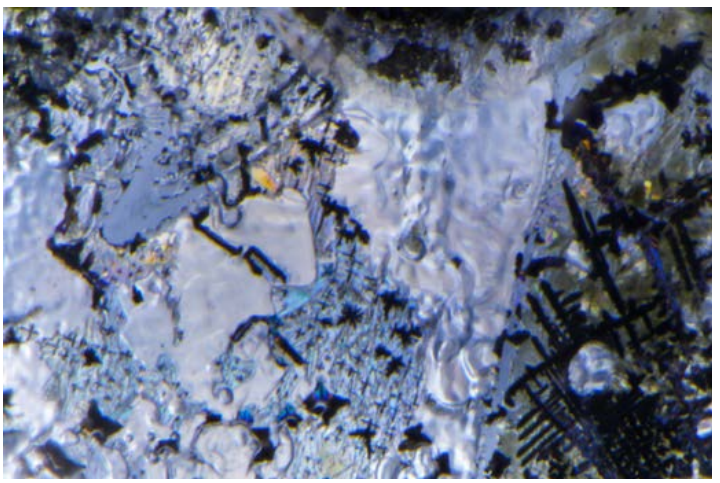

Figure 2. After treatment this stone showed distinct dissolution within a large fracture that was not present on the surface of the stone. Also seen here is the formation of dendritic graphite in the fracture. F.O.V. 1.59mm. Photomicrograph by Nathan Renfro.

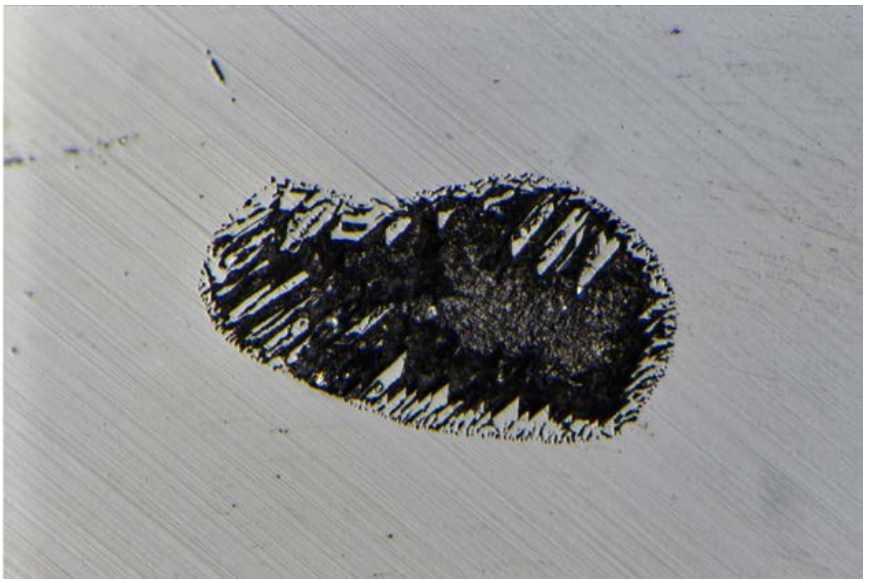

Figure 3. A couple of the samples showed distinct crystallization of corundum around the edges of cavities. F.O.V. 1.59mm. Photomicrograph by Nathan Renfro.

Another interesting point concerns discoid fractures. These fractures often occur around included crystals during heat treatment. They are typically glassy in appearance and often have a whitish fringe. Heated long enough and at high enough temperatures these discoid fractures can partially heal. In our test sample, not only did we have many instances of discoid fractures developing but they also partially healed – all in the short time the treatment lasts. For stones that have been heated before where glassy discoid fractures have formed and remain, this treatment effectively heals them, taking away the glassiness but leaving the fringe (Figure 4). So, they do not disappear but they are much less visible.

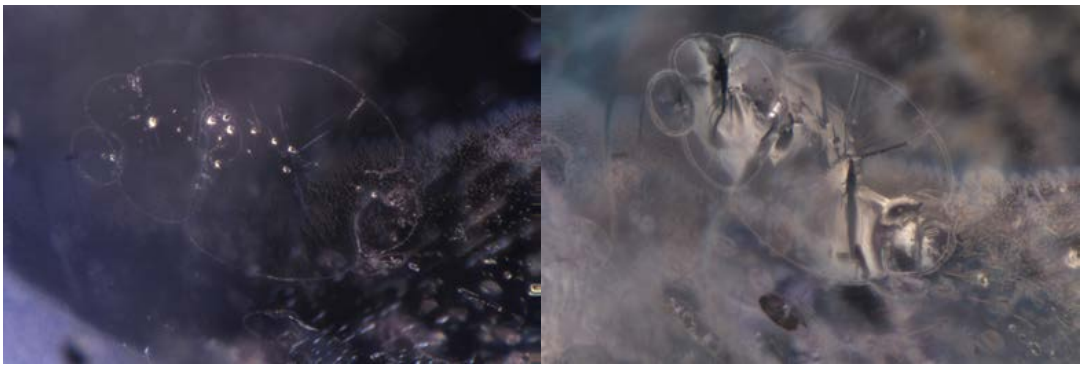

Figure 4. A. These glassy discoid fractures with whitish fringes were present in a test sample that had already been heated. B. After heating with pressure most of the glassy areas have healed but the fringes remain. F.O.V. 1.58mm. Photomicrograph by Jonathan Muyal.

Some stones developed subtle whitish wispy inclusions reminiscent of some that develop in blue beryllium treated sapphires that have been heated for weeks.

One of the major concerns of the trade was the rumor that this treatment could make fractures disappear. Our experience with these samples showed that while fractures certainly did heal, sometimes quite effectively, in no instance did they disappear. They might be less visible but they always still resembled the healing caused by traditional high temperature heat treatment (Figure 5). It is important to note that in some stones new fractures were created by the treatment.

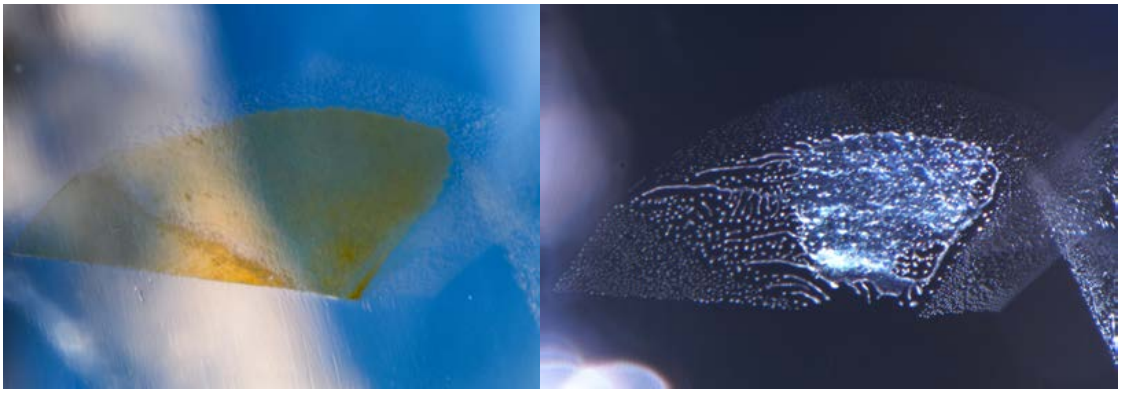

Figure 5. A. An orange stained fracture with some partial natural healing was present in this stone before heating. B. After heating with pressure the orange staining was gone and significantly more healing had taken place. F.O.V. 1.76mm Photomicrograph by Jonathan Muyal.

However, one inclusion we did see almost completely disappeared in some stones were clouds. Curiously, in other stones clouds sometimes appeared where there were none before.

The infrared spectrum of stones treated by this method often contain a band centered around 3048 cm^{-1} (Figure 6), which is considered to be diagnostic (Choi et al. 2018, Song et al., 2015). However, in this sample group we measured at least five different IR spectra, four of which did not show this band. Some variations in the IR spectra have been noted by others already (Peretti et al., 2018, LMHC, 2019).

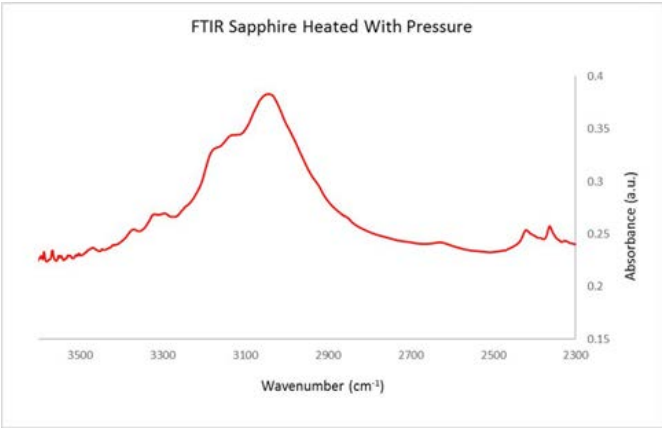

Figure 6. This is an example of the type of FTIR considered to be diagnostic of this treatment, with the main band centered around 3048 cm^{-1}. There were at least four other types of FTIR spectra noted in this group that did not show this band.

These are just some of the observations we have made so far. Still, there is much we don't yet know about the nature of this treatment. What does pressure have to do with this process? Is it pressure that makes the difference or is it more related to the rapid ramping up and ramping down of the temperature. Or, is one needed to control the other. We know it is a harsh treatment with a very large failure rate. Mr. Feris states that approximately 30% of the stones treated are useless after treatment. Can this be improved with further experimentation? It seems clear that the there is still much to be learned about the effects of pressure on the heat treatment process.

References

Choi H., Kim S., Kim Y., 2014 Appearance of new treatment method on sapphire using HPHT apparatus. International Consortium of Gem Testing Laboratories, Newsletter, Fall 2014, pp.1-2

Choi H., Kim S., Kim Y., Leelawatanasuk T., Atsawatanapirom N., Ounorn P. 2018 Sri Lankan Sapphire Enhanced by Heat and Pressure. The Journal of the Gemmological Association of Hong Kong, Vol. 39, pp. 16-25

Leelawatanasuk T., Atsawatanapirom N., Lhuaumporn T., Ounorn P., 2016 Blue sapphire undergone high pressure high temperature enhancement, GIT Gem testing laboratory, https://www.git.or.th/eng/testing center en/lab notes en/glab en/2016/07/BlueSapphire 26 072016.pdf

LMHC presentation on sapphires heated with pressure, Gemstone Industry and Laboratory Conference (GILC), February 2019, https://www.lmhc-gemmology.org/news/2019/2/21/lmhc-presentation -on-sapphires-heated-with-pressure-february-2019

Song J., Noh Y., Lon O. 2015. Color enhancement of natural sapphires by high pressure high temperature process. Journal of the Korean ceramic society. Vol. 52, No. 2, pp. 160-170.

Peretti A., Musa M., Bieri W., Cleveland E., Ahamed I., Alessandri M., Hahn L. 2018. Identification and characteristics of PHT ('HPHT') – treated sapphires – an update of the GRS research progress. http://gemresearch.ch/wp/wp-content/uplads/2018/11/GRS HPHT Update 2018 11 12 Sm.pdf

Little known absorption bands in infrared spectra of corundum: what do they mean?

Martial Bonnet[1], Emmanuel Fritsch[2]

[1] Centre de Recherches Gemmologiques, Nantes, France
[2] Institut des Matériaux Jean Rouxel (IMN) & University of Nantes, Faculté des Sciences et des Techniques, 2, rue de la Houssinière, BP 32229 Nantes, cedex 3 France,
* bonnet.martial.ch@gmail.com

Keywords: infrared, corundum, hole center

We studied five faceted medium yellow sapphires with similar colour (N1 to N5, 0.078 to 0.098 ct), sold as natural, which was confirmed by an internationally-recognized laboratory. All five showed infrared absorption bands little described in the literature (Figure 1). They were very clean, showed no Plato lines or ultraviolet luminescence. However, their infrared spectra contained bands known to occur in natural, processed or synthetic sapphire, and that are not inclusion-related. For example, the bands at about 3025, 2980, 2625, 2465, and 2415 cm^{-1} have been recorded in an orange synthetic sapphire grown by melting (Hummel, 2019). We have also found bands at about 3033, 3025 and 2980, which are recorded in Punsiri heat-treated sapphires, as well as in natural "basaltic" ones (Sangsawong et al., 2016).

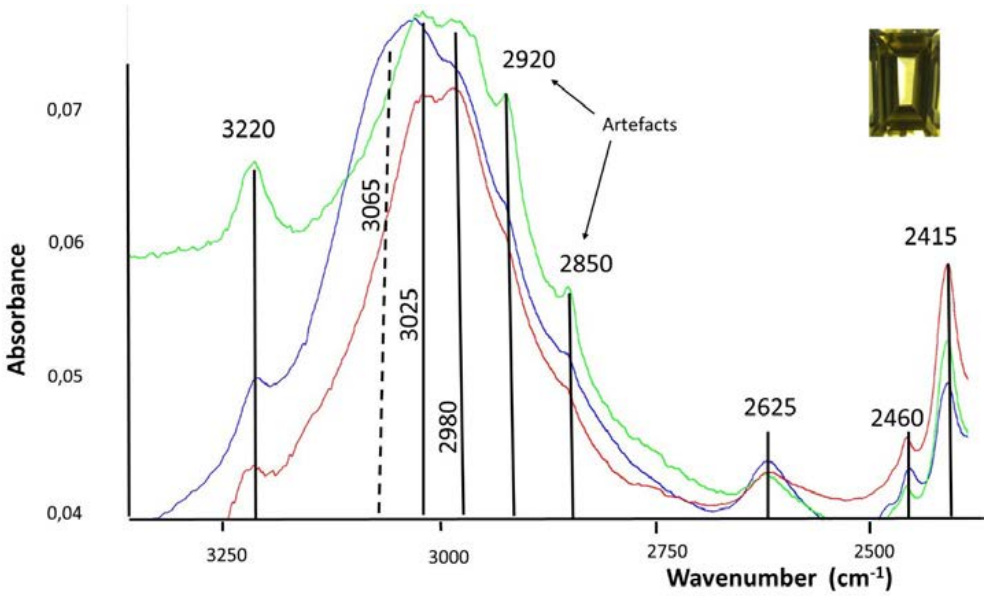

Figure 1: Infrared spectra of three of our studied samples, showing unusual, and at this point, un-interpreted infrared absorption bands. Red: N1; Green: N2; Blue: N4.

For the first time we attempt to consolidate these varied data based on approximate band positions and roughly estimated widths (Table 1).

Source	Sample	3320	3220	3214	3191	3120	3100	3065	3033	3025	3011	2980	2920	2780	2625	2490	2465	2460	2450	2415
Our samples	N1		X					?	X	X		X			X			X		X
	N2		X					?		X		X			X		X	X		X
	N3		X							X		X			X		X			X
	N4		X					X	X	?					X			X		X
	N5		X						X						X			X		X
Scarratt (2017)	Be diffused			X		X														
	"Punsiri" treated				X		X	X				?			X					X
Fukatsu et al. (2003)	Mg-doped synthetic	X?	X?	X?				X?	X?			X?	X	X	X?					
Hummel (2019)	1474 Be diffused							X								X	X			
	1718 melt							?			X	X							X	
	2504 melt							?		X		X			X		X			X
	GGTL1 natural		X					?	X			X			X		X			X
	205 hydrothermal		X					?	X						X		X			X

Table 1: Summary table of approximate infrared band positions (horizontal) as a function of our samples or spectra from the literature (vertical). We use color codes to indicate the approximate width of the bands, red for broad, green for medium and blue for "sharp" (these terms are relative only to the spectra analyzed). "x" indicates the presence of the band in the given sample," x?" signifies that this band is likely present, and "?" indicates the presence is possible but is difficult to ascertain

To simplify matters, we restricted ourselves to the range 3400-2400 cm^{-1}. We do not mention patterns that are already relatively well-known such as 3309 and 3160 cm^{-1} series (including the 2420 feature), and those observed in hydrothermal synthetics by Scarratt (2017). Peaks at 2920 and 2850 cm^{-1} are artefacts due to "fingerprints" (sebum from finger prints.) We end up with 19 bands, but comparison of apparent maxima and true maxima of individual Gaussian components proved challenging (hence the many question marks in Table 1). For example, the two components at 3040 and 2995 cm^{-1}, given by Fukatsu et al. (2003) may generate the apparent maxima around 3025 and 2980 cm^{-1}. Furthermore, the spectrum of Mg-doped sapphire by Fukatsu et al. (2003) is very different from the reputed Mg-related 3160 cm^{-1} series seen in natural gems. The only way to ascertain the exact position of the components, and possibly reconcile this work with previously published data, is to proceed to a decomposition with constraints of the unusual spectra recorded.

As many of these bands are generated by doping corundum with magnesium, a divalent ion (Mg^{2+}), it would be expected that a hole center will be generated for charge compensation of the substitution of Al^{3+}. We venture that many of the features observed by Fukatsu might be related to a hole center. This hole center is likely similar to that created by beryllium substitution, also a divalent ion. Thus it is not surprising that their related infrared absorptions would be in the same spectral range.

In the meantime, the similarity of these unusual spectra in natural, treated and synthetic corundum remains puzzling and unexplained.

References

Fukatsu N., Kurita N., Oka Y., Yamamoto S., 2003. Incorporation of hydrogen into magnesium-doped α-alumina, Solid State Ionics, 162-163, 147-159.

Hummel G., 2019. Etudes en spectroscopie infrarouge d'une collection de saphirs jaunes à orange, DUG diploma, Nantes University, 61 p.

Sangsawong.S., Pardieu V, Raynaud V, Engniwat S, 2016. « Punsiri » type FTIR Spectral Features in natural yellow sapphires, Gems & Gemology, 52-3, 325-327.

Scarratt K., 2017. Seeing infrared. Deconstructing the infrared spectra of corundun, 143-149. In Hughes R.W., Manorotkul W., Hughes B.: Ruby & Sapphire - A gemologist's guide, Lotus, Bangkok, Thailand.

PERSIAN AMBER: A *Myth* or Reality?

Bahareh Shirdam[1&2]*, Andy H. Shen[1], Soheila Aslani[2], Zhiqing Zhang[1]

[1] Gemological Institute, China University of Geosciences, Wuhan, 430074, China
[2] Gemological research laboratory, School of Mining engineering, College of engineering, University of Tehran, Tehran, Iran
shirdam@gmail.com*

Keywords: Persian Amber, Type III Fossilized Resin, FTIR, Py-GC-MS

"Persian", a famed trade name after the sky blue color of turquoise from Iran, had been contributed to various other gemstones from Iran such as Persian demantoid, Persian agate and recently Persian amber. Firstly published in 1969 (Abivardi., 2001), many dissimilar report had been recorded on amber specimen from Iran, some suggesting it to be natural amber and other categorizing it as copal. This article is the first scientific study on Persian amber, investigating optical and chemical characteristic of obtained samples from Iran.

Specimens found in central Iran zone (close to Tabas block, east-central Iran) came in different colors, transparency and size. While the most common color was yellow, they ranged from pale yellow to yellow, orange and brown. The size of material varied from 1 to 43 cm, transparent to translucent whereas bigger samples appeared translucent to almost opaque on the surface. Microscopic investigations showed a granular microstructure of different shapes and size that had been attributed to surface weathering. Disk like inclusions which were presumed to be sun spangles in primary observations, revealed a different texture and shape under higher magnification. While sun spangles are basically tension cracks resulted from heat and pressure, Persian sample's inclusions as displayed in figure 1, appear to have three dimension and varying shapes.

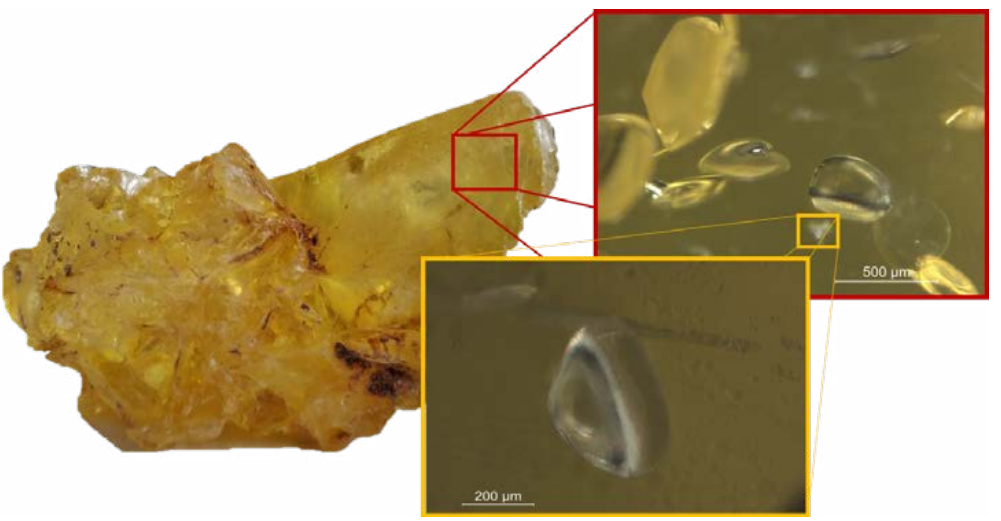

Figure 1- Persian amber and its inclusions

These inclusions are suggested to be palynomorph or plant pollen (Néraudeau et al, 2016) entrapped in resin due to its era climate and environmental condition.
Following the classic gemological examinations, specific difference of results drawn to separation of materials into two groups (I&II). Characteristic of both groups are explained in table 1.

Table 1- Classic examinations result

	Group I	**Group II**
Specific Gravity	1.23	1.21
UV Light	Blue	Yellow
Reaction to solvent	Not soluble in alcohol	partly soluble in alcohol
Fragrance	Only scented when exposed to fire	Scented even in room temperature
Reaction to fire	Burns away	Burns away

The chemical characterization of samples was investigated by FTIR and Raman spectroscopy followed by pyrolysis (Py)-GC-MS. As observed in figure 2, the obtained FTIR spectral of sample from Group I- Persian amber did not match the expected pattern of typical Baltic amber and resulted a spectra close to an aromatic polystyrene. While the existence of styrene inspire the possibility of materials being no more than synthetic resin, it also generate the theory of natural styrene which had been previously reported in type III fossilized resin (Grimaldi et al.,1989 & Anderson et al., 1995 & Anderson, 2006). Tracing the chemical composition of samples by Py-GC-MS, the presence of Cinnamic acid and its compounds confirmed the second theory; According to *Langenheim* (1995) study on type III fossilized resin, Persian amber is similar to Siegburgite which was categorized by isolation of cinnamic acid and styrene. Furthermore, 3- phenylpropanylcinnamate, a copolymer unit in Siegburgite fossil resin formerly proposed as a marker by *Pastorova et al* (1998) has been detected in samples from Iran.

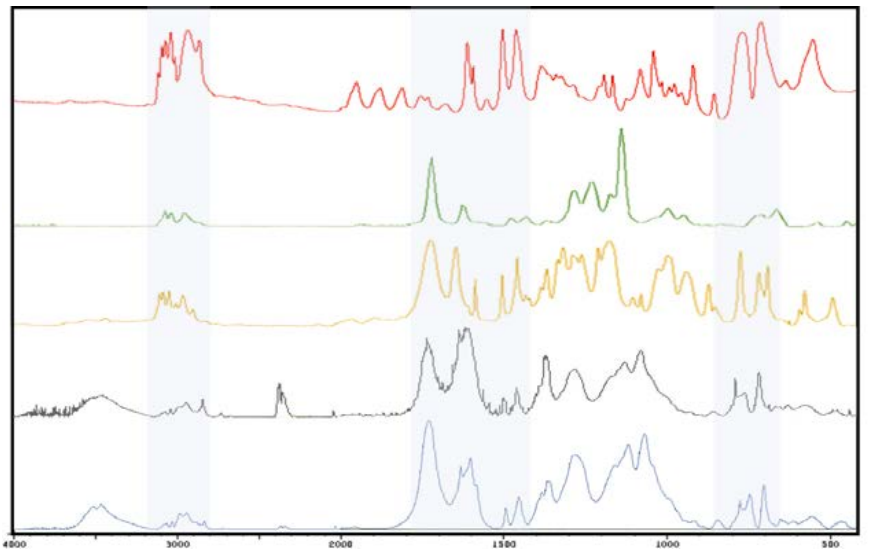

Polystyrene■, 3-Phenylpropanylcinnamate■, Allyl Cinnamate■,
Sample DYA-3(Group II)■, Sample YA-1(Group I)■

Figure 2- Comparison of obtained FTIR spectra with its possible compounds

In conclusion, even though this study classify Persian amber as a type III fossilized resin, but estimating the age of samples requires further study on Nuclear Magnetic Resonance (NMR) spectroscopy of materials which is a work in process; yet a related point to consider is the thermal behavior of materials which indicate a high degree of maturation. In fact one of the main reason for separation of Persian amber into two groups is the variation in sample's maturation which is suggested to be considerably higher in group I.

References

Abivardi C., 2001. Iranian Entomology. Springer-Verlag, Berlin-New York 515-520.

Anderson K. B., Crelling J. C., 1995. Amber, Resinite, and Fossil Resins. In: K.B. Anderson and J.C. Crelling (eds), ACS Symposium Series 617, Washington, 11-17.

Anderson K. B, 2006. The nature and fate of natural resins in the geosphere. XII. Investigation of C-ring aromatic diterpenoids in Raritan amber by pyrolysis-GC-matrix isolation FTIR-MS, Geochemical Transactions.

Grimaldi D., Beck C. W. , Boon J. J., 1989. Occurrence, chemical characteristics, and paleontology of the fossil resins from New Jersey, Am Mus Novit 2948, 1-27.

Néraudeau D., Perrichot V., Batten D.J., Boura A., Girard V., Jeanneau L., Nohra Y.A., Polette F., Martin S.S., Saint Martin J.-P., Thomas R., 2016. Upper Cretaceous amber from Vendée, north-western France: Age dating and geological, chemical, and palaeontological characteristics, Cretaceous Research.

Pastorova I., Weeding T., Boon J. J., 1998. 3-Phenylpropanylcinnamate, a copolymer unit in Siegburgite fossil resin: a proposed marker for the Hammamelidaceae, Org Geochem 29, 1381- 1393.

DNA FINGERPRINTING OF PRECIOUS CORALS AND PEARLS

Laurent E. Cartier[1*], Michael S. Krzemnicki1, Bertalan Lendvay[2], Nadja Morf[2], Joana B. Meyer[3]
[1] Swiss Gemmological Institute SSEF, Aeschengraben 26, 4051 Basel, Switzerland
[2] Institute of Forensic Medicine, University of Zürich, Winterthurerstrasse 190/52, 8057 Zürich, Switzerland
[3] Swiss Federal Research Institute WSL, Zürcherstrasse 111, 8903 Birmensdorf, Switzerland
*laurent.cartier@ssef.ch
* corresponding author's email

Keywords: Precious corals, pearls, DNA fingerprinting

Abstract
Organic gems such as pearls, precious corals and ivory are some of the oldest gems collected and used by mankind in jewellery. Although not geological in origin, such organic gem materials are products of biomineralization processes. Certain organic gem species are listed and protected by the Convention on International Trade in Endangered Species of Wild Fauna and Flora (CITES), but there are at present no techniques available for conclusive species identification by gemmologists and for the trade. DNA fingerprinting is a novel method in this regard and applications in gemmology will be presented.

Introduction

Organic gems such as pearls usually contain minute amounts of organic matter bound by a mineral matrix (Figure 1). Both the organic matter and the matrix may contain small amounts of DNA that can be extracted and analyzed using novel extraction and fingerprinting techniques. This method was developed and published in 2013 using different types of pearls and oyster species (Meyer et al., 2013), and a more recent study of a similar methodological approach was published by Saruwatari et al. (2018). The method has been further refined since 2013 by the authors so that the pearl does not need to be destroyed (i.e. quasi non- destructive) and the amount of required material has been considerably reduced. DNA fingerprinting can offer conclusive identification of the oyster species to which a pearl corresponds. Furthermore, the method has the potential to reveal the geographic origin of a pearl based on more specific fingerprinting.

Figure 1: Gem materials suitable for DNA testing include items such as these from the SSEF and H. A. Hänni collections: cultured pearls and associated shell material (P. maxima and P. margaritifera, ~15 cm tall), corals (including Corallium rubrum branches up to ~10 cm tall) and ivory (warthog and mammoth). Photo by Vito Lanzafame, SSEF. (Courtesy of Journal of Gemmology).

This method has also been applied to testing of precious coral and ivory, which also have minute amounts of organic matter in their mineral frameworks (Cartier et al., 2018; Lendvay et al., 2019). DNA fingerprinting can increase transparency (through origin and species determination) and prevent fraud by identifying protected species for other organic gems, and help in the documenting the provenance of certain organic gems (Figure 2).

Figure 2: A natural pearl necklace with pearls likely from Pinctada radiata of the Arabian/Persian Gulf. DNA fingerprinting could provide further documentation of the provenance for such exceptional pearls. Photo by Luc Phan, SSEF

This presentation will present the current status and methodological capabilities of DNA fingerprinting on pearls from a range of pearl producing oyster species (including *Pinctada margaritifera, Pinctada maxima* and *Pinctada radiata)*. Recent research led to the development of a DNA sequence reference database of seven *Pinctada* oyster species to assign any of their pearls to the exact species. New research that has focused on detailed DNA fingerprinting of the eight main precious coral species used in jewellery will also be presented. This involved a comprehensive study examining the best possible DNA extraction methods for precious corals and possibilities for sequencing and taxonomic attribution, as visible for a selection of these in Figure 3.

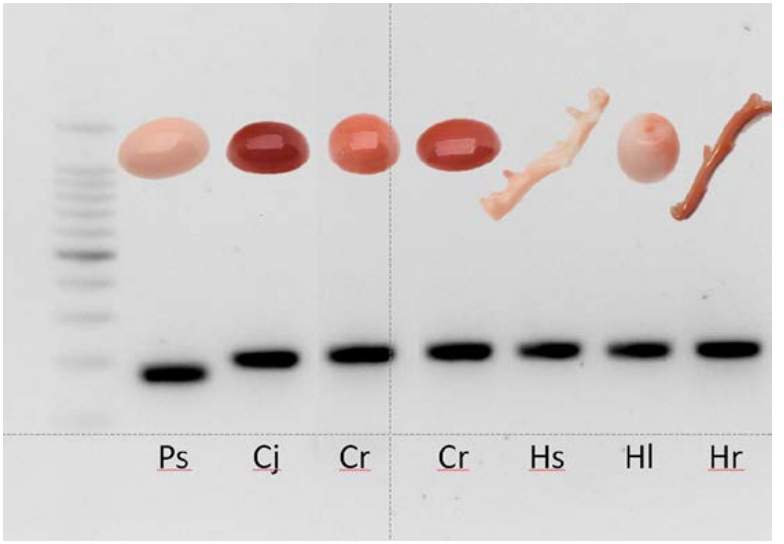

Figure 3: Gel electrophoresis photograph of the amplified DNA extracted from polished corals along a molecular size standard (on the left). Subsequent sequencing of the amplified DNA identified the coral species as Pleurocorallium secundum (Ps), Corallium japonicum (Cj), Corallium rubrum (Cr), Hemicorallium sulcatum (Hs), Hemicorallium laauense (Hl) and Hemicorallium regale (Hr). Photo: Bertalan Lendvay

Outlook

DNA fingerprinting as a tool in gemmology illustrates the importance of collaborating with researchers from other fields in order to develop new gemstone testing techniques for the 21st century. It provides an opportunity for conclusive species identification and potentially even geographic organic determination for certain types of pearls, precious corals and ivory specimens.

References

Cartier L.E., Krzemnicki M.S., Lendvay B., Meyer J.B., 2018. DNA Fingerprinting of Pearls, Corals and Ivory: A Brief Review of Applications in Gemmology. The Journal of Gemmology, 36 (2), 152-160.

Lendvay B., Morf N., Cartier L.E., Krzemnicki M.S., Kratzer A., 2019. Genetic species identification of precious corals processed for jewelry. SWFS 2019 Meeting, Denver (Colorado), oral presentation.

Meyer J.B., Cartier L.E., Pinto-Figueroa E.A., Krzemnicki M.S., Hänni H.A. and McDonald B.A., 2013. DNA fingerprinting of pearls to determine their origins. PLoS ONE, 8(10), article e75606, 11 pp., http://dx.doi.org/10.1371/journal.pone.0075606.

Saruwatari K., Suzuki M., Zhou C., Kessrapong P. and Sturman N., 2018. DNA techniques applied to the identification of Pinctada fucata pearls from Uwajima, Ehime Prefecture, Japan. Gems & Gemology, 54(1), 40–50.

NEW INSIGHTS ON X-RAY LUMINESCENCE OF NATURAL AND CULTURED PEARLS FROM FRESHWATER AND SALTWATER BIVALVES

Stefanos Karampelas[1*], Fatima Mohamed[1], Hasan Abdulla[1], Abeer Al-Alawi [1*]

[1] DANAT (Bahrain Institute for Pearls & Gemstones), WTC East Tower, Manama, Bahrain
*Stefanos.Karampelas@danat.bh

Keywords: Pearls, Manganese, X-ray luminescence

Natural and cultured pearls may be separated following the growth environment of the mollusc; they can be found in bivalves, gastropods and cephalopods and made of different calcium carbonate polymorphs, but the vast majority of natural and cultured pearls used in jewellery are found in bivalves and their surface is entirely made out of aragonite (Gauthier & Karampelas, 2009). Natural (or cultured) pearls can be found (or cultivated) in freshwater (FW) molluscs (i.e., living in rivers or lakes) or in saltwater (SW) molluscs (i.e., living in sea). Usually, the implanted bead in cultured pearls (both SW and FW) is cut from a freshwater bivalve shell (Cartier & Krzemnicki, 2013).

Freshwater cultured and natural pearls contain more manganese (Mn) than their saltwater counterparts (Schiffmann, 1971; Gütmannsbauer & Hänni, 1994). This is the reason eye visible (nowadays captured with a digital camera in most cases) reactions under X-rays (a.k.a. X-ray luminescence) are different for samples found in different water environment. Freshwater (natural and cultured) pearls luminesce green-yellow and saltwater pearls (natural and cultured without nuclei) remain essentially inert under X-rays (Lorenz & Schmetzer, 1986; Hänni et al., 2005; Scarratt, 2011). However, some cultured saltwater pearls containing a bead (made out of freshwater shell) can also give green-yellow luminescence under X-rays. This reaction is due to the manganese content of freshwater bead and the relatively thin nacre.

For the present study, 47 natural and cultured pearls from different bivalves were studied; 10 natural saltwater pearls from *P. radiata* fished off Bahrain (Arabia Gulf), 4 natural saltwater pearls from *P. margaritifera* fished off Egypt (Red Sea), 10 cultured saltwater pearls without beads from *P. maxima* fished off Indonesia, 7 natural freshwater pearls from Unionidae family fished from various North American rivers, 4 natural freshwater pearls from *Margaritifera margaritifera* fished from Spey river (Scotland), 12 cultured freshwater pearls without bead from *Hyriopsis sp.* from various places in China. The samples have various shapes and they reach up to 7 mm. X-ray luminescence was studied with a PXI GenX-100 under 100 kV and 5 mA and a Nikon D810 camera using a shutter (exposure) time of 5 seconds-F5.0 aperture and ISO Hi 2. ^{55}Mn of all samples was measured, in order to correlate it with X-ray luminescence reactions using LA-ICP-MS, which consists of a Thermo Fisher Scientific iCAP Q Induced Coupled Plasma-Mass Spectrometer (ICP-MS) coupled with a Q-switched Nd:YAG Laser Ablation (LA) device operating at a wavelength of 213 nm. MACS-3 standard, synthetic calcium carbonate ($CaCO_3$) pellet, was used to minimize matrix effects (Jochum et al., 2012). Raman spectra on some samples were acquired to identify calcium carbonate polymorph and link it with the X-ray luminescence reactions using a Renishaw inVia spectrometer with an excitation wavelength of 514 nm using a diode-pumped solid-state laser.

Most natural and cultured (without bead) saltwater pearls remain inert under X-rays and most of natural and cultured (without bead) freshwater pearls present medium to high yellow-green luminescence (see some examples in Figure 1 A and B). This luminescence is attributed to 9-fold coordination of oxygen around Mn^{+2} in aragonite (Sommer, 1972). As previously noticed on biogenic aragonite, X-ray luminescence intensity has a linear correlation with Mn^{+2} content (Sommer, 1972; Götte & Richter, 2009), the higher ^{55}Mn measured with LA-ICP-MS the more intense the yellow-green luminescence appears.

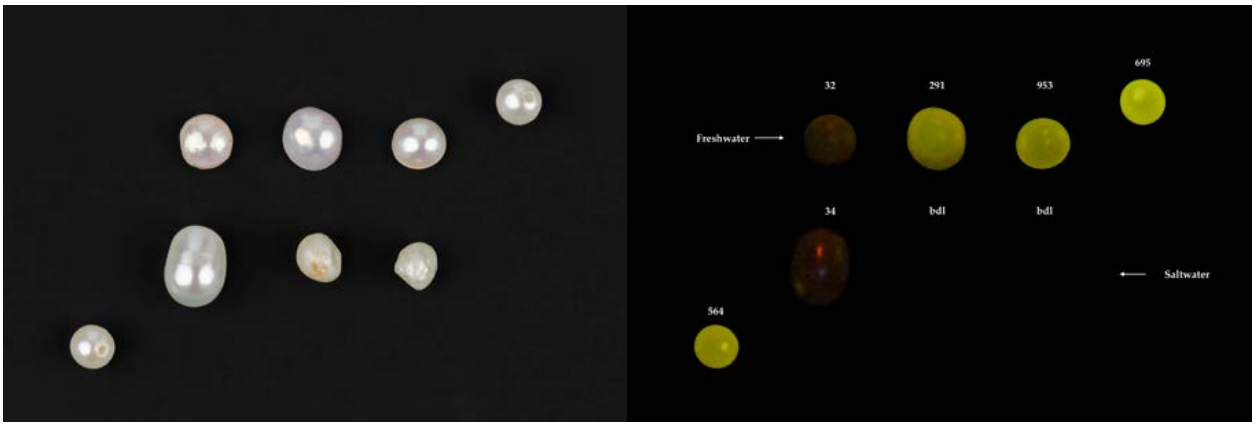

Figure 1: Three freshwater samples (upper row) and three saltwater samples (bottom row) under daylight (A) and X-rays (B). The concentrations of ^{55}Mn (average value on three different spots measured with LA-ICP-MS) in ppmw are mentioned in white over the samples (B; bdl: below detection limit). The two cultured freshwater pearls without bead upper right (diameter: 2.95 mm) and bottom left (diameter: 2.85 mm) are used as reference. Photos by Hasan Abdulla, DANAT.

A natural freshwater pearl from Unionidae family from North American rivers, contains ^{55}Mn of 32 ppmw presenting low yellow-green luminescence under X-rays and one of the studied cultured saltwater samples (without nuclei) contains ^{55}Mn of 35 ppmw is presenting similar yellow-green luminescence under X-rays (see again Figure 1B). These samples are challenging to be identified using X-ray luminescence. Additionally, the amount of manganese is around the detection limit in most EDXRF instrument (*ca.* 40 ppmw); these samples might be identified by EDXRF if barium is taken in consideration (barium is detectable in most freshwater samples and below the detection limit in saltwater samples) or with LA-ICP-MS using a set of various elements.

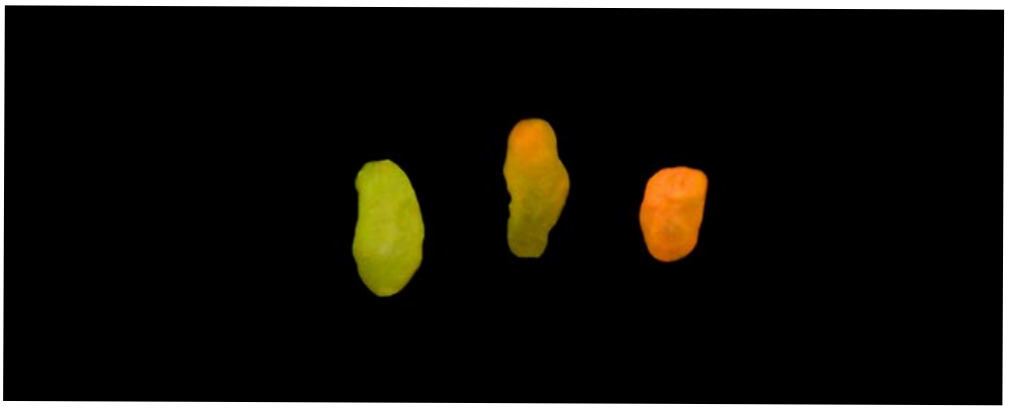

Figure 2: Three cultured freshwater pearls without bead from China under X-rays. The left sample presents yellow-green luminescence, the centre sample presents yellow-green luminescence as well as areas with orange luminescence and the right sample presents principally orange reaction under X-rays. Photos by Hasan Abdulla, DANAT.

Some (natural and cultured) freshwater samples present areas with orange luminescence under X-rays (see some examples in Figure 2). It was previously published that some cultured freshwater pearls from China without bead contain domains of calcite emitting Mn^{2+} linked orange cathodoluminescence (Habermann et al., 2001). However, Raman spectra acquired on the orange coloured sections under X-rays present bands linked to vaterite, not to calcite. Areas of vaterite were already previously identified in freshwater cultured pearls without bead from Japan and China (Qiao et al., 2006; Wehrmeister et al., 2007; Ma et al., 2009). CL and X-ray induced luminescence spectra of Mn^{2+} in calcite and vaterite are close, which suggests for both a 6-fold coordination of oxygen around it (Sommer, 1972).

References

Cartier L., Krzemnicki M.S., 2013. New developments in cultured pearls production: Use of organic and baroque shell nuclei. The Australian Gemmologist, 25 (1), 6-13.

Gauthier J.P., Karampelas S., 2009. Pearls and Corals: "Trendy Biomineralizations". Elements, 5 (3), 179-180.

Götte T., Richter D.K., 2009. Quantitative aspects of Mn activated cathodoluminescence of natural and synthetic aragonite. Sedimentology, 56 (2), 483-492.

Gütmannsbauer, W., Hänni, H.A., 1994. Structural and Chemical Investigations on Shell and Pearls of Nacre Forming Saltwater and Freshwater Bivalve Mollusks. Journal of Gemmology, 24 (4), 284-296.

Habermann D., Banerjee A., Meijer J., Stephan A., 2001. Investigation of manganese in salt- and freshwater pearls. Nuclear Instruments and Methods in Physics Research B, 181 (1-4), 739-743.

Hänni H.A., Kiefert L., Giese P., 2005. X-Ray Luminescence, a Valuable Test in Pearl Identification. Journal of Gemmology, 29 (5/6), 325-329.

Jochum K.P., Scholz D., Stoll B., Weis U., Wilson S.A., Yang Q., Schwalb A., Borner N., Jacob D.E., Andreae M.O., 2012. Accurate trace element analysis of speleothems and biogenic calcium carbonates by LA-ICP-MS. Chemical Geology, 318-319, 31-44.

Lorenz I., Schmetzer K., 1986. Possibilities and Limitations in Radiographic Determination of Pearls. Journal of Gemmology, 20 (2), 114-123.

Ma H., Su A., Zhang B., Li R.K., Zhou L., Wang B., 2009. Vaterite or aragonite observed in the prismatic layer of freshwater-cultured pearls from South China. Progress in Natural Science, 19 (7), 817-820.

Qiao L., Feng Q.L., Li Z., 2006. Special vaterite in freshwater lackluster pearls. Crystal Growth & Design, 7 (2), 275-279.

Scarratt K., 2011. Pearl identification-A practitioner's perspective. Gems & Gemology, 47 (2), 117-118.

Schiffmann C.A., 1971. Pearl identification: Some laboratory experiments. Journal of Gemmology, 12 (7), 284–296.

Sommer S.E., 1972. Cathodoluminescence of carbonates 1. Characterization of cathodoluminescence from carbonate solid solutions. Chemical Geology, 9 (1-4), 257-273.

Wehrmeister U., Jacob D.E., Soldati A.L., Häger T., Hofmeister W., 2007. Vaterite in freshwater cultured pearls from Chima and Japan. Journal of Gemmology, 31 (5/6), 269-276.

PINCTATA RADIATA SALTWATER CULTURED PEARLS FROM ABU DHABI (U.A.E.)

Abeer Al-Alawi[1*], Zainab Ali[1], Fatema Albedal[1], Stefanos Karampelas[1]

[1]DANAT (Bahrain Institute for Pearls & Gemstones), WTC East Tower, Manama, Bahrain
*Abeer.Alawi@danat.bh

Keywords: Cultured pearls, Saltwater, Beaded

A parcel of saltwater cultured pearls reportedly from a farm based in Abu Dhabi (U.A.E.) was examined. The owners mentioned that all samples were cultivated within *Pinctada radiata* (*P. radiata*) molluscs but supplied very limited further information on the process. This bivalve is rarely used for cultivation, as most saltwater pearls are cultivated within the bivalves *P. fucata*, *P. maxima*, *P. margaritifera* and less commonly within bivalves from *Pteria sp.* On the other hand, most natural pearls found in the Arabian Gulf are fished from *P. radiata*.

For the present work, 123 samples were studied. They have a range of colours which varies from white to cream to brownish-cream to yellow to grey and to dark grey, some of them with pink overtones, and various shapes such as round, near-round, near-button, near-oval, near-drop, near-baroque and baroque (Figure 1). Their weight ranges from 0.81 ct to 5.88 ct and their size from 4.84 x 4.77 to 15.07 x 11.51 mm, about half were of a high-quality; i.e., possessing high lustre, homogenous colour (sometimes having pink overtone) with few blemishes and of round to near-round shape (see again Figure 1).

Figure 1: A selection of cultured saltwater pearls with bead from P. radiata cultured off Abu Dhabi ranging from 4.85 mm to 8.50 mm. Photo: Hasan Abdula, DANAT.

Reaction of all the samples to long-wave (365nm) ultraviolet (LWUV) and short-wave (254nm) ultraviolet (SWUV) radiation was recorded using a 3W dual wavelength lamp. X-ray luminescence was studied using a PXI GenX-100 set to 100 kV and 5 mA and a Nikon D810 camera using a shutter (exposure) time of 5 seconds-F5.0 aperture and ISO Hi 2. X-ray microradiographs were acquired using a PXI GenX-90P set to 90 KV and 80 microA, 100-120 milliseconds exposure time per frame and 128 frames. Raman spectra were acquired using a Renishaw inVia spectrometer with an excitation wavelength of 514 nm using a diode-pumped solid-state laser from 200 to 2000 cm^{-1} and UV-Vis-NIR spectra from 250 to 1000 nm using a Cary 60 with DRA. Chemical analysis on all samples performed by LA-ICP-MS, using a Thermo Fisher Scientific iCAP Q Induced Coupled Plasma-Mass Spectrometer (ICP-MS) coupled with a Q-switched Nd:YAG Laser Ablation (LA) device operating at a wavelength of 213 nm. MACS-3 standard, synthetic calcium carbonate (CaCO3) pellet, was used to minimize matrix effects (Jochum et al., 2012).

The nacre thickness of the samples varied from 0.15 mm to 1.80 mm. The higher-quality pearls range in size from 7.00mm to 8.50mm, with beads from 5 to 7 mm and nacre thickness of 0.50 mm to 1.50 mm, with more than the half having a nacre thickness above 0.90 mm (figure 2). The largest samples (> 9 mm) are of baroque shape and present large areas of organic matter deposition. The two largest samples with 8 mm beads revealed large depositions of organic material and thin nacre.

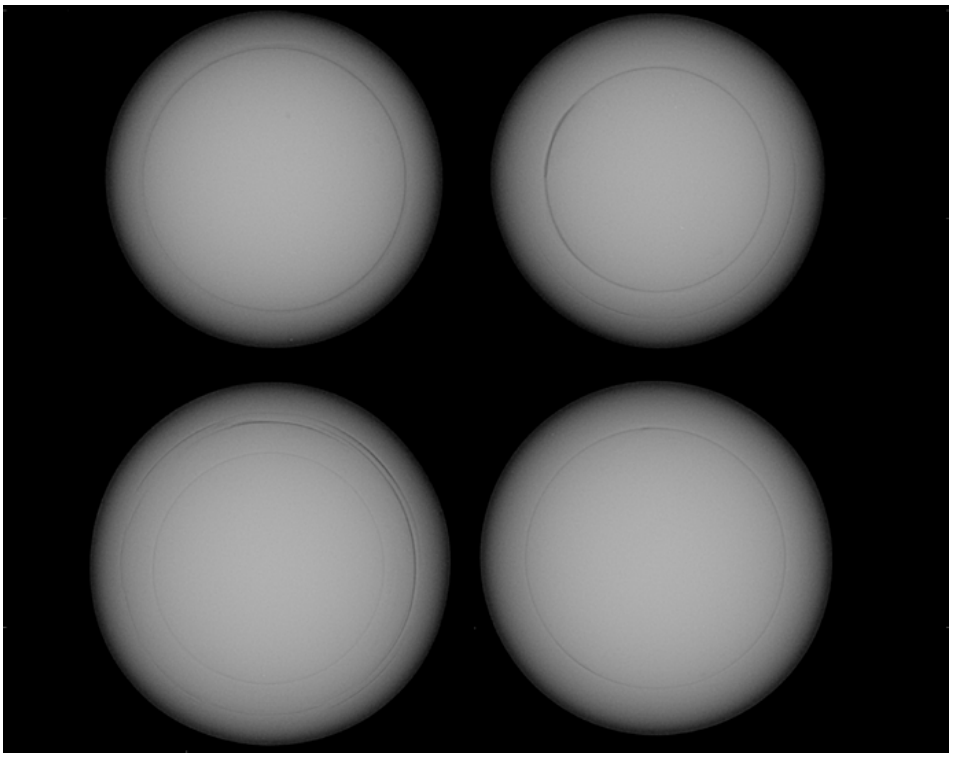

Figure 2: X-ray microradiographs of selected saltwater cultured pearls with bead from Abu Dhabi. The sample at the bottom left has 8.50 mm diameter and 1.50 mm nacre thickness, at the bottom right has 8.30 mm pearl and 1.15 mm nacre thickness, top right has 7.80 mm and nacre thickness of 1.40 mm and the sample at the top left has 8.00 mm diameter and nacre thickness of 1.00 mm.

All samples luminesce green to greenish-yellow under SWUV and yellow to green under LWUV. Only two samples present a slightly different reaction, yellowish-brown under SWUV and slightly brown to green under the LWUV. Luminescence under X-rays varied from a weak to a strong yellow-green. This is most likely due to the underlying bead being made from a freshwater shell (Hänni et al., 2005). Even the samples with the thickest nacre were presenting some X-ray induced luminescence.

Raman bands characteristic of aragonite (Urmos et al., 1991) were observed for all samples. Coloured samples also present two additional bands at 1130 cm^{-1} and 1530 cm^{-1} which are attributed to polyenic pigments. Similar Raman bands are also presented on pearls from different molluscs as well as on Akoya (*P. fucata*) cultured pearls (Fritsch et al., 2012; Otter et al., 2017).

A series of absorption bands (decrease of reflectance) in the visible range were recorded for all samples at 410 nm, 435 nm and 460 nm., also linked to polyenic pigments. Some samples recorded an additional band at around 495 nm. The bands recorded differ from those recorded in cultured saltwater pearls from other species (*P. maxima*, *P. margaritifera* and *Pteria sp.*) and are similar to those recorded for samples from Akoya -*P. fucata* (Karampelas et al., 2011; Karampelas, 2012; Otter et al., 2017). In table 1 chemical analysis of the most important elements of the cultured saltwater pearls from Abu Dhabi are presented. The results are similar to those obtained for natural saltwater pearls fished from *P. radiata* off Bahrain.

Table 1: Chemical analysis of the studied samples using LA-ICP-MS in ppmw. Three spots per sample were analysed. All the spots were made of aragonite.

Element	^{23}Na	^{24}Mg	^{55}Mn	^{88}Sr	^{137}Ba	^{208}Pb
Min	3810	55.2	bdl*	448	bdl*	bdl*
Max	6850	579	5.96	1260	0.84	0.48
Average	5229.5	232.9	1.01	752.9	0.21	0.027
Median	5160	212	0.84	722	0.19	0.023

bdl: below detection limit*

References

Fritsch E., Rondeau B., Hainschwang T., Karampelas S., 2012. Raman spectroscopy applied to gemmology, in Applications of Raman Spectroscopy to Earth Sciences and Cultural Heritage (edited by J. Dubessy, F. Rull and M.-C. Caumon), European Mineralogical Union and Mineralogical Society of Great Britain & Ireland, 12, 453-488.

Hänni H.A., Kiefert L., Giese P., 2005. X-Ray Luminescence, a valuable test in pearl identification. Journal of Gemmology, 29 (5/6), 325-329.

Jochum K.P., Scholz D., Stoll B., Weis U., Wilson S.A., Yang Q., Schwalb A., Borner N., Jacob D.E., Andreae M.O., 2012. Accurate trace element analysis of speleothems and biogenic calcium carbonates by LA-ICP-MS. Chemical Geology, 318-319, 31-44.

Karampelas S., 2012. Spectral characteristics of natural-color salt-water cultured pearls from Pinctada maxima. Gems & Gemology, 48 (3), 193-197.

Karampelas S., Fritsch E., Hainschwang T., Gauthier J.P., 2011. Spectral differentiation of natural -color salt-water cultured pearls from *Pinctada margaritifera* and *Pteria sterna*. Gems & Gemology, 47 (2), 117.

Otter L.M., Agbaje O.B.A., Huong L.T.T., Häger T., Jacob D.E., 2017. Akoya cultured pearl farming in Eastern Australia. Gems & Gemology, 53 (4), 423-437.

Urmos J., Sharma S.K., Mackenzie F.T., 1991. Characterization of some biogenic carbonates with Raman spectroscopy. American Mineralogist, 76 (3-4), 671-676.

Wehrmeister U., Jacob D.E., Soldati A.L., Häger T., Hofmeister W., 2007. Vaterite in freshwater cultured pearls from China and Japan. Journal of Gemmology, 31 (5/6), 269-276.

GREENLANDIC IVORY – PAST AND PRESENT USE

Anette Juul-Nielsen[1] & Hans Lange[2]
[1] Department of Geology, Ministry of Mineral Resources and Labour,
Government of Greenland, Imaneq 1A-201, 3900 Nuuk, Greenland
[2] Greenland National Museum & Archives, Hans Egedesvej 8, 3900 Nuuk, Greenland
* anjn@nanoq.gl

Keywords: Ivory, Greenland, Jewellery, Sculptures

Introduction

In Greenland there is a tradition for carving of organic material. Bones and wood were used by the early Inuits to make maps of the coastline and ivory was used for hunting equipment. The use of ivory changed with the arrival of Europeans and today the use of ivory is very different from the use by the first Inuits.

Past and present use of ivory in Greenland

Ivory has been used for centuries for jewellery, sculptures or other decorative items in many parts of the world. In Greenland, however, production and export of ivory was only introduced after the arrival of Europeans in Greenland in the late 10th century AD (Vésteinsson, 2016). The search for walrus ivory was probably one of the main reasons that led the first Europeans to Greenland (Vésteinsson, 2016). Prior to this, ivory was used by the Greenlandic Inuits in daily life as, for example, hunting equipment, but ivory does not seem to have been used for jewellery or sculptures. Some of the first Inuit-carved ivory material is from the 17th century AD and derives primarily from seal teeth (Figure 1). With the establishment of European trading posts in Greenland in the late 19th century AD, ivory sculptures and jewellery began to develop and the first ivory 'tupilak' representing mythical creatures came to light. Until the Second World War, most products were sold to buyers from Denmark but the arrival of American troops in Greenland boosted the sale of Greenlandic products (Borum, 1945). The ivory came from narwhal, sperm whale and walrus.

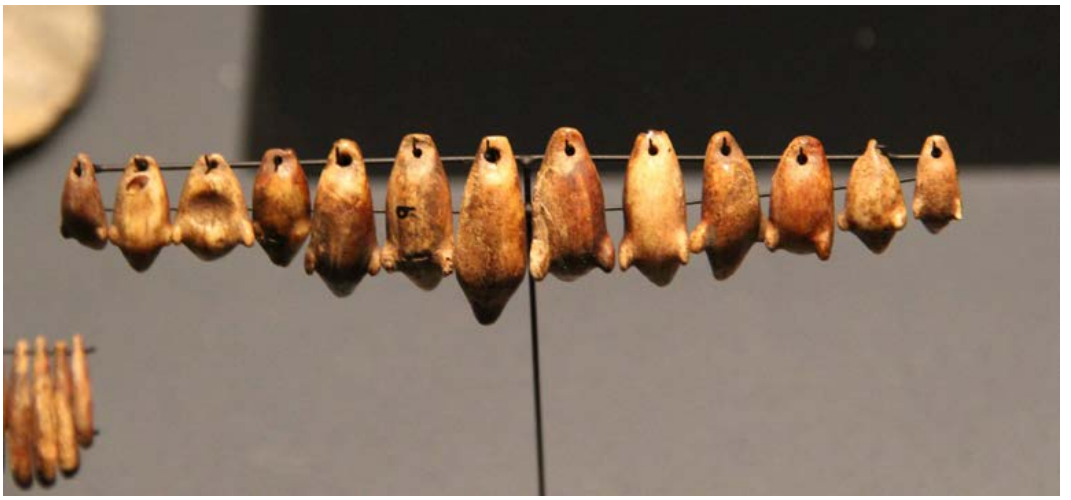

Figure 1. Necklace of ivory seal teeth from the 17th century AD found in East Greenland. (Photo: Greenland National Museum & Archives)

Today carving of ivory into jewellery or artistic sculptures such as 'tupilaks' is common. The ivory usually derives from narwhal and walrus hunted for their meat and skin. The walrus ivory consists of a thick outer cementum layer, a transition ring and a primary and secondary dentine layer (Espinoza & Mann, 1992). Narwhal ivory, in contrast, lacks the secondary dentine layer, making them easy to distinguish. The cementum often has deep cracks parallel to the length of the tusk, extending into the primary dentine layer. The tip of the walrus tusks is coated with thin enamel but this is often not preserved due to wear and tear by the animal. This also applies to the tip of the narwhal tusk. The narwhal ivory displays spiral growth that in cross-section shows as indentions in the otherwise circular tusk (Figure 2). Cracks tend to occur in the indented areas of the spiral extending from the outer cementum to the inner dentine layer. The cementum and dentine is separated by a distinct transition ring and the pulp cavity extends far into the tusk resulting in a hollow core. Due to the hollow core, it is usually only the tip of the narwhal tusk that is carved into sculptures, while the remainder of the tusk is primarily cut for jewellery.

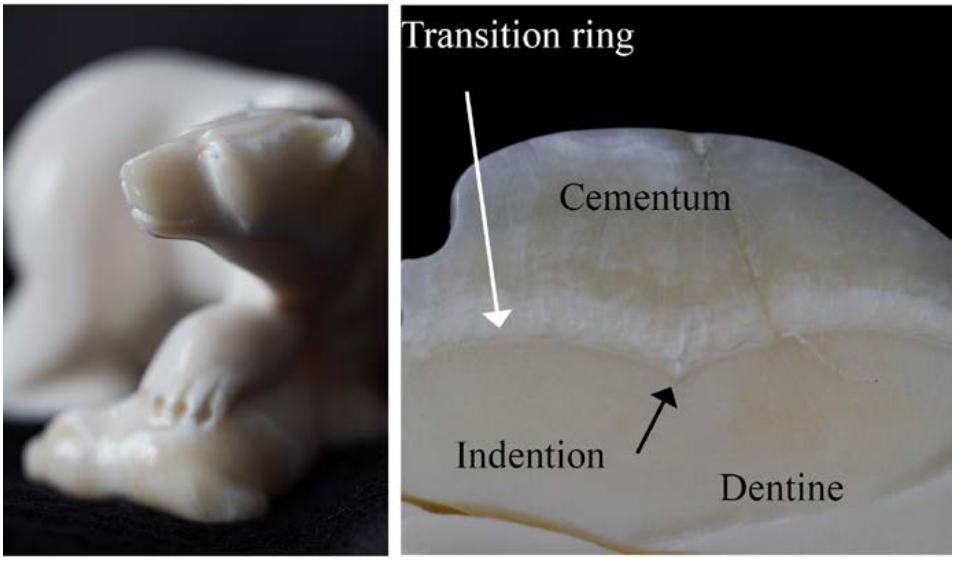

Figure 2. Narwhal ivory sculpture of a polar bear hunting for seal. The cementum, transition ring, dentine and hollow pulp cavity can be seen in the cross-section at the base of the sculpture. (Photo: A. Juul-Nielsen)

'Tupilaks', rings, brooches, and bead necklaces and bracelets are the most commonly sold narwhal and walrus ivory items (Figure 3), along with uncarved whole narwhal tusks for decoration. National ivory trade regulations allow for sale and purchase of narwhal and walrus ivory within Greenland, but not for export of narwhal ivory. Walrus ivory can be exported if accompanied by a CITES certificate. As a result, other materials such as reindeer antlers are instead used for export purposes.

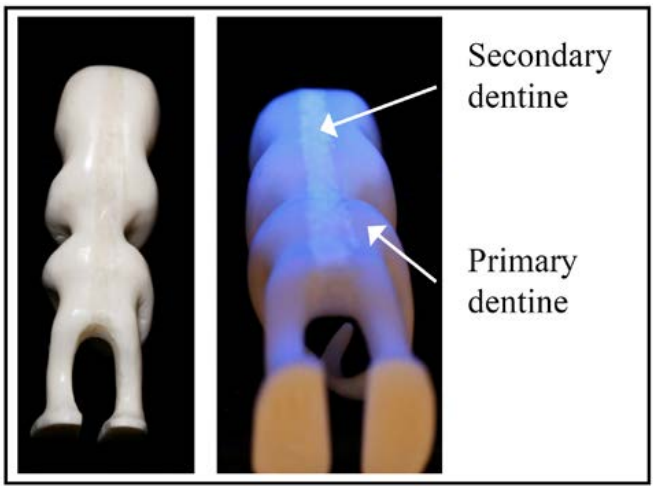

Figure 3. A walrus ivory polar bear sculpture made by Kim Eriksen (courtesy of Tupilak Travel; photo: A. Juul-Nielsen).

Conclusion

As part of the Greenlandic Inuit tradition of hunting the animals available in the Arctic for food, ivory producing animals such as walrus and narwhal are hunted in Greenland today as they have been for centuries. However, the use of the ivory has changed from hunting material equipment to the present day jewellery and sculptures.

References

Borum, V., 1945: Grønlandsk husflid i krigsaarene. Haandarbejdets Fremme, 4, 1945. Pp. 50-56.

Espinoza, E. O. & Mann, M.-J., 1922. Identification guide for ivory and ivory substitutes. World Wildlife Fund, 35 pp.

Vésteinsson, O., 2016. Kujataa – a subarctic farming landscape in Greenland. 264 pp.

UPDATE OF WORLDWIDE GEMSTONE DISCOVERY AND MINING ACTIVITIES AFTER 2000

Ahmadjan Abduriyim [1,2]

[1]Tokyo Gem Science LLC, [2]GSTV Gemological Laboratory
tgs@gemscience.tokyo

Keywords: Gemstone, mining locations, geographic origin

The gem market highly rates certain gemstones with a premium price when they originate from reputable sources (gem deposits). As a consequence, this increases the need for gem testing services by major gemological laboratories with a focus on geographic origin determination. In the past few decades, several new deposits of rubies and sapphires have been discovered in East African countries such as Tanzania (Schwarz et al., 2008, Pardieu and Schwarz., 2008), Mozambique (Pardieu,et al., 2009), and Madagascar (Hughes, 1997, Leuenberger, 2001, Pardieu and Rakotosaona, 2012, Pardieu et al., 2015, Pardieu et al., 2017). Sapphires also came from Sri Lanka (Zwaan 1982, Pardieu et al., 2012). Recently, several gemstone mines have been significantly developed by using high tech machineries, but many others are still worked using simple basic tools and techniques by local miners. To provide and collect information from current active gemstone mining countries, the author visited several well-known gem deposits in different countries to report their new discoveries and current mining activities. This aimed to update data on major gemstones which are usually focused on for their geographic origin determination, using the collected optical and chemical data for reference. A short summary of results from the 2017 to 2018 field trip is outlined here, with the detailed study results to be presented in this conference.

Brazil

The Belmont mine in the Itabira area is one of the largest and well-equipped mining operations in the world (Lucas 2012). In 2004, with a specific focus on geological research in the mining area, the mining company (Belmont Group) discovered a new productive emerald zone. Using a new optical selection process, they sorted out emeralds from the host rock more efficiently and precisely. In 2012, the Belmont Group started a joint-venture project with the Canaan mine (Mineração Canaã). This partnership enabled them to offer a wide range of emeralds to the world market extending into present times. From the author's 2018 field trip observation, good quality emeralds range from 3-4 to 6-8 in cm size and show good crystallization and color from Belmont mine, and new productions from an active mine in Nova- era, show a good quality but in small size in an extensive 150 meters deep shaft mine at Capoeirana area.

Figure 1. World class open pit emerald mine in Itabira, Minas Gerais state of Brazil.

Figure 2. Emerald crystals mined from metamorphic schist belt in Belmont mine.

Sri Lanka

In 2012, high quality blue sapphires were discovered in Kataragama area in south part of the island. Today, traditional artisanal mining methods are still used all over Sri Lanka, even for newly found alluvial deposits. The gem bearing soil and gravel is passed in baskets from one miner to another (miner collective) to reach the surface for washing. Our field trip in 2017 confirmed that, large amounts of pink and yellow sapphires were being produced from a big open-pit mine in Bogawantalawa, in southern Sri Lanka which has been discovered in 2015.

Figure 3. A new large open-pit mining in Bogawantalawa, Sri Lanka.

Figure 4. Yellow, pink and blue sapphires has been mined in the alluvial deposit in Bogawantalawa.

East Africa including Madagascar

In recent years, Madagascar, Tanzania and Mozambique have become the most important gem corundum producing countries. The decline in production of sapphires from Ilakaka, Sakaraha, and Andilamena in Madagascar was counterbalanced by recent discoveries of new sapphire deposits in North Madagascar, in the Didy, and Bemainty areas. In 2008, a new occurrence of high quality ruby discovered at Winza in Tanzania, today shows little active production. In contrast, large ruby deposits were discovered in Montepuez and Niassa districts in Mozambique in 2009. Specifically, in Montepuez, a multidisciplinary approach was adopted (Gemfields) to find both primary and secondary mining areas, using satellite imagery, core drilling, bulk sampling and geochemical studies. The mining operation at the so- called Maninge Nice area, yielded 115.4 ct/ton in primary and 349.8ct/ton in secondary deposits. An UV sorting technique and a new quality grading system for rough rubies was developed by Gemfields.

Figure 5. Large scale ruby mining process in Montepuez, Mozambique.

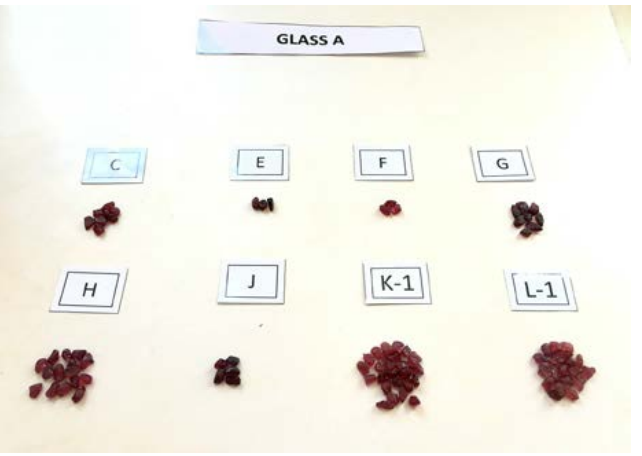

Figure 6. A grading system has been developed by Gemfields mining company based on the color, size, shape, clarity and the intensity of UV fluorescence of rough rubies.

References

Hughes R. W. (1997). Ruby & Sapphire. Boulder, CO, RWH Publishing.

Leuenberger, A., (2001). The new ruby deposits in eastern Madagascar: Mining and production. *Gems & Gemology*, Vol. 37, No 2, pp. 147-149.

Pardieu V., Schwarz D. (2008). Field report from Winza. *Rapaport Diamond Report*, Vol. 31, No. 26, pp. 173-175.

Pardieu V., Jacquat S., Senoble J., Bryl L.P., Hughes R., Smith M. (2009). Expedition report to the ruby mining sites in northern Mozambique (Niassa and Cabo Delgado provinces). http://www.gia.edu/gia- news-research-NR121709.

Pardieu V., Dubinsky E.V., Sangsawong S., Chauviré B. (2012) Sapphire rush near Kataragama, Sri Lanka (February–March 2012). GIA News from Research, www.gia.edu/research-resources/news-from-research/Kataragama_US_version_0503.pdf.

Pardieu, V., Rakotosaona, N., (2012). Ruby and sapphire rush near Didy, Madagascar (April - June 2012), http://www.giathai.net/pdf/Didy_Madagascar_US.pdf

Pardieu, V., Sangsawong, S., Detroyat, S., (2015). Rubies from a new deposit in Zahamena National Park, Madagascar, *Gems & Gemology*, Vol. 51, No 4, Gems News International, pp.454-456.

Pardieu V., Vertriest W., Weeramonkhonlert V., Raynaud V., Atikarnsakul U., Perkins R. (2017). Sapphires from the gem rush Bemainty area, Ambatondrazaka, Madagascar, https://www.gia.edu/doc/Sapphires-Gem-Rush-Bemainty-area-Ambatondrazaka-Madagascar-v2.pdf

Schwarz D., Pardieu V., Saul J.M., Schmetzer K., Laurs B.M., Giuliani G., Klemm L., Malsy A-K., Erel E., Hauzenberger C., Toit G.D., Fallick A.E., Ohnenstetter D. (2008). Rubies and sapphires from Winza, central Tanzania, *Gems & Gemology*, Vol. 44, No 4, pp. 322-347.

Zwaan P. C. (1982). Sri Lanka: The gem island. *Gems & Gemology,* Vol. 18, No. 2, pp. 62–71.

WRITING SCHOLARLY GEM LOCALITY ARTICLES: PERSPECTIVES FROM A GEOLOGIST, GEMOLOGIST, AND EDITOR

Brendan M. Laurs

Editor-in-Chief, The Journal of Gemmology, Gem-A, 1106 2nd St., #317, Encinitas, CA 92024 USA
brendanlaurs@gmail.com

Keywords: gem localities, field research, publication

Writing scholarly articles on gem localities can be challenging due to logistics in the field, the scope of information required, and the fluidity of the mining and production. Gathering first-hand information by visiting gem deposits is critical for obtaining reliable samples and researching the geology, mining and production of stones from a given locality. However, such expeditions often require abundant preparations and the cooperation of knowledgeable local guides. In addition to documenting the mines themselves, it is also worthwhile to visit local traders, markets, museums and geological surveys to obtain useful samples, information and publications. Publication of the research in a peer-reviewed journal will help ensure that the work is properly vetted and presented, and that it forms a permanent record in the literature.

Introduction

Some of the most interesting articles in the gem literature involve descriptions of exotic localities, particularly regarding new sources or mining areas. The most important factor for producing a successful gem locality article is obtaining first-hand information by conducting field research at the mine(s). However, few people realize the behind-the-scenes planning and coordination that are required for a successful expedition, particularly when the main goal is a scholarly contribution to the literature.

Figure 1: The new gem mineral pezzottaite was discovered at the Sakavalana pegmatite in a remote area of central Madagascar. Photo by B.M. Laurs, © GIA.

Visiting gem deposits in remote localities (e.g. Figure 1) takes considerable time and expense, but the benefits of performing field research 'on location' are numerous. In particular, such expeditions allow one to gain accurate information on the location, geology and mining activities at a given deposit, as well as an idea of future reserves. Also one can learn about the ore processing techniques and production (gem varieties, quality and quantity), and witness the trading and distribution of the material (Figure 2). Other benefits include purchasing research samples directly from the mine (Vertriest, 2018b) and obtaining hard-to-find maps and publications that are useful for future research. Visiting gem-producing countries may also allow one to make useful contacts with local traders and government officials, see cutting, processing, and treatment facilities, and visit local markets (Figure 3). In addition, it is sometimes possible to witness fair trade and sustainability initiatives that benefit the local population such as building schools, water wells and medical clinics. And finally, visiting gem deposits provides ancillary benefits of experiencing local cultures, flora, and fauna, typically in areas that are untouched by mass tourism. Although such experiences may not contribute directly to a locality article, they can be quite useful for presentations, blog posts, etc. that are important for outreach and exposure of one's work to the gemmological community.

Figure 2: At Mavuco, Mozambique, miners offer Cu-bearing tourmaline to intermediaries called 'runners' who bring the rough material from the mines to nearby trading centres. Photo by B.M. Laurs, © GIA.

Figure 3: Miners display mineral specimens and gem rough at the 'umbrella market' in Mogok, Myanmar. Photo by B.M. Laurs, © Gem-A.

Preparation and Execution of an Expedition

Extensive preparations are necessary to ensure a successful field expedition (see, e.g., Winser, 2004). Specifically, it is important to define the goal of the trip, invite research collaborators, arrange local guides, obtain visas, secure permission for visiting deposits and exporting samples, gather geological information and maps, and consider health and safety factors (including proper immunizations). Perhaps the most important logistical consideration is choosing reliable and knowledgeable field guides, who may consist of local citizens or foreign specialists. They will know local customs and safety issues, be able to provide access to mines (and thus should be the owner and/or know local miners), and take care of necessary logistics such as transportation, as well as room and board.

After arriving in the destination country, several tasks should be considered before actually visiting the mines. These include meeting with local contacts, obtaining any further permissions to access mines, visiting the geological survey office to obtain maps and publications (Figure 4), and becoming familiar with the area's gems and minerals by seeing local dealers, markets and museum collections (Figure 5). One should try to gain insights on recently produced gem material while learning about pricing and becoming aware of simulants and treatments that are locally present.

Figure 4: At the Geological Survey of Zambia in Lusaka, geologist Björn Anckar searches for maps and publications on gem-producing areas. Photo by B.M. Laurs, © GIA.

Figure 5: The National Museum of Geology in Maputo, Mozambique, is a good place to learn about the country's mineral resources. Dr Hanco Zwaan stands among cases containing various minerals from local pegmatites. Photo by B.M. Laurs, © GIA.

When visiting mining areas, particularly when only limited time is available, it is helpful to have specific goals in mind while remaining flexible to the fluidity of the situation. Some of the challenges associated with performing research on new gem discoveries were described by Vertriest (2018a). It is advisable to have at least two days for undertaking field studies in a particular area, and several days may be necessary to cover larger areas and/or accomplish more time-consuming tasks such as geological studies and purchasing samples. The combination of local attitudes toward foreigners, cultural differences, language barriers, and health and safety issues can be overwhelming, and it is helpful to have a list of questions in mind that pertain to matters such as 'who, what, where, when, and how'. This will help ensure that the fieldwork will produce the scope of information that is useful for a scholarly article. While it is tempting to focus only on sampling the gems themselves, it is also important to obtain samples of the host rocks/sediments and learn about the geology of the area—particularly if the goal is to understand the geological origin of a deposit and/or undertake future geographic origin determinations.

Sharing the Research

The information gleaned from a research trip can be shared in different ways, such as articles and presentations (or even a full-length book, if enough trips have been made to obtain a sufficient depth of information). Presentations are commonly given at conferences and shows, and additional audiences include gemmological alumni chapters, museum groups, and gem and mineral societies. However, preparing articles for peer-reviewed publication (e.g., Figure 6) ensures that one's findings will be presented in a rigorous, accessible, and attractive fashion, while also gaining widespread exposure and recognition for the research. Although this process can be laborious and time-consuming, the end product will be a valuable and informative contribution to gemmological knowledge that forms a permanent record in the literature.

FEATURE ARTICLE

Figure 1: These cabochons (up to 40 mm long) and rough pieces of Bumble Bee Stone (BBS) were produced in 2017. The samples are more orange than previously mined material that contained yellow areas. Photo by J. Ivey.

Bumble Bee Stone: A Bright Yellow-to-Orange and Black Patterned Gem from West Java, Indonesia

Emmanuel Fritsch and Joel Ivey

ABSTRACT: Bumble Bee Stone (BBS) is a bright yellow-to-orange and black patterned gem material. Although sometimes referred to as a jasper, it is actually a carbonate-rich rock rather than a silica-based gem. It is mined from sulphide-bearing veins near an active volcano in West Java, Indonesia. Its most remarkable characteristic is its bright yellow colour, which is caused by the presence of an unexpected sulfide, pararealgar. The orange colour in some samples consists of a mixture of pararealgar with realgar. Both minerals are polymorphs of As_4S_4, arsenic sulphide. Areas of black colouration are due to aggregates of micron-sized pyrite crystals ("sooty" pyrite). The successive growth layers, when cut through in different orientations, give rise to a variety of attractive patterns. BBS has been mined for the past 15 years, and new veins are still occasionally found.

The Journal of Gemmology, 36(3), 2018, pp. 228–238, http://doi.org/10.15506/JoG.2018.36.3.228

Figure 6: Publishing in peer-reviewed journals is an excellent way to ensure that one's research will reach a broad international audience.

The article preparation process involves several steps. The authors and collaborators should first decide the scope of each of their contributions, and thus take responsibility for producing specific parts of the resulting publication(s). The samples obtained on the trip need to be catalogued and prepared for analysis by a variety of techniques, which may include measurement of gem properties and observation of inclusions, spectroscopy, chemical analysis, and heat treatment or other experiments. Photos are obtained in the lab and selected from those taken in the field. Line-art is drafted (maps, spectra, diagrams, etc.) and data tables are compiled, all while the article is being written by the various authors. A detailed literature search should be performed (ideally both before and after the expedition). If the article is submitted to a peer-reviewed journal such as *The Journal of Gemmology* or *Gems & Gemology*, the authors may need to undertake revisions that require further work before it can be published. Such a vetting process frequently makes the article stronger and may prevent mistakes in the execution and presentation of the research. From fieldwork to publication, producing a full-length feature article can take several months to more than one year.

References

Vertriest W. (2018a) The dynamics of gem stone discoveries and the challenges for research. *XXII Meeting of the International Mineralogical Association*, Melbourne, Australia, 13–17 August, 330.

Vertriest W. (2018b) GIA's field gemology program: A modern approach to origin determination. *Gems & Gemology*, **54**(3), 283–284.

Winser S., Ed. (2004) *The Royal Geographical Society Expedition Handbook*. Profile Books, London, 416 pp.

Multi-element Analysis of Gemstones and its Applications in Geographical Origin Determination

Hao A.O. Wang[1*], Michael S. Krzemnicki[1], Susanne Büche[1], Ramon Schmid[1], Judith Braun[1]

[1] Swiss Gemmological Institute SSEF
Asechengraben 26, CH-4051, Basel, Switzerland,
*hao.wang@ssef.ch

Keywords: multi-element, LA-ICP-TOF-MS, sapphire, emerald, dimension reduction, PCA, t-SNE

In the past decades, multi-element information is becoming more and more important in gem testing, not only for material identification, filtering out synthetic and treated materials, but especially for determining geological origin of gemstones. Such information is not accessible by conventional gemmological testing instruments, hence making LA-ICP-MS a unique tool in gem testing labs. In the last IGC conference in Namibia, we have reported a study comparing advantages and disadvantages of LA-ICP-Quadrupole-MS and LA-ICP-Time-Of-Flight-MS (LA-ICP-TOF-MS, such as GemTOF at SSEF, see in Krzemnicki et al. 2017). As described two years ago, not only is the TOF-MS instrument capable of simultaneously acquiring almost all elements in the periodic table, also it excels in mass resolving power, which allows correction of mass interferences and improvement in quantification accuracy. In gemstone analysis, below ten parts per billion (ppb) limits of detection can be routinely achieved for heavy masses, and several hundreds of ppb for light isotopes.

LA-ICP-TOF-MS: Paradigm Shift of Multi-Element Analysis for Gemstones

During more than two years of measurements with GemTOF, the authors often encounter scenarios that a priori knowledge about multi-element content of the sample cannot be presumed, for example rarely occurring elements in gemstones, or solid or fluid inclusions in geological samples. Moreover, the isotope of interest for a specific element may also be changed in the post-data processing in case we encounter unforeseen mass interferences, which may be realized only after the measurement is done or the stone has left the premises. In this presentation, we would like to revisit the advantages of TOF-MS, especially the novel acquisition scheme of FIRST measure, THEN determine which isotopes are of interest. We would like to demonstrate how this paradigm-shift is useful for trace element analysis on gemstones.

Based on real case studies on sapphire and emerald specimens, we will present how simultaneous multi-element approach assists origin determination. Instead of pre-defining a list of isotopes in advance, routine analysis of blue sapphires using LA-ICP-TOF-MS detects rarely occurring trace elements such as beryllium (Be), zirconium (Zr), niobium (Nb), lanthanum (La), cerium (Ce), hafnium (Hf), thorium (Th). These elements have been observed more frequently in sapphires from Madagascar than Kashmir ones (Figure 1). Interestingly, radioactive thorium isotope (^{232}Th), as a rarely occurring isotope, decays to one of the lead isotopes (^{208}Pb) at a constant rate. By measuring intensities of parent and daughter isotopes, formation age of the stone can be estimated without using "time capsule" inclusions, such as zircon. This could sometimes be helpful, as the zircon inclusions are seldom found reaching surface of gemstones, hence difficult for age dating by LA-ICP-MS. In an example of a blue sapphire (Figure 2), conventional gemmological testing suggests Madagascar as its origin rather than Myanmar. During routine elemental analysis, rarely occurring ^{232}Th isotope was detected in this sapphire. Thanks to the full mass spectrum acquisition by GemTOF, without re-ablation, all of the Pb isotopes (^{204}Pb, ^{206}Pb, ^{207}Pb, ^{208}Pb) were collected si multaneously, and indicated no common Pb contamination. The estimated age (~500Ma) is in agreement with that of Madagascar samples expected in other study (Elmaleh, et al. 2015), which adds more evidence to the determination. More about our research in age dating of gemstones and pearls is given in a second contribution to this conference and abstract book (see Krzemnicki et al. 2019).

		Be	Zr	Nb	La	Ce	Hf	Th
Median Conc. [ppm]	Kashmir	<LOD	<LOD	<LOD	<LOD	<LOD	<LOD	<LOD
	Madagascar	<LOD	<LOD	<LOD	<LOD	<LOD	<LOD	<LOD
Occ. Freq. [%]	Kashmir	3.7	*1.7*	*4.3*	4.3	6.6	*2.9*	*6.0*
	Madagascar	17	*42*	*46*	14	18	*35*	*31*

Figure 1. Frequency of rarely occurring elements observed in blue sapphires from Kashmir and Madagascar. Median concentrations are below LODs. To the right, high Th signal and no common Pb have been found in sapphire, hence a candidate for Th-Pb age dating. The estimated age is around 500 Ma.

Figure 2. More than 100 ct sapphire from Madagascar. Age dating: ~500 Ma.

Multi-Dimension Data Visualization: PCA and t-SNE

Conventionally, trace element results of gemstones are shown in bivariate plots, tri-plots, and three dimensional scatter plots to compare their elemental similarities with reference samples from database. As an example, Figures 3a and 3b display a bivariate plot (Li-Cs) and a three dimensional scatter plot (Li-Fe-Cs) using SSEF emerald database. LA-ICP-TOF-MS intrinsically produces multi-element results (high dimensional dataset), therefore one would need to compare multiple bivariate-plots for a comprehensive data analysis, because direct visualization of the high dimensional dataset is challenging. Alternatively, statistical dimension reduction can be applied on the original dataset. Our high dimensional space of twenty element concentrations of more than 700 emerald analyses is projected onto a two dimensional space. Using this example, linear principle component analysis (PCA) and non-linear machine learning algorithms (t-SNE, Van Der Maaten, 2008) were applied on our datasets (Figures 4c and 4d). Both analyses are unsupervised, meaning colours (indicating various origins) of the scatter dots are labeled only after the reduction process. In this way, groups of data points are solely dependent on the elemental similarities among the analyzed gemstones and without prior information about their origins. Based on our research, we can see that, compared to PCA, we achieve a better separation of different origins when using t-SNE algorithm (Figures 3c and 3d). In this example, the emeralds from different geographical origins can be separated from each other. Emeralds from a new find in Afghanistan (black arrow in Figure 3d), which are gemmologically similar to Columbian material (Krzemnicki, 2017), can also be distinguished from more classic emeralds from Panjshir valley in Afghanistan and Columbia. It seems that non-linear dimension reduction algorithm t-SNE is more suitable for multi-element data visualization comparing to other types of linear algorithms.

Conclusions

Although the present study reveals the potential of elemental analysis combined with statistical analysis to separate gemstones from different origins and geological settings, it is important to mention that this method is often not a conclusive method. Especially for corundum, multi-element analysis is rather providing complementary information, to assist microscopic observations and further analyzed properties before concluding on an origin opinion. However, as shown in this study, such statistical methods can be a valuable tool, when studying elemental similarities of gemstones from various origins. Ongoing studies focus on combining elemental data with data from other analytical methods, such as (UV-Vis, FTIR, Raman) spectroscopy and microscopy, with the aim to advance our understanding of the geological conditions during formation of gemstones and finally deepen our knowledge about origin determination of gemstones as a service to the trade.

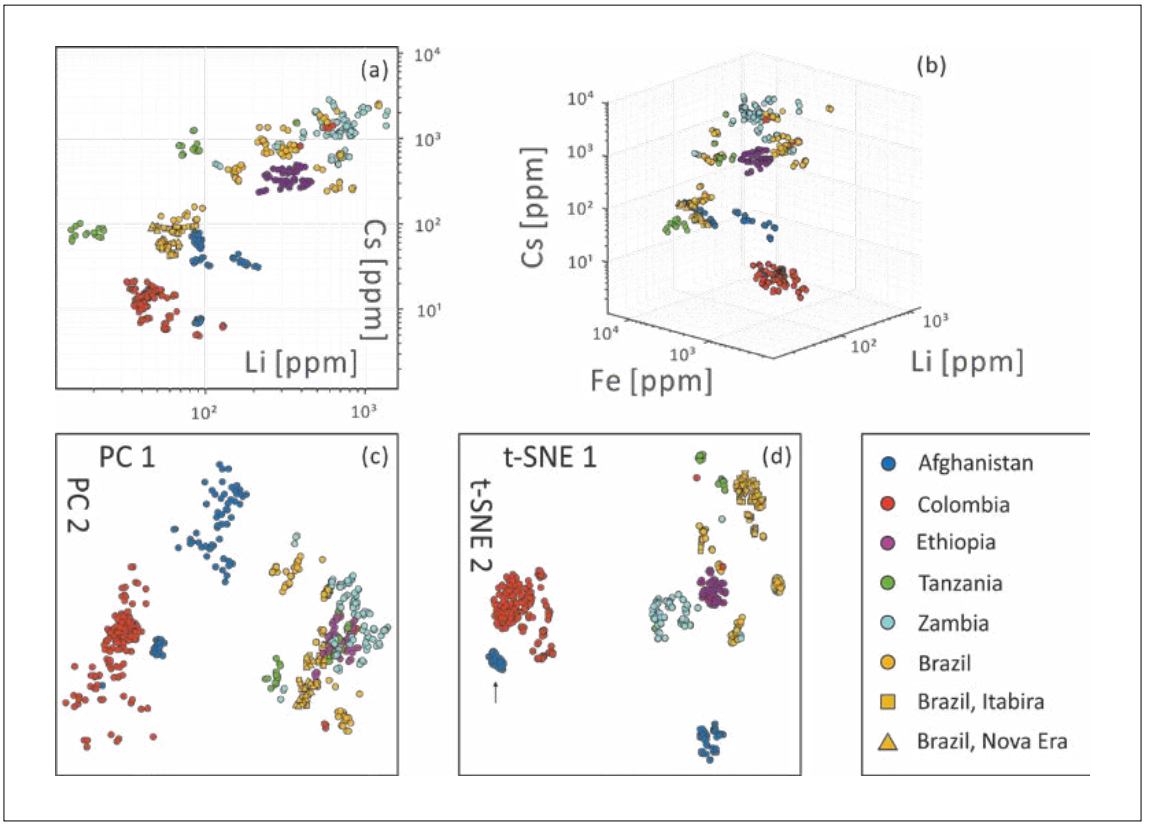

Figure 3. Multi-element data visualization using a) bivariate plot of Li and Cs concentrations (log scale); b) 3D scatter plot of Li-Fe-Cs concentrations (log scale); high dimensional elemental data visualization using c) linear Principle Component Analysis (PCA); and d) non-linear machine learning algorithm (t-SNE). Both PCA and t-SNE analyses result from 20 element concentrations and are unsupervised, meaning origin information (colour of scatter dots) are only draw after dimension reduction.

References

Elmaleh E., et.al., 2015, Zircon inclusions in blue sapphires. IGC Conference Abstract, 51–52.

Krzemnicki, M.S., Wang, H.A.O., et.al., 2017, GemTOF: A New and Highly Versatile Method to Analyze Trace Elements and Isotopes of Gemstones and Pearls. IGC Conference Abstract, 88-90.

Krzemnicki, M.S., 2017, New Emeralds From Afghanistan. Facette, 2017, 12-13.
Van Der Maaten, L.J.P., Hinton, G. E., 2008. Visualizing high-dimensional data using t-sne. Journal of Machine Learning Research, (9), 2579-2605.

Wang, H.A.O., Krzemnicki, M.S., et.al., 2016, Simultaneous High Sensitivity Trace- Element and Isotopic Analysis of Gemstones Using LA-ICP-TOF-MS. Journal of Gemmology, 35(3), 212-223.

Acknowledgement

The Swiss Association of Gemstone Dealers is acknowledged for generous donation and team members and foundation board of SSEF for their support and fruitful discussion.

Exploring gem commercial names using big data color analysis technology, expert traders' opinions and geographical and trade interpretation.

Menahem Sevdermish

GWLAB, Ramat Gan, Israel
smenahem@gemewizard.com

Big data analytics is the process of collecting, organizing and analyzing large data volumes to reveal hidden patterns and unfamiliar correlations, identify trends, and extract other useful information, which otherwise might be invisible – even for the data manager.

Big data analytics, within the gem and jewelry trade, is hardly used. Contrary to other luxury categories, which focus their sorting on many criteria, such as the type of item, color, texture, fabric, season and others, the gem and jewelry section is kept with general fixated inquiries, which scarcely offer insights.

One of the biggest challenges for the gem and jewelry market moving into e-commerce (remote trade) is to create a common language between traders, gemology professionals and consumers worldwide, and to promise a What-You-See-Is-What-You-Get (WYSIWYG) experience. This challenge is known for having very significant deviations and tolerances between the industry's key players. In addition, the effortless accessibility of information via online media resulting in increased awareness and involvement, is excellent in offering knowledge to the end consumer, though its accuracy is generally not fully verified.

During the past decade my team and I have devised and used a digitized, fully automatic big-data analysis system for large-scale gem and jewelry marketplaces and online websites, based on image color analysis and a contextual search engine. This system can generate unique analytics and insights.

During the years 2016-2018, we were given the opportunity to examine the validity of the system on vast amounts of data of a world-leading online retail marketplace and from major websites. The information gathered from this survey, together with volumes of documented data collected from prominent traders, provided us with important insights regarding the perception of traders and professionals of the known gem commercial names, such as Pigeon Blood, Royal Blue, Cornflower Blue, etc.

The information gathered from this survey was considered by gem traders as an eye opener. We found that the perception of which colors are represented in each of these commercial names differs according to geographical location and also among various leading gemological laboratories (save American labs, which prefer not to use commercial terminology), as apparent from their lab reports.

The process includes analysis of tens of thousands of gem images, accompanied by expert opinions regarding their colors and documented gemological reports of leading institutes. To support the accumulated digital information, hundreds of actual gems were collected from prominent dealers. The gems were photographed in appropriate lighting conditions to display their actual body color, as perceived by the human eye.

Once arranged in the database, we used the Gemewizard's Sampler scanning technology to compare the gem's image against Gemewizard's 6381 gem color combinations (arranged according to hue, tone and saturation levels). The Sampler analyzes the item image, locates the gem within the image, and retrieves its 'Color DNA'. The Color DNA is then converted to a Gemewizard pre-defined color code. For each gem type, a map of pre-defined

colors was built. These maps were defined using a worldwide online survey and by consulting with a team of experts from along the gem trade. The photographed gems were positioned within the map, with their reported commercial color definition opinions (from all sources).

For example, Pigeon's Blood is the trade name for a fiery Red vivid color of the highest quality ruby gem. According to traders, top quality rubies possess a slightly purplish Red (GW hue 31) to Red (hue 1) hue with a medium light to medium dark tone (GW tone grade 3 to 5) and a strong to vivid saturation (GW sat. level 5 to 6). This results in a vivid pinkish red appearance (see figure 1).

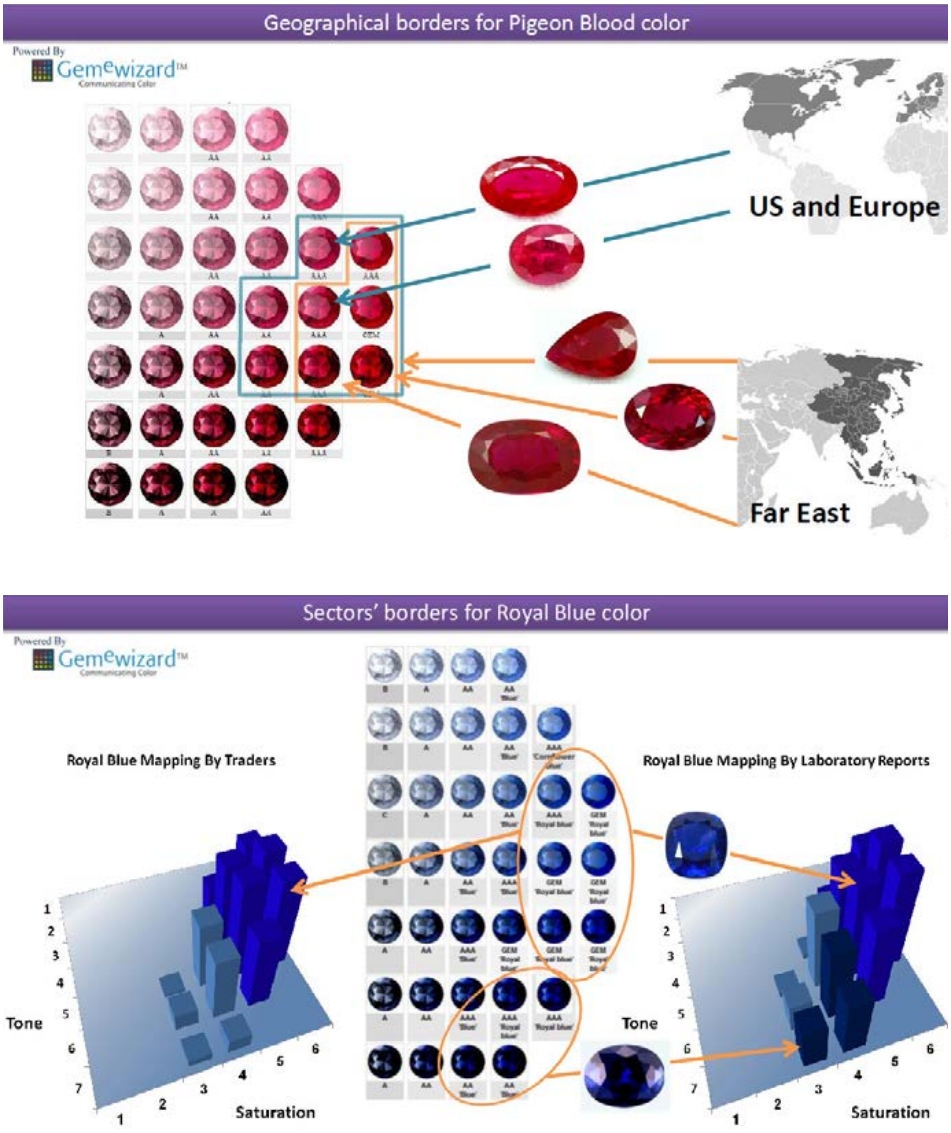

Figure 1: Color data on pigeon bloods and royal blue denomination

However, among the collected gemological laboratories' reports, according to our survey, the definition color borders are wider and inconsistent. While leading European-based laboratories draw a strict border of intense red to pinkish red appearance, Asian laboratories tend to allow darker-toned (tone 6 to 7) purplish- like colors as well, in order to achieve the designation.

Similar inconsistency was identified in blue-colored sapphires, with the two colors, which considered to be the most sought after – 'Royal Blue' and 'Cornflower Blue'.

According to most of the trade, the Royal Blue color is a medium light- to dark-toned (tone 3 to 6), moderately to vividly saturated (sat. 4 to 6) violetish Blue (hue 23) color. It resembles, somewhat, the color of iodine under an electric lamp. For the Cornflower Blue, the analysis was more complicated due to a wide variety of different opinions. Some traders define it as a specific shade of light toned (tone 3), strongly saturated (sat. 5) violetish Blue (hue 23), resembling the color of the renowned flower. Others, mainly in western countries, point towards a medium light to medium toned (tone 4 to 5), strongly-saturated (sat. 5) Blue (hue 22), lessening the violetish tint importance.

The laboratories, were again showing prominent inconsistencies. Several laboratories adopted a lenient approach where dark, less saturated, gems, depicting a very dark, almost black, color, were identified as Royal Blue. These colors were not considered as Royal Blue by the majority of the traders.

For the Cornflower issue, the solutions were more creative. The European laboratories choose not to use the term in their reports at all. In Asia, one laboratory chooses to divide the huge gap by adding a descriptive prefix of "intense-cornflower" to the deeper silky appearance (sat. 4 to 6). Another laboratory uses a set of commercial names for different shades, such as Pastel for light-toned (tone 2 to 3) highly saturated (sat. 4 to 5) straight blue (hue 22) gems and velvet for medium to medium dark-toned (tone 5 to 6) highly saturated (sat. 4 to 6) stones showing the violetish tint (hue 23).

These results present somewhat surprising results of strict borders drawn by the traders regarding commercial names, whilst the laboratories' reports show more leniency. This causes some distortion, while on the one hand, keeping a scientific approach but on the other hand, satisfying the customers (traders). It seems that there is some tension amongst the laboratories to produce saleable reports.

LASER DAMAGE IN GEMSTONES CAUSED BY JEWELLERY REPAIR LASER

Lore Kiefert[1*], Klaus Schollenbruch [1]

[1] Gübelin Gem Lab, Maihofstrasse 102, 6006 Luzern, Switzerland
*lore.kiefert@gubelingemlab.com

Keywords: ruby, sapphire, laser damage

Recently, several older sapphires as well as a pink sapphire were sent to the lab for certification, with what looked like cavity fillings at first sight (Figure 1). However, no filler could be detected. According to similar observations by other laboratories (see SSEF Facette 2019), such holes could have been derived by the uncareful use of a jewellery repair laser. In a quick first step, we had our jewellery department apply their repair laser on a sapphire from our reference collection and there were some surprising results: The holes did not appear where the laser hit the sapphire but rather where the laser beam exited the stone (Figure 2a and 2c), with a reflection feature (a second laser damage) at a completely different spot (Figure 2b and 2c).

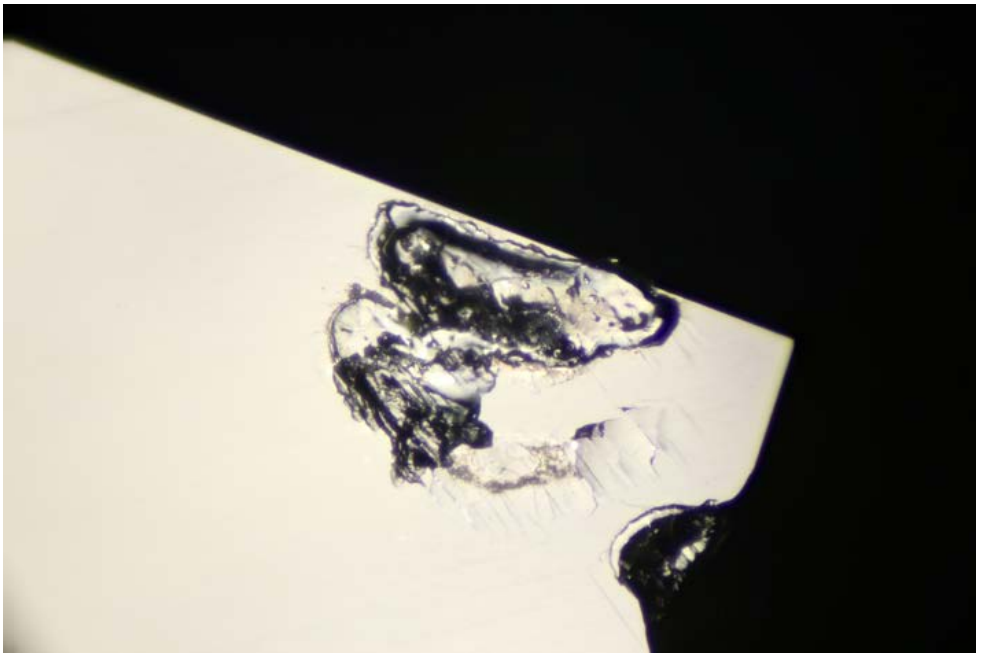

Figure 1: Melted surface on a Kashmir sapphire that came into the lab for testing. This damage is most likely caused by a repair laser.

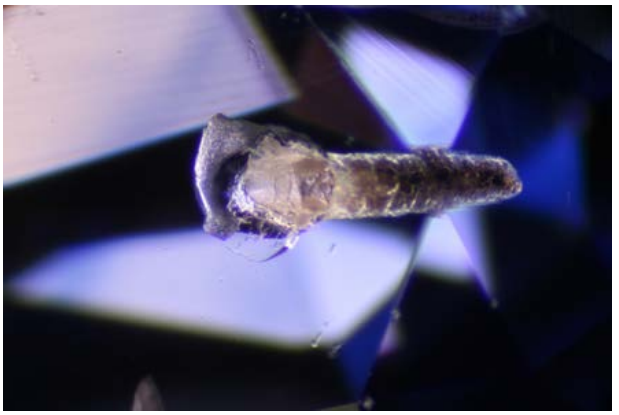

a

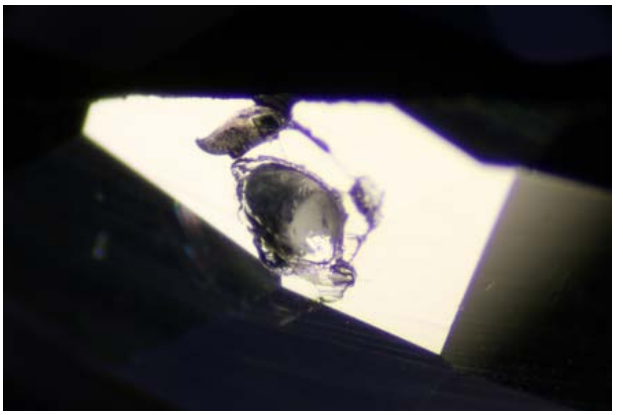

b

c

Figure 2:

a) Laser damage at the exiting side of a sapphire from our reference collection;

b) Laser damage at the opposite side where the first damage occurred, approximately at an angle of 90 degrees.

c) Sapphire showing the laser damage caused by a jewellery repair laser at Gübelin. The laser was pointed to the backside (blue arrow), but the damage occurred on the opposite side (oval red circle). A secondary damage was noted at a different surface (round circle), possibly due to a reflection effect.

This led to an experiment testing several other gemstones besides sapphire to see if the effect is repeatable (in sapphires), and what effect such a laser treatment has on other gemstones such as emerald, ruby, garnet, tanzanite, tourmaline. The chosen samples consisted of two sapphires in addition to the one for the first attempt, 4 rubies and 9 emeralds of different shape (cabochon and faceted) and qualities (unheated and heated, fractured, clean, clarity-enhanced), two tourmalines, one garnet and one tanzanite.

The results of these experiments are presented in the lecture.

Reference

SSEF Facette, International Issue No. 25, 2019, page 11. https://www.ssef.ch/wp-content/uploads/2019/02/facette-2019.pdf

Spectral fitting of UV/Vis/NIR spectra for the quantitative determination of Cr^{3+} and V^{3+} in gemstones, with special emphasis on ruby and emerald

Tom Stephan[1,2], Tobias Häger[2], Ulrich Henn[1], Wolfgang Hofmeister[2],

1German Gemmological Association, Idar-Oberstein, Germany
2 Center for Gemstone Research, Johannes Gutenberg-University, Mainz, Germany
t.stephan@dgemg.com

Keywords: Ruby, emerald, spectral fitting, absorption spectra

Gemstones incorporating chromium often contain also vanadium. Whereas the colour of rubies is influenced just by minor contributions of V^{3+} (Harder, 1969, Gübelin, 1975, Schmetzer, 1978, 1982, Fritsch & Rossman, 1988, Stephan et al., 2018), the impact of V^{3+} on the colour of emerald is stronger (Wood & Nassau, 1968, Schmetzer, 1978, 1982, Fritsch & Rossmann, 1988). The spin-allowed absorption bands of the chromophores strongly overlap each other, so a just visual distinction is difficult.
As an example for the influence of vanadium and chromium on the colour of chrysoberyl see Schmetzer et al. (2013).

For this study, the ultraviolet/visible/near-infrared (UV/Vis/NIR) absorption spectra of various natural and synthetic chromium- and/or vanadium-bearing rubies and emeralds were mathematically decomposed into Gaussian and Lorentzian curves to subdivide the overlapping Cr^{3+} and V^{3+} absorption bands, and the curve fitting software MagicPlot Pro has been used.

Based on oriented wafers of (natural and synthetic) rubies and emeralds solely coloured by Cr^{3+} or V^{3+}, four models were developed - one for each colour cause in each gemstone. Both, the applicability of the models and the transferability to the absorption spectra of natural rubies and emeralds from various occurrences as well as the correlation with chemical analyses were successfully tested.

The authors developed the models by defining Gaussian and Lorentzian curves in MagicPlot pro following these steps (exemplarily shown in figures 1-3 for ruby). Wavenumbers have been chosen for fitting, because these are directly proportional to the energy, whereas the wavelength is inversely proportional to the energy:

1- Subtraction of the background noise using a constant at the lowest point of the spectrum.

2- Modelling of the Tyndall-effect, which is a Rayleigh scattering of light at small particles (e.g. tiny inclusions). This effect occurs because the spectrometer used for measuring works without an Ulbricht-sphere. It has been modelled using a Gaussian bell curve with high half-width at half-maximum (HWHM). The maximum of this band is usually located in the UV- region.

3- Fitting of the absorption edge towards the UV-region ("cut off"). The shape of the cut off strongly depends on the spectroscope. For this reason, the authors fitted just the rise of the spectrum towards the UV-region.

4- Fitting of the Cr^{3+}- resp. V^{3+}-bands:
   a- Because of their asymmetry the two spin-allowed transitions of Cr^{3+} have been fitted each by two Gaussian bell curves, the spin-forbidden transition with one Gaussian bell curve.

b- The two spin-allowed transitions of V^{3+} have been fitted each by two Gaussian bell curves, too.

The authors chose the bands Cr1-5 and V1-4 to describe the absorption bands of Cr^{3+} and V^{3+}. Because of the asymmetry of the octahedral oxygen coordination in which both chromophores are incorporated in the structure of corundum and beryl, their spin-allowed absorption bands are asymmetric, too. Consequently, the authors used two Gaussian bell curves to describe each of these bands. Mathematically, the curves Cr1+2, Cr3+4, V1+2 and V2+3 shown in figure 1 and 2 are the best fitting results for the spin-allowed absorption bands of Cr^{3+} and V^{3+} in corundum.

5- Following the steps described above the absorption spectra were fitted. Afterwards, the actual models were created: The areas (thus intensities) of the curves Cr1-Cr5 resp. V1-V4 were joined together by setting the areas of the curves Cr1 resp. V1 to 1; the other curves were expressed as multiples. While using the models the parameters x-position and HWHM are fixed. Therefore, the programme varies the intensities but the relations between the bands always stay the same.

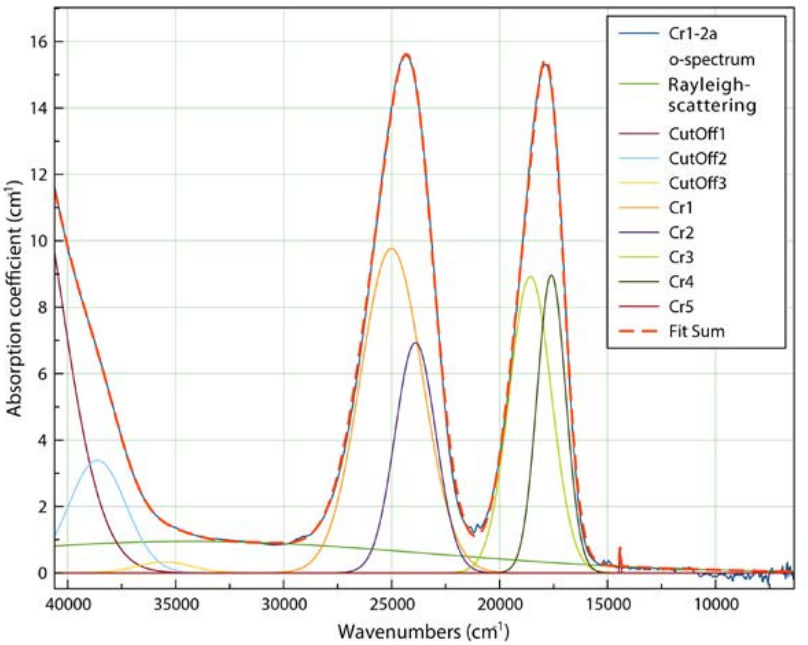

Figure 1

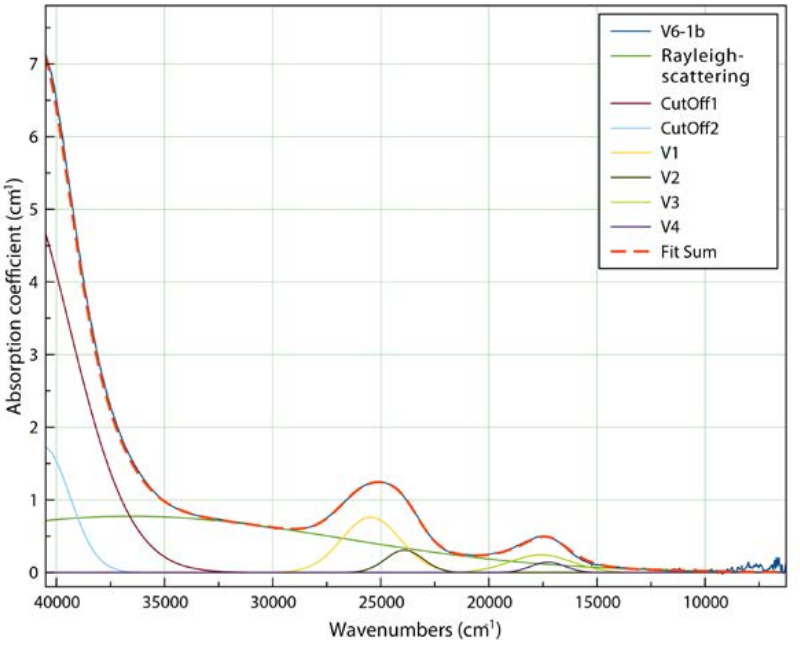

Figure 2

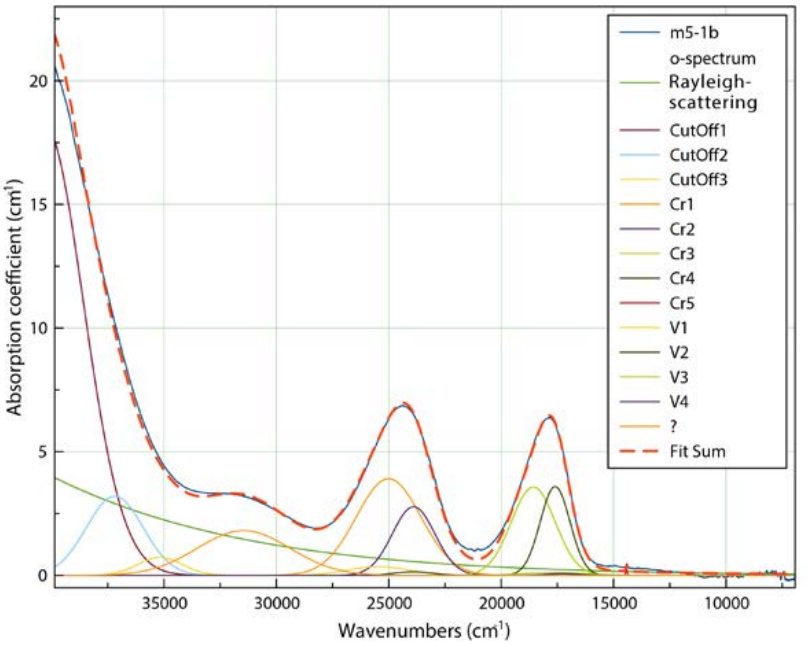

Figure3

The models were tested by fitting absorption spectra of various natural and synthetic rubies and emeralds with known sample thickness. For the fitted spectra the intensities of the curves Cr1 and/or V1 have been compared to their chemical analyses, resulting in diagrams with linear regression (figure 4). The regression line does not make it through zero because of the deviation of predicted and measured concentrations (see below), as well as the detection limit of the LA-ICPMS. For figure 4, the predicted concentrations compared to the measured concentrations of chromium show a deviation of 8.5-25% for Cr-concentrations < 1000 ppm, 2.5-16.1% for Cr-concentrations of 1001-2000 ppm and 0.2-8.7% for Cr- concentrations of 2001-5500 ppm.

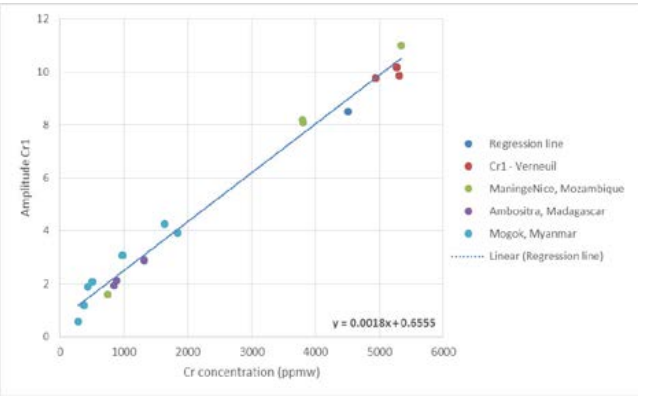

Figure 4

The investigations show that by using spectral fitting in the way described above in combination with the regression lines calculated (cf. figure 4), it is possible to determine the concentration of the colouring element also in samples with unknown chemistry. Despite the superposition of the absorption bands of both chromophores, the simultaneous application of Cr^{3+} and V^{3+} models is also possible. Therefore, the detection of vanadium in rubies and emeralds is made possible even at low concentrations. This, for example, allows first information on the samples origin.

Additional information can be obtained from the absorption spectra, such as:

1-Exact position and shape of the cut-off (absorption edge towards the UV-region).
2-The strength of the Tyndall-effect (Rayleigh scattering), to estimate the concentration and size of the light-scattering inclusions.
3-Detection of underlying colour causes.
4-Expression of the influence of a chromophore in percent by calculating the integral of each peak used for fitting, which allows a replicable and reproducible description of absorption spectra and the colour impression.

For faceted samples with unknown layer thickness it is difficult to use spectral fitting in the way described above. However, first and ongoing investigations show that there are some potential options:

1-Measuring through the girdle (esp. for small stones): the layer thickness equals the stone's diameter in the respective direction.
2-Measuring through table facet and culet/keel (esp. for flat stones): the layer thickness equals approx. to the stone's depth.
3- If the concentration of one chromophore is known, the Beer-Lambert-Bouguer law can be used to determine a correction factor to calculate the "real" layer thickness. This factor can be used again to calculate the layer thickness for other faceted stones of the same size, cut and proportions without knowledge of the chemistry.

Outlook

The results presented here are part of ongoing research in cooperation of the German Gemmological Association and the Johannes Gutenberg-university in Mainz, with the aim to prepare a fitting model for each colour cause of corundum and beryl, what would allow a simultaneous quantification of the concentration of all involved chromophores.

Furthermore, the method will be optimized in order to improve the deviation of measured and calculated concentrations, especially for low concentrations of the colouring trace element. Applicability for faceted samples requires further research, too.

Methods

Chemical analyses have been measured both with a mass spectrometer with laser ablation of the type *Agilent 7500c Quadrupol-ICP-MS* for trace elements as well as an electron microprobe of the type *JEOL JXA 8200* for the major elements.

Measurement of UV/Vis/NIR spectra has been undertaken using the spectroscope of the Center for Gemstone Research (*J&M Analytika AG),* which is coupled to a microscope. This instrument allows measurements between 200-1600 nm. Additionally, the spectroscope of the DSEF German Gem Lab (*Perkin Elmer Lambda 950S)* has been used, which measures from 200-2500 nm.

All spectra for this work have been fitted using the curve fitting software *MagicPlot Pro*. The models have been prepared manually by the authors and were refined afterwards by the software. After preparation of the models like described above, these models were used to fit the absorption bands of Cr^{3+} and V^{3+}. The other features like the Tyndall effect and the cut off were fitted manually for each spectrum and refined afterwards by the software.

References

Fritsch, E. & Rossman, G. R., 1988. An update on color in gems. Part III: Colors caused by band gaps and physical phenomena. Gems & Gemology, 24(2), 81-102.

Gübelin, E. J., 1975. The Color Treasury of Gemstones. Elsevier Phaidon, London.

Harder, H., 1969. Farbgebende Spurenelemente in den natürlichen Korunden. Neues Jahrbuch für Mineralogie, Abhandlungen, 110, 128-141 (in German).

Schmetzer, K., 1978. Vanadium III als Farbträger bei natürlichen Silikaten und Oxiden - ein Beitrag zur Kristallchemie des Vanadiums. Dissertation, Ruprecht-Karl-university, Heidelberg (in German).

Schmetzer, K., 1982. Absorptionsspektroskopie und Farbe von V^{3+}-haltigen natürlichen Oxiden und Silikaten - ein Beitrag zur Kristallchemie des Vanadiums. Neues Jahrbuch für Mineralogie, Abhandlungen, 144(1), 73-106 (in German).

Schmetzer, K., Krzemnicki, M. S., Hainschwang, T. & Bernhardt, H.-J., 1982. Natural and synthetic vanadium-bearing chrysoberyl. Journal of Gemmology, 33(7-8), 223-238.

Stephan, T., Häger, T., Henn, U. & Hofmeister, W., 2018. Quantitative Determination of Cr^{3+} and V^{3+} Contents in Rubies by Spectral Fitting of UV-Vis-NIR Spectra. Gems & Gemology, 54(3), 345-346.

Wood, D. L. & Nassau, K., 1968. The characterization of beryl and emerald by visible and infrared absorption spectroscopy. American Mineralogist, 53, 777-800.

Dissolved dislocations in gems: an overview

Martine Philippe [1], Emmanuel Fritsch[2]

[1]Retired gemologist, Paris, France, martine.philippe5@gmail.com
[2]Institut des Matériaux Jean Rouxel (IMN) & University of Nantes, Nantes, France, *emmanuel.fritsch@cnrs-imn.fr

Keyword: dislocation, dissolution, inclusion

Dislocations are crystallographic defects which are linear when simple, and correspond to defects usually induced during growth or deformation. The simplest variety is the edge dislocation (see figure 1). Other varieties exist and they can combine in rather complex patterns, such a loops or dislocation networks. At the atomic or molecular scale, they correspond to a very narrow volume (almost a line) of strain and atomic mismatch. This explains why they dissolve much faster than the rest of the crystal (as much as a thousand times faster). This means that a dissolved dislocation is found only in dissolved crystals. It creates a hollow volume, hair-like or needle-like, which follows and replaces the dislocation. It gets narrower as the dissolution progresses towards the inside of the crystal. Thus, these dissolved dislocations may on occasions be filled with supergene material (clays, iron oxides and so on). Although dislocations usually are not visible, they may on occasions be observed with classical gemological equipment, for example between crossed polarizers in CVD synthetic diamonds (Philippe & Fritsch, 2017a and b).

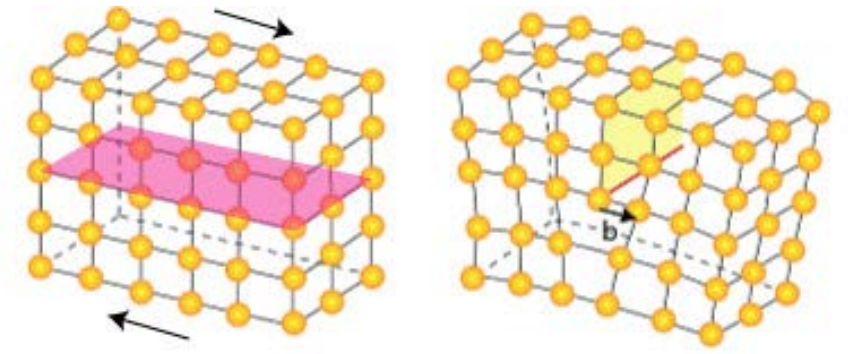

Figure 1 – Drawing of the atomic structure of a crystal submitted to strain (left, in pink), the shearing of this crystal along a plane induces an edge dislocation (right in pale yellow). The dislocation itself is the red line. from fr.wikipedia.org/wiki/Dislocation

Dissolved dislocations (dd) are often difficult to recognize as such, among inclusions, because they cover a wide variety of aspects, and they are by definition hollow. They often resemble, at least with the loupe, needle-like or hair-like inclusions, for which gemologists usually expect elongated crystal fibers.

Their occurrence is restricted of course to gem species which are essentially single crystals. They are relatively rare in corundum for example, but they are common in diamonds and danburite. They have been documented in a seemingly restricted number of gem species or families, about 20, including common ones, such as beryl, quartz, feldspars, garnets, spinel, topaz, and rarer ones, such as kyanite, spodumene, zoisite, scapolite, sinhalite, petalite and zircon (Philippe & Fritsch, 2017a and b; Gübelin & Koivula, 1986, 2005 and 2008). They have not been (yet) documented in fairly common gem species such as peridot, zoisite, cordierite, or chrysoberyl, and one may wonder why.

The presence of dissolved dislocations results from post-growth dissolution of the crystal. This affects of course the surface first, but leads to various patterns when it follows dislocations. It may reveal growth dislocations, starting at an inclusion for example, reversing the process that lead to the very existence of the gem.

They can be recognized because they necessarily reach the surface of the faceted gem, with a section narrowing as the dissolution progresses along the dislocation inside the stone (Figure 2).

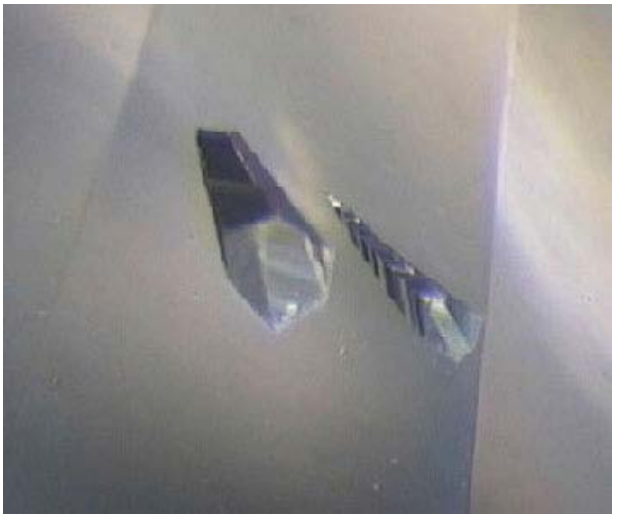

Figure 2: Typical dissolved dislocations in diamond, with a polygonal section, and a tapered shape pointing inside. Photo by Aurélien Delaunay (Field of view about 0.85 mm).

Their general shape and section is dictated by crystallography and the many events that can affect a dislocation: they could be straight, tubular or lath-like. They are often kinked or "bent", and may rarely appear as branches, loops or networks (most commonly in garnets figure 3). They have rarely been called "dissolved dislocations", although it has been demonstrated that it is what they are. In the gemological literature, they are often named "etch channels" or "corrosion tubes ". They are not to be confused with growth tubes or laser drill holes for example.

Because of their peculiar appearances, dissolved dislocations may be mistaken for needle-like crystals, fibers or even bacterial boreholes. It is possible that these features may become properly identified in a great many more gem species than now, once the identification criteria are better-known.

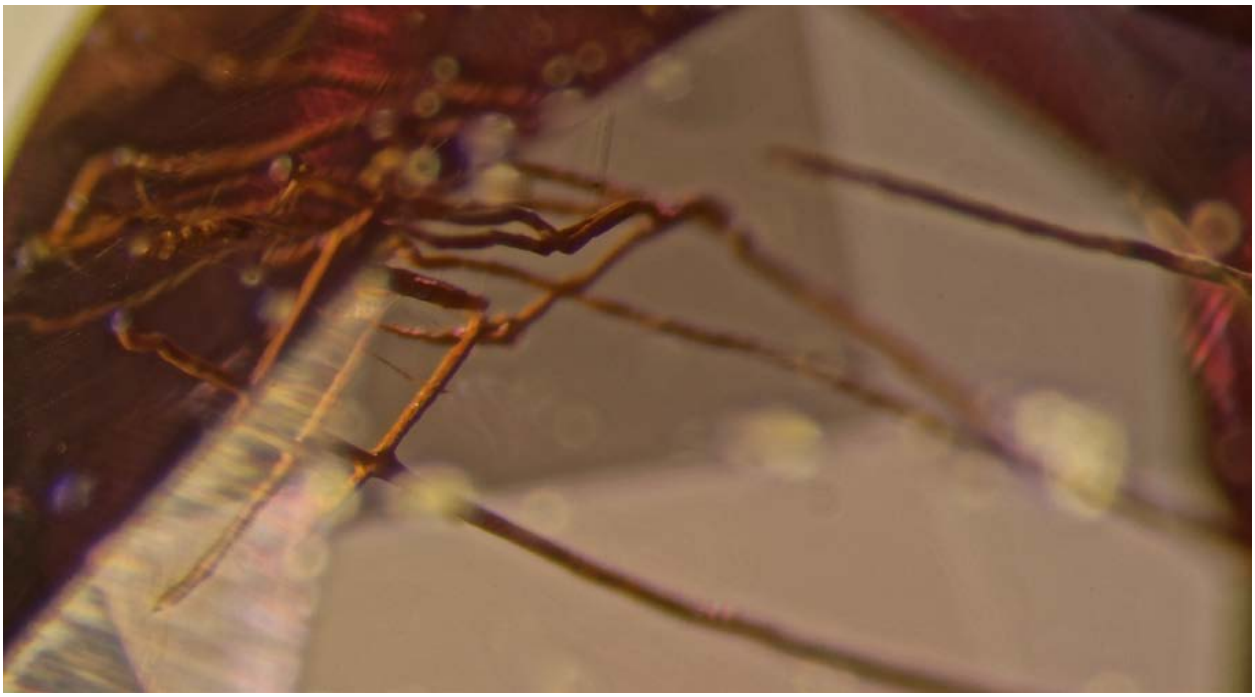

Figure 3: Branch- or root-like dissolved dislocations in a color-change garnet. Photo Martine Philippe (Field of view approx. 5 mm).

References

Gübelin E.J., Koivula J.I., 1986. Photoatlas of Inclusions in Gemstones. Volume 1 – ABC Edition, Switzerland – 532 pages

Gübelin E.J., Koivula J.I., 2005. Photoatlas of Inclusions in Gemstones. Volume 2 – Opinio Publishers, Switzerland – 829 pages

Gübelin E.J., Koivula J.I., 2008. Photoatlas of Inclusions in Gemstones. Volume 3 – Opinio Publishers, Switzerland – 672 pages

Philippe M., Fritsch E., 2017a. Dissolved dislocations: Inclusions that are not so easy to identify [in French]. Revue de Gemmologie a.f.g., 200, 11-22.

Philippe M., Fritsch E., 2017b. Dissolved dislocations : Inclusions that are not so easy to identify. Part II [in French]. Revue de Gemmologie a.f.g., 201, 12-16.

LFG
PARIS
Laboratoire Français
de Gemmologie

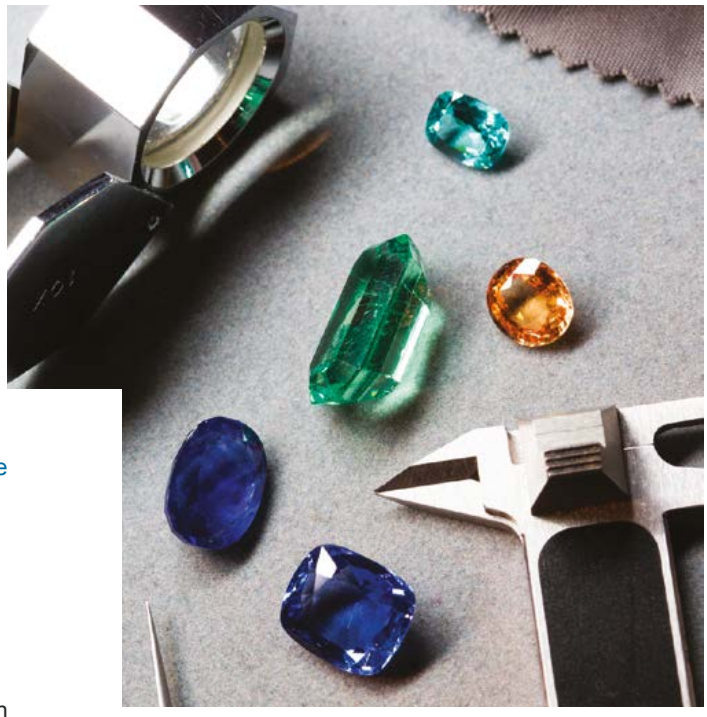

The Laboratoire Français de Gemmologie (LFG) is the oldest gemmological laboratory in the world, as it was founded in 1929 in Paris.
It became part of the French Jewellery Union in 2011. The LFG is a totally independant organism which provides expertise for the information and protection of the trade and its customers. It is the reference laboratory for High Jewellery houses of the Place Vendôme, and is active worldwide.

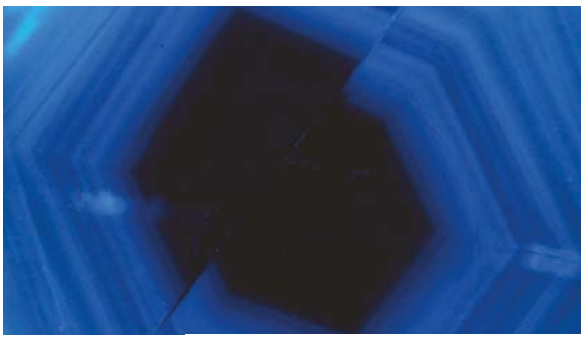

30, rue Notre Dame des Victoires - 75002 Paris - Tél. : 33 (0) 1 40 26 25 45 - Fax : 33 (0) 1 40 26 06 75
www.laboratoire-francais-gemmologie.fr

Création : Egga, 01 40 27 01 04

To support international events in their area,
the University of Nantes and the Bretagne Loire university
(grouping several universities in the West of France)
have joined forces with two territorial organizations,
the Pays de la Loire region (to which Nantes belongs)
and the Nantes metropolis (Nantes and 23 surrounding towns).
They share the sponsorship, each paying a portion
according to the nature, size, and location of the event.

UNIVERSITÉ DE NANTES

UNIVERSITE
BRETAGNE
LOIRE

Nantes
Métropole

Région
PAYS
de la
LOIRE

A REVIEW OF COMMERCIALLY AVAILABLE TURQUOISE IMITATIONS

Gagan Choudhary[1], Sandeep Vijay[1]

Gem Testing Laboratory, Jaipur, India
*gagan@gjepcindia.com

Keywords: turquoise, imitation, ceramic, composite

Turquoise, best known for its splendid blue colour, has been used for adornment since antiquity. Chemically a hydrous copper aluminium phosphate, it has a cryptocrystalline structure composed of fine, randomly oriented groups of triclinic crystals (Webster, 1994). This cryptocrystalline structure gives rise to the gem's porosity, making it susceptible to body oils, ordinary solvents, or even dirt, which can alter its colour. For decades, turquoise has been impregnated with wax, plastics, or polymers—a process known as stabilization, which enhances not only the material's durability but also its colour and surface lustre (e.g. Lind et al, 1983; Nassau, 1994). Another established treatment is the dyeing of pale-coloured turquoise to give it a rich blue colour (see, e.g., Kammerling, 1994). In addition to the above mentioned treated counterparts, due to increasing popularity of this gem material, we at the Gem Testing Laboratory, Jaipur have seen a significant rise in number and types of imitations being presented as turquoise in recent years, both rough and fashioned.

Figure 1: A composite image of greenish blue to bluish green natural turquoise (centre three specimens) with black veins (spider-web turquoise), dyed magnesite with brown and black veins (1-a), dyed chalcedony (1-b), dyed dolomite (1-c), dyed alunite (1-d), composite turquoise with metallic flakes along polymer veins (2-a), ceramic (turquoise/barite/gibbsite) without veins (2-b), ceramic (turquoise/barite/gibbsite) with black veins, imitating 'spider-web' turquoise (2-c) and an opaque glass (2-d).

The samples

Based on the type of samples received for identification since January 2017, turquoise imitations are broadly classified into two groups, as follows:

Group 1: Mainly consists of colour-treated (dyed) natural materials, such as turquoise, magnesite, howlite, alunite, chalcedony and dolomite.

Group 2: Comprises man-made materials, including composites made from turquoise and/or magnesite grains and chips, in various patterns, such as, with or without black/brown veins, with or without pyrite/marcasite, and with or without metallic (Zn/Cu) flakes/veins. Another common imitation-type in this group includes reconstructed or ceramic materials composed of mineral powder, especially of turquoise (often called 'synthetic' in trade), gibbsite or barite, pressed and bonded in a polymer, with a colouring agent; these ceramic-imitations are also available in various patterns, as described above for composite-imitations. Further to composite- and ceramic-imitations, translucent to opaque glass is also occasionally encountered.

In addition to the above mentioned two groups, some natural-coloured blue materials, such as ceruleite and chrysocolla have also been encountered, simulating turquoise. Due to their limited encounter, these materials are not being discussed here.

Identification and separation

Non-destructive spectroscopic methods of analyses, such as infrared, absorption or Raman, along with EDXRF analyses are the most useful tools to characterize and separate natural turquoise from treated counterparts or its imitations. However, textural observations under a microscope remain the most important tool, especially while determining presence of colour concentrations in natural dyed materials, or deep crevices with polymer veins or randomly oriented mineral grains in composites (e.g. Choudhary 2010), or fine granular texture with 'blue-dots', commonly referred to as 'cream-of-wheat' effect in synthetic turquoise (Rockwell, 2005). In routine, we use a combination of qualitative EDXRF analysis, Raman spectroscopy and microscopic observations to identify and separate various types of turquoise imitations, the key features of which are summarized in table 1.

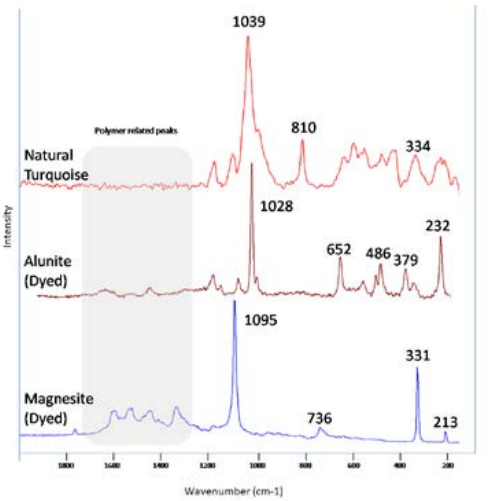

Figure 2: Raman spectroscopy has been useful tool for separation of natural turquoise from its simulants and imitations. Presented here are representative Raman spectra of natural turquoise, dyed alunite and dyed magnesite.

Table 1: Key features in commonly encountered turquoise imitations

Group	Material	Features		
		Microscopic observation	**Qualitative EDXRF analysis**	**Raman Spectroscopy**
Natural turquoise (including 'stabilized')		White clouds, various mineral inclusions, black/brown veins	Al, P, Fe, Cu, K (minor), Zn (in veined)	Peaks at ~ 215, 230, 335, 420, 480, 550, 595, 635, 810, 1040, 1105 and 1180 cm^{-1}
Group 1 Colour-treated (dyed) natural materials"	Turquoise	White clouds, various mineral inclusions, black/ brown veins, colour concentrations	As above	As above
	Magnesite		Mg, Ca, Fe	Peaks at ~ 215, 330, 737, 1095, 1764 cm^{-1}
	Howlite		Ca, Si, Fe	Peaks at ~ 255, 305, 370, 475, 550, 600, 675, 736, 860, 985, 1120, 1450, 1751 cm^{-1}
	Alunite		Al, Si, K, Ca	Peaks at ~ 230, 380, 480, 507, 555, 650, 1025, 1080, 1185 cm^{-1}
	Dolomite		Mg, Ca, Fe	Peaks at ~ 300, 720, 1098 and 1760 cm^{-1}
	Chalcedony	Banding, white clouds, colour concentrations (occasionally)	Si, Fe	Peaks at 205, 355, 395, 464, 502, 695 and 1160 cm^{-1}

Group 2 Man-made materials"	Composite (turquoise and/or magnesite grains)	Deep crevices with polymer (coloured / colourless) veins, randomly oriented mineral grains	As above given for turquoise and magnesite	As above given for turquoise and magnesite
	Ceramic1 (made from turquoise powder)	Smooth or fine-granular texture, 'cream-of-wheat' effect, dispersed dark blue spots, white clouds	Al, P, Ti, Fe, Cu	Majorly polymer-related features (turquoise peaks overwhelmed by polymer features). Additional peaks from dark blue spots at ~ 220, 447 and 607 cm^{-1}, corresponding to TiO_2 (rutile).
	Ceramic (made from barite powder)		Al, S, Cu, Ba	Peaks at ~ 455, 620, 985 and 1145 cm^{-1}.
	Ceramic (made from gibbsite powder)		Al, Fe, Ti	Peaks at ~ 240, 320, 380, 395, 540, 565, 620, 650 and 890 cm^{-1}
	In addition to the mineral-related peaks listed above, Raman spectra displayed additional peaks associated with polymer at ~ 1340, 1450, 1530, 1600, 1640 and 1720 cm^{-1}			
	Glass	Gas bubbles (often seen as hemispherical cavities on surface), flow lines, occasionally devitrification effect	Si, K, Ca, Cr, Fe, Cu, Zn, As	Broad features: ~ 360-630, 720-840, 970-1200 cm^{-1}

Note to table 1

1. This material is classified as 'ceramic' and not 'synthetic' because of the difference in chemistry (presence of Ti), compared to natural turquoise, while the Raman spectra of the dispersed 'blue dots' correspond to TiO_2 (rutile), acting as the colouring agent in these studied samples; synthetic turquoise is expected to be coloured by Cu^{2+}/Fe^{3+}, as natural turquoise.

Conclusions

Availability of wide range of imitations and simulants has created a lot of confusion within the turquoise trade, as most of the discussed materials cannot be identified and classified with classical gemmological testing. Since, most of the natural turquoise available in the marketplace is 'stabilized' using colourless or coloured polymers, gemmological characteristics such as RI and SG are not useful for their identification. However, a combination of observational features under a microscope, qualitative EDXRF analyses and Raman spectroscopy helps to identify and separate turquoise from its simulants and imitations.

References

Choudhary G., 2010. A new type of composite turquoise. Gems & Gemology, 46(2), 106-113

Kammerling R.C., 1994. Gem Trade Lab Notes: Turquoise, dyed and impregnated. Gems & Gemology, 30(2), 120–121

Lind T., Schmetzer K., Bank H., 1983. The identification of turquoise by infrared spectroscopy and x-ray powder diffraction. Gems & Gemology, 19

Nassau K., 1994. Gemstone Enhancement: History, Science and State of the Art, 2nd ed. Butterworth-Heinemann, Oxford, UK, 98pp

Rockwell K., 2005. Lab Notes: Synthetic turquoise necklace. Gems & Gemology, 41(3), 261-262

Webster R., 1994. Gems: Their Sources, Descriptions and Identification, 5th ed. Revised by P. Read, Butterworth-Heinemann, Oxford, UK, 254pp

A HISTORY OF GEM-QUALITY CUBIC ZIRCONIA

Claude Drouin.[1], Emmanuel Fritsch [2]
[1] Gemmologist, Cambridge, England
[2] Institut des Matériaux Jean Rouxel (IMN) & University of Nantes, Faculté des Sciences et des Techniques, 2, rue de la Houssinière, BP 32229 Nantes, cedex 3 France,
* claude.drouin@tiscali.co.uk

Keywords: cubic zirconia, history, skull melting, cold crucible.

As gem-quality cubic zirconia is today's most abundant (and possibly best) diamond imitation on the market, it is interesting to have an objective look at its history, and identify the many countries and individuals that led to today's product (Figure 1). In 1936, two German mineralogists described cubic zirconia crystals (ZrO_2) as inclusions in natural zircons. This discovery was never repeated, but cubic zirconia is since considered a synthetic material. Then up to 1969, many different teams of researchers around the world tried to grow big single crystals of good quality. They had to face two main problems: firstly, the very high fusion temperature required and secondly, the stabilization in the cubic system of the single crystals at room temperature.

Figure 1: Typical recent gem-quality, near-colourless cubic zirconia from a variety of manufacturers. Photo by C. Drouin & P. Phillips.

In the 1930's the high melting point of the zirconium dioxide was well-known and zirconia had already been stabilized to produce the high refractory ceramics for the furnace industry. The ceramics were typically 96% zirconia and 4% calcium oxide CaO. Phase diagrams have been established for many stabilizers including the ones relevant today to grow single gem- quality crystal, CaO and Y_2O_3.

UK: The Oxford cold crucible

In the early 1960s, the need for large, pure synthetic crystals for industrial use (not gem production) lead to various developments around the world. In England, the final stage of this efforts was an expensive, complicated and fragile 'Oxford Cold Crucible' engineered with ultimate modifications to improve the design (Smith, 1979)

France: the first large fully stabilized cubic zirconia crystals

In the 1960s, French teams worked to grow such crystals using a new technique: melting in a cold crucible or "skull" melting. For example, in 1964, Perez Y Jorba and Collongues in Paris investigated the fusion of refractory oxides without a crucible by high frequency heating (Perez Y Jorba et al., 1964). Roulin and his colleagues in Grenoble elabo-

rated a "self crucible", a cold crucible apparatus made of two split halves, assembled to make an electrically insulated chamber. The cubic zirconia crystals obtained must have had sizeable dimensions since they cut from it a parallelepiped 15 x 3.5 x 3.5 mm for further studies. (Roulin et al., 1969).

USSR: cubic zirconia becomes a gem (Fianite)

In the 1970s, they started to submit patents on "monocrystals based on stabilized zirconium or hafnium dioxide and method of production thereof" (Aleksandrov et al., 1979). The stabilizer used was yttria, yttrium oxide Y_2O_3. The crystals were named "Fianit" in honor of the
Lebedev Institute of Physics, 'Fizicheski Institut Akademii Nauk' (FIAN). The optical performance of the Russian crystals for laser use were 'disappointing' but 'in an ironic stroke of luck, one of the technicians cut and faceted a CZ crystal and a new diamond simulant was born (Wenckus, 1991). The size of the Russian apparatus became larger, up to 50 cm diameter, and several laboratories produced this crystal (Figure 2). Also, they started putting dopants in the crystals to obtain interesting colours.

Figure 2: Photo of early Russian equipment Kristall-401. Courtesy Dr. Mikhail Borik.

Switzerland and Djevalite

Switzerland was involved at the very beginning of the production of gem-quality calcium- stabilized cubic zirconia and in 1976 Kurt Nassau reports on two faceted stones studied. This material was bought in Europe under the name of 'Djevalite' and was then said to be produced by Djevahirdjian S.A,in Monthey, Switzerland by a flux technique (in fact cold crucible). This happened during the late 1970s and early 1980's.

USA gets in the chase

Following a conference in 1972 in Tsakhkador, USSR, Joseph "Joe" Wenckus got interested in skull melting and started a long friendship with a Russian investigator, Osiko. In 1977 he patents a cold crucible (Wenckus et al., 1977; Figure 3), which evolved into a 125 litres reactor. After many tweaks and improvements, in 1998, Ceres Corporation in the US produced around 20 tons monthly of single cubic zirconia crystal in 110 cm diameter crucible holding a charge of 2.5-3.5 tons. 98% is used as diamond simulant (Lomonova & Osiko, 2003).

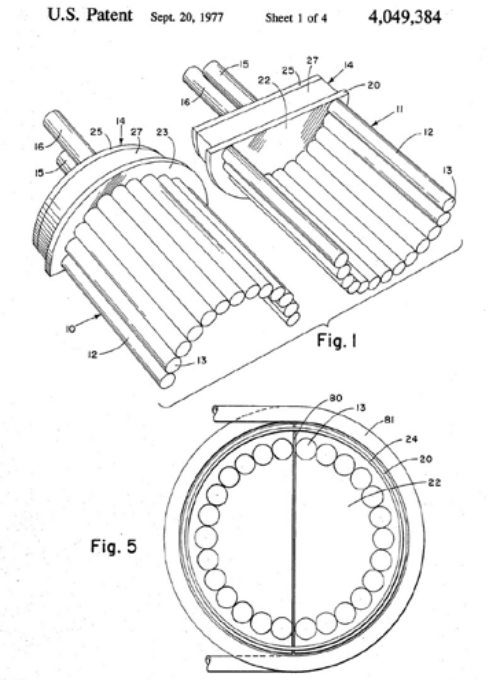

Figure 3: Illustration extracted from Wenckus et al. (1977) showing the principle of the American cold crucible.

China & India: mass production of CZ

China was not a pioneer for the synthesis cubic zirconia. However in 2009, it was estimated that half of the world production of 4,500 tons was produced in China (Xu et al., 2009). Chinese did research on the process and very practical papers were published with obvious economical interest in mind; low cost and high yield. India got in the game apparently recently, is considered the second world producer, behind China and ahead of Russia, with reportedly high quality gems.

References

Alexandrov V.I., Osiko V.V., Tatarinsev V.M., Udovenchik V.T.,1979. Monocrystals based on stabilized zirconium or hafnium dioxide and method of production thereof, United States Patent 4,153,469, issued 8 May 1979.

Lomonova E.E. & Osiko V.V., 2003. Growth of zirconia crystals by the skull melting technique, in Crystal Growth Technology, Scheel H.J. & Fukuda T. editors, John Wiley & sons, Chichester, England. 461-485

Nassau K., 1976. A New Diamond Imitation: Cubic Zirconia, Gems & Gemology, 15-5, 143-144.

Perez Y Jorba M., Collongues R., 1964. Sur le chauffage et la fusion sans creuset par induction haute fréquence de quelques oxydes réfractaires, Revue Internationale des Hautes Températures et des Réfractaires, 1, 21-25.

Roulin Y, Vitter G., Déportes C., 1969. Nouveau dispositif de fusion en autocreuset. Fusion d'oxydes réfractaires dans une enceinte multitubulaire, Revue Internationale des Hautes Températures et des Réfractaires, 6, 153-157.

Smith B.A., 1979. Some aspects of the design and construction of the cold crucible, Materials Research Bulletin, 14, 431-439.

Wenckus J.F., Nenashi W.P., Catonguay A., 1977. Cold crucible system, United States Patent 4,049,384 issued 20 September 1977.

Wenckus J.F., 1991. Cubic Zirconia: The Great Impostor, Proceedings of the International Gemological Symposium, Keller A.S., editor, Gemological Institute of America, Santa Monica, 88-89.

Xu J., Lei X., Jiang X., He Q., Fang Y., Zhang D., He X., 2009. Industrial growth of yttria-stabilized cubic zirconia crystals by skull melting process, Journal of Rare Earths, 27-6, 971-974.

GEMMOLOGICAL APPLICATIONS OF ARDUINO

K.E. Fox[1], K.R. Fox[2]

[1] Earth Sciences Museum, University of Waterloo, Waterloo, Canada; kefox.ca@gmail.com
[2] Peterborough, Canada; kfox17@cogeco.ca

Keywords: specific gravity, Arduino, strain gauge, load cell, Neopixel, dark-field, illuminator

Introduction

Over the past 15 years a strengthening "Maker Movement" has spurred development of an ecosystem of open-source hardware and code such as that offered by the Arduino company and others, along with a wealth of web-shared designs and libraries that enable the creation of technology enabled DIY (do-it-yourself) projects. Popular for grown-up toy-making, these resources also have practical applications. For example, the authors have used readily available components and online guidance as the backbone for construction of a microscope dark-field illuminator and specific gravity (SG) systems for gemmological work.

Microscope illuminator

An Adafruit NeoPixel RGBW (red-green-blue-white) LED ring (Adafruit, 2019a) has been interfaced with an Adafruit Pro Trinket microcontroller board (Adafruit, 2019b) similar to the Arduino Uno to retrofit thermally cool illumination to a vintage Bausch and Lomb StereoZoom microscope (Figure 1). Although not intended to compete with modern gemmological microscopes, the system is cost-effective and provides the option of coloured LED illumination to replace coloured filters for enhancing visibility of colour banding in gems (Hughes, 1988). Of seven yellow sapphires inspected to-date against a light background using blue illumination, six showed the curved banding of Verneuil synthetics, and one natural stone displayed straight banding. Once the banding has been identified and oriented in blue light, photos can be converted to black and white and contrast-enhanced to accentuate the effect (Figure 2).

Figure 1. Dark-field illuminator with exposed NeoPixel ring. The light diffuser shown to the left foreground of the image fits over the LED ring. K.E. Fox photo.

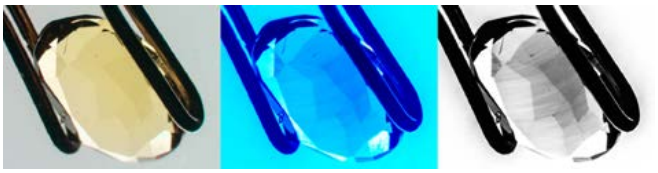

Figure 2. The banding in this yellow Vernueuil sapphire becomes visible in blue light and can be accentuated in a post-processed B&W image. Immersed in water. K.E. Fox photo.

Specific gravity measurement – instrumentation

An Arduino-based specific gravity measurement system is a useful aid for the identification of objects seen at gem & mineral shows, including jade, gem rough and carvings, all of which may be heavier than the average faceted gemstone. Hydrostatic weighing is a time-proven method for SG determination (Webster, 1983), but can be simplified by suspending the unknown directly from a digital weighing sensor.

In the current work, two SG measurement systems have been constructed using strain gauge load cell sensors designed for weights up to 100 g, and up to 5 kg. A load cell (orange in Figure 3) incorporates four small strain gauges (red in Figure 3), which are very thin metal conductors deposited on plastic film substrates which are glued to four points on the surface of a specially designed metal bar and wired in Wheatstone bridge configuration (Sparkfun, 2019). When correctly mounted as in Figure 3, a suspended weight causes deformation of the bar with compression of two diametrically opposed strain gauges and tension on the other two. This produces resistance changes which are used to generate a voltage difference between the two arms of the bridge, thus providing a highly sensitive measure of weight.

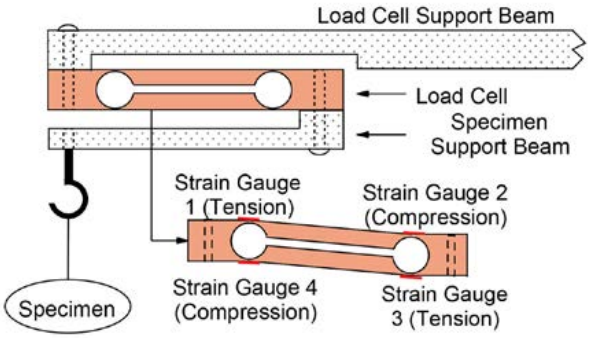

Figure 3. Mounting configuration for the load cell. An exaggerated view of the distortion under load is shown toward the lower right. K.R. Fox diagram.

Key components of the system are shown in the block diagram in Figure 4. The apparatus for the lower weight range is based on the TAL221 100 g mini load cell produced by HT Sensor Technology Ltd and marketed by various resellers, including Sparkfun in the US for ~US$9. It is interfaced to Sparkfun's Load Cell Amplifier-HX711 (~US$10). An open-source Arduino Uno microcontroller board allows output from the load cell to be manipulated and displayed on an LCD (liquid crystal display) or sent to a computer via USB cable. Pushbuttons activate routines that zero the reading, save the specimen's weight in air and weight in water, and calculate the specific gravity. The 100 g system is depicted in Figure 5.

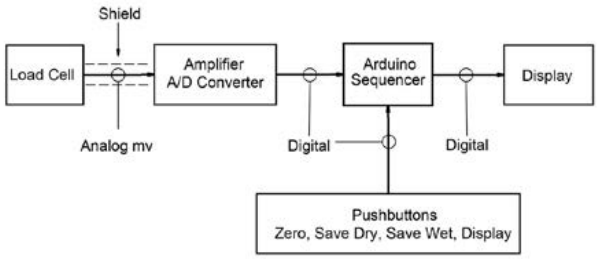

Figure 4. Block diagram of the specific gravity measurement system. K.R. Fox diagram.

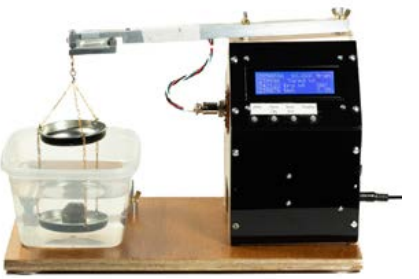

Figure 5. Hundred-gram SG system. K.E.Fox photo.

Specific gravity – results and discussion

Continuous data acquisition during operation allows quantification of noise and baseline drift, and inspection of signals during measurement. The residual voltage produced by the unloaded load cell can be "zeroed-out" using the reading taken when the tare button is pushed. The tared signal values for the 100 g load cell range from ~1,189,000 for a 90 g weight down to ~620 for a 50 mg weight. Peak-to-peak random noise is ~300, and introduces uncertainty into both the tared zero and the measured weights. Additional slow drift can cause excursions up to 1000 over a couple of hours, but less than 100 over the period of an SG measurement. The calibration plot shows excellent linearity from 90 g to 50 mg. Table 1 gives the results of repeat measurements of specific gravity for several specimens. Performance over most of the load cell range is very good, and although reproducibility for the 2 g topaz specimen is clearly degraded over even the 5 g quartz, the average SG is still within the expected range and thus potentially useful for the identification of unknowns.

Table 1. Specific gravity reproducibility

Material	Weight (g)	# Repeats	SG Average	SG Stddev	Expected SG
Faceted Topaz	2.17	10	3.559	0.077	3.53 - 3.56[1]
Faceted Quartz	4.68	10	2.655	0.013	2.65[1]
Moonstone cab	16.14	10	2.594	0.005	2.56 - 2.59[1]
Calcite rhomb	18.36	10	2.715	0.005	2.71[1]
Rosin chunk	20.24	10	1.090	0.000	1.06-1.08[2]
Unknown cobble	44.72	10	2.625	0.005	?
Bismuth plug	57.14	11	9.790	0.014	9.79[2]

[1]Webster, 1983; [2]Glover, 2002.

Conclusions

Arduino-based solutions for illumination and SG measurement have proven their value for gem identification at gem & mineral shows. Opportunities exist for further optimization of illumination conditions for viewing growth banding, and SG systems could be refined with improved signal processing and the addition of electrical shielding. Combined with 3D printing of mechanical components to reduce dependence on the home machine shop, the DIY "Maker" ecosystem offers new opportunities for addressing gemmological needs.

References

Adafruit, 2019a. Adafruit NeoPixel überguide. Available from https://www.adafruit.com/product/2863, [Accessed Apr 2, 2019].

Adafruit, 2019b. Introducing Pro Trinket. Available from https://learn.adafruit.com/introducing-pro-trinket, [Accessed Apr 2, 2019].

Glover, T.J., 2002. Pocket ref, 2nd ed. Sequoia Publishing Inc, CO, pp. 428 & 435.

Sparkfun, 2019. Load cell amplifier HX711 breakout hookup guide. Available from https://learn.sparkfun.com/tutorials/load-cell-amplifier-hx711-breakout-hookup-guide, [Accessed Apr 2, 2019].

Hughes, R.W., 1988. Identifying yellow sapphires – two important techniques. Journal of Gemmology, 21(1), 23-25.

Webster, R., 1983. Gems, their sources, descriptions and identification, 4th ed. Butterworth & Co Ltd, London, pp. 650 – 656.

OPTICAL PROPERTIES OF HACKMANITE AND SODALITE

Seung Kwon Lee [1]*, Randy Luo [2]

[1] Wooshin Gemological Institute of Korea, 06022, Seoul, South Korea
[2] China National Jewellry Quality Supervision and Inspection Center, Beijing city, China
* sklee1201@hanyang.ac.kr

Keywords: Sodalite, Hackmanite, Tenebrescence, Photochromism

The sodalite-group minerals ($M_8T_{12}O_{24}X_2$) are an important rock-forming mineral group in which M is a metal ion (typically Na, Ca, Mn or Zn), T is an element in tetrahedral coordination in such way that cubo-octahedral cages are formed, where each atom of Al or Si is located at the center of a tetrahedral cage of oxygens. X is an anion such as Cl^- or S^{2-}. In each cage there is a X ion tetrahedrally coordinated by M ions forming a body-centered cubic structure (Finch et al., 2016). Hackmanite is an important variety of sodalite exhibiting tenebrescence. It is the geological word for photochromism, which is the reversible light-
induced color change of minerals. Since the work of Kirk in 1955, the nature of the impurity activating the photochromism of sodalite has been ascribed to S-based species, but the exact nature of the impurity (S^{2-}, S_2^{2-}, SO_4^{2-}, etc.) is still a source of debate. However, S_2^{2-} ion is the one the most frequently assumed.

Eight rough samples of hackmanites and sodalites (see Fig. 1) were studied using Raman scattering, Photoluminescence (PL), Energy-Dispersive X-ray Fluorescence (EDXRF), Fourier-transform infrared (FTIR) and UV-Visible absorption spectroscopies. Exposure to short-wave UV for several minutes visibly changed the color of 6 of the 8 stones. All samples have sulfur ions (see Fig. 3 and its caption) and similar chemical compositions detected by EDXRF. Also, Raman spectra (see Fig. 2) of all the samples are indistinguishable from the spectrum of sodalite.

Figure 1. 6 hackmanites and two blue sodalities used for this study. SH5 and SH8 samples have no tenebrescence.

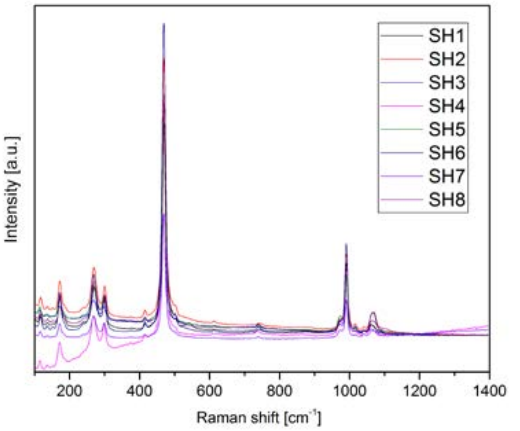

Figure 2. Raman spectra of 8 samples

The present study examines the light emitted by a suite of sodalite-group minerals in response to excitation at 405 nm. The origin of the emission bands observed in these samples might be attributed S_2^- (646 nm) ions in the cage (Finch et al., 2016). We compare each sample's luminescence as a function of sulfur atoms concentration (see Fig. 3). Fluorescence and tenebrescence in natural sodalites might appear by S but charge transfer between [S_2^-, V_{cl}^-] and [S_2^-, V_{cl}] occurs a geometrical relaxation of the system, leading to a large reorganization of the electronic states (Curutchet et al., 2017).

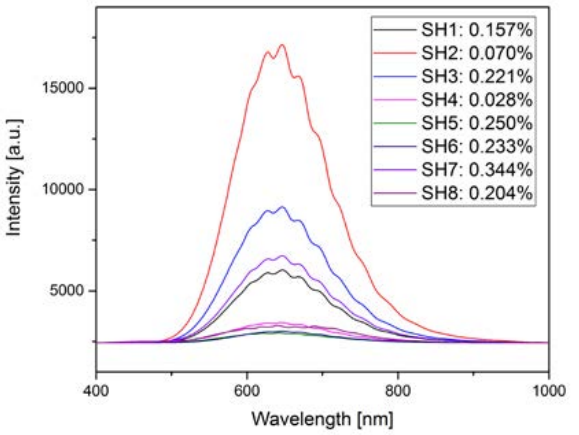

Figure 3. Each sample's PL spectra and sulfur concentration [SO_3 %] by EDXRF.

The blue sodalites, SH5 and SH8 samples, only show the fluorescence in spite of the similar chemical compositions of hackmanites in this study. The sodalites might have intrinsic and/or extrinsic quenchers so as to disperse energy in excited states. Further studies on various sodalite and hackmanite may identify the origin of non-radiative relaxation.

References

Curutchet A. and Le Bahers T., 2017. Modeling the Photochromism of S-Doped Sodalites Using DFT, TD-DFT, and SAC-CI Methods. Inorg. Chem., 56 (1), 414–423

Finch A., Friis H. and Maghrabi M., 2016. Defects in sodalite-group minerals determined from X-ray-induced luminescence. Physics and Chemistry of Minerals, 43(7), 481-491

Kirk R.D., 1955. The luminescence and tenebrescence of natural and synthetic sodalite. American Mineralogist, 40(22), 22–31.

PROVENANCE OF EMERALD FROM PRINCE LIANGZHUANG'S TOMB IN MING DYNASTY, HUBEI, CHINA

Zemin Luo[1*], Mingxing Yang [1], Qin Fang [2], Ren Lu [1], Luwu Cai [2], Yang Hu [1]

[1] Gemmological Institute, China University of Geosciences, China
[2] Hubei Province Museum, China
*hellenzemin@gmail.com

Keywords: Prince Liangzhuang's tomb, Emerald, Provenance, Egypt, Austria

Abstract: More than 18 species and 700 pieces of colored gemstones were unearthed from Prince Liangzhuang's tomb (1411-1441A.D.) in Hubei province, China in 2001 (Yang et al., 2004). Among these gemstones, 50 samples were identified as emerald. Emerald's popular deposits have dramatic change in history, divided by the age of exploration. The current well-known emerald origins, such as Colombia, Afghanistan, as well as Brazil, were all found in and after 16th century (Giuliani et al., 2000; Groat et al., 2008). The famous emerald deposits before 16th century over the world were known as Egypt, Austria and Pakistan (Giuliani et al., 2000; Groat et a l., 2008), as shown in Table 1. This raised an interesting question that where and how the prince Liangzhuang's emerald stones come from.

Table1 The countries and corresponding mines produced Emerald before and in 16th century

Emeriald origins	Main mines and mining time	Reference
Egypt	Cleopatra mine, ~1500 B.C. Wadi Sikait, 1th B.C.~6th A.D.	Giuliani et al., 2000 ; Groat et a l., 2008
Austria	Habachtal, Romans or even the Celts	Giuliani et al., 2000 ;Groat et al., 2008
Pakistan	Swat-Mingora, Gallo-Roman era	Giuliani et al., 2000
Colombian	Chivor(1545 A.D.),Muzo(1594 A.D.)	Giuliani et al., 2000

As most of the emerald unearthed in Prince Liangzhuang's tomb have been mounted on noble metal, only one emerald sample (No.5.26732) was un-mounted. Therefore, gemmological tests was thoroughly performed on this un-mounted emerald sample, including micro-inclusions observation, optical absorption spectra and mineral phase identification by using UV-Vis spectra, Infrared spectra and Raman spectra. Fig 1 exhibits the appearance of the emerald sample. UV-visible absorption spectrum is shown in Fig 2. We found the typical Cr-related fluorescence peak centred at 684 nm. The broad absorption peaks centred around 610 nm and 430 nm were usually attributed to Cr^{3+} selective absorption.

To analyse its possible provenance, we detected the chemical components of the emerald sample by Laser ablation plasma mass spectrometer (LA-ICPMS). Comparing the trace elements contents and distribution with the published data of emerald from Egypt, Austria and Pakistan (Abdalla and Mohamed, 1999; Calligaro et al., 2000; Groat et al., 2008) (Table 2), we found that the emerald from Liangzhuang's tomb has quite similarity with that from Egypt or Austria. For instance, the contents of Cr, Zn, Ga, Rb, Cs and Li in Liangzhuang's emerald are more closed to those in Austria or Egypt, while emeralds from Pakistan show much higher concentrations of Cr and V. We inferred that the origin of the non-mounted emerald from Prince Liangzhuang's tomb probably came from Egypt or Austria, or some

other locality which has been forgotten in time. The emerald gem trade between east and west may have already existed before the age of exploration and the Maritime Silk Road explored by Zhenghe(15th century).

Fig 1 Emerald sample unearthed from Prince Liang Zhuang's Tomb, Ming Dynasty, Hubei, China. (a)Front figure ;(b)Back figure;(c)Top figure;(d)Bottom figure.

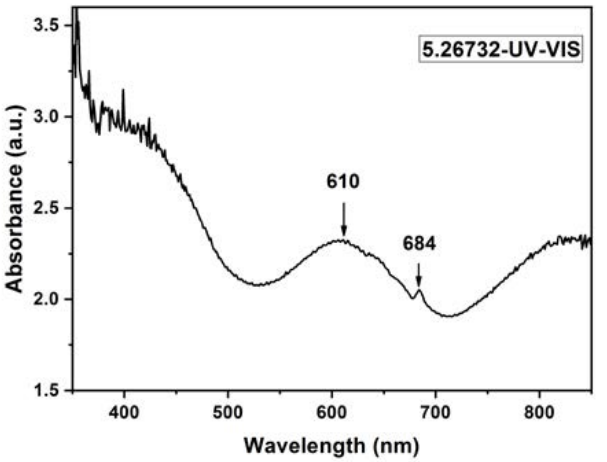

Fig 2 UV-visible absorption spectra of emerald from Prince Liang Zhuang's tomb

Table 2 The elemental content (weight ppm) for reference and Liangzhuang's emerald

Elements	Liangzhuang's	Egypt	Austria	Pakistan
Cr	975(625)	2600(1820) [a] 872(246) [b]	1390(720) [a] 821 b	5930(1930) [a] 3700(1294) [b]
V	71(7)	330(60) [a] -- b	170(100) [a] -- b	320(250) [a] 255(105) [b]
Zn	21(3)	18(10) [a]	14(6) a	4(1) [a]
Ga	16(1)	9(1) [a]	11(4) [a]	5(2) [a]
Rb	46(6)	24(12) [a]	18(13) [a]	6(3) [a]
Cs	397(33)	160(90) [a]	370(390) [a]	120(80) [a]
Li	160(23)	110(20) [a]	190(210) [a]	350(130) [a]

Standard deviations are given in parenthesis. [a] refers to Table 1 in Calligaro et al., 2000; [b] was calculated based on Table 1 in Groat et al., 2008 not considering 121-123 which showed much different contents of Cr, V, and Fe from other samples; -- means lower than the detection limit.

References

Abdalla H.M., Mohamed F. H., 1999. Mineralogical and geochemical investigation of emerald and beryl mineralisation, Pan-African Belt of Egypt: genetic and exploration aspects, Journal of African Earth Sciences, 28 (3), 581-598.
Calligaro T., Dran J.-C., Poirot J.-P., Querr G., Salomon J., Zwaan J.C., 2000. PIXE/PIGE characterisation of emeralds using an external micro-beam. Nuclear Instruments & Methods in Physics Research, 161–163(3), 769-774.
Giuliani G., Chaussidon M., Schubnel H-J., Piat D.H., Rollion-Bard C., France-Lanord C., Giard D., Narvaez D., Rondeau B., 2000. Oxygen Isotopes and Emerald Trade Routes Since Antiquity. Science, 287, 631-633.
Groat L.A., Giuliani G., Marshall D.D., Turner D., 2008. Emerald deposits and occurrences: A review. Ore Geology Reviews. 34(1), 87-112.
Gubelin E.J., 1982. Gemstones of Pakistan: emerald, ruby and spinel. Gems & Gemology, 18(3), 123-139,
Yang M.X., Di J.R., Fan L.W., Zhou Y., Liang Z., Li L., Zhu H., 2004. Characters of Gemstones from Liangzhuang King 's Tomb in Ming Dynasty in Zhongxiang, Hubei Province. Journal of Gems and Gemology. 6(3), 22-24.

Acknowledgements

This paper is CJHI contribution CJHIWZ-2019005. The authors acknowledge the financial support of a Grant (CJHIXM-201823) from Center for Jewelry Heritage and Innovation, a Hubei Provincial Key Research Base for Humanity and Social Sciences.

Characteristics of Tairus Synthetic Hydrothermal Ruby and Blue Sapphire

Nalin Narudeesombat [1], Namrawee Susawee[1], Pimtida Bupparenoo [1], Apitchaya Buathong[1], Supparat Promwongnan[1] and Thanong Leelawatanasuk[1]

[1] The Gem and Jewelry Institute of Thailand (Public Organization), ITF-Tower Building, Silom Road, Suriyawong, Bangrak, Bangkok, 10500 Thailand
* lthanong@git.or.th

Keywords: hydrothermal, ruby, sapphire, gemstone

Introduction

Gem quality synthetic corundum has been circulated in the gem market for almost a century and there are various techniques to grow the high quality crystal, such as flame fusion process (aka Verneuil), crystal pulling (aka Czochralski), flux growth and hydrothermal techniques. Hydrothermal synthetic ruby and sapphire, in particular, have been reportedly commercialized for a decade but this type of synthetic is still rarely seen in gem market. In this study, a suite of 8 hydrothermal synthetic rubies and blue sapphires from Tairus were studied and their characteristic are reported in this article.

Figure 1: Eight synthetic hydrothermal rubies and blue sapphires ranging in weight from 0.48 to 3.04 cts. (Photo by A. Buathong)

Material and Methods

The facetted samples used in this study weight from 0.48 to 3.04 cts.(see figure 1) Basic gem instruments were used for the measurement of the stone's properties. Internal features were observed with both standard gem microscope and immersion scope in methylene iodide solution. Their internal and extermal features were examined and recorded by a gem microscope with Canon EOS 7D camera attached. In addition, fluorescence images were taken by using a DiamondView™ instrument.

The chemical compositions were analyzed by an Energy-dispersive X-ray Fluorescence (EDXRF) spectroscopy of Eagle III system. The IR spectra in the Mid-IR range (4000-500 cm-1) were obtained by using a Thermo Nicolet 6700 Fourier-transform infrared (FTIR) spectrometer at the resolution of 4.0 cm-1 and 128 scans. UV-Vis-NIR absorption spectra were measured in the range of 300 – 800 nm by a UV-Vis-NIR spectrophotometer (Model Lambda 950 series, Perkin Elmer).

Gemological Properties

The basic gemmological properties of synthetic hydrothermal ruby and blue sapphire used in this study fall in normal ranges of corundum RI: 1.770-1.762, SG: 3.94-4.02, LWUV: inert to strong red, SWUV: moderate-red to moderate chalky green.

Microscopic Features

Under a gem microscope, these stones showed many diagnostic internal features of hydrothermal synthetic origin, namely, zig-zag (chevron) growth pattern, minute particles, seed plate and breadcrumb-like inclusions (Figure 2). Zig-zag or irregular growth line (Figure 3) and seed plate (Figure 3b) were also clearly seen under an immersion microscope with cross-polarized light.

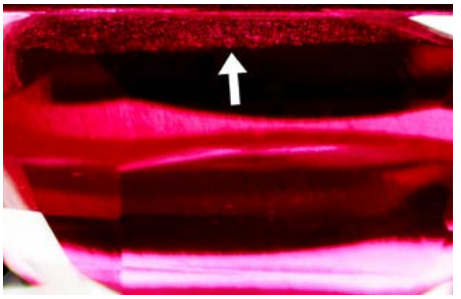

(a) breadcrumb-like inclusions along seed plate (SR3-FoV 1.25 mm)

(b) zone of breadcrumb-like inclusions (SR4-FoV 0.63 mm)

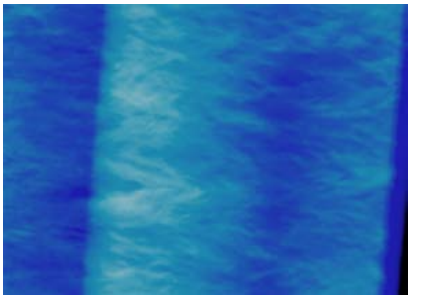

(c) zig-zag growth pattern viewing from the crown facet (SB1-FoV 0.75 mm)

Figure 2: The microscope features of the synthetic ruby and blue sapphire specimens. Dark Field (Photos by P. Bupparenoo)

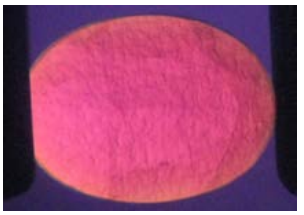

(a) zig-zag growth pattern (SR1-FoV 5.7 mm)

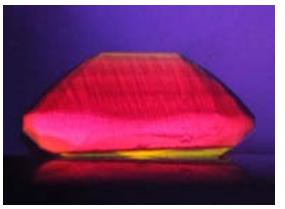

(b) seed plate and zig-zag growth pattern (SR3-FoV 7.1 mm)

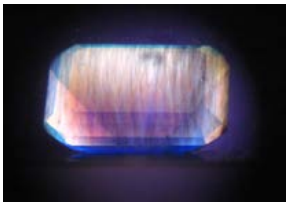

(c) irregular growth pattern (SB1-FoV 10.6 mm)

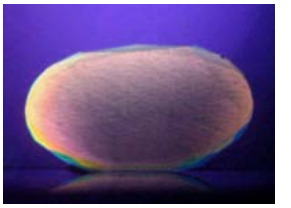

(d) zig-zag growth pattern (SB3-FoV 8.3 mm)

Figure 3: Internal features of the synthetic ruby and synthetic blue sapphire specimens under immersion (Photos by N. Susawee)

Luminescence images

Luminescence images under DiamondViewTM (Figure 4) with high intensity shortwave UV radiation powered at 50% showed strong red to chalky red fluorescence of zig-zag (chevron) pattern, breadcrumbs and minute particles in all ruby samples. All synthetic blue sapphire samples also displayed strong blue to chalky blue fluorescence of zig-zag (chevron) pattern, minute particles and seed plate.

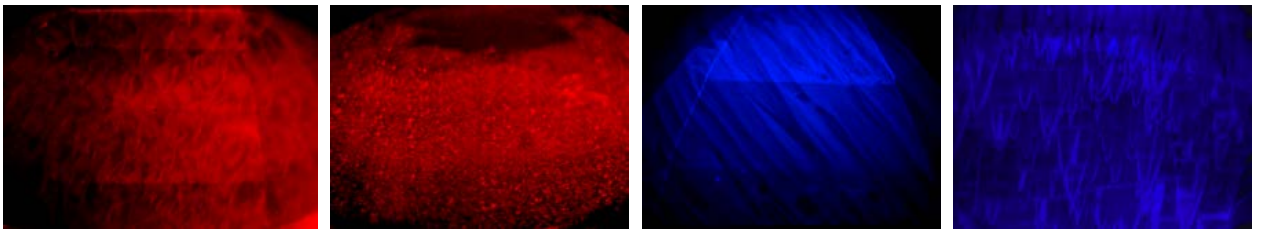

(a) zig-zag growth pattern (SR3-FoV 3.6 mm) *(b) minute particles (SR2-FoV 4.0 mm)* *(c) zig-zag growth pattern (SB1-FoV 4.5 mm)* *(d) zig-zag growth pattern (SB4-FoV 3.6 mm)*

Figure 4: The luminescence images of the synthetic ruby and synthetic blue sapphire specimens. (Photos by A. Buathong)

Spectroscopic Features

The mid-IR spectra of the synthetic ruby samples displayed several characteristic absorption peaks at 3562, 3482, 3380, 3304, 3231 and 3000 wavenumber (cm-1) (Figure 5 left). For the spectra of synthetic blue sapphire samples, several absorption peaks were also found at 3563, 3530, 3483, 3310, 3232 and 3184 wavenumber (cm-1) (Figure 5 right). All those peaks indicated the water band (OH-related absorption peaks) of hydrothermal synthetic corundum (Bidny et al., 2010)

UV/Vis/NIR spectra of synthetic ruby revealed two broad absorption bands of chromium (Cr3+) at center around 400 and 550 nm for both o- & e-rays (Figure 6 left). These absorption patterns are in good agreement with the rather high chromium contents of these ruby samples (0.58-0.84 wt.% Cr2O3, see Table 2). The spectra of the synthetic blue sapphire samples (Figure 6 right) revealed broad absorption peaked at around 550 nm for the o-ray and at around 700 nm for the e-ray due to Fe/Ti IVCT without any peaks related Fe3+ (450, 377/387 nm). Small humps at 400 may relate to the presence of small amounts of vanadium in those samples (~0.01 wt.% V2O5, see Table 2). Furthermore, both synthetic ruby and sapphire showed total absorption cut-off wavelength at around 300 nm. (Figure 6). In comparison, these UV-Vis spectra are similar to those of synthetic ruby and sapphire growth by other technique.

FTIR spectroscopy

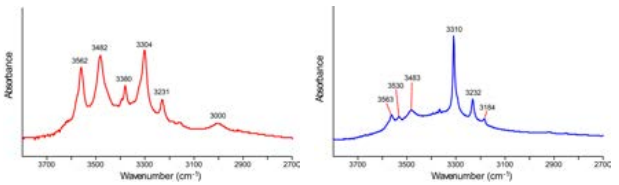

Figure 5: Infrared absorption spectra of sample SR1 (left) and sample SB1 (right). The curves have been corrected for a spurious absorption attributed to CO2.

UV-VIS spectroscopy

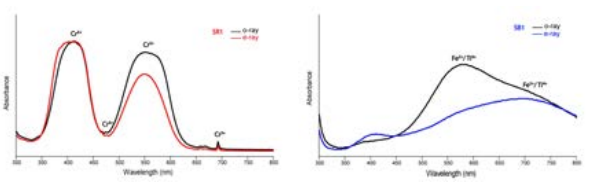

Figure 6: A representative polarized UV-Vis-NIR absorption spectrum of synthetic ruby (sample SR1) (left) and synthetic blue sapphire (sample SB1) (right).

Chemical characteristic

Chemical compositions of the eight samples analyzed by EDXRF revealed low to below detection limit of Ga contents of both synthetic hydrothermal ruby and blue sapphire samples (Tables 2). Furthermore, trace amount of copper almost always detected on the exposed seed plate of synthetic ruby samples. However, the presence of Cu has been previously reported as inclusion in Tairus synthetic sapphires (Thomas et al., 1997).

Table 2: Chemical composition of synthetic hydrothermal ruby and synthetic hydrothermal blue sapphire samples by EDXRF analysis.

Element oxides	Concentration Range (wt.%)										
	synthetic hydrothermal ruby							synthetic hydrothermal blue sapphire			
	SR1	SR2		SR3		SR4		SB1	SB2	SB3	SB4
Area	Body	Body	Seed plate	Body	Seed plate	Body	Seed plate	Body	Body	Body	Body
Al_2O_3	99.38	99.26	99.90	99.10	99.79	99.28	99.89	99.84	99.91	99.83	99.84
TiO_2	0.01	0.01	0.01	0.01	bdl	0.01	0.01	0.05	0.02	0.06	0.04
V_2O_5	bdl	bdl	bdl	bdl	bdl	bdl	bdl	0.01	0.01	0.01	bdl
Cr_2O_5	0.58	0.72	0.01	0.84	bdl	0.69	bdl	bdl	bdl	bdl	bdl
Fe_2O_3	0.02	0.01	0.02	0.04	0.17	0.01	0.02	0.07	0.06	0.08	0.09
Ga_2O_3	bdl	0.01	0.01	0.01	bdl	bdl	0.01	bdl	bdl	bdl	bdl
CuO	-	-	0.05	-	0.03	-	0.08	-	-	-	-

bdl = below detection limit

Discussion and Conclusions

Synthetic Ruby and blue sapphire grown by hydrothermal process sharing many internal features similar to those of other hydrothermal synthetic gemstone, such as chevron (zig-zag) growth pattern, zones of breadcrumb-like inclusions etc. Besides, their internal characteristics, the luminescence image induced by DiamondView also shown the prominent inhomogenity of the growth features. The Mid-IR spectra also revealed distinct series of OH-related absorption peaks that unique for this type of synthetic process. Very low to below-detection-limits of gallium contents also give a clue for synthetic origin of these corundum. In conclusion, the collected data from this study are clearly indicate the hydrothermal growth condition of these synthetic corundum. Furthermore, their spectroscopic data are consistent with result reported in previous studies of similar material (Thomas et al., 1997).

References

Bidny, S.A., Dolgova, S.O., Baksheev, A.I., and Ekimenkova, A., 2010. New data for distinguishing between hydrothermal synthetic, flux synthetic and natural corundum. The Journal of Gemmology, 32(1-4), 11-13

Sun, Z., and DeGhionno, D., 2014. Flux-Grown Synthetic Ruby with Hydrothermal Synthetic Seed Crystal, Available from https://www.gia.edu/gems-gemology/summer-2014-labnotes-flux-grown-synthetic-ruby.

Saeseaw, S., Pardieu, V., Weeramonkhonlert, V., Sangsawong, S., and Muya,l J., 2015. An analysis of synthetic ruby overgrowth on corundum, Available from http://www.giathai.net/wp-content/uploads/2015/06/Synthetic-ruby-overgrowth-on-natural-corundum-Thai-v2.pdf

Thomas, G.V., Mashkovtsev, I.R., Smirnov, Z.S., and Maltsev, S.V., 1997. Tairus Hydrothermal Synthetic Sapphires Doped with Nickel and Chromium, Available from https://www.gia.edu/doc/Tairus-Hydrothermal-Synthetic-Sapphires-Doped-with-Nickel-and-Chromium.pdf

Amber from Khamti, Sagaing region, Myanmar.

Thet Tin Nyunt[1], Tay Thye Sun [2], Cho Cho [3], Naing Bo Bo Kyaw[3], and Wai Yang Lai Aung[4]

[1] Deputy Director General, Department of Higher Education, Ministry of Education, Nay Pyi Taw, Myanmar.
[2] Far East Gemological Laboratory, 12 Arumugam Road #04-02, LTC Building B, Singapore 409958.
[3] Myanma Gems Enterprise, Nay Pyi Taw, Myanmar.
[4] Department of Geology, University of Yangon, Yangon, Myanmar.
* Corresponding email: thettinnyunt@gmail.com

Keywords: amber, Khamti, Geology, FTIR

Introduction

Myanmar amber or Burmite is mainly found at the Tanai, Hukawng valley in Kachin State and some at Hti Lin (Tilin) in Magway Region. Another amber deposit is at Pat-tar bum (Pat-ta bum), near Nampilin stream, Khamti (Hkamti), Khamti Township, Sagaing Region, about 100km southwest of Tanai. This mine also known as Old Amber Mine, was abandoned since the British Colonel period and restarted in 2010. The study area, Pat-tar bum lies about 25km southeast of khamti in khamti Township, Sagaing Region i.e. 25° 40′ 12.10″ and 25° 42′ 54.60″ and longitude 95° 50′ 46.26″ and 95° 2′ 34.04″. Within Pat-tar bum, there are several mine sites where the key author and some of the co-authors visited the sites at Lachun (Laychun) Maw (most productive), Kyat Maw, Nat Ein Thar Maw, Palatar Maw, Shan Maw, Gyar Maw and Kyauk Tan Maw.

Brief geology of Khamti region

The regional geology of Khamti is made up of Triassic rocks found in the eastern part of the famous Jade Mine Area i.e. Pharkant. Ultramafic and basic intrusions mainly peridotite and serpentinite (mostly Jurassic) (Myanmar Geosciences Society, 2014) are well occupied in jade mine area, southern part of Khamti and northwest of Pharkant. Low grade metamorphic rocks, Kanpetlet schists and similar schists of Naga Hill are encountered in the eastern part. These metamorphic rocks are mainly schist such as glaucophane schists, graphite schists, epidote schist, etc. Orbitolina fossil (Cretaceous) bearing limestone disperse around the region (Kyu Kyu Thin, 2016; Mitchell 2018). Sedimentary units of Miocene age of Upper Pegu Group are widely exposed in the western, middle and north eastern part. Amber could be found in the Orbitolina fossil bearing Cretaceous limestone and intercalated with sandstone and carbonaceous shaley limestone (Fig.1).

Figure 1: Amber from Pat-tar Bum Khamti region showing a range of colour from yellow, brown, orangy yellow, and brownish yellow. (Photo by Tay).

Materialand methods

Twenty-one samples from Pat-tar bum
were examined using basic gemmological methods. All samples were examined using Fourier Transform Infrared spectroscopy of JASCO FTIR-4100 in the range 400 - 4000 cm^{-1}, with a resolution of 4 cm^{-1}, accumulating 100 scans.

Results

Gemmological data

The colour of Khamti amber varies from yellow, brown, greenish yellow, orangy- yellow, golden yellow and brownish yellow. The materials can be transparent to opaque. The refractive index spot reading ranges from 1.53 to 1.54, and specific gravity ranges from 1.03 to 1.09. The specimen with higher SG was attributed to attachment of calcite layer on the amber. Under magnification, flattened gas bubbles and some are brownish in appearance, flow marks, some brownish inclusions probably organic debris could be observed. Although no insect found in this lot of study, but the co-author Naing Bo Bo Kyaw has acquired various insects like spider, flies, some kind of worms, bits of feather like and plant-like inclusions from this location. Under ultraviolet radiation, Khamti amber tends to fluoresce very strong chalky yellowish-blue under long wave and weak chalky yellowish-blue or greenish under short wave. Some of the deep brownish material shows weak chalky blue or yellow under long wave ultraviolet light and inert under short wave ultraviolet light.

Infrared spectroscopy data

Peaks at 2925 cm^{-1}, 1725 cm^{-1}, 1460 cm^{-1}, 1375 cm^{-1}; also between 1300-1000 cm^{-1} and a weak pair of peaks between 855 cm^{-1} – 810 cm^{-1} are significant and common to samples from Khamti region. The absorption frequency of less than 3000 cm^{-1} in the C-H stretching region implies the absence of unsaturated or aromatic compounds. The peaks from 3000 cm^{-1} to 2850 cm^{-1} can be attributed to the C-H stretch of sp^3-hydridized C-H bonds of methyl and methylene groups. These are supported by the methylene (CH_2) bending absorption at 1460 cm^{-1} and the methyl (CH_3) bending absorption at 1375 cm^{-1}. The strong peak at 1725 cm^{-1} indicates the C=O stretch of a carbonyl group. The presence of a second peak close to this value could indicate the presence of more than one type of carbonyl compound. The presence of broad peaks between 1250 cm^{-1} – 1000 cm^{-1} could be attributed to C-O stretching and could indicate the presence of ester.

As Khamti amber has the characteristic IR peaks at 2925 cm^{-1}, 1725 cm^{-1}, 1460 cm^{-1}, 1375 cm^{-1}; between 1300 cm^{-1} – 1000 cm^{-1} and between 855 cm^{-1} – 810 cm^{-1} similar to amber from Hti Lin and Tanai regions, it could be concluded that Khamti amber is quite similar to Hti Lin and Tanai regions (Tay, 2015; Liu, 2018).

Discussion & Conclusion

The occurrence of amber in the Orbitolina fossil bearing limestone (Cretaceous) indicates that the formation of Khamti amber is older than Cretaceous. Gemmological properties of R.I., S.G., ultraviolet lighting data and IR peaks shows that the Khamti amber is quite similar to Hti Lin and Tanai regions.

References
Kyu Kyu Thin, 2016. 'Mineralogy and occurrences of jadeite jade from Nansibon Area, Hkamti Township, Sagaing Region', Unpublished M.Sc. Thesis, Department of Geology, University of Yangon, pg. 94.

Mitchell, A., 2018. 'Geological Belts, Plate Boundaries and Mineral deposits in Myanmar', Published by Elservier, Inc. Chapter 13, Hukawng Basin, the Amber Mines, and the Orbitolina limestone, pg.433-438.

Regional Geological Map of Myanmar Geosciences Society, 2014.

Tay T.S., Kleismantas A., Thet Tin Nyunt, Zheng M.R, Krishanswamy M. and Loke H.Y., 2015. Burmese amber from Hti Lin, the Journal of Gemmology, Vol.34, No.7, pg.606-615.

Shang I Liu, 2018. 'Burmese amber from Khamti, Sagaing Region', Journal of Gemmology, 36(2) pp107-110.

Acknowledgement
We are very grateful to Prof. Dr Day Wa Aung, Head of Geology Department and also Prof. Dr Htay Lwin, Department of Geology, University of Yangon for their permission to study this area. We also express our sincere thanks to Khaing Nan Shwe Co., for their generous support and also to Daw Ma Gjam, Ko Aung Naing, Dr Ko Hein for providing financial support to attend the International Gemmological Conference (IGC), Nantes, France. Also many thanks to Mr Murali Krishnaswamy, Head of Year 4 and Lecturer at Chemistry dept., NUS High School who has kindly assist in checking the FTIR data on the amber, U Tin Khaw Than and Loke Huiying for data discussion.

TURQUOISE FROM ZHUSHAN COUNTY IN HUBEI PROVINCE OF CHINA

Quanli Chen[1*], Xianyu Liu[1,2], Zuowei Yin[1], Pengfei Zhang[1]

[1] Gemmological Institute, China University of Geosciences, Wuhan, China, 430074. *chenquanli_0302@163.com
[2] College of Jewelry, Shanghai Jian Qiao University, Shanghai, China, 201306.
* Corresponding author's email

Key Words: Turquoise; Zhushan County; Infrared absorption spectra; Structure, Hubei Province

Abstract: China has been a significant source of turquoise for decades. One area of Zhushan County in Hubei Province has produced some attractive turquoise material. The turquoise from Zhushan County is often of high quality, with a dense texture and an attractive uniform coloration. Turquoise in China's Zhushan County occurs in a compressed fractured zone among beds of siliceous and carbonaceous-siliceous slates. Rough and polished samples were studied using standard gemological methods, as well as FTIR and UV-Vis-NIR spectroscopy in this paper. The Zhushan County turquoise occurs mainly as veinlets, blocks, and nodular aggregates. It is generally compact, massive, and shows a waxy luster. Its color is predominantly a medium bluish green. Light bluish green, light green, and yellowish green are also fairly common, while "azure" blue is rare. The Zhushan County turquoise showed the following properties: RI:1.61–1.62; Mohs hardness:5–5.5; and SG:2.57–2.72. Microscopic examination of thin sections shows microcrystalline platelike and spherulitic structures. The turquoise matrix was composed mainly of carbonaceous material, limonite, and a clay mineral. Secondary quartz is locally present in the matrix as elongate bladed aggregates. Brownish black veinlets/patches and irregular white blebs are typical features of turquoise from Zhushan County. The chemical constituents of the Zhushan County turquoise are w(Al_2O_3)=33.46~36.30%, w(P_2O_5)=31.12~33.80%, w(CuO)=3.75%~7.63%, w(Fe_2O_3)=1.13% ~6.58%, w(FeO) = 0.06% ~0.32%, showing they belong to the turquoise-chalcosiderite family(Frost et al., 2006). The bluer samples contained higher Cu and lower Fe concentrations. The infrared absorption spectra show typical phosphate, water, and hydroxyl vibrations for turquoise. UV-Vis-NIR absorption spectra have strong, sharp bands caused by Fe^{3+} and wide bands caused by Cu^{2+}. Most of the gemological and spectral characteristics of turquoise from Zhushan County are similar to those found in samples from elsewhere in China's Hubei Province(Qi et al., 1998; Luan et al., 2004).

Figure 1. This map shows the location of turquoise deposits in Zhushan County, Hubei Province.

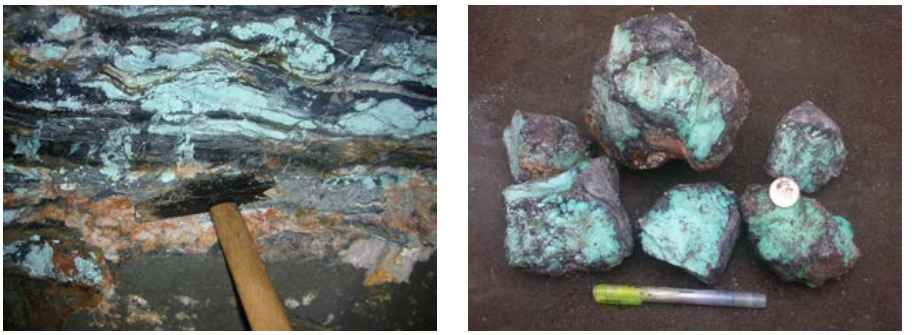

Figure 2. The turquoise occurs as lenses and fracture fillings in a compressed fractured zone between beds of siliceous and carbonaceous-siliceous slates(left). Blocky turquoises are commonly produced from the Zhushan County deposits(right). Photos by Quanli Chen.

Figure 3. This carving, called "Seven female celestials," was made from a large piece of Zhushan County turquoise. It measures about 56 cm high and 35 cm wide. Photo by Quanli Chen. Nodular specimens are usually displayed as ornamental stones (right, 33 ×26 cm). Photos by Quanli Chen.

References

Frost R.L., Reddy B.J., Martens W.N., Weier M. (2006) The molecular structure of the phosphate mineral turquoise—A Raman spectroscopic study. Journal of Molecular Structure, No. 788, No. 1–3, pp. 224–331, http://dx.doi.org/10.1016/j.molstruc.2005.12.003.

Luan L.J., Han Z.X., Wang C.Y., Zhang Y.W. (2004) Elementary research on color-forming mechanism of turquoise. Northwestern Geology, Vol. 37, No. 3, pp. 77–82 [in Chinese].

Qi L.J., Yan W.X., Yang M.X. (1998) Turquoise from Hubei Province, China. Journal of Gemmology, Vol. 26, No. 1, pp. 1–12.

THE VIVID WORLD OF JADEITE

Elizabeth Su

(Gemsu Rona (Shanghai) Jewellery Co. Ltd. , China)
L102, No. 99, East Beijing Road, Shanghai, China 200011 esu_gems@yahoo.com

Keywords: Vivid Jadeite, Top Quality Jadeite, Inclusions

I have been working in the jadeite industry for more than 16 years. During my tenure as a gemologist and merchant, I have experienced not only boom cycles within the jadeite industry, but also bust cycles during economic decline. I have been schooled in the most high-end part of the jadeite. In this article, you will, through my eyes and experiences, peruse the report of top colour and top quality jadeite. There are 32 super samples of green, purple, yellow to orange, colourless, inky and multi-colour jadeite. For some typical or special jadeite structures and inclusions, we used gemological microscope for magnification observation and recorded them by photos.

Top green jadeite is the most important and expensive, normally the price of purple jadeite is 1/10 of green one.

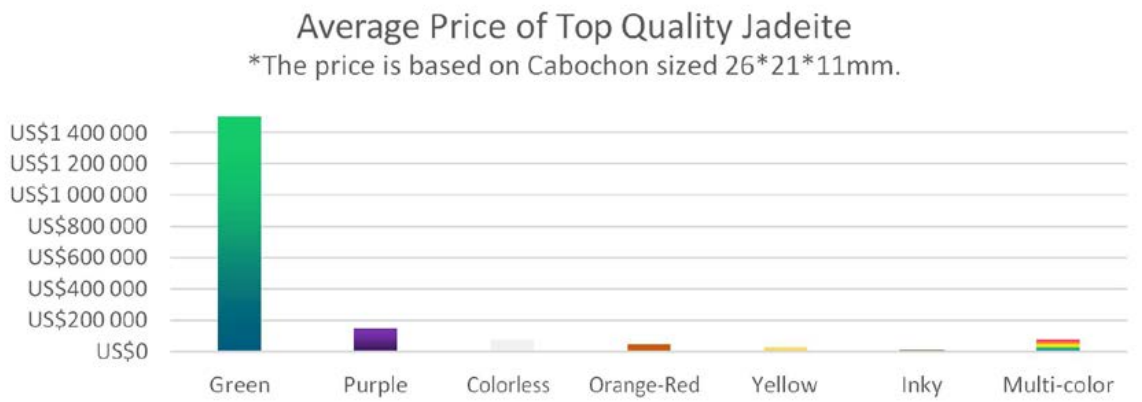

Figure 1 Average Price of Top Quality Jadeite

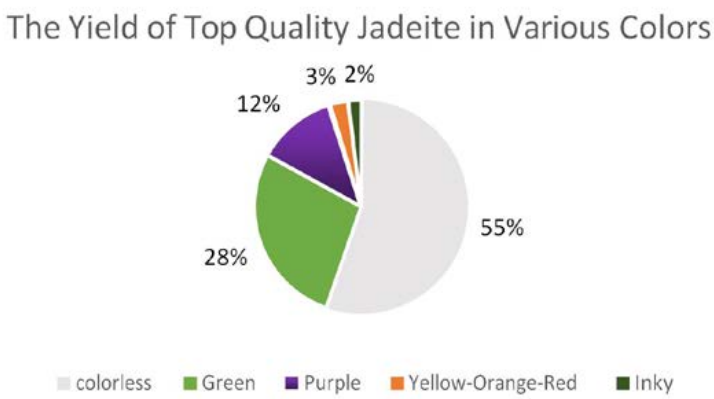

Figure 2 The Yield of Top Quality Jadeite in Various Colors

These four jadeite cabochons are the best samples of top jadeite with extremely fine structure, very good translucency, more even size of microcrystalline. It's a kind of colloidal texture which has countless super tiny jadeite crystals in more orderly arrangement and more uniform fineness. In the transmitting light will shows a visual effect as thick as glue. It's absolutely icy~glassy jadeite with bright and vivid green just like four pieces of jelly.
Price US 38000/4ps

Figure 3 MuNa Mine Jadeite Cabochons

This pair of pendant is the excellent example of high-class jadeite. The crystal grain is microgranular the fineness is uniform and the crystal particles are invisible to the naked eye. Extra low impurity no crackers extremely fine texture charming vivid green colour good translucency. When we move it the light suddenly overflows the colour.
Price: US 119000

Figure 4 A Pair of Old Mine Glassy Pendant

Icy yellow-orange jadeite is extremely rare in the nature. The vivid orange icy jadeite has very find texture excellent translucency vivid colour. Some colours are evenly distributed and some colours change gradually.
Price: Us1200-Us7500

Figure 5 A Set of Yellow-Orange Jadeite Jewellery

This intense vivid purple jadeite cabochon necklace is the only one in the market which shows the unique top vivid colour
Price: Us 2388000

Figure 6 A Jewellery set of Intense Vivid Purple Jadeite

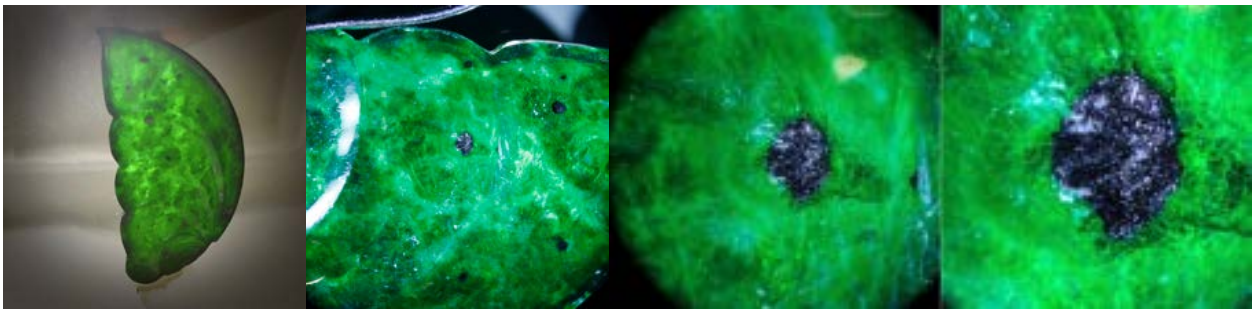

Figure 7 Magnification of Jadeite inclusions

The jadeite slice with butterfly wings shape is a vivid color with good translucency piece. Because it's a thin slice and also because it has a lot of small black spots scattered so the price is not expensive. On closer inspection it's a common chromite inclusions in green jadeite.
Price:Us750

Figure 8 Natural Multi-colour Jadeite Bangle

This natural jadeite bangle has tricolor combination: vivid yellow, apple green and white, with fine texture and medium translucency.
Weight 67g, Size:55mm
Price:US 418000

References

XU Mengjun1,LI Ji2, 2010, Study and Interpretation to Jade Culture and Jade Market

Acknowledgements

The author is grateful for support from Alida Marais, colleagues of Gemsu Rona, and great thanks to Mr.Duan Gang for many helpful discussions.

Mineralogical characterization of the unusual gemstone parisite–(Ce)

Manuela Zeug[1*], Lutz Nasdala[1], Radek Škoda[2], Chutimun Chanmuang N.[1], Martin Ende[1], Christoph Hauzenberger[3], Dan Topa[4], Manfred Wildner[1], Richard Wirth[5],

[1] Institut für Mineralogie und Kristallographie, Universität Wien, Althanstr. 14, 1090 Wien, Austria
[2] Department of Geological Sciences, Masaryk University, Kotlářská 2, 61137 Brno, Czech Republic
[3] NAWI Graz Geozentrum, Universitätsplatz 2, 8010 Graz, Austria
[4] Naturhistorisches Museum Wien, Burgring 7, 1010 Wien, Austria
[5] Helmholtz-Zentrum Potsdam – GFZ, Telegrafenberg, 14473 Potsdam, Germany
*manuela.zeug@univie.ac.at

Keywords: Parisite-(Ce), Muzo mine, Polycrystal

The first description of "parisite" appeared in the middle of the 19th century, referring to a specimen from the Muzo emerald-mining area, Boyacá Dept., Colombia (Bunsen, 1854). The Italian mineralogist Lavinio de Medici-Spada named "parisite" after the former mine owner and manager, Mr. José J. Paris. Only after 1890, parisite-group minerals were also found in other locations, including Mountain Pass, California; Bayan Obo, Inner Mongolia; Phalaborwa, South Africa; Mt. Malosa, Malawi; Mont St. Hilaire, Quebec; and Narsarsuk, Greenland. According to current nomenclature rules of the International Mineralogical Association (IMA), individual mineral species are now named according to the dominant rare earth element (REE) by quoting that REE as a suffix. Among others, parisite-group minerals include parisite–(Ce), parisite–(Nd) and parisite–(La) (e.g. Cook, 2000; Menezes Filho et al., 2018).

At a first glance, the Ca-Ce-fluorocarbonate mineral parisite–(Ce) does not seem to be an attractive gem material (Fig. 1). Most specimens are brownish, occasionally with yellow, orange or reddish hue. Their hardness is decidedly low for any potential use as gems (about 4.5 on the Mohs scale). Transparent and flawless crystals without inclusions or impurities are rare. In addition, specimens are decidedly brittle and hence not easy to handle for gem cutters. In spite of the above, however, parisite–(Ce) is quite well present in the Colombian gem trade, perhaps because of its common, attractive colour change between daylight and artificial illumination. Also, parisite–(Ce) is an interesting mineral from the crystal-chemical point of view. Here we report results of a study that aimed at characterising parisite–(Ce) from La Pita mine, Municipality de Maripí, Boyac á Dept., Colombia (Fig. 1).

Figure 1: Three parisite–(Ce) crystals (from left to right: 2.48 ct; 0.26 ct; 1.98 ct) from the La Pita mine, eastern Cordillera, Colombia.

Minerals that contain noticeable amounts of REEs tend to be strongly luminescent, which can then easily obscure the Raman spectrum. In case of the Muzo material under investigation, it was nevertheless possible to identify two fluorocarbonate minerals in one crystal, from the symmetric carbonate-stretching Raman bands around 1100 cm^{-1} (Figs. 2, 3B).

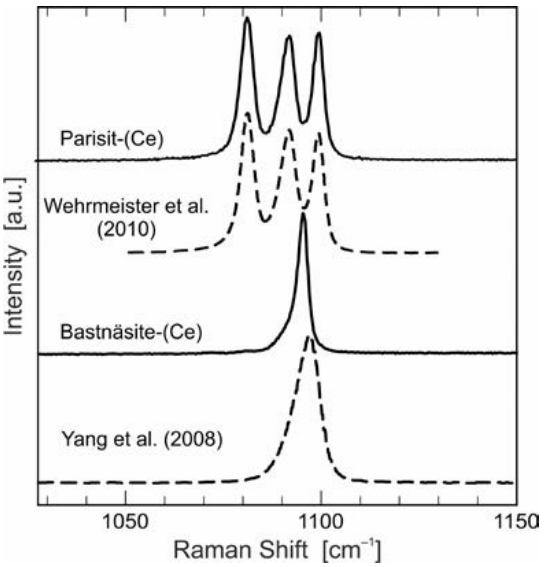

Figure 2: Raman spectra showing the symmetric CO3 stretching range. Spectra obtained in parisite–(Ce) and bastnäsite–(Ce) zones (compare Fig. 3B below) are shown in comparison with published references. Differences in band positions compared to reference spectra are due to differences in samples' chemical compositions.

The crystal-structural composition of parisite–(Ce) is remarkably complex. This is due to stacking sequences, which show commensurate or incommensurate stacking patterns consisting of parisites, bastnäsites, synchisites, röntgenite–(Ce) or other REE-fluorocarbonates (Ciobanou et al., 2017). The ideal stacking sequence of parasites is $[2(REE)FCO_3 \cdot CaCO_3]$, which corresponds to one bastnäsite and one synchysite layer (e.g. Ciobanou et al., 2017). It was already found by Donnay and Donnay (1953) that in most cases, parasite-group minerals form polycrystals because of the syntactic intergrowth of at least two mineral species. For decades, this complex polytypism made it difficult to unravel the crystal structure of parasite. Donnay and Donnay (1953) found parisite–(Ce) to be trigonal with space group R3, whereas Ni et al. (2000) found a monoclinic crystal system with m or 2/m symmetry. We have determined a monoclinic unit-cell of parisite–(Ce) and hence agree with the results of Ni et al. (2000). Our results reveal that parisite–(Ce) crystals may be even more complex than has previously been thought. There exist various stacking sequences, showing commensurate or incommensurate stacking sequences, which exist down to the atomic scale (Fig. 3). Figure 3B shows the syntactic intergrowth of bastnäsite–(Ce) (two bright-BSE lamellae) and parisite-(Ce) (medium- to low-BSE lamellae) determined by means of Raman spectroscopy.

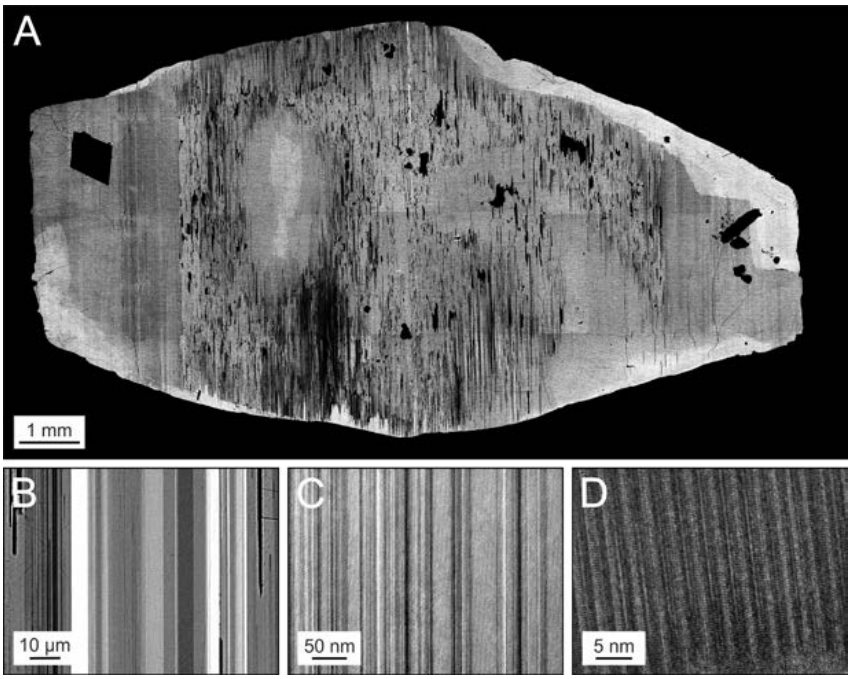

Figure 3: Images of parisite–(Ce). (A) Patchwork image, consisting of numerous individual back-scattered electron (BSE) photographs, of an entire polished crystal. (B) Detail enlargement. Raman point analyses revealed that the two bright-BSE lamellae are bastnäsite–(Ce) whereas all other, medium- to low-BSE lamellae consist of parisite–(Ce). (C) Bright-field image obtained in the transmission electron microscope (TEM). (D) High-resolution TEM lattice fringe image. The two latter show that disordered stacking sequences exist down to the atomic scale.

References

Bunsen, R., 1854. Ueber den Parisit, ein neues Cerfossil. Annalen der Chemie und Pharmacie, 53, 147–156.

Ciobanu, C.L., Kontonikas-Charos, A., Slattery, A., Cook, N.J., Kathy Ehrig, K., Wade, B.P., 2017. Short-range stacking disorder in mixed-layer compounds: a HAADF STEM study of bastnäsite-parisite intergrowths. Minerals, 7(11), 227.

Cook, R.B., 2000. Connoisseur's choice: Parisite Muzo district, Colombia. Rocks and Minerals, 75(4), 250–252.

Donnay, G., and Donnay, J.D.H., 1953. The crystallography of bastnaesite, parisite, roentgenite and synchysite. American Mineralogist, 38, 932–963.

Menezes Filho, L.A.D., Chaves, M.L.S.C., Chukanov, N.V., Atencio, D., Scholz, R., Pekov, I.V., da Costa, G.M. Morrison, S.M., Andrade, M.B., Freitas, E.T.F., Downs, R.T., Belakovskiy, D.I., 2018. Parisite-(La), $CaLa_2(CO_3)_3F_2$, a new mineral from Novo Horizonte, Bahia, Brazil. Mineralogical Magazine, 82, 133–144.

Ni, Y., Post, J.E., Hughes, J.M., 2000. The crystal structure of parisite-(Ce), $Ce_2CaF_2(CO_3)_3$. American Mineralogist, 85, 251–258.

Wehrmeister, U., Soldati, A.L., Jacob, D.E., Häger, T., Hofmeister, W., 2010. Raman spectroscopy of synthetic, geological and biological vaterite: a Raman spectroscopic study. Journal of Raman spectroscopy, 41, 193–201.

Yang, H., Dembowski, R.F., Conrad, P.G., Downs, R.T., 2008. Crystal structure and Raman spectrum of hydroxyl-bästnasite-(Ce), $CeCO_3(OH)$. American Mineralogist, 93, 698–701.

Acknowledgements
We thank Darwin Fortaleche, Bogotá, for his help in acquiring samples, and Andreas Wagner, Wien, for sample preparation. We are indebted to Gerlinde Habler, Wien, for her help with the preparation of FIB foils.

AMBER WITH VIOLET FLUORESCENCE FROM MYANMAR

Zhiqing ZHANG, Andy H. SHEN*

Center for Innovative Gem Testing Technology, Gemmological Institute,
China University of Geosciences, Wuhan, 430074, CHINA
* ahshen1@live.com

Keywords: Amber, Infrared spectra, violet fluorescence

Introduction

Normally amber shows yellowish white or blue fluorescence, when excited with long-wave UV light (typical wavelength = 365nm). Recently, we obtained thirty-eight transparent brownish yellow amber beads from Myanmar (exact origin not available) showing unique violet fluorescence (see Figure 1 (a), (b)). Gemologically, they all showed S.G. about 1.05,
R.I. around 1.54 and conchoidal fractures. We collected the mid-infrared spectra by Bruker Tensor 27 with 4 cm^{-1} resolution in reflection mode. Additionally, fluorescence spectra of these Burmese ambers and of a piece of amber from Dominican Republic as a reference were collected using a Jasco FP8500 fluorescence spectrometer. Specific testing conditions were set as 2.5 nm bandwidth and 5 nm data interval for the excitation spectra, 1 nm bandwidth and 1 nm data interval for the emission ones.

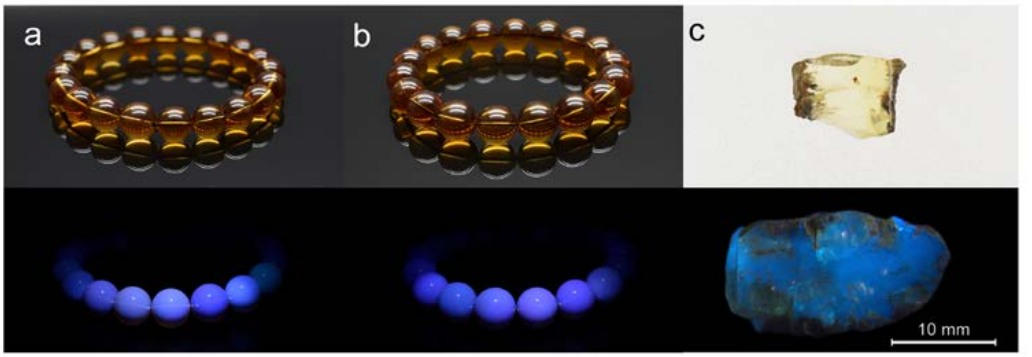

Figure 1 The upper row photos showed samples illuminated with D65 light, while the lower row showed the same samples illuminated with a solid state 365 nm UV light LED torch. (a) and (b) are Burmese beads (with diameters around 10.15 mm and 10.55 mm, respectively) shown bluish violet fluorescence. Amber fragment from Dominican Republic in (c) showed a typical blue fluorescence; the scale bar applies to the Dominican sample under UV light only. Photo by Z. ZHANG.

Infrared Absorption features

Infrared absorption features were measured as reflection then subsequently converted to absorption. Two types of IR spectra were observed from these beads (Figure 2). Curve (a) is
similar to previously published spectra on Burmite (Tay et al. 2015; Xing et al. 2015; Zhang et al. 2017); while curve (b), the biggest difference is the presence of double peak around 1751 cm^{-1}. In other spectral range, strong absorptions at 2929 cm^{-1} and 2862 cm^{-1} were observed in functional group region (4000-1500 cm^{-1}). In the fingerprint region (1500-400 cm^{-1}), both type spectra show same absorption locations near 1460 cm-1, 1377 cm^{-1}, 1224 cm^{-1} and 1022 cm^{-1}.

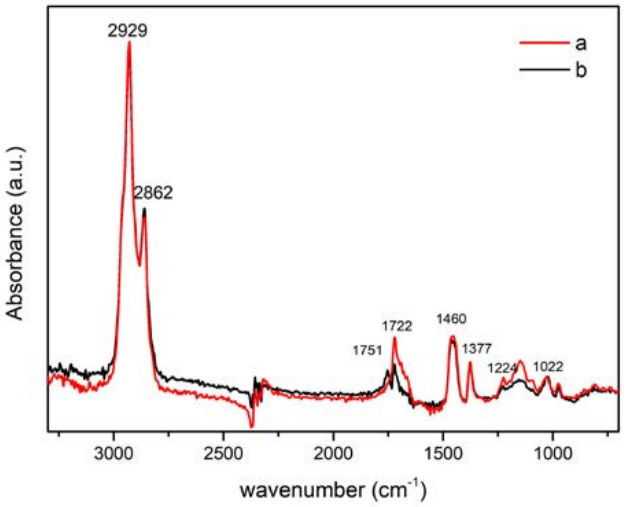

Figure 2 Two types of infrared spectra were obtained from these beads. Type (a) is a typical Burmite spectrum and type (b) is somewhat different spectrum. There is no direct correlation to their fluorescence features.

Fluorescence features

In this study, all beads reveal same luminescence behavior - emission range were focused in two spectral regions: 330 nm to 360 nm and 380 nm to 430 nm. The latter wavelength range covered the violet color wavelength thus resulting in the violet fluorescence color visually. As shown in Figures 3 (a) and (b), the optimal excitation wavelength for generating emission bands at 386 nm, 406 nm and 430 nm is 355 nm. Therefore, when using a typical gemological long-wave UV light (mostly 365 nm UV source), these three emission bands still appear - thus the observed violet fluorescence. Additionally, another group of emission peaks at 332 nm, 345 nm and 363 nm are all in the UV region, not visible to the bare eyes.

By contrast, normal ambers from Dominican Republic are with blue fluorescence (Figure 3 (c), (d)). Their fluorescence spectra show emissions at 445 nm, 474 nm and 508 nm, the last two main emission peaks are in the blue – thus the observed blue fluorescence. All these emissions can be best excited by the excitation wavelengths near 440 nm and 415 nm. When excited with a typical gemological long-wave UV light source (mostly 365 nm UV source), these three emission centers still appear but with lower intensity.

Interestingly, no clear correlation between the types of IR absorption and their fluorescence spectra was observed among all these samples. Therefore, determining the nature of compounds causing these violet luminescence features, will need further, careful studies.

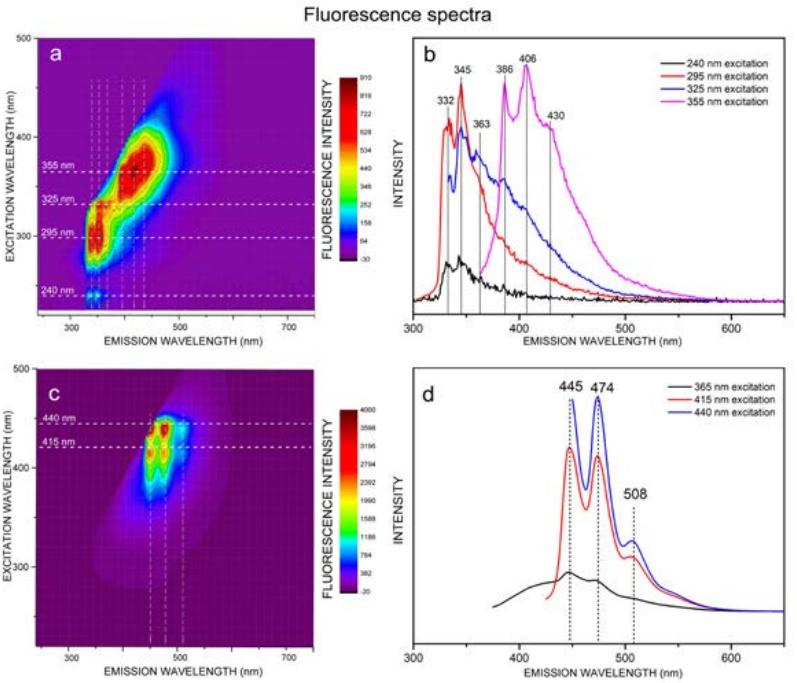

Figure 3 Typical three dimensional fluorescence spectra were shown. (a) and (b) are the spectra of a typical amber with violet fluorescence from Myanmar. (c) and (d) are the spectra from a typical amber from Dominican Republic with blue fluorescence.

References

Beck C., Wilbur E., Meret S., Kossove D., Kermani K. 1965. The infrared spectra of amber and the identification of Baltic amber. Archaeometry, 8(1), 96-109.

Tay T.S., Kleismantas A., Nyunt T.T., Zheng M., Krishnaswamy M., Ying L.H. 2015. Burmese amber from Hti Lin. The Journal of Gemmology, 34(7), 606-615.

Xing Y., Qi L., Mai Y., Xie M. 2015. FTIR and ^{13}C NMR spectrum characterization and significance of amber from different origins. Journal of Gems and Gemmology, 17(2), 8-16. DOI:10.3969/j.issn.1008-214X.2015.02.002 (in Chinese with English abstract).

Zhang Z., Lin Q., Shen A.H. 2017. Characteristic of oxygen content in black amber from Myanmar. Journal of Gems and Gemmology, 19(1), 17-21. DOI: 10.15964/j.cnki.027jgg.2017.01.003 (in Chinese with English abstract).

INTERNATIONAL GEMMOLOGICAL CONFERENCE

Nantes - France
August 2019

www.igc-gemmology.org